SUPERCRITICAL FLUID EXTRACTION OF PARAFFIN WAX

by

James Christoffel Crause

Dissertation presented for the Degree

of

DOCTOR OF PHILOSOPHY IN ENGINEERING
(Chemical Engineering)

in the Department of Chemical Engineering
at the University of Stellenbosch

Promoter

Prof. Izak Nieuwoudt

STELLENBOSCH
DECEMBER 2001

Declaration

I, the undersigned, hereby declare that the work contained in this dissertation is my own original work and that I have not previously in its entirety or in part submitted it at any university for a degree.

Synopsis

In this study the deoiling and fractionation of paraffin wax using supercritical fluid extraction (SCFE) has been investigated. SCFE was compared with state-of-the-art processes such as wax crystallisation, static crystallisation and short path distillation.

Ethane and carbon dioxide were investigated as supercritical solvents for the supercritical fluid extraction of paraffin wax. Supercritical phase equilibrium data for ethane – n-alkane and CO_2 – n-alkane systems close to the mixture critical region were obtained from the literature, and were correlated with several equations of state. Statistical mechanical equations of state failed to correlate the data close to the mixture critical region due to the neglect of density fluctuations which influences phase behaviour close to critical points, or due to inadequate mixing rules. It was found that simple cubic equations of state such as Soave-Redlich-Kwong, Peng-Robinson and Patel-Teja could correlate the data using two interaction parameters. This can be attributed more to their flexibility as correlating tools than to their fundamental accuracy. The Patel-Teja EOS was modified by fitting it to predict low vapour pressure data for long-chain n-alkanes. This modified Patel-Teja EOS was then fitted to the phase equilibria by adjusting two interaction parameters per binary system. The interaction parameters for each solvent (ethane or CO_2) system were then fitted to generalised correlations to enable extrapolation to solvent – n-alkane systems for which no equilibrium data were available. The Simplified Perturbed Hardchain theory (SPHC) equation of state was used to correlate lower-pressure solubility data used to model the extract separator.

A pilot plant SCFE unit was constructed and used to obtain experimental fractionation data of a low-molecular weight Fischer-Tropsch wax. The experimental results indicate that fractionation of the wax is possible and that the separation efficiency is enhanced by returning some of the extract to the column as reflux. An equilibrium stage model was constructed and used to simulate the extraction experiments. It was possible to obtain good agreement between the experimental results and model predictions.

Deoiling of petroleum waxes with a low n-paraffin content (which are not currently deoiled commercially) was investigated. Experimental SCFE and SPD results indicated that selective deoiling is not possible, since the separation is based on differences in molecular weight (or vapour pressure). Simulations of wax crystallisation or solvent extraction and practical tests indicate that deoiling is possible, based on differences in structure and

therefore melting point of the components in the wax. Practical problems associated with crystallisation or solvent extraction such as filtration, the use of chlorinated solvents and low yields currently prevent the commercial deoiling of these waxes. During crystallisation of these waxes a soft wax cake is formed which impedes the operation of static crystallisation.

A detailed study of the economics of n-paraffin wax deoiling using SCFE was conducted. Flow sheets were proposed to minimise the energy consumption of the SCFE process. Comparison of SPD, static crystallisation and SCFE indicates that a SPD plant will be the cheapest option for deoiling the wax feed investigated. Fractionation of heavier waxes using SPD might not be economically feasible, since the distillation temperature increases dramatically with increasing molecular weight, which leads to higher energy cost. For medium to long chain n-paraffin waxes SCFE should be very competitive, since the capacity of the supercritical solvent can be manipulated to extract longer chain waxes without increasing the extraction temperature. Static crystallisation appears to be the more expensive deoiling option, due primarily to the large initial capital investment cost.

Opsomming

Die olieverwydering en fraksionering van paraffienwasse met behulp van superkritiese ekstraksie is in hierdie studie ondersoek. Die modellering van moderne olieverwyderings- en fraksioneringsmetodes soos waskristallisasie, statiese kristallisasie en kortpad distillasie is ook ondersoek.

Etaan en koolstofdioksied is ondersoek as superkritiese oplosmiddels vir die superkritiese ekstraksie van paraffienwasse. Literatuurdata van superkritiese fase-ewewigte vir etaan – n-alkaan en CO_2 – n-alkaan stelsels naby die mengselkritiese punt is versamel en gekorreleer met verskeie toestandsvergelykings. Statisities-meganiese toestandsvergelykings kon nie data naby mengselkritiese punte korreleer nie, moontlik weens digtheidsvariasies wat afwykings van klassieke gedrag teweegbring, of onakkurate mengreëls. Eenvoudige kubiese toestandsvergelykings soos Soave-Redlich-Kwong, Peng-Robinson en Patel-Teja kon op die ewewigsdata gepas word deur gebruik van twee interaksieparameters. Dit kan eerder toegeskryf word aan hulle buigsaamheid eerder as hulle fundamentele akkuraatheid. Die Patel-Teja toestandsvergelyking is gemodifiseer deur dit te pas op lae dampdruk data van langketting n-alkane. Hierdie gemodifiseerde toestandsvergelyking is gepas op die fase-ewewig data deur twee interaksieparameters te gebruik per binêre sisteem. Die interaksieparameters vir die oplosmiddel stelsels (etaan of CO_2) is gekorreleer met algemene vergelykings sodat dit vir ekstrapolasie na oplosmiddel – n-alkaan stelsels gebruik kan word waarvoor ewewigsdata nie beskikbaar is nie. Die "Simplified Perturbed Hardchain" teorie (SPHC) toestandsvergelyking is gebruik om laer druk oplosbaarheidsdata te korreleer vir gebruik in die modellering van die ekstrak skeier.

'n Superkritiese ekstraksie loodsaanleg is gebou en gebruik om eksperimentele fraksioneringsdata van 'n lae molekulêre massa Fischer-Tropsch was te genereer. Vanaf die eksperimentele resultate blyk fraksionering van was moontlik te wees. Die doeltreffendheid van die skeiding kan verhoog word deur terugvloei van ekstrak na die kolom. 'n Ewewigsmodel is opgestel en gebruik om die ekstraksie eksperimente te modelleer. Deur die ekstraksiedruk en aantal stadia te verander kon goeie ooreenstemming met eksperimentele resultate verkry word.

Die verwydering van olie uit petroleumwasse met 'n lae n-paraffien inhoud (wat nie tans kommersiëel ontolie word nie) is ondersoek. Eksperimentele resultate vir superkritiese ekstraksie en kortpad distillasie dui daarop dat selektiewe olieverwydering nie moontlik is nie, omdat die skeiding gebaseer is

op verskille in molekulêre massas en dus (of dampdrukke). Simulasies van waskristallisasie dui op die moontlikheid van olieverwydering gebaseer op verskille in strukture van die komponente in die was. Praktiese probleme geassosieer met kristallisasie of oplosmiddel ekstraksie soos filtrasie, lae opbrengste en gebruik van gechlorineerde koolwaterstowwe as oplosmiddel belemmer die kommersialisering van olieverwydering vir hierdie tipes wasse.

'n Gedetaileerde studie van die ekonomiese lewensvatbaarheid van superkritiese olieverwydering is uitgevoer. Vloeidiagramme is voorgestel om die energieverbruik van die superkritiese ekstraksieproses te minimeer. Vergelyking van kortpad distillasie, statiese kristallisasie en superkritiese ekstraksie dui daarop dat kortpad distillasie die goedkoper opsie vir die olieverwydering van die spesifieke was is. Fraksionering van swaarder wasse met kortpad distillasie sal moontlik nie haalbaar wees nie omdat die distillasietemperatuur drasties toeneem met molekulêre massa. Die skeiding van medium tot langketting wasse met superkritiese ekstraksie behoort meer mededingend te wees, want die kapasiteit van die superkritiese oplosmiddel kan maklik verstel word om langer kettinglengtes wasse te ekstraeer sonder om die temperatuur te verhoog. Statiese kristallisasie blyk die duurder olieverwyderingsopsie te wees hoofsaaklik weens die hoë kapitaalkoste van so 'n aanleg.

Acknowledgements

Prof. Nieuwoudt introduced me to this topic. I want to thank him for his enthusiasm and frequent support.

Table of contents

CHAPTER 1. WAX PROCESSING – AN INTRODUCTION

1.1. Background

Some of the industrial uses of paraffin wax are listed in Table 1-1. Most applications require wax with a low oil content. A large fraction of the total deoiled wax is used in the paper and packaging industry (Nasser, 1999). Some of the more specialised applications require wax with low polydispersity or narrow melting point ranges, such as thermostat wax, hot melt adhesives or thermal transfer wax. One of the interesting areas of wax usage is as phase change medium for the storage of energy (Sharma and Singh, 1979; Haji-Sheikh et al., 1983).

Paraffin wax is obtained from two sources namely crude oil or the Fisher-Tropsch process. Usually the refined lubricating oil fraction from the vacuum distillation process is first dewaxed to produce a wax-free lubricating oil and a slack wax. This slack wax is then subjected to a deoiling step to produce a deoiled wax and a soft wax (also called foot oil). These deoiled waxes contain mostly n-paraffins, with some iso-paraffins and cyclo-paraffins.

The following wax deoiling and fractionation methods are currently used (Sequeira, 1994; WolfMeier et al., 1996):

Wax sweating

In general wax sweating entails slowly heating solid wax, and to remove the oil and low melting point waxes. An example of such a wax sweating process is the process described by Irwin and Aufhauser (Irwin and Aufhauser, 1975): Molten wax is poured between perforated metal sheets with a spacing of 3-6mm (see Figure 1-1). Tubes passing through the sheets are used as heat exchanger. After the cell consisting of the perforated metal sheets is filled with the molten wax, cold water is circulated through the heat exchanger tubes to solidify the wax. After all the wax has solidified, the cell with the solid wax is slowly heated. The oil and low melting point waxes slowly melt and drain to the bottom of a cell. The slow heating continues until the remaining solid wax has obtained the desired oil content. The remaining solid wax is then melted by additional heating, and collected. Wax sweating is the oldest deoiling process, and has been mostly replaced by newer processes.

Table 1-1. Industrial uses of paraffin wax (WolfMeier, Schmidt et al., 1996; Sinowax, 2000; Wax.org, 2000)

Application	Function/Effect	
	During processing	On finished goods
Adhesives, hot melts	Viscosity regulation, open time	Rapid set off
Carbon paper	Dispersing agent and binder	Clarity of reproduction
Cardboard, paper	Improvement of properties of substrate and adhesion	Coating, impregnation, surface gloss, laminating
Ceramics	Binder for sintering	Improved surface and reduction of rejects
Cheese	Encapsulation, moisture control	Coating, surface protection
Chewing gum	Dispersion of rubber and gum base additives	Chewability of gumbase
Cosmetics	Binder, consistency regulation	Component of ointments, pastes, creams, lipsticks
Paints and coatings	Viscosity regulation	Matting, surface protection, slip agent
Pharmaceuticals	Dispersion or surface treatment aid	Surface protection, glazing agent, release retardant in drugs
Plastics and rubber	Lubricant (PVC), release agent (PA)	Improved surface appearance
Polishes	Major ingredient	Surface protection of leather, floors, cars
Printing inks	Dispersion promoter	Improved rub resistance, slip, gloss
Photocopier toner	Dispersing aid	Print clarification

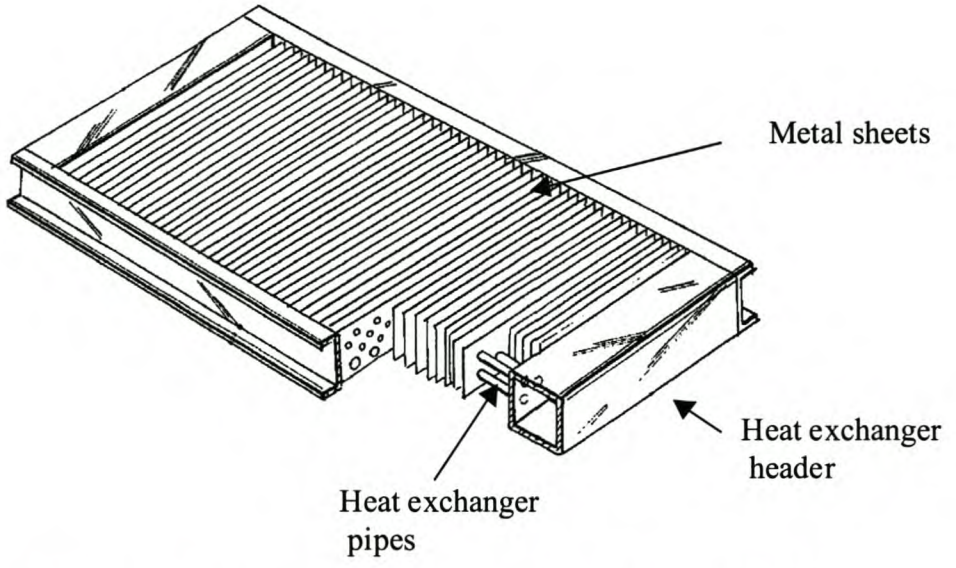

Figure 1-1. Wax sweating cell (Irwin and Aufhauser, 1975).

Static crystallisation

Sulzer Chemtech AG has made refinements to the wax sweating process, and has recently installed a 100 000 ton / year deoiling plant for Schümann Sasol (Jans and Stepanski, 1999; Engstler et al., 2000). The static crystallisation process is as follows: A batch of molten wax is slowly cooled in a heat exchanger. The molten wax is cooled and wax crystals form on the exchanger surface. The heat exchanger surface slopes downward and the crystals slide along this surface to a collector.

Wax recrystallization

The wax feed is dissolved in warm solvent. This solution of wax and solvent is then chilled, and the harder wax precipitates. The resulting solvent-wax pulp is filtered, and the wax cake is washed with cold solvent (see Figure 1-2). The filtration temperature determines the melting point of the wax product. This process can also be used to fractionate the hard wax by doing multiple filtrations at different temperatures (West, 1985).

Warm-up deoiling (Pulping, solvent extraction)

In this process solid wax pellets or flakes are contacted with a liquid solvent at a constant temperature. The oil and some of the soft waxes dissolve in the solvent. The solvent and solid wax is then separated by filtration. The extraction can be performed in steps, with an increase in the extraction temperature, resulting in fractionation of the wax feed. The solvent is recovered from the solvent-wax solution by distillation (Katayama, 1993; Meyer and Hildebrand, 2000). This process is more cost-effective than the wax recrystallization process, since the hard wax is not melted and

recrystallized before filtration. The process flow diagram is similar to Figure 1-2, but the chiller between the mixer and filtration unit is absent.

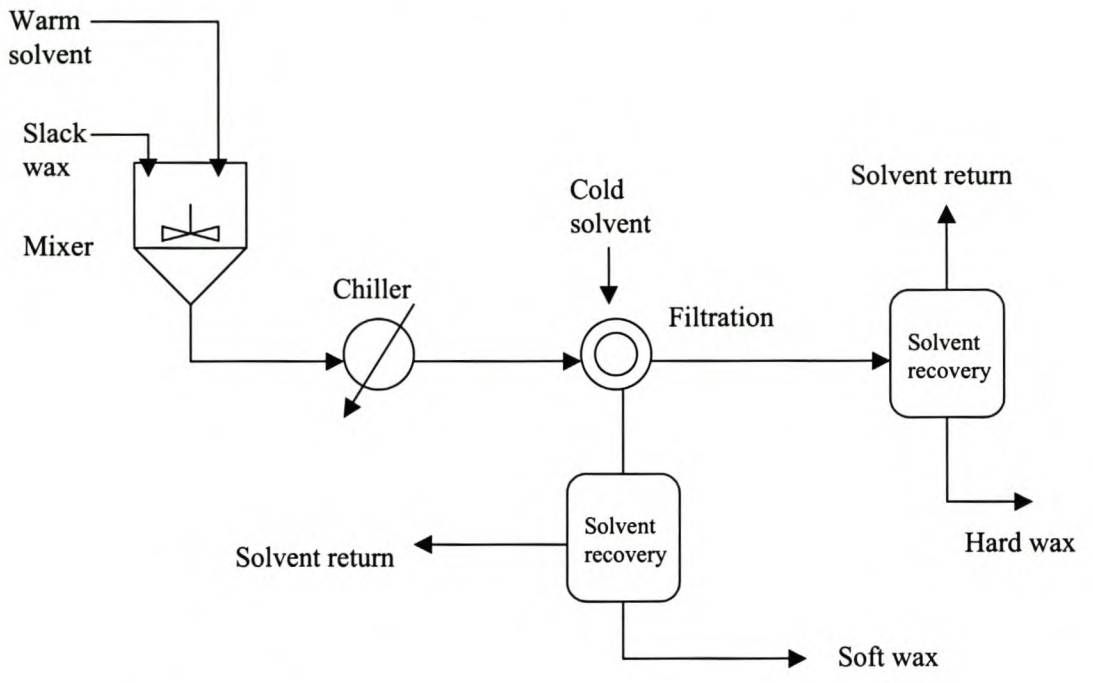

Figure 1-2. Process flow diagram of the wax recrystallisation process.

Spray deoiling

Molten wax is sprayed into the top of a tower, and cold air is blown into the tower from the bottom. The hard wax solidifies and collects at the bottom of the tower. This wax is then washed with cold solvent to remove oil that adheres to the wax.

Short path distillation (molecular distillation)

Molten wax is fed to a cylindrical vessel. The wax is wiped onto the vessel wall with a wall wiper. The process operates under low pressure, and some of the wax evaporates from the heated wall and condenses on a cold surface. This process is mostly used to fractionate hard wax (Jones et al., 1991; Nieuwoudt, 1994; Pope, 2000).

The choice of solvents used in the above solvent based processes depends on the oil content and composition (iso-paraffins, cyclo-paraffins, low molar mass n-paraffin). A whole range of solvents are used in the solvent based processes:

- Ketones such as MEK and MIBK.
- Chlorinated solvents such as 1,2-dichloroethane and dichloromethane.
- Aromatics such as benzene and toluene.

Drawbacks of current deoiling and wax fractionation processes:

- Residual oil trapped in wax matrix (wax sweating).
- Residual solvent left in wax product.
- Lack of sharp cuts.
- High temperatures (short path distillation fractionation of waxes).

Since some of the deoiled and fractionated wax is used in products that are in contact with food (packaging) or humans (cosmetics), residual solvent in the wax product is undesirable. Currently the solvent is recovered from the wax by distillation or flash vaporisation, which is energy intensive. Short path distillation operates at higher temperatures, which can lead to thermal decomposition, especially during the fractionation of hard waxes.

Form the discussion above it is clear that the wax deoiling and fractionation process needs to be changed in order to overcome some of the inherent problems of current processes. The cut sharpness of wax fractionation also needs improvement, since wax fractions having narrow melting point ranges can be used in products having high commercial value.

1.2. An alternative wax processing technology - Supercritical fluid processing

It is believed that supercritical fluid extraction should be investigated as an alternative to solvent based deoiling due to the following reasons:

- Low viscosity and high diffusivity of supercritical solvents suggest a small mass transfer resistance in the supercritical phase.
- Easily adjustable solvent power.
- Low surface tension, leading to excellent wetting characteristics.
- Low solvent residue in product, since the fluid is normally a gas at ambient conditions.
- Low operating temperatures to prevent product decomposition.

Every pure component exhibits the qualitative phase behaviour as shown in Figure 1-3. The critical point is the point where the vapour-liquid line terminates. Above the critical point no separate liquid or gas phases can be observed. This region is called the supercritical fluid region.

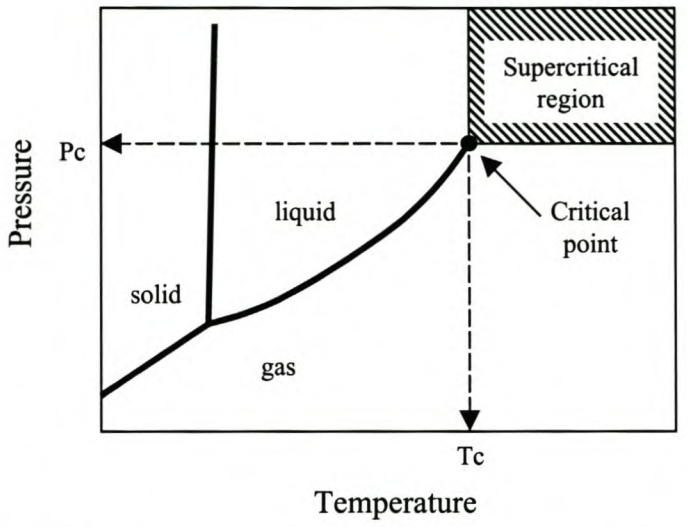

Figure 1-3. Pressure-temperature diagram for a pure component.

Fluids in the supercritical region exhibit characteristics intermediate to those of gases and liquids. The viscosity of supercritical CO_2 is shown in Figure 1-4. The viscosity of the supercritical fluid at pressures as high as 400 bar (0.09 mPa.s) is much lower than liquid solvents such as hexane (0.28 mPa.s) or MEK (0.38 mPa.s) at 30°C.

The self-diffusivity of CO_2 is shown in Figure 1-5, with the range of diffusivities of solutes in organic liquids (McHugh and Krukonis, 1993). The self-diffusivity of CO_2 is about one to two orders of magnitude higher than the diffusivity of solutes in liquids. The low viscosity and high diffusivity of supercritical fluids, compared with conventional solvents, lead to comparatively high mass transfer rates in the supercritical fluid phase. A pure supercritical fluid has no surface tension, since there is no separate liquid and vapour phases. When subcritical components dissolve in the supercritical fluid, the supercritical phase gets a small surface tension (if the system is in the two-phase region), which is much less than that of liquid solvents.

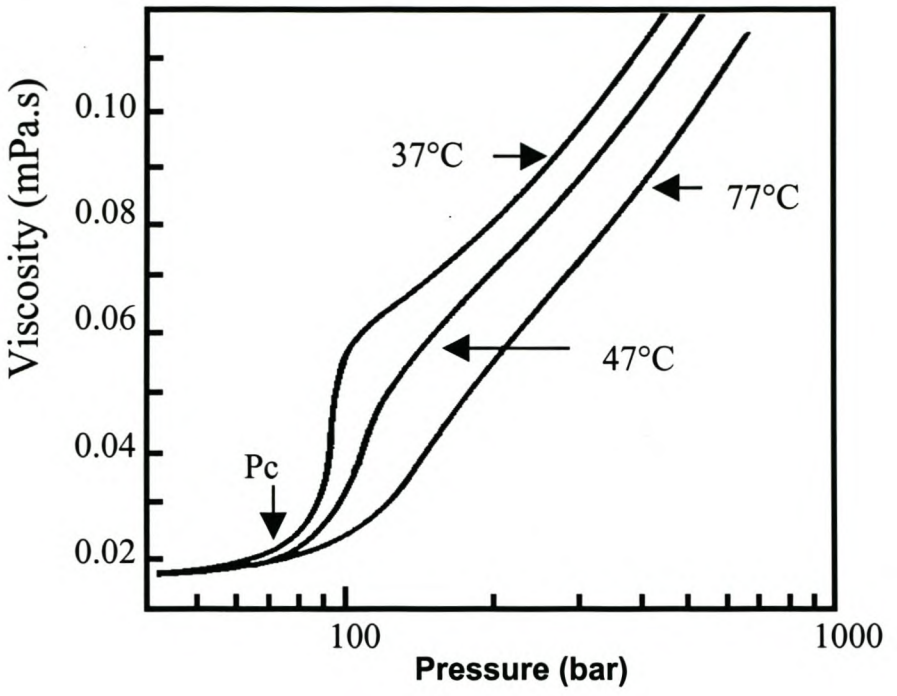

Figure 1-4. Effect of temperature and pressure on supercritical CO_2 (McHugh and Krukonis, 1993).

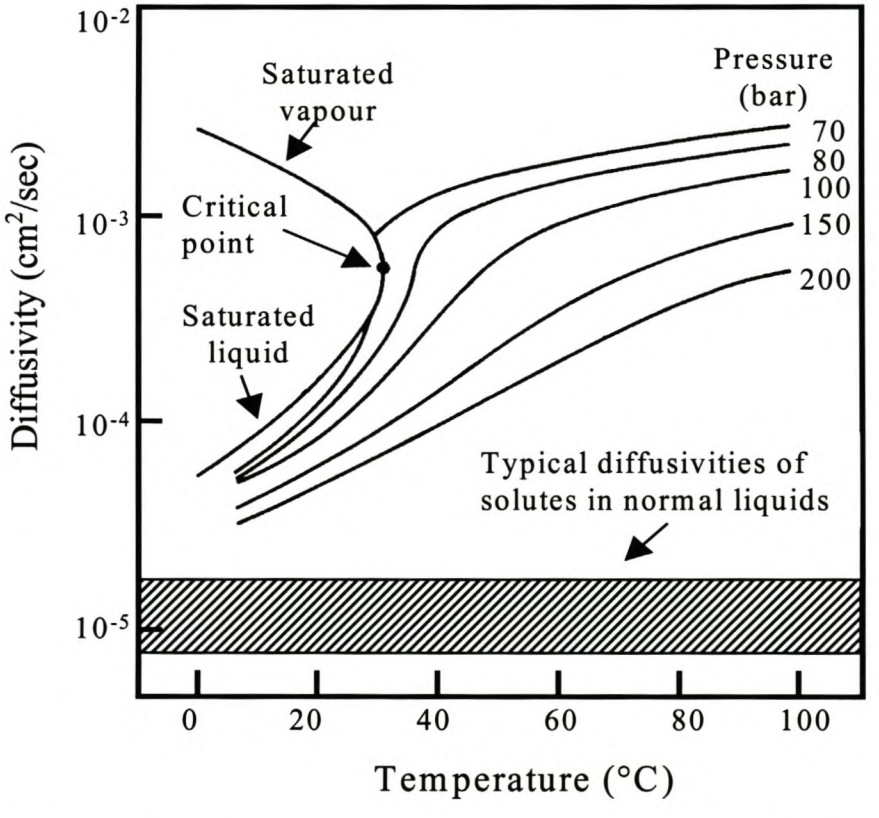

Figure 1-5. Diffusivity behaviour of carbon dioxide (McHugh and Krukonis, 1993).

The typical behaviour of pure component density in the vicinity of its critical point is shown in Figure 1-6. It can be seen that the density of a component close to its critical point is strongly dependent on both temperature and pressure. By operating in the critical region, the temperature and pressure can be used to regulate density, which regulates the solvent power of a supercritical fluid (McHugh and Krukonis, 1993). This is clearly illustrated in Figure 1-7, where a dramatic increase in solubility is observed when the critical pressure of ethylene (50.5 bar) is exceeded.

The interested reader is referred to (McHugh and Krukonis, 1993) and (Brunner, 1994) for a more in-depth discussion of supercritical fluids and supercritical extraction principles.

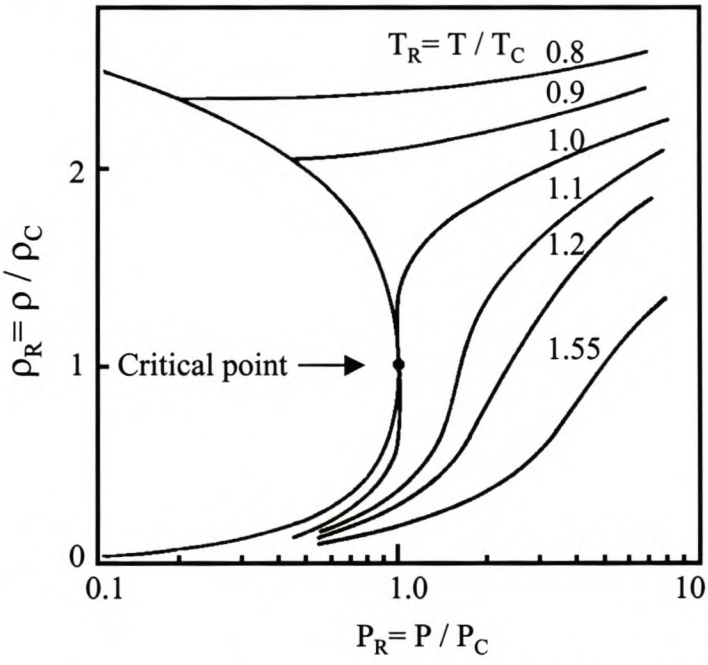

Figure 1-6. Variation of reduced density with temperature and pressure (McHugh and Krukonis, 1993).

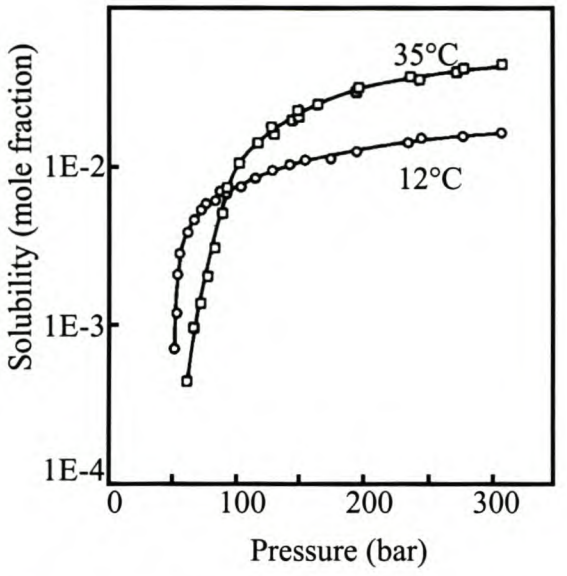

Figure 1-7. Solubility of solid naphthalene in supercritical ethylene (McHugh and Krukonis, 1993).

1.3. Supercritical fluids background

In 1822 Baron Cagniard de la Tour studied the changes in sound made when a liquid was heated inside a sealed cannon barrel. He observed discontinuities in the sound at a certain point, leading him to describe what is known today as the critical point (Cagniard de la Tour, 1822). In 1869 Dr. Thomas Andrews (Andrews, 1875-76) described his experimental apparatus for the measurement of critical points, and observations of the critical properties of carbon dioxide to the Royal Society. Hannay and Hogarth (Hannay and Hogarth, 1879) used a modification of Andrews's apparatus to measure the solubilities of inorganic salts in ethanol at a temperature above the critical temperature of ethanol. They observed an increase in solubility with an increase in pressure, and a decrease in solubility with a decrease in pressure. In 1896 Villard (Villard, 1896) published a review of supercritical solubility phenomena. He described the ability of methane, ethylene, carbon dioxide and nitrous oxide to dissolve a number of liquid and solid hydrocarbons such as carbon disulphide, camphor, stearic acid and paraffin wax. In 1954 Francis (Francis, 1954) published an extensive quantitative study on the solvent properties of near-critical liquid carbon dioxide. He collected solubility data for 261 components, and ternary phase diagrams for 464 systems.

The first commercial supercritical extraction application (deasphalting of residuum oil) appeared more than a century after de la Tour's studies.

1.3.1. SCFE applications

Petroleum Industry

In 1936 Wilson, Keith and Haylett (Wilson et al., 1936) described a process using propane to deasphalt residuum lube oil (see Figure 1-8). In this propane deasphalting process the residuum oil is mixed with compressed liquid propane (McHugh and Krukonis, 1993). All the feed components except the asphalt dissolve in the propane, and the asphalt fraction is separated from the propane-oil mixture in a settler. The propane-oil mixture is then cooled to precipitate waxes from the propane mixture. Heating of the remaining propane-oil mixture decreases the solvent power of the propane, and resins, heavy ends and naphthenics are sequentially precipitated, leaving only the light paraffins in solution.

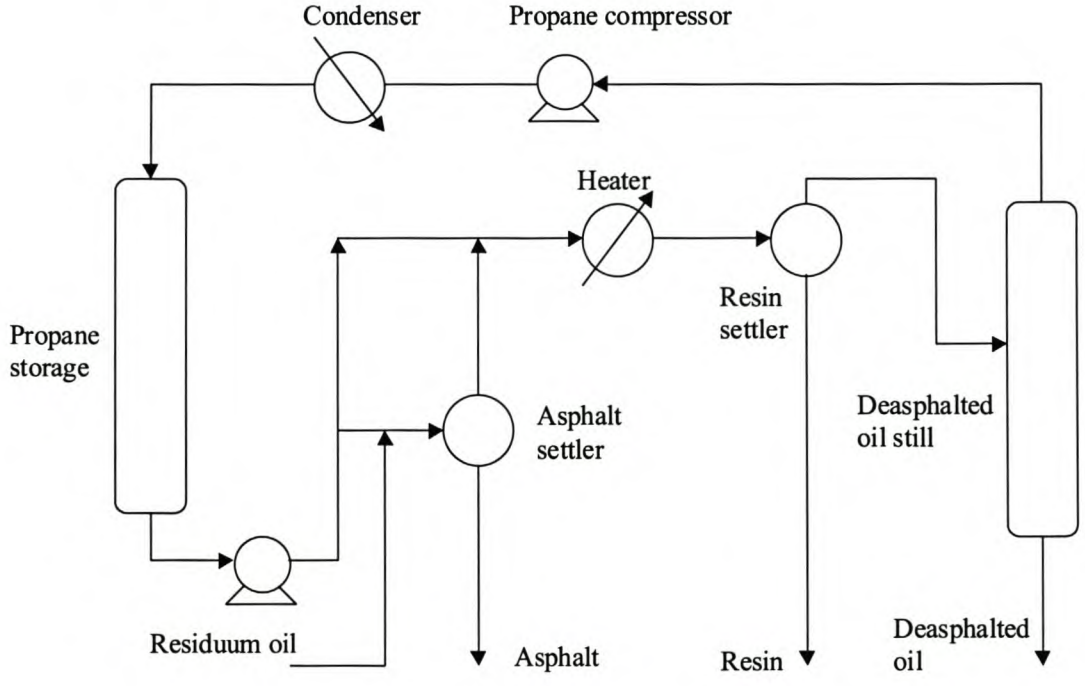

Figure 1-8. Propane deasphalting process showing asphalt and resin removal units (adapted from (Wilson, Keith et al., 1936)).

Other commercial deasphalting processes are the Residuum Oil Supercritical Extraction (ROSE®) process (Nelson and Roodman, 1985; Sequeira, 1994) from Kerr McGee, the Demex (Sequeira, 1994) process from UOP and the Solvahl-Asvahl process (Nieuwoudt, 1994; IFP, 2000) from IFP North America. These processes are based on the same principles as the propane deasphalting process, but use different light hydrocarbons as solvent, and are aimed at different grades of feedstock.

Products for human consumption

The Solexol process is similar to the propane deasphalting process, and is used to extract polyunsaturated triglycerides from vegetable oils and vitamin A from fish oils. The process was developed by the M.W. Kellogg company in 1946 (Passino, 1949; Dickson and Meyers, 1952). As with the early petroleum processes, the Solexol process is not a strictly supercritical extraction process since the extraction temperature is below the critical temperature of the solvent. At least six Solexol plants with capacities of up to 34000 ton/a were in operation by the 1950's (Dickson and Meyers, 1952).

Camilli Albert & Laloue started a commercial flavours extraction plant in Grasse, France in 1989. Natural oils are extracted from vanilla, ginger, paprica and rosemary. Flavex, Rehlingen, Germany is operating a 300 ton/a plant for the extraction of plant oils from basil leaves, ginger, parsley roots, vanilla and camomile flowers (Parkinson and Johnson, 1989).

Other areas where supercritical extraction is used on a commercial scale is coffee and tea decaffeination, nicotine extraction, hops extraction and the extraction of oils from plants. Most of these developments were as a result of tougher regulations that specified lower levels of solvents in food, e.g. the Food and Drug Administration of USA (FDA) ruled that methylene chloride could no longer be used to produce decaffeinated tea imported to the USA (Korner, 1984).

The decaffeination of coffee has been the subject of a large amount of research in Europe (especially Germany) and the USA (McHugh and Krukonis, 1993). McHugh shows a list of 19 patents on the decaffeination of coffee for the period up to the end of 1984. Since then even more patents have been registered. The Zosel process (pioneered by Kurt Zosel) was commercialised in 1978 (Worthy, 1981). The decaffeination process uses supercritical carbon dioxide to extract caffeine from wet coffee beans. The caffeine dissolved in the carbon dioxide is either adsorbed on activated carbon, or absorbed in water. A supercritical coffee decaffeination plant with a 30 000 ton/a capacity was built in Bremen, Germany (Nieuwoudt, 1994). In 1988 Kraft General Foods started up a similar decaffeination plant in Houston, USA, with an estimated capacity of 23 000 ton/a (McHugh and Krukonis, 1993). In 1988 SKW Trostberg started a tea decaffeination plant for the Lipton company, with a capacity of 6 800 ton/a (McHugh and Krukonis, 1993). SKW Trostberg also uses this plant to extract citrus oils from citrus peels.

Polymer processing

The high-pressure polyethylene process was developed in the late 1930s by Imperial Chemical Industries (ICI) (McHugh and Krukonis, 1993). In this process polymerisation of ethylene takes place at high temperatures (150-250 °C) and high pressure (2 700 bar). The ethylene is both the reactant and supercritical solvent, since the polyethylene product dissolves in the supercritical ethylene. Downstream of the reactor the pressure of the ethylene-polyethylene mixture is reduced to precipitate the dissolved polyethylene. The polymer free ethylene is then recycled to the reactor (see Figure 1-9). High pressure low density polyethylene plants with capacities ranging between 136 000 to 227 000 ton/a have been in operation since the 1950s (McHugh and Krukonis, 1993). Fractionation of the polymer product can be achieved by stepwise reduction of the pressure of the ethylene-polyethylene solution, as described by patents held by du Pont ((Krase, 1945; Krase and Lawrence, 1946), ICI (Hunter and Richards, 1945) and Phillips Petroleum (Cottle, 1963). The production of polyethylene is probably the largest commercial application of supercritical fluid processing.

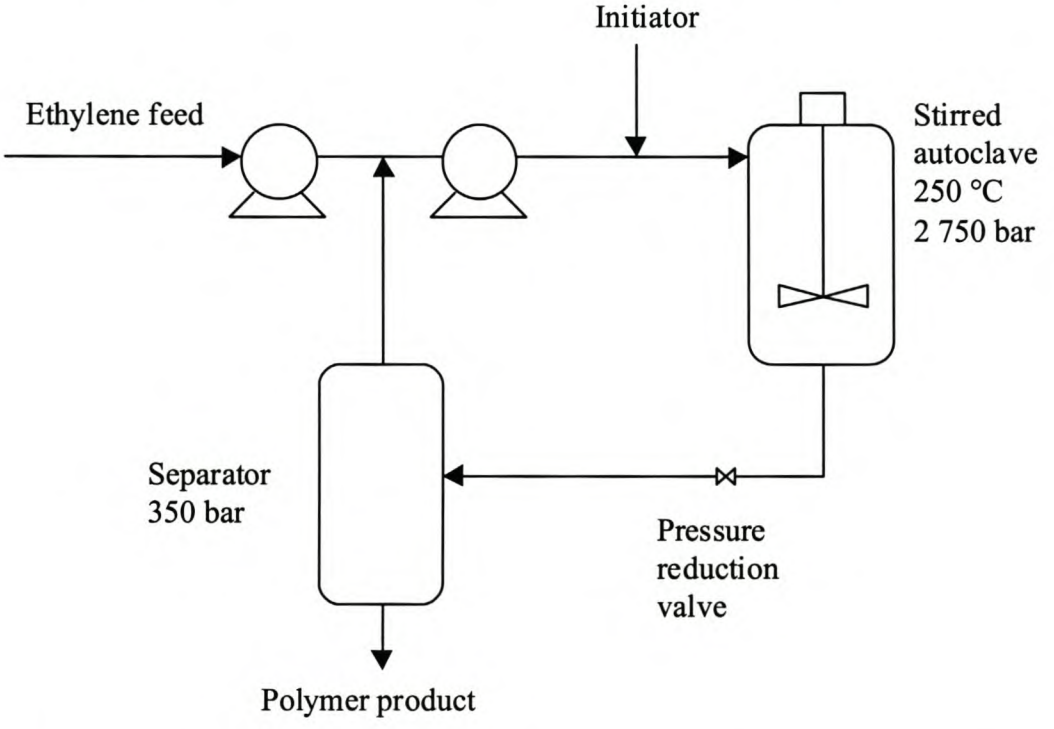

Figure 1-9. Simplified diagram of the high-pressure polyethylene process

1.3.2. Potential applications

There is currently great interest in supercritical fluid technology, with a journal (Journal of Supercritical Fluids) devoted to the subject. There are also numerous publications at international symposia (over 300 papers and posters were presented at the 5th International Symposium on Supercritical Fluids, Atlanta, 2000). Some of the more promising fields are highlighted below.

Activated carbon regeneration

Activated carbon can be used to adsorb organics from wastewater. When the activated carbon is loaded, it is usually regenerated by heating. The high regeneration temperature results in high energy usage and thermal degradation of the carbon. In 1978 a process using supercritical carbon dioxide to regenerate spent activated carbon was described (Modell et al., 1978). This is still an area of active research, see e.g. Tomasko et al. (Tomasko et al., 1993), Madras et al. (Madras et al., 1993) and Chihara et al. (Chihara et al., 1997).

Supercritical water as reaction medium

Supercritical water exhibits less molecular ordering, with a reduced effective hydrogen bonding potential. This leads water to behave like a non-polar solvent showing complete miscibility with organics such as benzene and gases like oxygen and carbon dioxide. The supercritical medium also shows enhanced mass transport properties. These unique properties make supercritical water an interesting medium for reactions. The main focus of research has been on the destruction of organic material, pollutants and toxic chemicals. A supercritical water oxidation pilot plant for the destruction of military dyes, smokes and pyrotechnics, with a capacity of 840 kg/day, has been reported by the Foster Wheeler Company (Crooker et al., 2000). The US Army also uses a supercritical water reactor for the destruction of military smoke and dyes, with a capacity of 3500 kg/day (Rice et al., 2000). It has also investigated the oxidation of wastewater from polyethylene terephthalate processes (Cocero et al., 2000) and the synthesis and growth of inorganic materials (Kolis, 2000).

Coal benefication

Coal can be extracted with supercritical fluids to yield an extract that can be hydrogenated to produce distillate oil, and a residue that can be gasified. Water is a good choice as extraction medium, since it prevents repolymerisation of the products (Fong, 1989).

Pitch fractionation

Depending on the molecular weight, mesophase composition and softening point, petroleum pitch fractions can be used in a wide range of applications. For example a heavy pitch fraction that forms a 100% mesophase can be used as a precursor for high performance carbon fibres. Hutchenson et al. (Hutchenson et al., 1991) and Zhuang et al. (Zhuang and Thies, 2000) have published studies on the fractionation of petroleum pitch using supercritical toluene.

Polymer fractionation and purification

The products from polymer reactions usually contain a highly polydisperse polymer product, with some residual solvents and oligomers. Supercritical fluid extraction offer advantages for the fractionation of the polymer product, and the removal of residual solvent, monomers and oligomers (Kiran, 1994; Kleintjens, 1994). These low vapour pressure materials are usually processed with short path distillation, but heat lability of the substances limits the separation capability of short path distillation (Krukonis, 1985). McHugh and Krukonis (McHugh and Krukonis, 1993) presents a detailed discussion on the published research relating to the fractionation and purification of polymers such as ethylene based polymers, polysiloxilanes, polycarbosilanes and silicone polymers. Conceptually polymer fractionation is done by partially or fully dissolving the polymer in a supercritical solvent. Decreasing the pressure and/or increasing the temperature reduces the solvent power. This is done in a step-wise manner to obtain polymer fractions with decreasing chain lengths.

Microparticles

Sometimes the particle size and particle size distribution of a product must be reduced to increase the effectiveness of the product, e.g. chemicals, pharmaceuticals, dyes and polymers. Sometimes simple grinding is not suitable as commonition process, e.g. for size reduction of explosives and certain polymers. During their investigation of solubility in supercritical fluids, Hanney and Hogarth (Hannay and Hogarth, 1879) observed a fine snow-like crystalline precipitation upon a sudden reduction of pressure of a solution of a solid in a supercritical fluid. Rapid expansion of a supercritical solvent (RESS) is a technique used to reduce the solvent power of a supercritical fluid (Krukonis, 1984; McHugh and Krukonis, 1993; Debenedetti, 1994). The sudden reduction in solvent power leads to high supersaturation levels, producing small particles. Quite uniform conditions can be obtained with RESS, leading to monodisperse particle formation.

Another process utilising supercritical fluids to produce small particles is the gas antisolvent (GAS) process. In the GAS process a solid is dissolved in a liquid solvent. A supercritical gas is then dissolved in the liquid, which reduces the solubility of the dissolved solid in the solvent, resulting in the precipitation of the solid. The process can generally be used if two conditions are met: the solid must have a low solubility in the gas, and the gas must be very soluble in the liquid solvent. The GAS process has been used to produce small particles of the explosives RDX and nitroguanidine (McHugh and Krukonis, 1993). A detailed review of publications relating to particle design using supercritical fluids has been published by Jung and Perrut (Jung and Perrut, 2001).

Fractionation of paraffins

de Haan (de Haan, 1991) investigated the use of carbon dioxide to recover pure paraffins from liquid paraffin-aromatics mixtures. Nieuwoudt (Nieuwoudt, 1994) investigated the use of LPG to fractionate heavy paraffin wax. He compared the separation efficiency of short path distillation with supercritical extraction, and concluded that sharper cuts could be made with supercritical extraction than with short path distillation. The use of carbon dioxide as supercritical solvent for the batch fractionation of waxes has been patented by Katayama (Katayama, 1992).

Extraction of organics from water

Light hydrocarbons such as propane, n-butane or i-butane can be used to extract alcohol from alcohol-water mixtures. Brignole et al. (Brignole et al., 1987) claimed that the energy requirements of this process were one third that of the conventional benzene drying system.

Impregnation

The low viscosity and low surface tension of a supercritical fluid makes it an ideal candidate for the transport of chemicals into porous media. It is also known that a supercritical fluid can cause swelling of a porous polymer. This aids the transport of chemicals, fragrances and pharmaceuticals into the polymer (McHugh and Krukonis, 1993). When the pressure is reduced, the dopants are trapped inside the matrix, and get released at a greatly reduced rate.

Fractionation of plant and animal oils

In addition to the use of SCFE to extract essential oils from solid matrices, it is also investigated for fractionation of these oils to recover valuable products such as flavour compounds (Budich et al., 1999), antioxidants (Esquivel et al., 1999) and fatty acids from fish oil (Riha and Brunner, 1999; Riha and Brunner,

2000). A detailed overview of the fractionation and extraction of essensial oils is given by (Reverchon, 1997)

There are several other potential applications for supercritical fluid technology. McHugh and Krukonis (McHugh and Krukonis, 1993) discusses several other applications such as:

- Supercritical fluid chromatography
- Polymer fibre spinning
- Isomer separation
- Enzymatic reactions
- Heterogeneous catalysis
- Formation of porous polymers

1.4. Choice of solvent

The choice of a solvent for the supercritical fluid extraction process is very important, since it will have an impact on the solubility and selectivity. This will influence operating parameters such as solvent to feed ratio, temperature and pressure. A high solubility of the wax in the solvent will lead to low solvent to feed ratio's, leading to lower operating costs. In Figure 1-7 it can be seen that the capacity of a solvent greatly increases when the pressure is increased above the critical pressure of the solvent. The temperature for the extraction of solids using supercritical fluids should be close to the critical temperature of the solvent. For liquid – supercritical fluid extraction the density difference between the liquid and supercritical phase should be large enough to allow easy phase separation, which means that the extraction temperature should be slightly above the critical temperature of the solvent.

It is also important that the extraction temperature is higher than the congealing temperature of the wax, in order to ensure that the wax is a liquid. This will simplify the handling and transport of the wax, and it will also have a positive impact on mass transfer in the wax phase. The congealing point of the waxes used in this study varies between 30 and 65 °C.

Ethane (critical temperature = 32.2 °C) and carbon dioxide (critical temperature = 31.1 °C) is chosen as the supercritical solvents for this work. Carbon dioxide is a commonly used solvent in supercritical extraction, due to its low toxicity, low cost and non-flammability. Although ethane is flammable, it has a lower critical pressure.

1.5. Aims of this work

This work will investigate the technical feasibility of using supercritical extraction to de-oil and fractionate paraffin wax. After proving the feasibility of deoiling n-paraffin wax with SCFE, it will be compared with current state-of-the-art deoiling and fractionation processes to judge the economic feasibility of SCFE for deoiling wax mixtures. The following state-of-the-art processes were selected based on energy efficiency and availability of production plant information: static crystallisation and short path distillation.

The work presented in this dissertation is structured as follows: In chapter 2 two simple models are presented to model SPD. These models are compared with experimental SPD results obtained for this work. Chapter 3 covers the equilibrium modelling of static crystallisation of n-paraffin wax. Chapters 4 and 5 discuss the modelling of SCFE. Chapter 4 covers the phase equilibrium correlation and prediction of supercritical solvent - n-paraffin equilibria using equations of state. Chapter 5 discusses the equilibrium stage modelling of SCFE, and compares experimental SCFE data, obtained in this work, with simulations. This is followed by a short qualitative study on the deoiling of mixed n-paraffin/iso-paraffin waxes using static crystallisation, SPD and SCFE in chapter 6. Chapter 7 is an economic case study on the deoiling of an n-paraffin mixture, comparing the economics of static crystallisation, SPD and SCFE.

CHAPTER 2. MODELLING OF SHORT PATH DISTILLATION

Short path distillation (SPD) is one of the technologies used currently to fractionate paraffin wax (Fischer and Bethge, 1992; Nieuwoudt, 1994). In this chapter the performance of SPD is modelled and compared with experimental data. This will be used later in a comparative study where SCFE is compared with current wax deoiling technologies.

The main part of a short path distillation (SPD) unit is a vertical double-jacketed cylinder with an internal condenser and a rotating wall wiper system. Liquid is fed onto the heated wall and spread uniformly with the wall wipers. The wall wipers mix the liquid film to promote heat transfer between the wall and liquid and reduce liquid side temperature and composition gradients. The unit operates at very low total pressure, which results in relatively low liquid temperatures compared with vacuum distillation. The design of a SPD unit eliminates flooding problems associated with the high vapour velocities in vacuum distillation columns.

SPD has the following characteristics:

- Relatively low liquid temperatures compared to vacuum distillation.
- Short residence time and little holdup, since the only holdup in the unit is a thin liquid film.
- Small thermal gradients and little liquid mass transfer resistance in the liquid film because of mixing with wall wipers.
- Lower temperature and residence time makes this an attractive process for the separation or recovery of heat labile components.

Current applications of SPD are (Fischer and Bethge, 1992; Fischer, 2000; Pope, 2000):

- Recovery and concentration of edible oils and vitamins such as vitamin E, carotene and polyunsaturated fatty acids from plant and animal oils.
- Polymer devolatilization and monomer stripping from di-isocyanites.
- Wax fractionation.
- Solvent recovery.
- Pharmaceutical and biomaterial concentration.

2.1. Theory

When the pressure is very low (10^{-1} -10 Pa), molecular distillation conditions can be assumed, where the mean free path of the gas molecules is large enough that the evaporated molecules reach the condenser unhindered by other molecules. This assumption implies that there is no vertical mixing in the vapour phase. Langmuir and Knudsen (Burrows, 1960; Cvengroš and Lutišan, 1995; Nguyen and Le Goffic, 1997) used the kinetic theory of gases to derive an equation describing the rate of evaporation of a pure component from a cylindrical liquid surface (see Figure 2-1):

Eq. 2.1 $$dV = \frac{P^{sat}}{\sqrt{2\pi R M_r T}} 2\pi r dz$$

where P^{sat} is the saturation pressure of the liquid at temperature T and V is the molar rate of evaporation. The following assumptions are made to derive equation 2.1:

- The liquid film is quiescent.
- There are no residual molecules in the gap between the evaporator surface and the condenser surface.
- All the molecules leaving the evaporator surface reach the condenser without colliding with other molecules.
- The condenser temperature is low enough to ensure a negligible vapour pressure at the condenser surface.

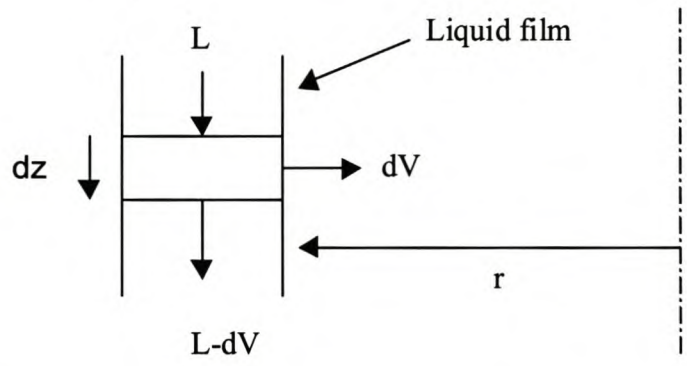

Figure 2-1. Evaporation from a liquid film.

The evaporation rate of a component from a liquid mixture, assuming an ideal liquid mixture where Raoult's law is valid, is then given by

Eq. 2.2 $$dv_i = \frac{x_i P_i^{sat}}{\sqrt{2\pi R M_{r,i} T}} 2\pi r dz$$

It is assumed that there is no liquid side resistance to mass transfer, which should be reasonable since the liquid film gets stirred with wall wipers to promote liquid mixing and heat transfer.

The composition of the condensing vapour is given by

Eq. 2.3 $$Y_i = \frac{dv_i}{\sum_j dv_j}$$

Eq. 2.2 and Eq. 2.3 can be rewritten in a form relating the liquid composition to the condensed vapour composition, which can be used in standard flash calculations. The composition of the vapour at the liquid interface can be calculated assuming Raoult's law:

Eq. 2.4 $$y_i P = x_i P_i^{sat}$$

Combining Eq. 2.4 and Eq. 2.2, Eq. 2.3 can be written as

Eq. 2.5 $$Y_i = \frac{y_i / \sqrt{M_{r,i}}}{\sum_j \left(y_j / \sqrt{M_{r,j}} \right)}$$

The equilibrium ratio (K-value) of a component where the vapour and liquid is in equilibrium is defined as:

Eq. 2.6 $$K_i = \frac{y_i}{x_i}$$

This corresponds to the case where the total pressure is such that a significant number of molecules evaporated from the liquid return to the liquid surface due to intermolecular collisions, resulting in equilibrium between the vapour condensing at the condenser and the liquid surface.

An analogous K-value describing the distilled vapour to liquid composition ratio for molecular evaporation is defined as:

Eq. 2.7 $$K_i^{'} = \frac{Y_i}{x_i} = \frac{K_i}{\sqrt{M_{r,i}} \cdot \sum_j \left(y_j / \sqrt{M_{r,j}} \right)}$$

Eq. 2.2 can be solved using discrete elements, Δz, see e.g. (Kawala, 1992; Cvengroš and Lutišan, 1995; Nguyen and Le Goffic, 1997) and (Batistella and Maciel, 1996). These discrete elements can be viewed as a series of flash calculations, with the amount of liquid evaporated depending of the size of the finite element Δz (see Figure 2-2).

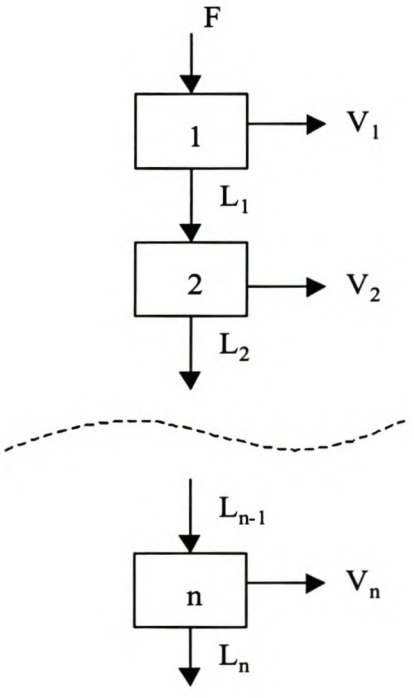

Figure 2-2. Model for evaporation from a falling film.

The vapour to liquid flow rate leaving an equilibrium stage, *n*, is defined as

Eq. 2.8 $$\beta_n = \frac{V_n}{L_n + V_n}$$

A mass balance over a stage gives

Eq. 2.9 $$L_n x_{n,i} = L_{n-1} x_{n-1,i} - V_n Y_{n,i}$$

Combining Eq. 2.8, Eq. 2.9 and Eq. 2.7 gives:

Eq. 2.10 $$x_{n,i} = \frac{x_{n-1,i}}{1 + \beta_n (K'_{n,i} - 1)}$$

Analogous to a flash, the ratio of the residue to feed flow rate for SPD is defined as

Eq. 2.11 $$\beta_{SPD} = 1 - \frac{F}{L_n}$$

The composition of SPD residue can be approximated by solving the *n* equilibrium stages over the height of the SPD unit. A further simplification is to select the vapour to feed fraction of each equilibrium stage equal ($\beta_1 = \beta_2 = \ldots = \beta_n = \beta$). The relation between β_{spd}, β, and the number of equilibrium stages, *n*, can be determined as follows:

First stage:

Eq. 2.12 $$L_1 = (1 - \beta) F$$

Second stage:

Eq. 2.13 $$L_2 = (1 - \beta) L_1 = (1 - \beta)^2 F$$

For *n* stages:

Eq. 2.14 $$L_n = (1 - \beta) L_{n-1} = (1 - \beta)^n F$$

Comparison of Eq. 2.11 and Eq. 2.14 gives the relation between β_{spd}, β, and the number of equilibrium stages, *n*:

Eq. 2.15 $$1-\beta_{SPD} = (1-\beta)^n$$

To simulate an SPD run for a specified β_{SPD}, the number of flash calculations (n) is chosen, and the β value for the flash calculations is calculated from Eq. 2.15. Eq. 2.10 is then solved using the Rachford-Rice algorithm (Rachford and Rice, 1952). The simulation are done assuming a constant liquid temperature, since numerical studies indicate that the liquid film temperature quickly reaches a steady state (Batistella and Maciel, 1996; Cvengroš et al., 2000). The liquid temperature is then adjusted to give the desired residue to feed ratio.

This method of solving the composition profile for the residue is analogous to the numerical integration of equation 2.2 over the height of the SPD heated surface, by using finite Δz increments. The difference between the two methods is that for a fixed β value for all the stages, Δz is adjusted in order to get a fixed vapour to feed ratio for an interval. This has the advantage that the analogous "step length" is reduced when the vapour flux is high, and a larger "step length" is used when the vapour flux is low.

The above simulation method can only calculate the residue composition for a specified residue to feed ratio, given a constant temperature or pressure, by approximating the integration of equation 2.2 over the height of the heated surface with a series of flash calculations as described above. A more rigorous treatment of molecular distillation is given by Burrows (Burrows, 1960), while Kawala (Kawala, 1992), Nguyen and Le Goffic (Nguyen and Le Goffic, 1997) and Batistella and Maciel (Batistella and Maciel, 1996) published some numerical simulation results for various SPD scenarios. The SPD simulations done in this work is intended to predict the separation efficiency of SPD, in contrast to the other numerical studies that yielded capacity, rating or profile results.

It was also decided to simulate a separation by doing a single stage flash at the experimentally observed pressure, by changing the temperature until the calculated and measured distillate to feed ratio was matched. This calculated temperature was usually 20 – 30 °C less than the heating jacket temperature. This calculated temperature was then used in the molecular distillation simulation. This method for estimating the surface temperature is necessary since the liquid film temperature cannot be measured during an experiment.

The vapour pressure correlations used are given in Appendix A.

2.2. Experimental set-up

See Figure 2-3 for a schematic of the SPD column set-up. The inner diameter of the jacketed evaporating surface is 150 mm with a wetted height of 290 mm. The condenser has an outer diameter of 51 mm and a height of 250 mm. The rotating wall wiper has three arms, each with a length of 250 mm, with PTFE rollers. An electrical motor, via a variable speed gearbox and a magnetic coupling drives the wall wiper. The unit is evacuated with a rotating vane vacuum pump, capable of obtaining absolute pressures down to 10 Pa. The pressure inside the unit can be controlled by bleeding air through a needle valve.

The pressure inside the unit is monitored with a Pirahni type pressure transducer, connected to the SPD unit with a length of ¼" tubing, to protect the sensor of the pressure gauge from condensable vapour inside the SPD unit. The jacket is heated with heating oil from an external oil bath, which also regulates the temperature of the circulating oil. The condenser is cooled with running tap water.

Molten wax is fed to the unit via a feed vessel of 600 mL capacity. The flow rate of the wax to the SPD unit is controlled with a manually operated needle valve. The flow rate is controlled by adjusting the needle valve in order to maintain a particular absolute pressure inside the unit. The dissolved air in the wax feed influences the pressure inside the unit, which gives an indication of the relative flow rate of the wax into the unit. The average feed flow rate of the wax is obtained by collecting and weighing the residue and distillate, while noting the time interval.

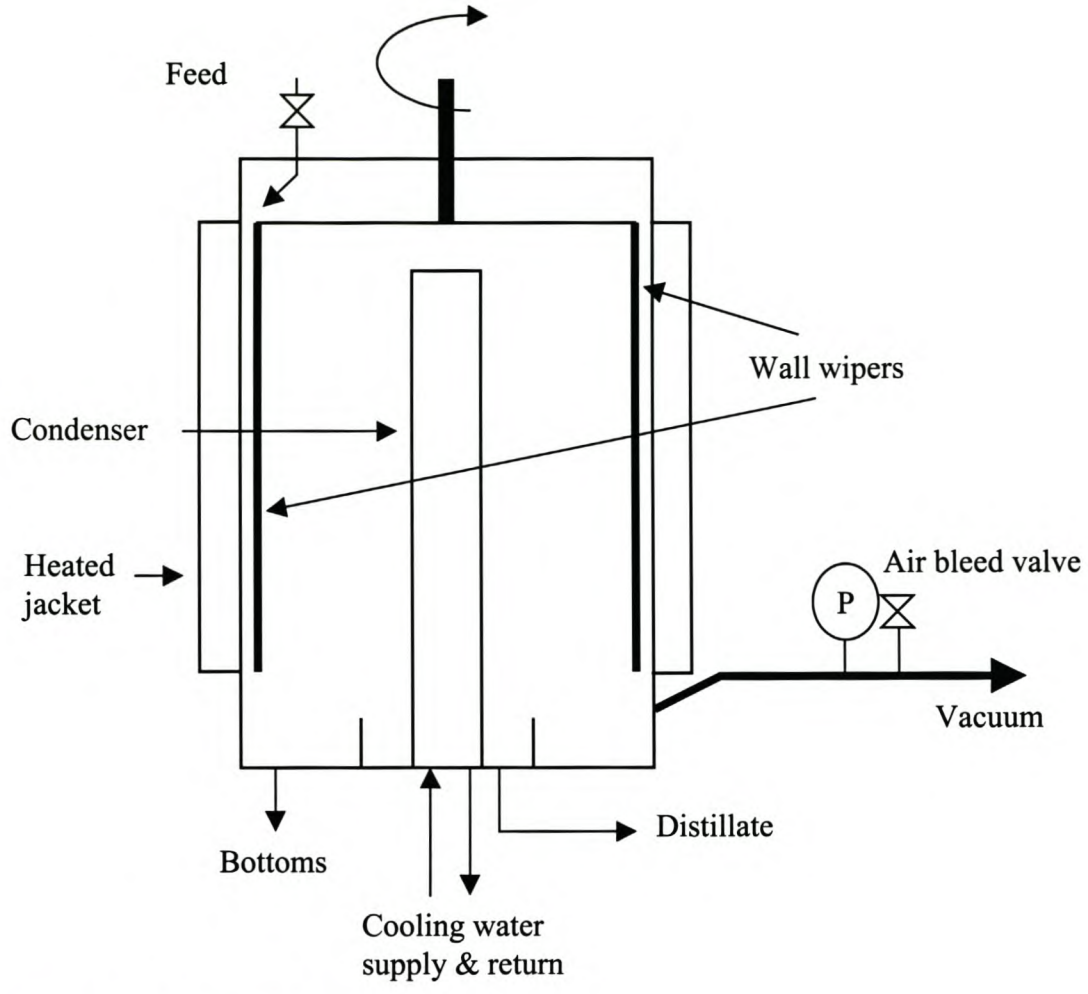

Figure 2-3. Diagram of SPD unit.

2.3. Analysis of wax

A Fischer-Tropsch wax from Sasol consisting of mostly n-alkanes was used in this work. A gas chromatograph using a megabore column (15m BPX-5) and a flame ionisation detector was used to determine the composition of an n-paraffin wax sample. The wax sample was dissolved in toluene and diluted to about 0.5% by weight. The temperature program was as follows: 4 minutes at 60 °C, ramp to 100 °C at 20 °C/min, ramp to 250 °C at 7 °C/min. Response factors were calculated using a standard solution containing equal amounts of pure n-C_{12}, n-C_{16}, n-C_{18}, n-C_{20}, n-C_{24}, n-C_{28} and n-C_{36}.

2.4. Results

Some typical SPD data for the Fischer-Tropsch wax are shown below in Figure 2-4 to Figure 2-6. Only three graphs are shown to illustrate the common trends observed. The complete set of SPD data is tabulated in

Appendix B. The experiments cover a pressure range of 30 – 120 Pa, and heating oil temperatures of 140 –170 °C.

Note that only the total distillate composition of a run is shown to minimise cluttering of the graphs. The experimentally obtained distillate composition is compared with the total distillate composition calculated with the SPD model described in section 2.1 (labelled SPD in the graphs), and with the vapour composition of a single stage flash (labelled flash in the graphs).

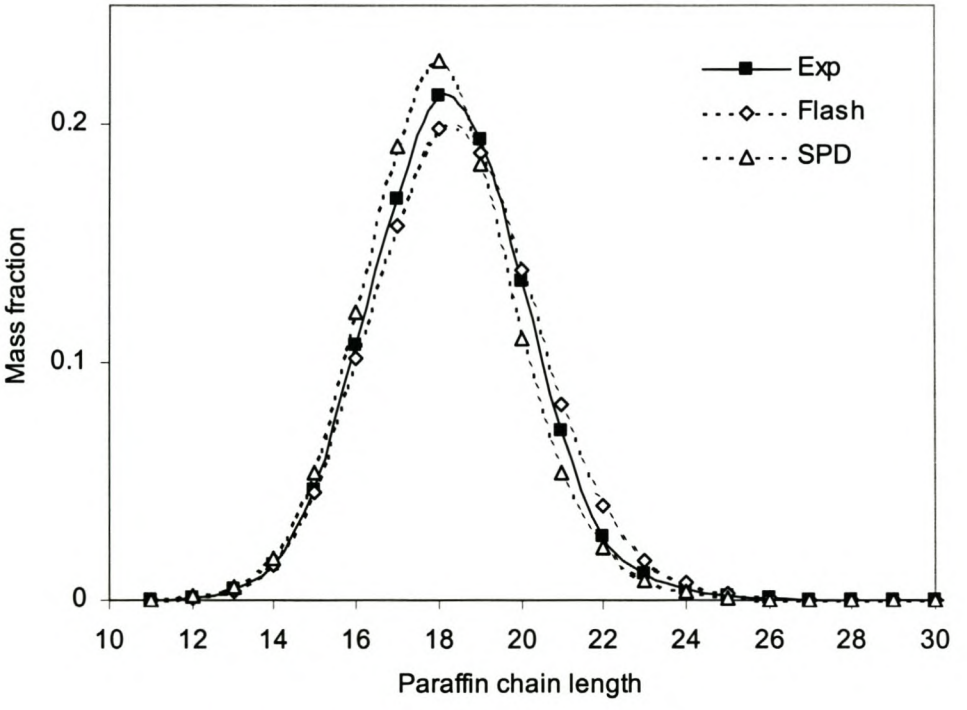

Figure 2-4. SPD distillate composition for run 1.

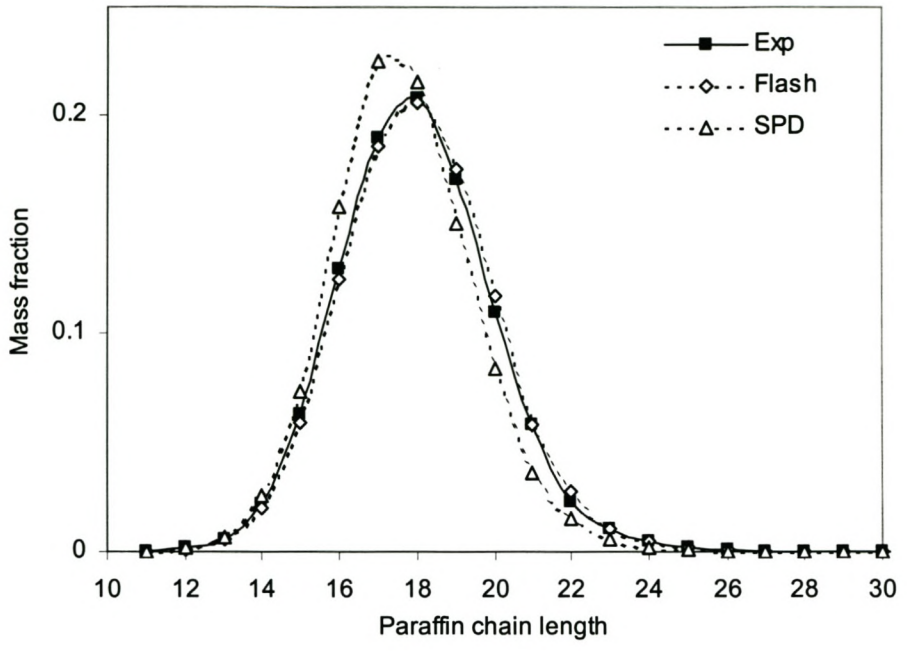

Figure 2-5. SPD distillate composition for run 2.

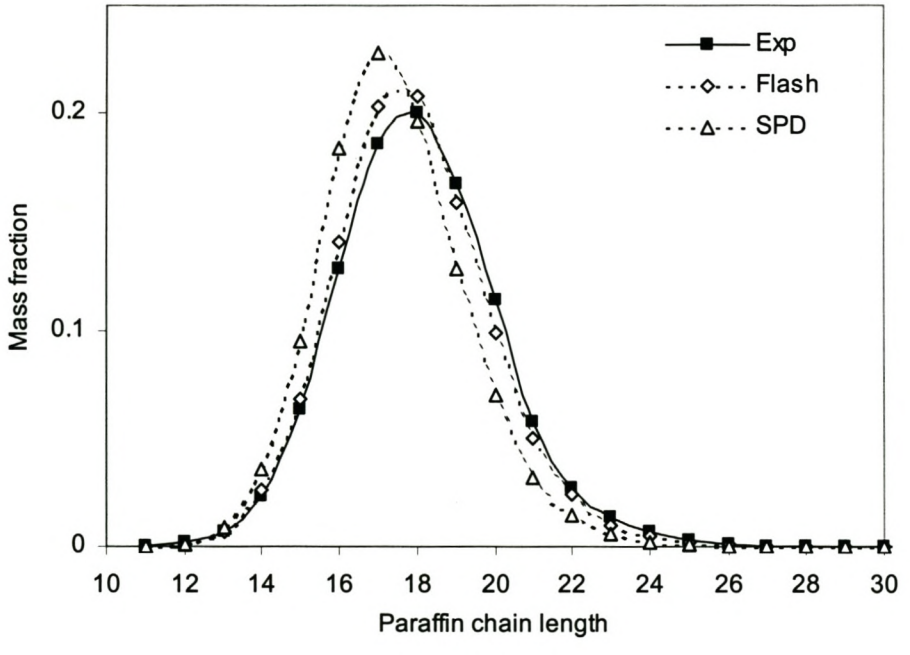

Figure 2-6. SPD distillate composition for run 3.

2.5. Discussion

In all the experiments the separation efficiency of SPD was less than predicted by molecular distillation theory. This is evident from the graphs above, where the experimental distillate composition is biased towards heavier components, compared with the simulated SPD distillate. This result is not surprising, since the experimental conditions do not fulfil all the requirements for molecular distillation. The pressure range of 30 – 120 Pa is higher than the upper limit of 10^{-1} – 10 Pa where molecular distillation effects are expected (Cvengroš, 1995; Nguyen and Le Goffic, 1997; Cvengroš, Lutišan et al., 2000). At these higher pressures the mean free path of the evaporating molecules are such that the probability of molecular collisions in the vapour space is very high, and some of the evaporated molecules return to the liquid surface. The condensate temperature is maintained at about 40 – 60 °C, to prevent congealing of the wax on the condenser surface. At this temperature the distillate vapour pressure is about 1 – 10 Pa, leading to some re-evaporation of the distillate. This reduces the effective composition of the distillate from that predicted by Eq. 2.7 to something approaching the equilibrium value predicted by Eq. 2.6.

Another factor that reduces the separation efficiency is back mixing of the vapour. At higher pressures evaporated molecules can, through multiple collisions, reach a part of the liquid film far from where it originally evaporated. In the worst case scenario, back mixing of the vapour phase can lead to separation efficiencies less than the equilibrium value predicted by Eq. 2.6.

The relatively high pressures during the SPD fractionation are mainly due to two factors: the feed wax was not degassed before entering the SPD unit, and the vacuum pump was operating at maximum capacity. Although this does not give the maximum obtainable separation efficiency, higher capacity can be achieved if the SPD is operated at a higher pressure.

From the results it appears as if a simple flash calculation, assuming an ideal liquid mixture, can be used to adequately represent the separation efficiency of wax fractionation with SPD. This model will be used later in chapter 6 to design a SPD wax deoiling plant. The economics of that SPD deoiling plant will be compared with the economics of wax deoiling using different technologies.

2.6. Nomenclature

Symbol	Description	Unit
F	Feed rate	mol/s
K	Equilibrium vapour to liquid composition ratio	
K'	Liquid to condensed vapour composition ratio	
L	Liquid flow rate	mol/s
M_r	Molar weight	g/mol
P	Pressure	Pa
R	Universal gas constant	J/mol.K
r	Radius of heated surface	m
T	Temperature	K
V	Molar rate of evaporation	mol/s
v	Component molar rate of evaporation	mol/s
x	Liquid mole fraction	
y	Vapour mole fraction at liquid surface	
Y	Vapour mole fraction at condenser surface	
z	Height of heated surface	m

Subscripts

i	Component index
j	Component index
n	Flash index
SPD	Short path distillation

CHAPTER 3. WAX MELTING AND RECRYSTALLISATION

Wax deoiling processes such as wax sweating, wax recrystallisation and solvent extraction (Sequeira, 1994; WolfMeier, Schmidt et al., 1996) are commonly used in industry for the deoiling of petroleum wax. In this chapter wax crystallisation processes are modelled, and the models compared with experimental data. The models tested in this chapter will be used in chapter 6 in a comparative study of SCFE with current wax deoiling technologies.

3.1. Modelling

Wax sweating, wax recrystallisation and solvent extraction are based in principle on crystallisation. Equilibrium between the solid and liquid composition for a component *i* is given by:

Eq. 3.1 $$\hat{f}_i^L = \hat{f}_i^S$$

which can be rewritten as:

Eq. 3.2 $$x_i \gamma_i^L f_i^L = s_i \gamma_i^S f_i^S$$

or

Eq. 3.3 $$\frac{x_i \gamma_i^L}{s_i \gamma_i^S}^S = \frac{f_i^S}{f_i^L}$$

The ratio of the pure component fugacities, $\frac{f_i^S}{f_i^L}$, can be derived from a thermodynamic cycle shown in Figure 3-1. The change in Gibbs energy from state a to state f is related to the fugacities of the liquid and solid of component *i*:

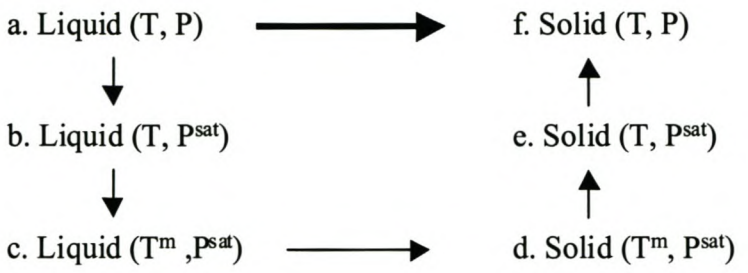

Figure 3-1. Thermodynamic cycle for transition of a pure liquid to a solid.

Eq. 3.4 $$\frac{\Delta G(a \to f)}{RT} = \ln\left(\frac{f_i^L}{f_i^S}\right)$$

The change in Gibbs energy from state a to state f can also be written in terms of changes in enthalpy and entropy:

Eq. 3.5 $$\Delta G(a \to f) = \Delta H(a \to f) - T\Delta S(a \to f)$$

The enthalpy change from state a to f is the sum of the changes in state:

Eq. 3.6 $$\Delta H(a \to f) = \Delta H(a \to b) + \Delta H(b \to c) + \Delta H(c \to d) + \Delta H(d \to e) + \Delta H(e \to f)$$

Using the definition of constant pressure heat capacity

Eq. 3.7 $$\left(\frac{\partial H}{\partial T}\right)_P = C_P$$

and deriving the following expression from the Maxwell relations

Eq. 3.8 $$\left(\frac{\partial H}{\partial P}\right)_T = v - T\left(\frac{\partial v}{\partial T}\right)_P$$

Eq. 3.6 can be rewritten in terms of the enthalpy of melting and the heat capacity:

Eq. 3.9

$$\Delta H(a \to f) = \int_{P}^{P^{sat}} \left[v - T\left(\frac{\partial v}{\partial T}\right)_P \right]^L dP + \int_{T}^{T^m} C_p^L dT - \Delta H^m + \int_{P^{sat}}^{P} \left[v - T\left(\frac{\partial v}{\partial T}\right)_P \right]^S dP + \int_{T^m}^{T} C_p^S dT$$

The change in entropy from state a to f is given by:

Eq. 3.10

$$\Delta S(a \to f) = \Delta S(a \to b) + \Delta S(b \to c) + \Delta S(c \to d) + \Delta S(d \to e) + \Delta S(e \to f)$$

Eq. 3.11

$$\Delta S(a \to f) = \int_{P}^{P^{sat}} \left[-\left(\frac{\partial v}{\partial T}\right)_P \right]^L dP + \int_{T}^{T^m} \frac{C_p^L}{T} dT - \frac{\Delta H^m}{T^m} + \int_{P^{sat}}^{P} \left[-\left(\frac{\partial v}{\partial T}\right)_P \right]^S dP + \int_{T^m}^{T} \frac{C_p^S}{T} dT$$

The effect of pressure (at atmospheric pressure) on the molar volume is negligible. Further, assuming the difference between the liquid and solid heat capacity is constant, Eq. 3.9 and Eq. 3.11 can be integrated and inserted into Eq. 3.5:

Eq. 3.12

$$\Delta G(a \to f) = \Delta v\left(P^{sat} - P\right) + \Delta C_P \left(T^m - T - T \cdot \ln\left(\frac{T^m}{T}\right)\right) - \Delta H^m \left(1 - \frac{T}{T^m}\right)$$

$$with\ \Delta C_P = C_P^L - C_P^S\ and\ \Delta v = v^L - v^S$$

Substituting Eq. 3.12 into Eq. 3.4 gives (Pan and Radosz, 1999):

Eq. 3.13

$$\ln\left(\frac{f_i^L}{f_i^S}\right) = -\frac{\Delta H_i^m}{RT}\left(1 - \frac{T}{T_i^m}\right) + \frac{\Delta Cp_i^m}{R}\left(\frac{T_i^m}{T} - 1 - \ln\left(\frac{T_i^m}{T}\right)\right) + \frac{\Delta v\left(P^{sat} - P\right)}{RT}$$

At atmospheric pressure the pressure correction term contributes very little compared to the other terms, and will be neglected (Coutinho et al., 1995). Define K_i^S as the ratio of the liquid to solid mole fraction of component i:

Eq. 3.14
$$K_i^S = \frac{x_i}{s_i} = \frac{\gamma_i^S}{\gamma_i^L} \exp\left(-\frac{\Delta H_i^m}{RT}\left(1 - \frac{T}{T_i^m}\right) + \frac{\Delta Cp_i^m}{R}\left(\frac{T_i^m}{T} - 1 - \ln\left(\frac{T_i^m}{T}\right)\right)\right)$$

Some n-alkanes go through solid-solid phase transition close to their melting points (Finke et al., 1954; Schaerer et al., 1955). If this transition temperature, T_i^t, is between T and T_i^m, an additional correction similar to the melting transition needs to be made to Eq. 3.14:

Eq. 3.15
$$K_i^S = \frac{x_i}{s_i} = \frac{\gamma_i^S}{\gamma_i^L} \exp\left[-\frac{\Delta H_i^m}{RT}\left(1 - \frac{T}{T_i^m}\right) - \frac{\Delta H_i^t}{RT}\left(1 - \frac{T}{T_i^t}\right) + \frac{\Delta Cp_i^m}{R}\left(\frac{T_i^m}{T} - 1 - \ln\left(\frac{T_i^m}{T}\right)\right)\right]$$

Eq. 3.14 or Eq. 3.15 can be used with the Rachford-Rice flash algorithm (Rachford and Rice, 1952) to calculate the equilibrium composition of a multicomponent solid-liquid mixture. In addition to the pure component properties (T_i^m, ΔH_i^m, ΔCp_i etc.) needed in Eq. 3.14 or Eq. 3.15, the liquid and solid activity coefficients are needed for calculations. Activity coefficient models for the liquid and solid phases are discussed below.

3.1.1. Liquid activity coefficient models

In some cases ideal liquid activity can be assumed, e.g. for alkane solutions of similar size. In wax recrystallization the size difference between the solvent and the paraffin wax is substantial, and large negative deviations from Raoult's law are observed (Polyzou et al., 1999). For mixtures of solvents and polymers the Flory-Huggins theory (Flory, 1953) and modifications are used to predict liquid phase activity coefficients (Reid et al., 1987). The empirical Buchowski equation (Buchowski et al., 1980) has been used to correlate the solubility of solids (Provost et al., 1998; Zhu et al., 1999), but its extension to multicomponent systems is not straightforward.

Kontogeorgis et al. (Kontogeorgis et al., 1996) compared several classical and free volume based liquid activity models with molecular simulation results for athermal polymer systems, and concluded that free-volume based models should be used to model polymer systems.

Polyzou et al. (Polyzou, Vlamos et al., 1999) investigated several liquid activity coefficient models to determine the accuracy of these models for symmetrical and unsymmetrical alkane systems. They concluded that symmetric systems are best described by an ideal solution ($\gamma_i^l = 1$), while free volume type models such as Flory free-volume (Flory-FV) (Kontogeorgis et al., 1994) and chain free-volume (chain-FV) (Kontogeorgis et al., 1997) best describe asymmetric systems. The ideal solution model and Flory-FV and chain-FV models were selected to predict liquid activity coefficients.

(Kontogeorgis, Nikolopoulos et al., 1997) derived an activity coefficient model starting with the generalised van der Waals partition function by assuming the excess Gibbs energy is equal to the excess Helmholtz energy at low pressure:

Eq. 3.16 $$G^E \approx A^E$$

The excess Helmholtz free energy can be calculated from the Helmholtz free energy of mixing:

Eq. 3.17 $$A^E = \Delta A^{mix} - RTx_i \ln x_i$$

The Helmholtz free energy of mixing is calculated as follows:

Eq. 3.18 $$\Delta A^{mix} = A^{mix} - \sum x_i A_i$$

The Helmholtz free energy is obtained form the partition function by:

Eq. 3.19 $$A = -kT \ln Q$$

The generalized van der Waals partition function for a fluid is given by (Tassios, 1993):

Eq. 3.20 $$Q = \frac{q_{\text{int}}^N}{N!\Lambda^{3N}} V^N \left(\frac{V_f}{V}\right)^N \left(\exp\left(-\frac{\varphi^{attr}}{2kT}\right)\right)^N$$

The second term in Eq. 3.20 represents the combinatorial contribution, the third term the free volume correction contribution and the last term is the attractive (energetic) contribution to the partition function (Elbro et al., 1990). V^N is the combinatorial term (V is the volume) and V_f^N the free volume term (V_f is the volume between molecules). The simple Flory-Huggins equation (Flory, 1953) can be derived by considering only the combinatorial contribution to the partition function (Elbro, Fredenslund et al., 1990) at high density:

Eq. 3.21 $$Q^{comb} = V^N$$

Assuming the mixture volume is given by a linear combination of the component molar volumes in the mixture, the excess Gibss energy can be determined using Eq. 3.16 - Eq. 3.19:

Eq. 3.22 $$G^E = \sum_i x_i \ln\left(\frac{\phi_i^V}{x_i}\right)$$

The volume fraction is calculated as:

Eq. 3.23 $$\phi_i^V = \frac{x_i v_i}{\sum_{j=1}^{n} x_j v_j}$$

The Flory-Huggins equation is obtained by partial molar differentiation of Eq. 3.22 (Elbro, Fredenslund et al., 1990):

Eq. 3.24 $$\ln \gamma_i^{Flory} = \ln\left(\frac{\phi_i^V}{x_i}\right) + 1 - \frac{\phi_i^V}{x_i}$$

This simple model ignores free volume effects and density dependent internal energy effects and does not yield accurate results when predicting activity coefficients in solid-liquid systems (Coutinho, Andersen et al., 1995; Kontogeorgis, Nikolopoulos et al., 1997; Polyzou, Vlamos et al., 1999). Later Patterson (Patterson, 1969), Flory (Flory, 1970) and others (Chen et al., 1990; Bogdanic and Fredenslund, 1994) established that free volume effects are

important in polymer systems, and other systems with large differences in size.

Considering both the combinatorial and free volume contributions to the partition function at high density:

Eq. 3.25 $$Q^{comb-FV} = V^N \left(\frac{V_f}{V} \right)^N = V_f^N$$

The corresponding liquid activity coefficient model (Flory-FV) is as follows (Elbro, Fredenslund et al., 1990):

Eq. 3.26 $$\ln \gamma_i^{Flory-FV} = \ln \left(\frac{\phi_i^{FV}}{x_i} \right) + 1 - \frac{\phi_i^{FV}}{x_i}$$

The free volume fraction is given by:

Eq. 3.27 $$\phi_i^{FV} = \frac{x_i v_i^{Flory-FV}}{\sum_{j=1}^{n} x_j v_j^{Flory-FV}}$$

Several methods for calculating the free volume have been presented (Flory, 1970; Elbro, Fredenslund et al., 1990; Kontogeorgis, Coutsikos et al., 1994). Of these free volume models, the Flory free volume term yielded the best results (Kontogeorgis, Coutsikos et al., 1994). The free volume is calculated as:

Eq. 3.28 $$v_i^{Flory-FV} = \left(v_i^{1/3} - v_i^{W\,1/3} \right)^{3c}$$

with v_i the liquid volume and v_i^W the van der Waals volume of component *i*. The van der Waals volume is used to estimate the hard core volume of the molecule. Parameter c represents the external degrees of freedom of molecule *i*. Coutinho et al. (Coutinho, Andersen et al., 1995) investigated different *c* values and suggested a value of $c = 1.1$. This value is used in this work.

Beret, Donohue and Prausnitz (Beret and Prausnitz, 1975; Donohue and Prausnitz, 1978), using principles developed by Prigogine (Prigogine, 1957) (rotational and vibrational contributions to the partition function can be replaced by equivalent translational contributions), proposed the following partition function for hard sphere chain fluids:

Eq. 3.29 $$Q = \frac{q_{\text{int}}^{N}}{N!\Lambda^{3N}} V^{N} \left(\frac{V_f}{V}\right)^{N} \left(\frac{V_f^{c-1}}{V^{c-1}}\right)^{N} \left(\exp\left(-\frac{\varphi^{attr}}{2kT}\right)\right)^{Nc}$$

The number of internal degrees of freedom is $3c$, which is a measure of the flexibility of a molecule. It is further assumed that, for mixtures, c_{mix} is a linear function of the pure component c parameters. For athermal mixtures (mixtures without significant energetic interactions) at high densities only the combinatorial and free volume terms in Eq. 3.29 are important, and the partition function reduces to (Kontogeorgis, Nikolopoulos et al., 1997):

Eq. 3.30 $$Q^{comb-FV} = \left(\frac{V_f^{c}}{V^{c-1}}\right)^{N}$$

Using Eq. 3.16 - Eq. 3.19, the excess Gibbs free energy can be calculated from Eq. 3.30 (Kontogeorgis, Nikolopoulos et al., 1997):

Eq. 3.31 $$G^{E} = \sum_i x_i \ln\left(\frac{\phi_i^{V}}{x_i}\right) + \sum_i x_i c_i \ln\left(\frac{\phi_i^{FV}}{\phi_i^{V}}\right)$$

The liquid activity coefficient expression for the chain-FV model is obtained from Eq. 3.31 (Kontogeorgis, Nikolopoulos et al., 1997) by differentiation:

Eq. 3.32 $$\ln \gamma_i^{chain-FV} = \ln\left(\frac{\phi_i^{V}}{x_i}\right) + 1 - \frac{\phi_i^{V}}{x_i} + c_i \ln\left(\frac{\phi_i^{FV}}{\phi_i^{V}}\right) + c\left(\frac{\phi_i^{V}}{x_i} - \frac{\phi_i^{FV}}{x_i}\right)$$

Parameter c is a linear function of composition:

Eq. 3.33 $$c = \sum_i x_i c_i$$

Parameter c_i is obtained as follows:

Eq. 3.34 $$c_i = \frac{r_i}{q_i}$$

r_i and q_i are normalised van der Waals volume and area parameters respectively, as used with the UNIQUAQ liquid activity model. The volume fraction term is given by Eq. 3.23 and the free volume fraction is calculated as:

Eq. 3.35 $$\phi_i^{FV} = \frac{x_i v_i^{chain-FV}}{\sum_{j=1}^{n} x_j v_j^{chain-FV}}$$

The free volume term is similar to the more empirical p-FV model (Kontogeorgis, Coutsikos et al., 1994):

Eq. 3.36 $$v_i^{chain-FV} = \left(v_i - v_i^W\right)^{p_i}$$

The exponent in Eq. 3.36, p_i, should be close to unity for a polymer solution in a solvent and is defined, for a binary sytem, as (Kontogeorgis, Nikolopoulos et al., 1997):

Eq. 3.37 $$p_1 = p_2 = 1 - \left(\frac{r_1}{r_2}\right)^{1.5}$$

where r_1 and r_2 are normalised van der Waals volume parameters as used with the UNIQUAQ liquid activity coefficient model, and $r_1 < r_2$. No extension to multicomponent mixtures for the exponent, p_i, is given by Kontogeorgis (Kontogeorgis, Nikolopoulos et al., 1997). In this work Eq. 3.37 is extended to multicomponent mixtures as follows:

Eq. 3.38 $$p_i = 1 - \left(\frac{r_i}{r_{avg}}\right)^{\pm 1.5}$$

The sign of the exponent, 1.5, is chosen such that $p_i \geq 0$. The average volume parameter is defined as follows:

Eq. 3.39 $$r_{avg} = \sum_{j=1}^{n} x_j r_j$$

For a dilute binary mixture (either $x_1 \approx 0$ or $x_2 \approx 0$) Eq. 3.38 and Eq. 3.39 correctly reduce to Eq. 3.37. It must be noted that Eq. 3.37 is not dependent on concentration. It was developed to fit infinite dilution activity coefficients. The multicomponent extension (Eq. 3.38) can be viewed as the exponent, p_i, of component *i* that is infinitely diluted in a liquid mixture having the average size parameter, r_{avg}, defined by Eq. 3.39. Eq. 3.38 and Eq. 3.39 introduce composition dependence not present in the original binary formulation of the exponent p_i. Some effort was made in this work to develop a composition independent multicomponent extension of Eq. 3.37, but this resulted in equations that suffer from the Michelsen-Kistenmacher inconsistency (Michelsen and Kistenmacher, 1990).

3.1.2. Modelling results of long chain n-alkane solubility in n-alkane solvents

The liquid activity coefficient models described above were used to predict solubility of published data for long chain n-alkanes in n-alkane solvents. Only systems with n-alkane solvents were selected, since both the Flory-FV and chain-FV models were derived for athermal mixtures.

From the average errors listed in Table 3-1 it can be seen that the Flory-FV and chain-FV models predicts solubilities with comparable accuracy, with the chain-FV model having a slightly lower overall error for the systems tested.

Assuming ideal liquid phase activity coefficients also gives a reasonable prediction of solubilities. Different pure component property correlations were tested. Butler et al. (Butler and MacLeod, 1961) reported a correlation for the lumped enthalpy of melting and solid-solid transition, which gives comparable results to the correlations developed in this work (see **Appendix C**). The Butler correlation does not predict the solubility of the shorter n-alkanes (n-C_{12} and n-C_{16}) very well, probably caused by the inability of this correlation to predict the melting + solid-solid transition enthalpy change for these components (see **Appendix C**, Figure 111).

Table 3-1. Percentage errors[a] between experimental solubility data and predicted solubilities of various liquid activity models.

System	Flory-FV[b]	Chain-FV[b]	Ideal[b]	Ideal[c]	Source
n-C_6/n-C_{12}	23.2	23.2	23.2	30.8	1
n-C_6/n-C_{16}	4.6	5.6	3.2	20.2	1
n-C_6/n-C_{17}	69.0	69.5	57.5	26.5	1
n-C_6/n-C_{32}	20.5	18.3	28.0	22.8	1
n-C_6/n-C_{16}	0.8	1.2	1.9	3.1	2
n-C_6/n-C_{24}	15.2	5.2	32.3	32.5	2
n-C_7/n-C_{23}	21.5	19.9	13.6	20.2	3
n-C_7/n-C_{25}	15.1	13.3	9.7	14.9	3
n-C_7/n-C_{26}	15.4	13.8	14.7	10.5	3
n-C_7/n-C_{28}	12.3	10.4	15.9	12.2	3
Overall	19.8	18.0	20.0	19.4	

1. (Hoerr and Harwood, 1951)
2. (Dernini and de Santias, 1976)
3. (Provost, Chevallier et al., 1998)

a. $$error = 100 \times \frac{1}{n} \sum \frac{\left| x^{\exp} - x^{\mathrm{mod}\,el} \right|}{x^{\exp}}$$

b. Physical properties calculated with correlations presented in Appendix C.

c. Physical properties correlations taken from (Butler and MacLeod, 1961).

3.1.3. Solid phase activity coefficients

Initially researchers modelled the precipitation of multicomponent n-alkanes as an ideal solid solution (e.g. (Butler and MacLeod, 1961; Won, 1989; Pedersen et al., 1991; Erickson et al., 1993)), but this lead to limited success. Studies by (Snyder et al., 1993) and (Pedersen et al., 1991) indicated that the solid wax phase might not consist of a solid solution, but rather that large hydrocarbons are mutually insoluble in the solid state and precipitate as separate pure solids. Recently (Lira-Galeana et al., 1996) and (Vafaie-Sefti et al., 2000) used this multisolid concept to model wax precipitation of crude oils. They obtained good results when predicting the fraction wax precipitated from a solution of crude oil, but this multiphase model is mostly applicable to the precipitation of wax mixtures containing components of different chemical structure such as n-alkanes, naphthenes and aromatics.

A recent study done by Chevallier (Chevallier et al., 1999) on the structure of the solid phase of semicontinuous mixtures of n-alkanes indicates that a single homogeneous solid solution of n-alkanes exists at room temperature.

Won (Won, 1986) used a modified regular solution theory model to estimate the ratio of the liquid to solid activity coefficients. Coutinho and co-workers investigated the use of lattice model theory (Coutinho et al., 1996) and local composition models such as the Wilson model (Coutinho and Stenby, 1996) and NRTL and UNIQUAQ models (Coutinho, 1999) to describe solid phase nonidealities in solid-liquid equilibrium for n-alkanes. This approach lead to reasonable prediction of solid-liquid equilibria for ternary and quaternary systems. Pauly et al. (Pauly et al., 1998) measured solid-liquid phase equilibria for n-decane - multi-paraffins systems and concluded that the Flory-FV model, describing liquid activities, with the Wilson equation, describing solid phase activities, best modelled wax appearance temperatures and fraction of wax precipitated.

Two local composition models (Wilson and NRTL) are used in this work to model the solid phase activity coefficients and their derivations will be given briefly below. Wilson started with Eq. 3.22, the Flory-Huggins equation and introduced two important modifications (Wilson, 1964); a) The volume fractions were calculated from local volume fractions. b) The local volume fractions were calculated from a Boltzmann probability function. The distribution of molecules *i* and *j* around a molecule of type *i* is given by:

Eq. 3.40
$$\frac{x_{ij}}{x_{ii}} = \frac{x_j \exp\left(\frac{-\lambda_{ij}}{RT}\right)}{x_i \exp\left(\frac{-\lambda_{ii}}{RT}\right)}$$

where λ_{ij} indicates the energy of interaction between molecule *i* and *j*. The local volume fraction of component *i* can then be calculated from local molar composition:

Eq. 3.41
$$\phi_i = \frac{v_i x_i \exp\left(\frac{-\lambda_{ii}}{RT}\right)}{\sum_j v_j x_j \exp\left(\frac{-\lambda_{ij}}{RT}\right)} = \frac{x_i}{\sum_j \frac{v_j}{v_i} x_j \exp\left(\frac{-(\lambda_{ij}-\lambda_{ii})}{RT}\right)}$$

Substituting Eq. 3.41 into Eq. 3.22 gives the Wilson expression for excess Gibss energy:

Eq. 3.42 $$\frac{G^E}{RT} = \sum_i x_i \ln \sum_j \frac{1}{x_j \Lambda_{ij}} = -\sum_i x_i \ln \sum_j x_j \Lambda_{ij}$$

The interaction parameters, Λ_{ij}, are defined in terms of interaction energies between molecules of type *i* and type *j* (Wilson, 1964):

Eq. 3.43 $$\Lambda_{ij} = \frac{v_i}{v_j} \exp\left[\frac{-(\lambda_{ij} - \lambda_{ii})}{RT}\right]$$

Differentiation of Eq. 3.42 leads to the activity coefficient expression (Gmehling and Onken, 1977):

Eq. 3.44 $$\ln \gamma_i = 1 - \ln\left(\sum_j x_i \Lambda_{ij}\right) - \sum_j \frac{x_k \Lambda_{ki}}{\sum_j x_j \Lambda_{kj}}$$

To apply the Wilson equation to the solid phase, Coutinho and Stenby (Coutinho and Stenby, 1996) replaced the component liquid molar volumes with local mole fractions, reducing Eq. 3.43 to:

Eq. 3.45 $$\Lambda_{ij} = \exp\left(-\frac{\lambda_{ij} - \lambda_{ii}}{RT}\right)$$

The like-pair potential, λ_{ii}, relates the interaction energy between two molecules of type *i*. It can also be seen as the cohesion energy (Hildebrand and Scott, 1964). Tassios (Tassios, 1971) and Wong et al. (Wong and Eckert, 1971) proposed that λ_{ii} can be calculated from the configurational energy as follows:

Eq. 3.46 $$\lambda_{ii} = -\frac{2}{z}\left(\Delta H_i^{vap} - RT\right)$$

z is the liquid phase coordination number, assumed to be 10, and ΔH_i^{vap} is the heat of vaporisation. In solid systems this interaction energy can be related to the enthalpy of sublimation (Coutinho et al., 1996):

Eq. 3.47 $$\lambda_{ii} = -\frac{2}{z}\left(\Delta H_i^{subl} - RT\right)$$

The coordination number, z = 6 for axial interactions in an orthorhombic structure. In this work the enthalpy of sublimation is taken as the sum of the enthalpies of solid-solid transition, melting and vaporisation:

Eq. 3.48 $$\Delta H_i^{subl} = \Delta H_i^{tr} + \Delta H_i^{m} + \Delta H_i^{vap}$$

Enthalpies of vaporisation are calculated from the group contribution method of Basarova et al. (Basarova and Svoboda, 1995). The unlike pair potential, λ_{ij}, is taken as the London dispersion forces acting over the contact surface between two molecules. This contact area, and thus interaction potential, will be the same between shorter molecules of type *i*, and between molecules of type *i* and *j*, if molecule *i* is shorter than *j* (Figure 3-2). Thus, if molecule *i* is shorter than molecule *j* (Coutinho, Knudsen et al., 1996):

Eq. 3.49 $$\lambda_{ij} = \lambda_{ji} = \lambda_{ii}$$

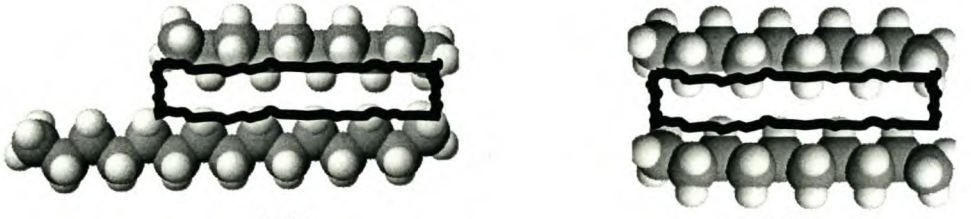

Figure 3-2. Contact area between n-alkane molecules of unequal and equal length.

Renon and Prausnitz (Renon and Prausnitz, 1968) used Guggenheim's quasi-chemical theory to obtain an expression for the local mole fraction of molecule *i* surrounded by molecule *j*, taking into account nonrandomness of mixtures. The result is similar to Eq. 3.40, except for the parameter α_{ij}, which corrects Eq. 3.40 for nonrandom behaviour:

Eq. 3.50 $$\frac{x_{ij}}{x_{ii}} = \frac{x_j \exp\left(\alpha_{ij} \frac{-g_{ij}}{RT}\right)}{x_i \exp\left(\alpha_{ij} \frac{-g_{ii}}{RT}\right)}$$

The g_{ij} and g_{ii} in Eq. 3.50 are the residual Gibbs free energy of interactions between molecule *i* surrounded by molecule *j* or *i* respectively. The local mole fractions are related by

Eq. 3.51 $$\sum_j x_{ij} = 1$$

From Eq. 3.50 and Eq. 3.51 the local mole fraction is obtained:

Eq. 3.52 $$x_{ij} = \frac{x_i \exp\left(\alpha_{ij} \frac{-(g_{ij} - g_{ii})}{RT}\right)}{\sum_k x_k \exp\left(\alpha_{ik} \frac{-(g_{ik} - g_{ii})}{RT}\right)}$$

The following substitutions can be made to simplify Eq. 3.52 and further equations:

Eq. 3.53 $$\tau_{ij} = \frac{(g_{ij} - g_{ii})}{RT} \; and \; G_{ij} = \exp(-\alpha_{ij}\tau_{ij})$$

Using the two-liquid theory of Scott (Scott, 1956), the excess Gibbs energy is given by (Renon and Prausnitz, 1968):

Eq. 3.54 $$G^E = \sum_i x_i \sum_j x_{ij} (g_{ij} - g_{ii})$$

Substituting Eq. 3.52 into Eq. 3.54 the excess Gibbs free energy for the NRTL equations is obtained:

Eq. 3.55 $$\frac{G^E}{RT} = \sum_i x_i \frac{\sum_j \tau_{ij} G_{ij} x_j}{\sum_l G_{il} x_l}$$

The NRTL liquid activity coefficient model is obtained by differentiation of Eq. 3.55 giving (Gmehling and Onken, 1977):

Eq. 3.56 $$\ln \gamma_i = \frac{\sum_j \tau_{ij} G_{ij} x_j}{\sum_l G_{il} x_l} + \sum_j \frac{x_j G_{ji}}{\sum_l G_{jl} x_l} \left(\tau_{ji} - \frac{\sum_n x_n \tau_{jn} G_{jn}}{\sum_l G_{jl} x_l} \right)$$

Coutinho (Coutinho, 1999) proposed that the NRTL equation be used to predict solid n-alkane activity coefficients. The interaction energies are obtained in a similar fashion as for the Wilson equation (Wong and Eckert, 1971; Coutinho, 1999), from Eq. 3.46 - Eq. 3.49, giving:

Eq. 3.57 $$\tau_{ij} = \frac{\lambda_{ij} - \lambda_{ii}}{RT}$$

The non-randomnes parameter, α_{ij}, is related to the coordination number of the system:

Eq. 3.58 $$\alpha_{ij} = \frac{2}{z}$$

The maximum coordination number for axial interaction in an orthorhombic alkane crystal is z = 6 (Coutinho and Stenby, 1996). This gives a fixed value of α_{ij} = 0.33. In this way the NRTL activity coefficient model is used in a predictive manner, with the binary interaction parameters calculated from pure component properties.

3.1.4. Modelling results for multi-alkane precipitation

Solvents normally do not co-precipitate with the heavy n-alkanes, and their solid phase composition is set to zero. Several researchers presented correlations to predict the miscibility limits between different n-alkanes (Matheson and Smith, 1985; Dorset, 1990). A correlation presented by Bhat (Bhat, 1996) is used in this work to determine whether an n-alkane will co-precipitate with the next heavier n-alkane in the mixture:

Eq. 3.59 $$n_{max} = 1.16 n_{min} + 2.07$$

n_{max} is the carbon number of the longest n-alkane that will co-precipitate with the shorter n-alkane with carbon number n_{min}.

Solvent crystallisation data published by Pauly et al. (Pauly, Dauphin et al., 1998) (n-C_{20} – n-C_{30} with n-C_{10} as solvent) was simulated using the liquid and solid activity coefficient models discussed in sections 3.1.1 and 3.1.3. It was found that the solid phase activity models had a greater influence on phase calculations than the liquid phase activity models. The Flory-FV and chain-FV models were found to have almost identical influences on solid-liquid calculations. For this reason only one liquid activity coefficient model will be used with the Wilson and NRTL solid phase models for phase calculations. Following Coutinho (Coutinho and Stenby, 1996; Coutinho, 1999), the Flory-FV model is selected to model the liquid phase activity coefficients. Three combinations of liquid and solid activity coefficient models were used with Eq. 3.14 and Eq. 3.15 to perform equilibrium calculations:

- The liquid and solid phases were assumed ideal ($\gamma_i^S = \gamma_i^L = 1$), labeled *ideal* in the figures.
- The solid phase is modelled using the Wilson equation and the liquid phase modelled with the Flory-FV model, labelled *Wilson+FloryFV* in the figures.
- The solid phase is modelled using the NRTL equation and the liquid phase modelled with the Flory-FV model, labelled *NRTL+FloryFV* in the figures.

From Figure 3-3 and Figure 3-4 it can be seen that the use of a solid phase activity model with the Flory-FV model results in a large improvement in the prediction of total wax dissolved at a temperature, compared with the ideal solid and liquid model.

The composition profiles of the two mixtures at 283.15 K is shown below in Figure 3-5 and Figure 3-6. All three models give fair representations of the experimental composition profiles for the two mixtures shown. The Wilson + Flory-FV models gives qualitatively the same results as the ideal liquid and solid models, but the temperature prediction of the Wilson + Flory-FV models are more accurate. The NRTL + Flory-FV models gives slightly different composition predictions, but the general trend is still the same as the other two models. Qualitatively similar results were obtained at other temperatures.

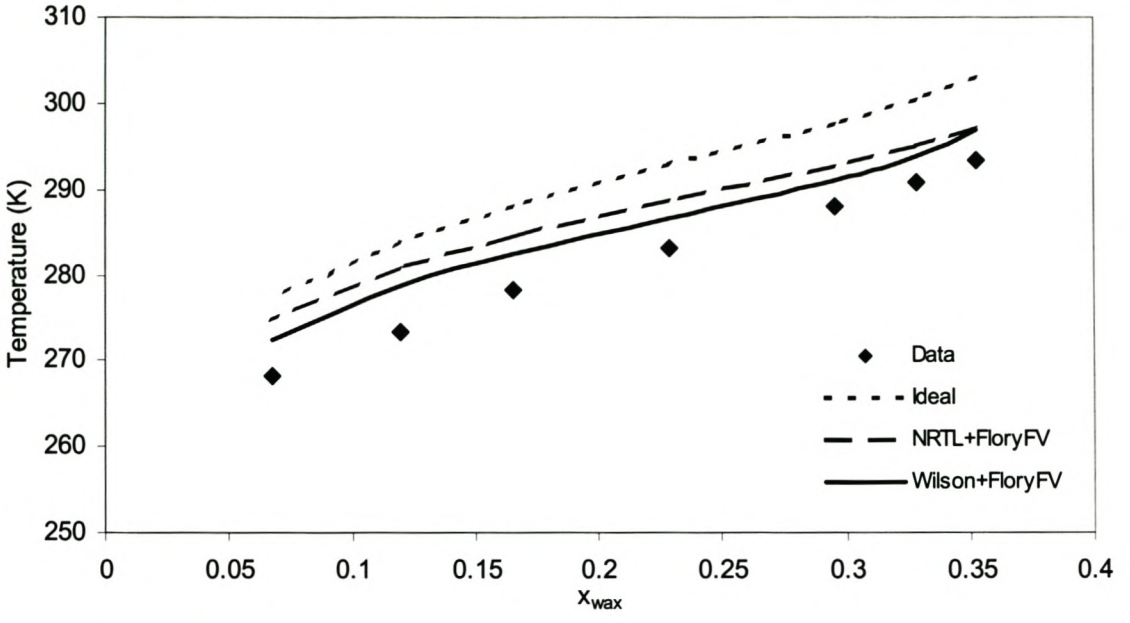

Figure 3-3. Fraction wax dissolved in n-C_{10} vs. temperature for mixture A (Pauly, Dauphin et al., 1998).

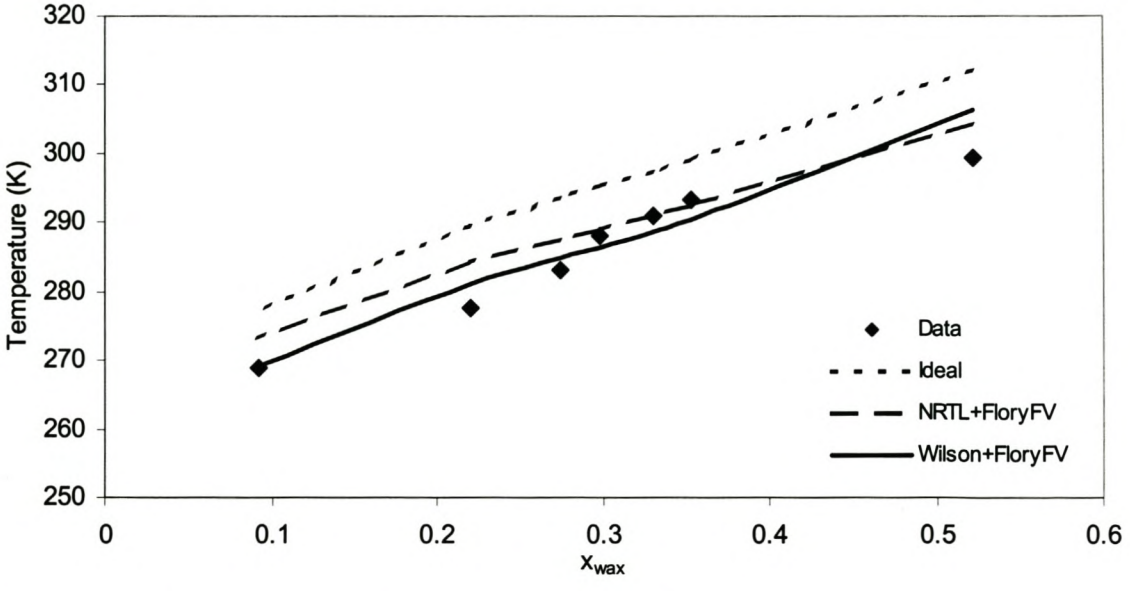

Figure 3-4. Fraction wax dissolved in n-C_{10} vs. temperature for mixture B (Pauly, Dauphin et al., 1998).

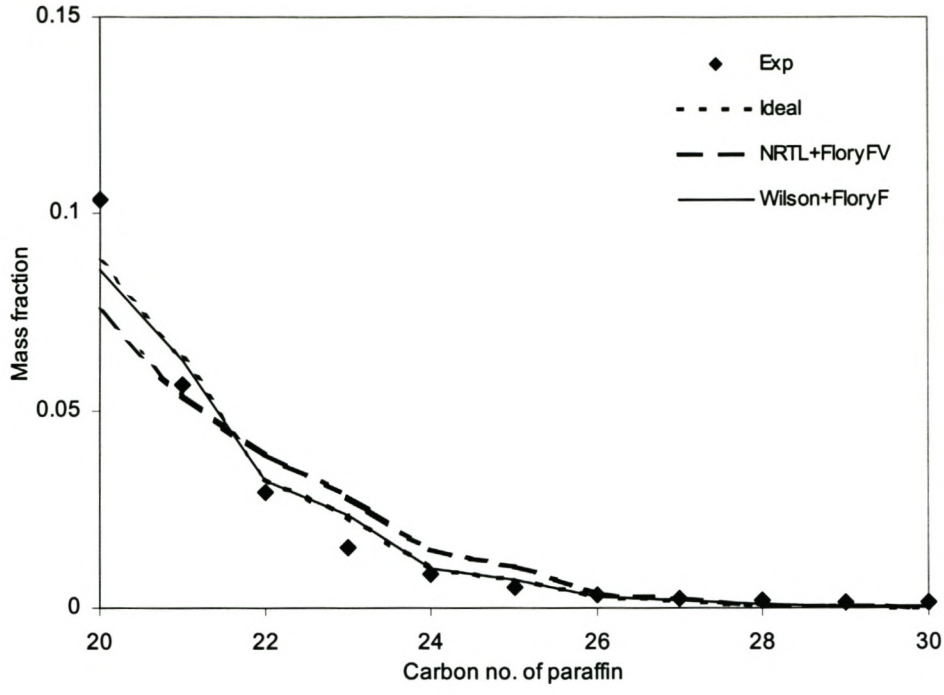

Figure 3-5. Liquid composition of mixture A (Pauly, Dauphin et al., 1998). Liquid consists of 77.1% solvent.

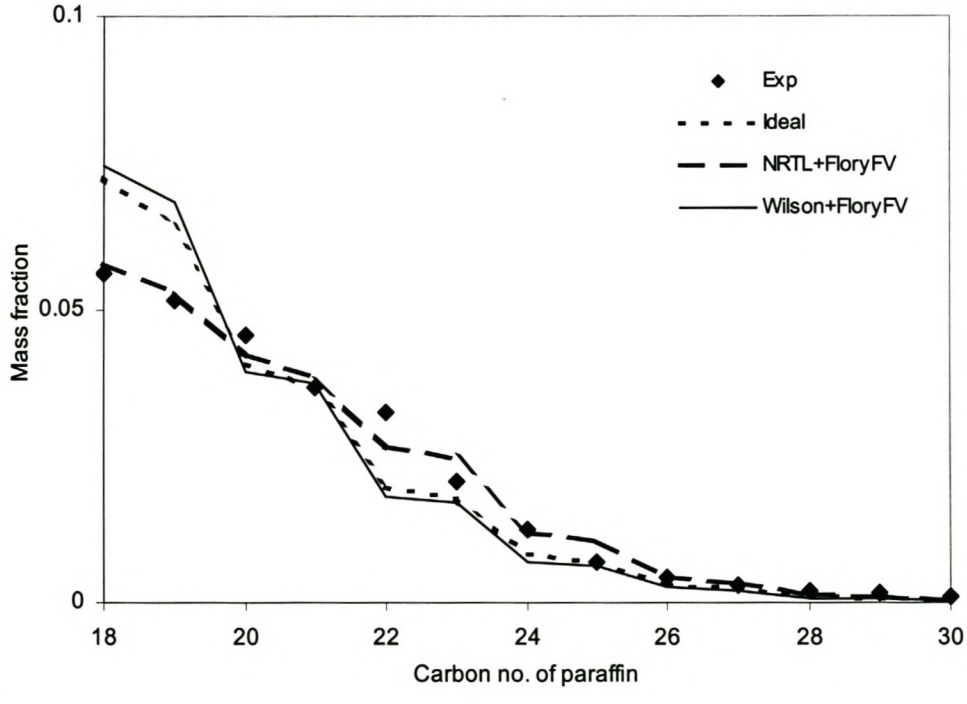

Figure 3-6. Liquid composition of mixture B (Pauly, Dauphin et al., 1998). Liquid consists of 72.6% solvent.

In Figure 3-7 the solid phase predicted and experimental compositions are shown for a data set from (Pauly, Dauphin et al., 1998). The NRTL+Flory-FV models overestimate the amount of light paraffins in the solid, and underestimate the amount of intermediate paraffins in the solid phase. The Wilson + Flory-FV and ideal models give better predictions, but still overestimate the amount of n-C_{20} in the solid phase. Other researchers have also found that most models overpredict the amount of light paraffins precipitated in the solid phase (Coutinho and Ruffier-Meray, 1997; Pauly, Dauphin et al., 1998). The solid phase composition predictions are especially bad when small amounts of wax have precipitated from solution.

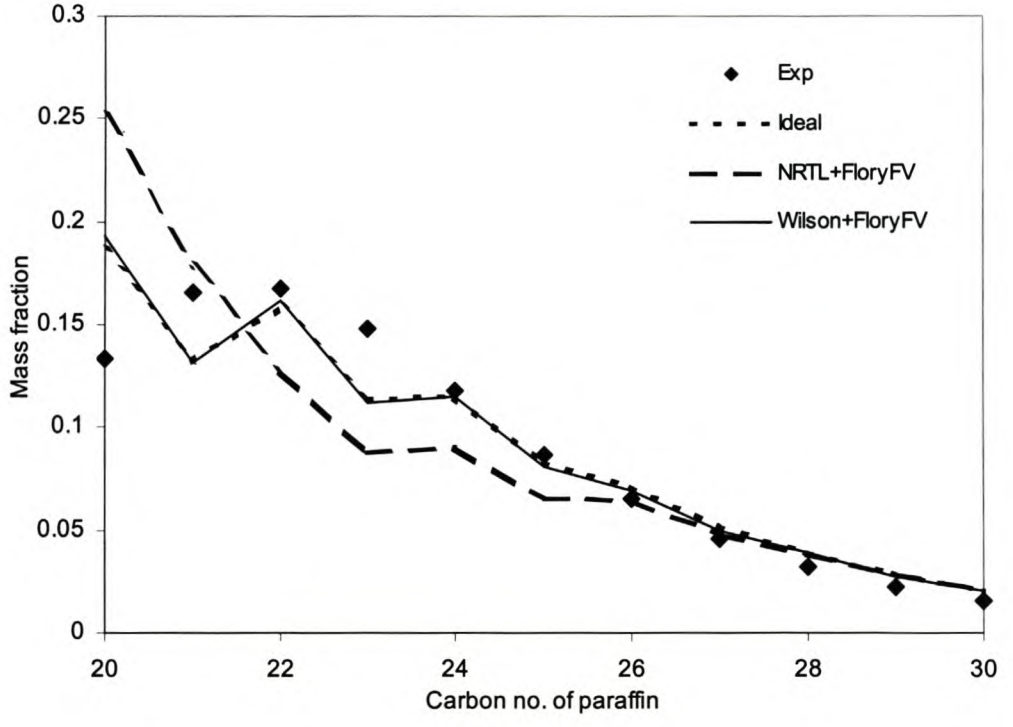

Figure 3-7. Solid composition of mixture A (Pauly, Dauphin et al., 1998). Liquid consists of 77.1% solvent.

Wax recrystallisation data published by Butler and MacCleod (table 4 and Figure 16 in (Butler and MacLeod, 1961)) were simulated with the Wilson and NRTL solid phase models, using the Flory-FV model for the liquid phase. The solvent used was a mixture of 50% MEK and 50% toluene. These two solvents have significant energetic interactions in the liquid phase. Since the free volume liquid activity models ignore energetic interactions, the residual part of the UNIFAC liquid activity model (Larsen et al., 1987) is included when calculating liquid activity coefficients (Coutinho, 1999):

Eq. 3.60 $$\ln \gamma_i^L = \ln \gamma_i^{comb-FV} + \ln \gamma_i^{residual}$$

The simulated composition of the wax product is shown in Figure 3-9 and Figure 3-9. All three models give good qualitative descriptions of the solid phase compositions, with the ideal model predicting the lowest separation sharpness. The NRTL + Flory-FV model underpredicts the composition of the light paraffins. The Wilson + Flory-FV model gives an excellent prediction of the composition in Figure 3-9, but the predicted solid composition shown in Figure 3-9 is biased towards the heavier paraffins.

These solid phase predictions are remarkably accurate, since the models are totally predictive.

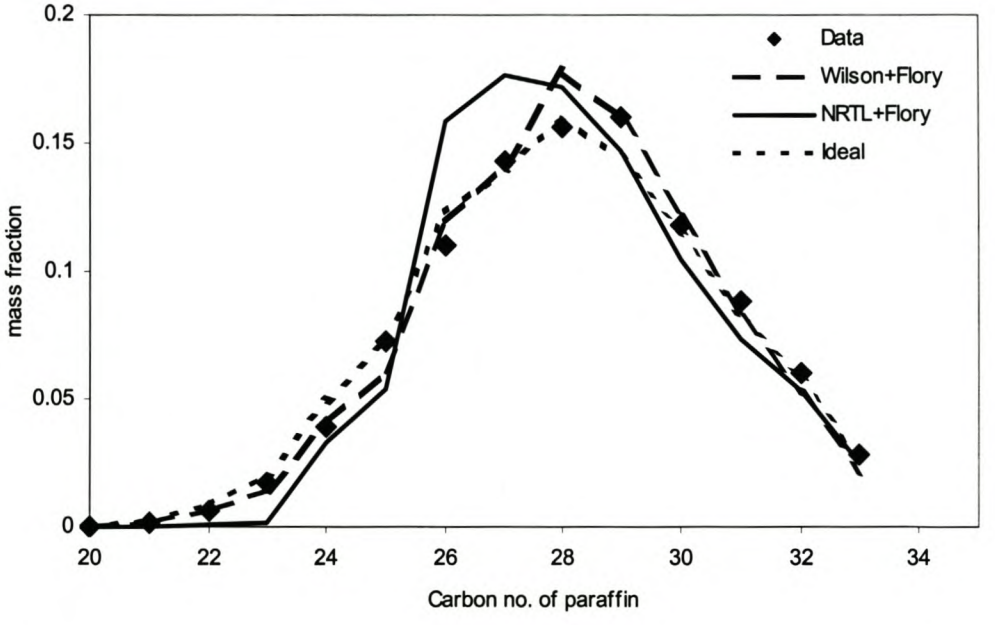

Figure 3-8. Comparison of precipitated wax composition from solvent crystallisation (from table 4 in (Butler and MacLeod, 1961)) with model predictions.

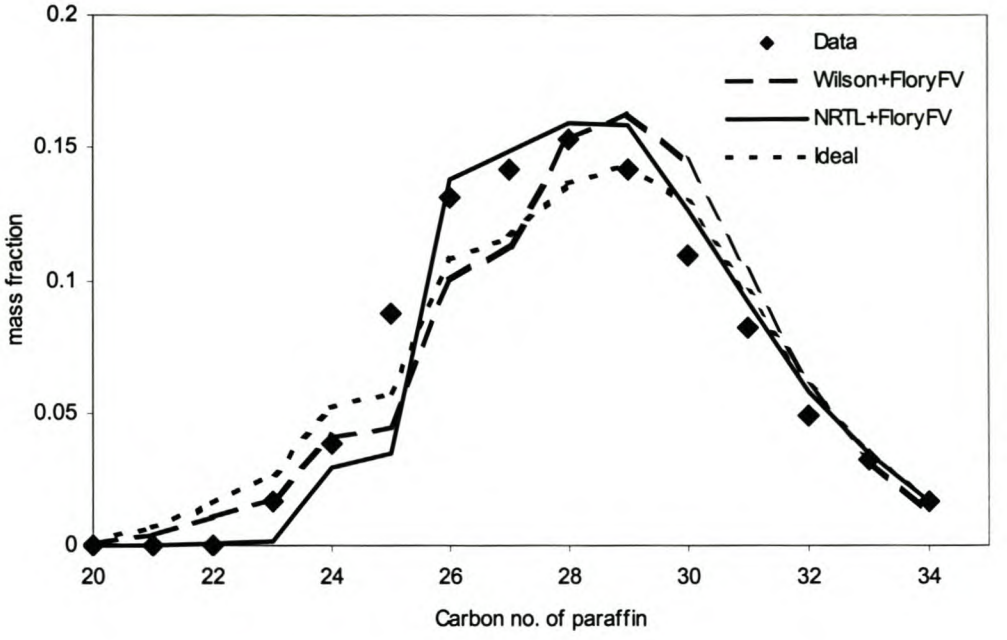

Figure 3-9. Comparison of precipitated wax composition from solvent crystallisation (from figure 16 in (Butler and MacLeod, 1961)) with model predictions.

3.2. Conclusions and recommendations

Several liquid and solid activity models have been tested against experimental data and compared with the ideal liquid and solid assumption. The following conclusions regarding the improvements of the various activity coefficient models can be made:

- Free volume type liquid activity models such as Flory-FV and chain-FV give slightly improved liquid solubility predictions for single n-alkane waxes in n-alkane solvent.
- There are little or no real differences between the Flory-FV and chain-FV models, when used to predict multicomponent solubility.
- The Wilson and NRTL solid activity models, with the Flory-FV model, give improved calculated total wax solubility results, compared with the ideal model.
- Both the Wilson and NRTL models give good predictions of the liquid phase in wax crystallisation.
- Assuming ideal solid and liquid phases also gives qualitative predictions of solid and liquid phases, but the solubility limit for multicomponent wax mixtures are overestimated by several Kelvin.

- The Wilson + Flory-FV models and the NRTL + Flory-FV models gave very good composition predictions for the wax crystallisation data of (Butler and MacLeod, 1961).

The use of a free volume type liquid activity model such as Flory-FV or chain-FV, together with a solid activity model such as either Wilson or NRTL should lead to a qualitative description of wax recrystallisation. These models are also expected to be applicable to wax melting.

Various types of wax crystalising technologies are currently used in deoiling paraffin wax. The modelling done in this chapter will be used later to simulate the separation performance of wax deoiling using static crystallisation, which will be compared with wax deoiling using supercritical extraction.

3.3. Nomenclature

Symbol	Description	Unit
A	Helmholtz free energy	J/mol
c	1/3*Internal degrees of freedom	
C_p	Constant pressure heat capacity	J/mol/K
f	Fugacity of pure component	Pa
$\hat{f}$	Fugacity of component in mixture	Pa
G	Gibbs free energy	J/mol
g_{ij}	Gibbs energy of interaction	
H	Enthalpy	J/mol
K	Equilibrium ratio, x/s	
k	Boltzman's constant	J/K/molecule
M_r	Molar weight	g/mol
N	Number of molecules	
p	Exponent in Eq. 3.36	
Q	Molecular partition function	
q	Specific contribution to Q	
q_i	Normalised van der Waals area for copmonent *i*	
R	Universal gas konstant	J/mol.K
r	Normalised van der Waals volume	
S	Entropy	J/mol
s	Solid mole fraction	
T	Temperature	K
v	Molar volume	mol/m^3

x	Liquid mole fraction	
z	Maximum coordination number	
α	Nonrandomness parameter	
ϕ	Volume fraction	
γ	Activity coefficient	
φ	Attractive energy between molecules	J
Λ	de Broglie wavelength	m
Λ_{ij}	Wilson interaction parameter	
λ	Interaction energy	J/mol
τ	NRTL interaction parameter	

Subscripts

i, j	Component index

Superscripts

comb	Combinatorial
E	Excess property
FV	Free volume
L	Liquid
m	Melting
mix	Mixture property
res	Residual
S	Solid
sat	Saturation
subl	Sublimation
t	Transition
W	van der Waals

CHAPTER 4. PHASE EQUILIBRIUM MODELLING IN SUPERCRITICAL FLUID EXTRACTION

Accurate phase equilibrium data is needed when modelling the separation efficiency of a process, and also when predicting how such a process might perform under different circumstances. Equilibrium phase composition ratio's (K-values) are generally needed to model equilibrium stage processes (see section 5.1). Equations of state are normally used to correlate and predict high pressure and supercritical phase equilibria. The state-of-the art in equations of state is such that their predictive capabilities are limited, and are usually tuned or fitted to experimental data. In this chapter relevant experimental phase equilibrium data sets from the literature are identified, and several equations of state are fitted to this data.

4.1. Available phase equilibrium data

Supercritical extraction consists of two basic steps namely a high-pressure extraction step followed by an extract-solvent separation step. The separation step is done at conditions where the solubility of the extract in the solvent is minimised. In this work the separation of the extracted wax from the solvent is accomplished by pressure reduction. Phase equilibrium models are needed to predict wax solubilities in ethane and CO_2 at high pressure to model the extraction step, while the extract separation step requires phase equilibrium models valid at moderate pressures. Two sets of experimental data have been compiled from literature; a high pressure set (see Table 4-1) to be used to model the extraction column and a moderate pressure set (see Table 4-2) to be used to model the separator.

Not all published equilibrium data involving CO_2 or ethane and an n-alkane were used. Examples of data sets not used in this work includes solid-liquid-vapour and liquid-liquid-vapour data from (Peters et al., 1991), solubility of a solid in supercritical fluid (Suleiman et al., 1993; Yau and Tsai, 1993; Smith et al., 1996) and partial miscibility data (Kim et al., 1967; Wagner et al., 1968).

Table 4-1. High pressure ethane or CO_2 phase equilibrium data.

System	Temperature (°C)	Pressure (bar)	Data in mixture critical region	Source
ethane – n-C_{16}	40 – 80	50 – 150	Y	1
	80	50 – 100	N	2
ethane – n-C_{20}	47 – 77	3 – 120	Y	3
ethane – n-C_{24}	60 – 80	95 – 145	Y	1
	47 – 77	5 – 125	N	4
ethane – n-C_{28}	65 – 80	120 – 165	Y	1
CO_2 – n-C_{12}	40 – 60	80 – 86	Y	1
	50 – 80	60 – 140	N	2
CO_2 – n-C_{14}	50 – 80	100 – 170	N	2
				5
CO_2 – n-C_{16}	40 – 50	85 – 170	Y	1
	50 – 80	100 – 200	N	2
	80	100 – 200	Y	6
CO_2 – n-C_{18}	80	125 – 210	N	2
CO_2 – n-C_{19}	80	100 – 275	Y	6
CO2 – n-C_{20}	43 – 75	77 – 293	Y	1
	80	150 – 250	N	2
	80	100 – 300	Y	6
CO2 – n-C_{24}	56 – 84	155 – 300	N	1
	80	100 – 475	N	6
CO2 – n-C_{28}	65 – 93	140 – 290	N	1
	80	100 – 250	Y (Graphical data)	7
	35 – 50	120 – 280	N	8
CO2 – n-C_{36}	70 – 94	200 – 300	N	1

1. (du Rand, 2000)
2. (de Haan, 1991)
3. (Peters and de Roo, 1987)
4. (Peters et al., 1987)
5. (Gasem et al., 1989)
6. (Kordikowski and Schneider, 1993)
7. (Pohler et al., 1996)
8. (McHugh et al., 1984)

Table 4-2. Solubility data used to develop a generalised SPHC correlation.

System	Temperature range (°C)	Pressure range	Source
ethane – n-C_{12}	100	7 – 50	7
ethane – n-C_{20}	37 – 77 50 – 150	3 – 70 5 – 70	1 2
ethane – n-C_{22}	47 – 87	2 – 70	3
ethane – n-C_{24}	57 – 87	2 – 70	4
ethane – n-C_{28}	75 – 150	5 – 50	2
ethane – n-C_{36}	100 – 150	4 – 40	2
ethane – n-C_{44}	100 – 150	4 – 30	2
CO_2 – n-C_{16}	40 – 70	7 – 70	5
CO_2 – n-C_{19}	40 – 60	10 – 80	6
CO_2 – n-C_{20}	50 – 100	5 – 75	7, 8
CO_2 – n-C_{21}	40 – 60	10 – 80	6
CO_2 – n-C_{22}	50 – 100	10 – 70	9
CO_2 – n-C_{24}	100 – 200	10 – 50	10
CO_2 – n-C_{28}	75 – 100	8 – 90	7
CO_2 – n-C_{32}	100 – 200	10 – 50	10
CO_2 – n-C_{36}	100 – 150	5 – 80	7
CO_2 – n-C_{44}	100 – 150	5 – 70	7

1. (Peters and de Roo, 1987)
2. (Gasem et al., 1989)
3. (Peters et al., 1988)
4. (Peters, van der Kooi et al., 1987)
5. (Charoensombut-Amon et al., 1986)
6. (Fall et al., 1985)
7. (Gasem and Robinson, 1985)
8. (Huie et al., 1973)
9. (Fall and Luks, 1984)
10. (Tsai and Yau, 1990)

4.2. Equations of state

Equations of state have been developed along two routes: empirical formulation and theoretical development based on statistical mechanics theory. Although the statistical mechanics based EOS have a strong theoretical background, there are still some parameters that have to be obtained by fitting constants to experimental data. These equations of state are also very complex, and several simplifications have to be made in order to obtain a usable EOS. The pressure explicit forms of these equations are usually high order polynomials in volume that have to be solved with iterative techniques (see e.g. (Topliss et al., 1988)).

On the other hand, empirical equations of state have a much simpler form and can be constrained to satisfy critical constraints (see Eq. 4.2). The pressure explicit forms of these equations are normally cubic in volume, which can be solved analytically. Although their empirical nature might not lend to extrapolation, thet has been used successfully in the petroleum industry for years, and many of these empirical cubic EOS are found in simulation packages. The are also very flexible, and with parameters fitted on pure component properties, fairly accurate. However, this class of equations of state does not always predict mixture properties accurately, although various mixing and combining rules have been developed to improve phase equilibrium predictions.

In this section several equations of state are investigated, firstly to determine their suitability to predict pure component properties (vapour pressure and specific volume) of the components used in this study, and secondly their ability to correlate experimental phase equilibria. The prediction of the solvent properties was seen as very important, since it cannot be expected to predict mixture properties accurately if pure component properties are not predicted accurately. Hence the capability of an EOS to predict ethane and carbon dioxide properties was tested. The ability of an EOS to predict wax properties was tested by using n-eicosane as representative of the wax mixture components.

The calculation of pure component vapour pressure and multi-component phase equilibrium follows from standard thermodynamic principles described in engineering thermodynamics textbooks (see e.g. (Tassios, 1993; Smith et al., 1996)).

Many of the equations listed below use critical constants to calculate EOS parameters. The critical constants used in this work are given in Appendix A.

4.2.1. Soave-Redlich-Kwong equation of state

Until the 1970's, the Redlich-Kwong (Redlich and Kwong, 1949) equation of state was the best available 2 parameter EOS. This EOS gave adequate results for pure component properties of simple molecules, but its application to multicomponent equilibrium calculations often gave poor results. Its *a* parameter also had a fixed temperature dependence. In 1972 Giorgio Soave (Soave, 1972) published a modification of the Redlich-Kwong EOS (SRK):

Eq. 4.1 $$P = \frac{RT}{v-b} - \frac{a(T)}{v(v+b)}$$

Parameters *a* and *b* are obtained by evaluation of the following conditions:

Eq. 4.2 $$\left(\frac{\partial P}{\partial v}\right)_{T_c} = \left(\frac{\partial^2 P}{\partial v^2}\right)_{T_c} = 0$$

This leads to:

Eq. 4.3 $$a(T) = 0.42747\alpha \frac{R^2 T_c^2}{P_c}$$

and

Eq. 4.4 $$b = 0.08664 \frac{RT_c}{P_c}$$

The parameter α is written in terms of the acentric factor, ω:

Eq. 4.5 $$\alpha = \left(1 + m\left(1 - \sqrt{T_r}\right)\right)^2$$

Eq. 4.6 $$m = 0.48 + 1.574\omega - 0.17\omega^2$$

The SRK EOS predicts a constant critical compressibility factor of 0.333, which is approximately correct for small molecules, but differs considerably for larger molecules. The saturation curves and compressed fluid volumes for ethane and carbon dioxide was calculated with the SRK EOS (see Figure 4-1). The SRK accurately predicts vapour phase volumes, but dense phase volumes are not accurately predicted, both on the saturation curve and in the compressed fluid region. The vapour pressure curve for n-eicosane is also predicted quite accurately (see Figure 4-2), but the calculated saturated liquid volume (see Figure 4-3) deviates by an average of 33% from the pure component correlation.

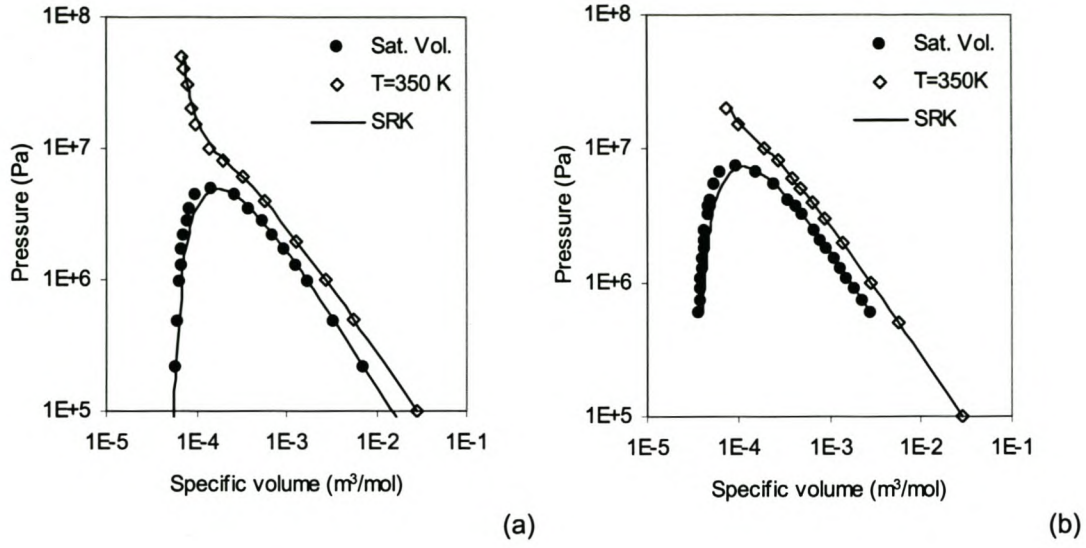

Figure 4-1. Plot of experimental volumes (symbols) compared with calculated volumes (curves) from the SRK EOS. a) Ethane (RMS errors: P^{sat} = 1.8%, V_l^{sat} = 12.4%). b) Carbon dioxide (RMS errors: P^{sat} = 0.5%, V_l^{sat} = 14.9%). Experimental data compiled by Liley (Liley et al., 1997).

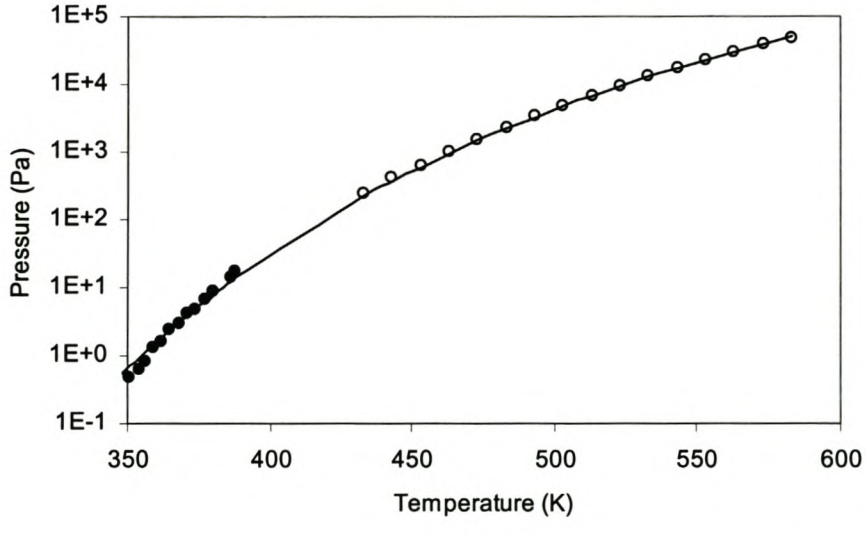

Figure 4-2. Vapour pressure of n-Eicosane. — SRK EOS. Experimental data from Piacente et al. (Piacente et al., 1994) (•) and Morgan et al. (Morgan and Kobyashi, 1994) (o). RMS error for Piacente et al. data = 29%.

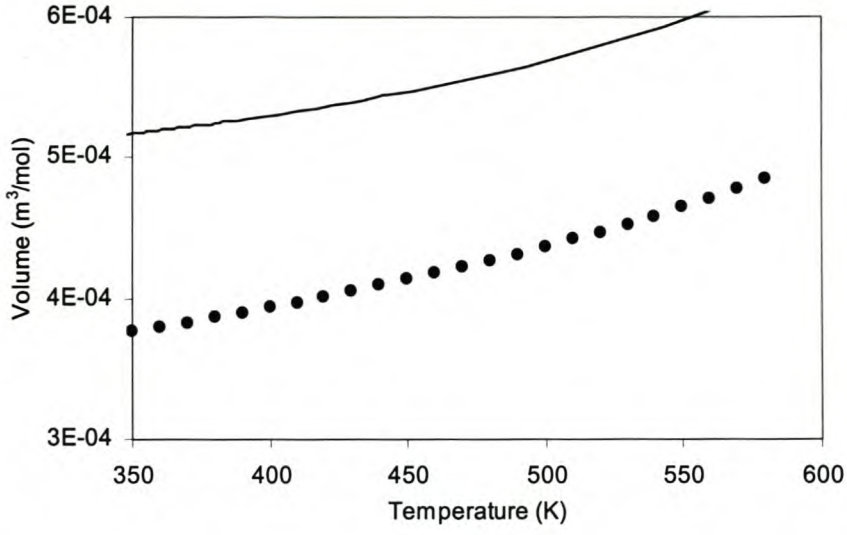

Figure 4-3. Saturated liquid volume of n-eicosane. — SRK EOS. Data points (•) calculated from the correlation tabulated by Thomas (Liley, Thomas et al., 1997). RMS error = 33%.

Compared with other cubic EOS, the SRK EOS gives the best prediction of n-eicosane vapour pressure in the low temperature region (350 K – 400 K). This is the temperature range of relevant to this work.

The poor liquid volume predictions can be addressed by applying a volume correction to the calculated molar volume, first proposed by Martin (Martin, 1967). Later Peneloux and Rauzy (Peneloux and Rauzy, 1982) proposed a linear volume correction term to improve the liquid density predictions of the SRK EOS. They showed that a linear volume translation does not affect vapour pressure calculations. Several other researchers have since published various volume translation correlations for the SRK EOS (Chou and Prausnitz, 1989; Ji and Lempe, 1997; Wang and Gmehling, 1999). A comparison of several volume translation methods is given by de Sant' Ana (de Sant' Ana et al., 1999). Although volume translation improves the liquid volumetric predictions of an EOS, it was not incorporated in this work, because current volume translation procedures do not yield consistent improvement in volume predictions over a wide range of conditions. The more accurate methods also require several component-specific parameters, which might be difficult to predict for compounds having little or no experimental data available.

Mixture parameters for use in multiphase equilibrium calculations are calculated using quadratic mixing rules for both the *a* and *b* parameters:

Eq. 4.7 $$a_m = \sum_i \sum_j x_i x_j a_{ij}$$

Eq. 4.8 $$b_m = \sum_i \sum_j x_i x_j b_{ij}$$

Eq. 4.9 $$a_{ij} = (1 - k_{ij})\sqrt{a_i a_j}$$

Eq. 4.10 $$b_{ij} = (1 - l_{ij})\frac{(b_i + b_j)}{2}$$

The interaction parameters k_{ij} and l_{ij} are fitted to phase equilibrium data, and are used to correct inaccuracies in the underlying equation of state.

4.2.2. Peng-Robinson equation of state

The Peng-Robinson equation of state (PR) is a modification of the Redlich-Kwong equation of state and was published by Peng and Robinson in 1976 (Peng and Robinson, 1976). It is similar to the SRK equation in many respects and was designed to improve the poor liquid density predictions for the SRK method. As with the SRK equation, the *a* term in the Redlich-Kwong equation was replaced with a more general temperature dependent term, *a(T)*. The expression is as follows:

Eq. 4.11 $$P = \frac{RT}{v - b} - \frac{a(T)}{v(v + b) + b(v - b)}$$

with

Eq. 4.12 $$a(T) = 0.457235\alpha \frac{R^2 T_c^2}{P_c}$$

Eq. 4.13 $$\alpha = \left(1 + m\left(1 - \sqrt{T_r}\right)\right)^2$$

Eq. 4.14 $$m = 0.37464 + 1.54226\omega - 0.26992\omega^2$$

Eq. 4.15 $$b = 0.0778\frac{RT_c}{P_c}$$

It should be noted that the PR EOS predicts a fixed critical compressibility factor of 0.3074. The P*v* diagrams of ethane and CO_2 are shown below in Figure 4-4. The PR EOS gives an improved prediction of liquid volumes in the critical region, compared with SRK.

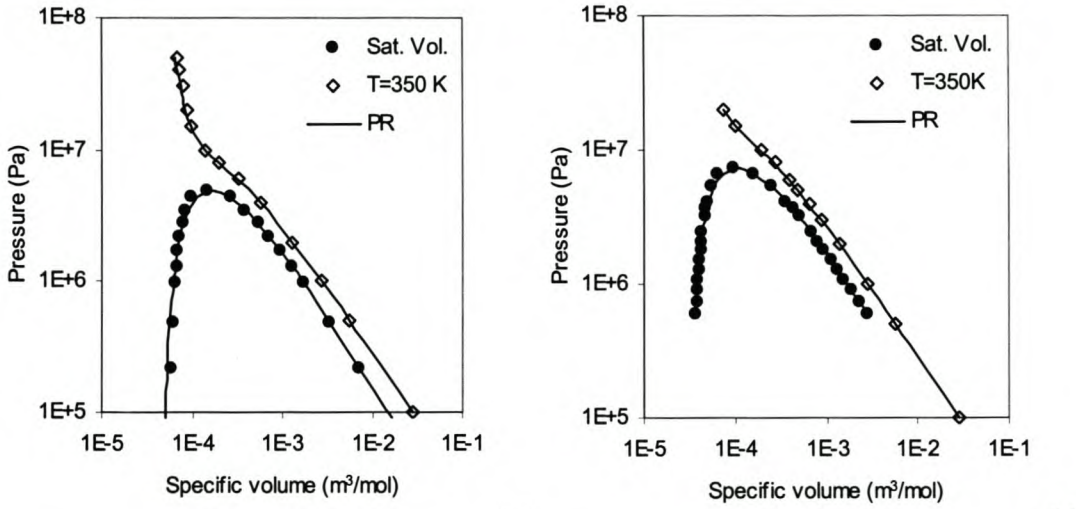

Figure 4-4. Plot of experimental volumes (symbols) compared with calculated volumes (curves) from the PR EOS. a) Ethane (RMS errors: P^{sat} = 0.9%, V_l^{sat} = 8.2%). b) Carbon dioxide (RMS errors: P^{sat} = 0.7%, V_l^{sat} = 7.5%). Experimental data compiled by Liley (Liley, Thomas et al., 1997).

The vapour pressure and liquid volume of n-eicosane calculated with PR is shown below in Figure 4-5 and Figure 4-6. The PR EOS does not give accurate vapour pressure predictions in the low temperature region. The liquid volume predictions are also not very good, with an average error of about 20 %. This is a slight improvement from the 33% error of the SRK EOS. Similar to the SRK EOS, volume translation corrections can be made to improve the liquid volume predictions of the PR EOS (see eg. (Monnery et al., 1998)).

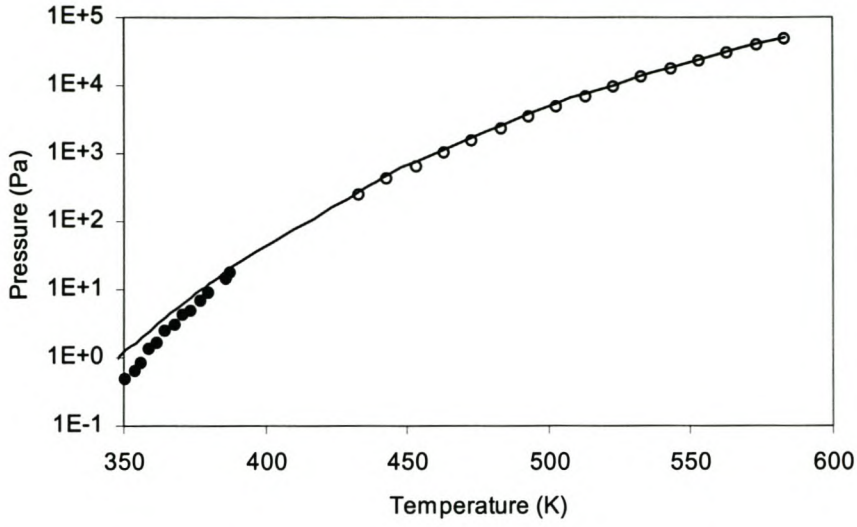

Figure 4-5. Vapour pressure of n-Eicosane. — PR EOS. Experimental data from Piacente et al. (Piacente, Fontana et al., 1994) (•) and Morgan et al. (Morgan and Kobyashi, 1994) (o). RMS error for Piacente et al. data = 101%.

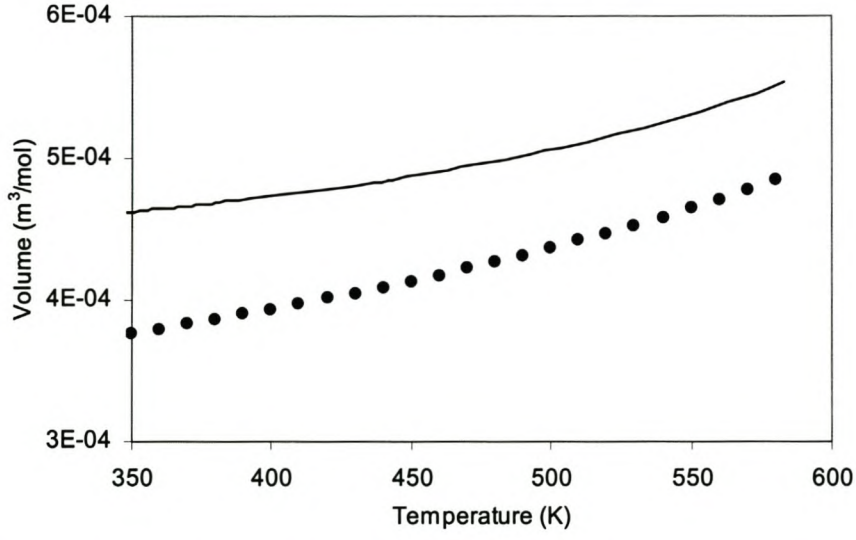

Figure 4-6. Saturated liquid volume of n-eicosane. — PR EOS. Data points (•) calculated from the correlation tabulated by Thomas (Liley, Thomas et al., 1997). RMS error = 19%.

Mixture parameters for use in multiphase equilibrium calculations are calculated using quadratic mixing rules for both the *a* and *b* parameters:

Eq. 4.16 $$a_m = \sum_i \sum_j x_i x_j a_{ij}$$

Eq. 4.17 $$b_m = \sum_i \sum_j x_i x_j b_{ij}$$

Eq. 4.18 $$a_{ij} = (1 - k_{ij})\sqrt{a_i a_j}$$

Eq. 4.19 $$b_{ij} = (1 - l_{ij})\frac{(b_i + b_j)}{2}$$

The interaction parameters k_{ij} and l_{ij} are fitted to phase equilibrium data.

4.2.3. Stryjek and Vera modification of Peng Robinson equation of state

In 1986 Stryjek and Vera (Stryjek and Vera, 1986) published a modified Peng-Robinson EOS (PRSV). They retained the general form of the α term of the EOS (see Eq. 4.13), but modified the parameter m to better predict vapour pressures at low reduced temperatures:

Eq. 4.20 $$m = m_0 + m_1\left(1 + \sqrt{T_r}\right)\left(0.7 - T_r\right)$$

with

Eq. 4.21 $$m_0 = 0.378893 + 1.4897153\omega - 0.17131848\omega^2 + 0.0196554\omega^3$$

and m_1 an adjustable parameter characteristic of a pure component. Stryjek and Vera (Stryjek and Vera, 1986) lists m_1 values for over ninety components. Unfortunately they do not propose a method to predict these m_1 values, which makes its use somewhat difficult. They also recommend that m_1=0 are used when $T_r > 0.7$. Pv diagrams for ethane and CO_2 have been constructed using the PRSV EOS with $m_1 = 0$ (Figure 4-7). The quality of fit is virtually identical to the PR EOS, even when fitting the m_1 parameter to the data. Since the modification of the PRSV EOS is only supposed to correct low pressure calculations, this is not surprising.

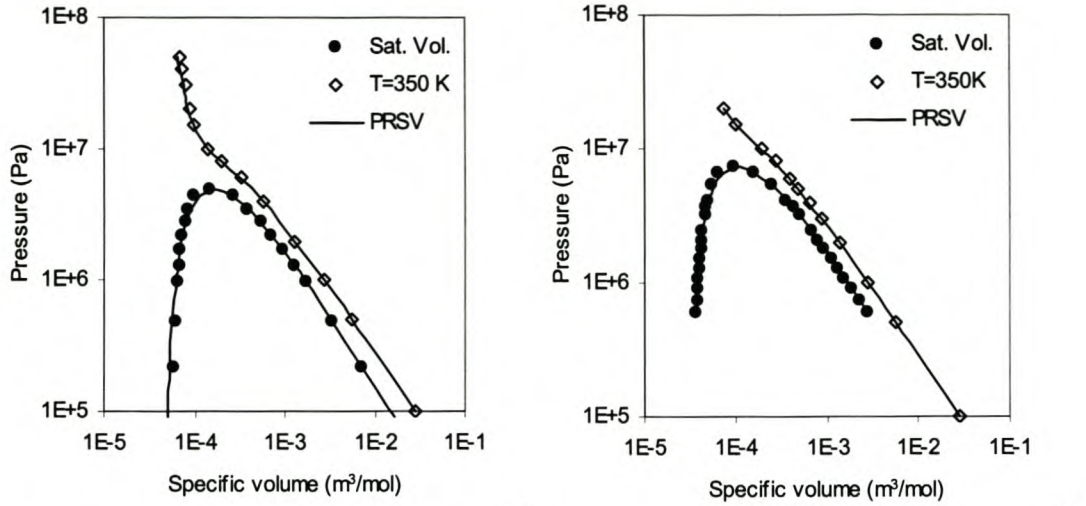

Figure 4-7. Plot of experimental volumes (symbols) compared with calculated volumes (curves) from the PR EOS. a) Ethane (RMS errors: P^{sat} = 0.9%, V_l^{sat} = 8.2%). b) Carbon dioxide (RMS errors: P^{sat} = 0.5%, V_l^{sat} = 7.5%). Experimental data compiled by Liley (Liley, Thomas et al., 1997).

The vapour pressure curve for n-eicosane is plotted using the PRSV EOS with the $m_1 = 0$, and with $m_1 = 0.05$. The results are plotted below in Figure 4-8 and Figure 4-9. The predicted vapour pressure curves are almost identical over the whole temperature covered, except at the lower temperatures. At the lower temperatures use of the m_1 parameter improves somewhat on the predicted vapour pressures. Since only a slight improvement in vapour pressure calculations are obtained, and the m_1 parameters of Stryjek and Vera (Stryjek and Vera, 1986) do not lie on a smooth line, a value of $m_1 = 0$ will be used in this work.

Saturated liquid volumes of n-eicosane are compared with liquid volumes calculated using the PRSV EOS (see Figure 4-10). The calculated liquid volumes are comparable with that of the PR EOS.

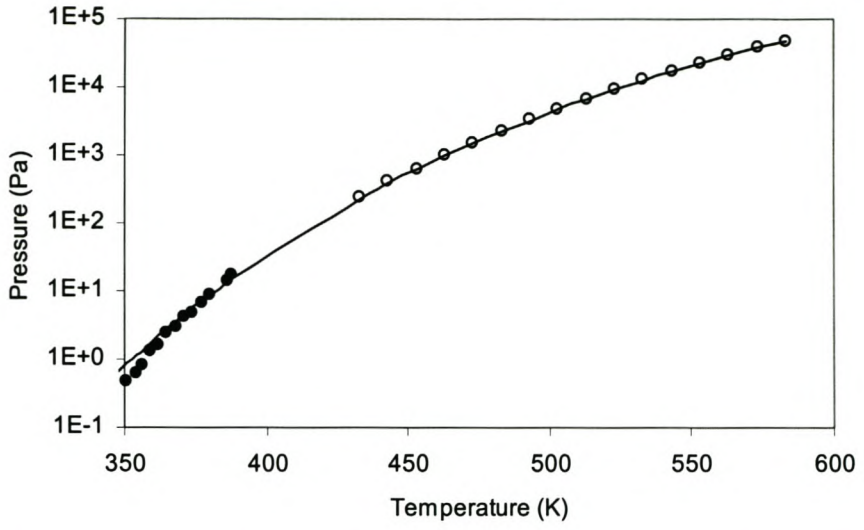

Figure 4-8. Vapour pressure of n-Eicosane. — PRSV EOS with $m_1 = 0$. Experimental data from Piacente et al. (Piacente, Fontana et al., 1994) (•) and Morgan et al. (Morgan and Kobyashi, 1994) (o). RMS error for Piacente et al. data = 45%.

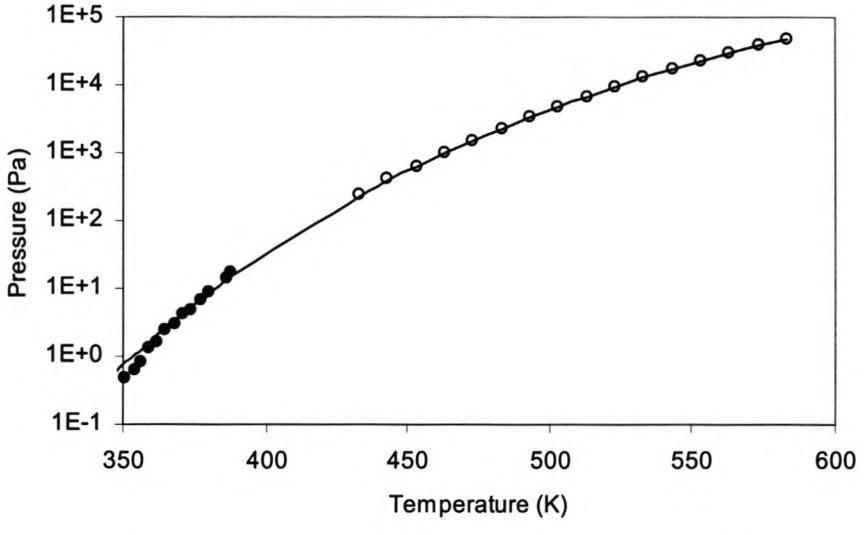

Figure 4-9. Vapour pressure of n-Eicosane. — PRSV EOS with $m_1 = 0.05$. Experimental data from Piacente et al. (Piacente, Fontana et al., 1994) (•) and Morgan et al. (Morgan and Kobyashi, 1994) (o). RMS error for Piacente et al. data = 30%.

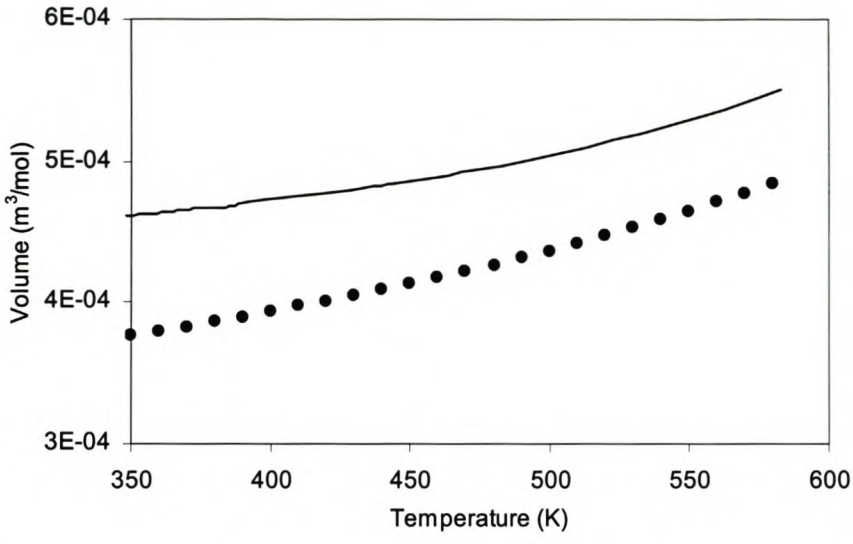

Figure 4-10. Saturated liquid volume of n-eicosane. — PRSV EOS. Data points (•) calculated from the correlation tabulated by Thomas (Liley, Thomas et al., 1997). RMS error = 19%.

4.2.4. Patel-Teja equation of state

In order to overcome the fixed critical compressibility factor predicted by the SRK and PR equations, Patel and Teja (Patel and Teja, 1982) proposed a three-parameter EOS. This EOS also greatly improves the prediction of saturated liquid densities, compared to the SRK and PR equations.

Eq. 4.22 $$P = \frac{RT}{v-b} - \frac{a(T)}{v(v+b)+c(v-b)}$$

Parameters *a*, *b* and *c* are obtained by use of Eq. 4.2, with the following additional constraint:

Eq. 4.23 $$\frac{P_c v_c}{RT_c} = \zeta_c$$

Patel and Teja did not set ζ_c to the experimental value of the critical compressibility, but treated it as an adjustable parameter. Parameters *a*, *b* and *c* are evaluated as follows:

Eq. 4.24 $$a(T) = \alpha \Omega_a \frac{R^2 T_c^2}{P_c}$$

Eq. 4.25 $$b = \Omega_b \frac{RT_c}{P_c}$$

Eq. 4.26 $$c = \Omega_c \frac{RT_c}{P_c}$$

with

Eq. 4.27 $$\Omega_c = 1 - 3\zeta_c$$

Eq. 4.28 $$\Omega_a = 3\zeta_c^2 + 3(1 - 2\zeta_c)\Omega_b + \Omega_b^2 + 1 - 3\zeta_c$$

Ω_b is the smallest positive root of the following equation:

Eq. 4.29 $$\Omega_b^3 + (2 - 3\zeta_c)\Omega_b^2 + 3\zeta_c^2\Omega_b - \zeta_c^3 = 0$$

The α function used is similar to that used by Soave and Peng and Robinson:

Eq. 4.30 $$\alpha = \left(1 + m\left(1 - \sqrt{T_r}\right)\right)^2$$

Eq. 4.31 $$m = 0.452413 + 1.30982\omega - 0.295937\omega^2$$

The parameter ζ_c was correlated with the acentric factor as follows:

Eq. 4.32 $$\zeta_c = 0.329032 - 0.076799\omega + 0.0211947\omega^2$$

The PT EOS ability to predict the saturation curve and compressed fluid volumes of ethane and carbon dioxide was investigated as an indication of this equation's suitability to predict solvent properties at conditions close to that encountered in this work. In Figure 4-11 it can be seen that the PT EOS gives an equally good prediction of the saturation curve and the compressed fluid volume isotherm for both ethane and carbon dioxide.

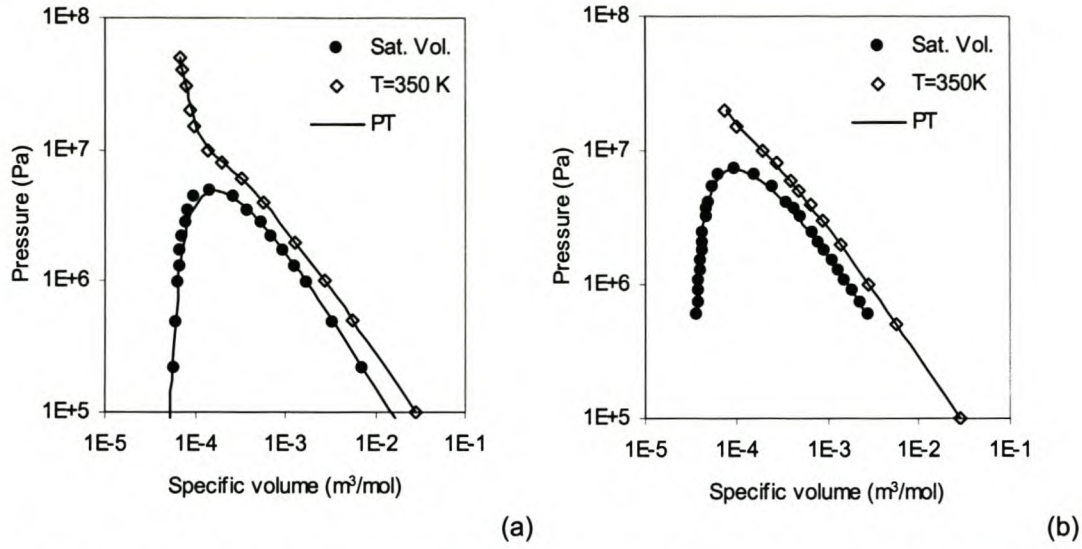

Figure 4-11. Plot of experimental volumes (symbols) compared with calculated volumes (curves) from the PT EOS. a) Ethane (RMS errors: P^{sat} = 1%, V_l^{sat} = 8.2%). b) Carbon dioxide (RMS errors: P^{sat} = 6.2%, V_l^{sat} = 10%). Experimental data compiled by Liley (Liley, Thomas et al., 1997).

This EOS was also used to calculate the saturation pressure curve of n-eicosane. The resulting curve is shown in Figure 4-12, together with experimentally measured data. The predicted vapour pressures are quite accurate above about 380 K, but below this temperature systematic deviation between the experimental and calculated data is evident. Unlike the SRK and PR equations, the PT EOS gives quite a good prediction of the saturated liquid volume (see Figure 4-13), with a root mean square error of only 4%.

It is possible that the acentric values used to fit Eq. 4.31 and Eq. 4.32 differ from the values used in this work, but this could not be confirmed since the acentric values used by Patel and Teja (Patel and Teja, 1982) were not reported. The *m* value in Eq. 4.30 and the parameter ζ_c were simultaneously fitted to vapour pressure and density data for several long-chain n-alkanes in the range n-C_{12} to n-C_{36}.

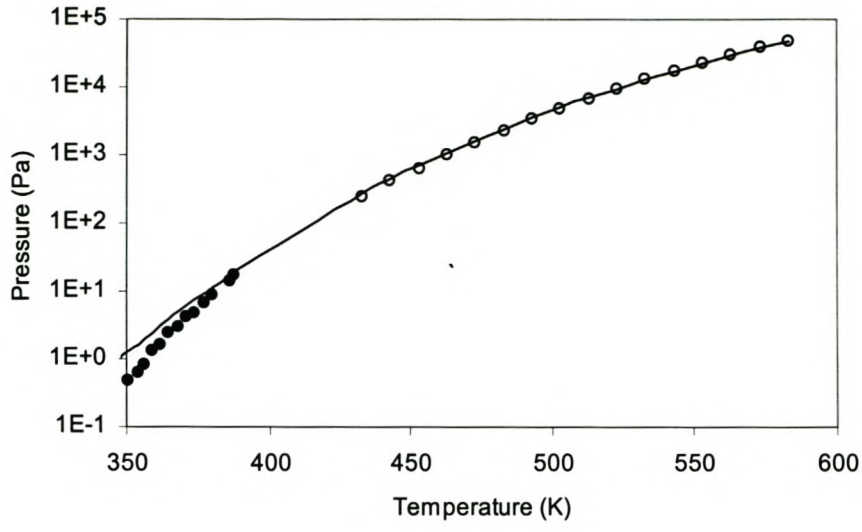

Figure 4-12. Vapour pressure of n-eicosane. — PT EOS. Experimental data from Piacente et al. (Piacente, Fontana et al., 1994) (•) and Morgan et al. (Morgan and Kobyashi, 1994) (o). RMS error for Piacente et al. data = 100%.

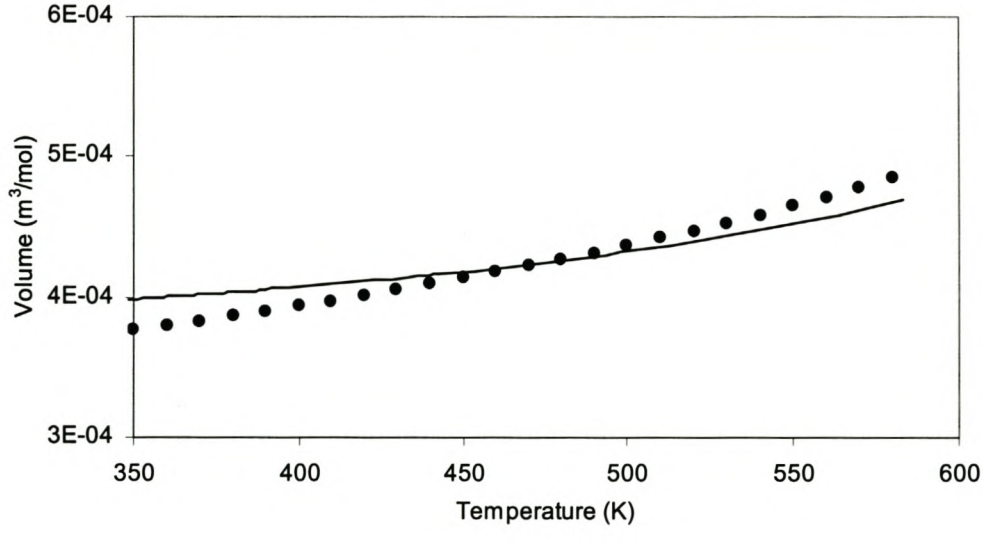

Figure 4-13. Saturated liquid volume of n-eicosane. — PT EOS. Data points (•) calculated from the correlation tabulated by Thomas (Liley, Thomas et al., 1997). RMS error = 4%.

The literature sources for the vapour pressure and liquid volume data used in the regression are shown in Table 4-3.

Table 4-3. Pure component vapour pressure and liquid volume data sources.

n-Alkane	Data source	
	Vapour pressure	Liquid volume
n-C_{10}	1	1
n-C_{12}	2	4
n-C_{14}	2	4
n-C_{16}	2	4
n-C_{18}	2	4
n-C_{19}	2	4
n-C_{20}	2, 3	4
n-C_{24}	2, 3	5
n-C_{28}	2, 3	5
n-C_{36}	3	5

1. (Liley, Thomas et al., 1997), table 2-249
2. (Morgan and Kobyashi, 1994)
3. (Piacente, Fontana et al., 1994)
4. (Liley, Thomas et al., 1997), table 2-30
5. Correlations from Pro/II® 5.1, Simulation Science Inc.

The m and ζ_c parameters of the PT EOS were fitted to the data by using the Levenberg-Marquardt algoritm (Levenberg, 1944; Marquardt, 1963) using the following error function:

Eq. 4.33
$$E = \left(0.8 \frac{\left| P^{\exp} - P^{calc} \right|}{P^{\exp}} + 0.2 \frac{\left| v^{\exp} - v^{calc} \right|}{v^{\exp}} \right)^2$$

A greater weight was assigned to the vapour pressure error than the liquid volume error, since accurate vapour pressure prediction is more important in phase equilibrium calculations than accurate volume calculations. The resulting parameters were correlated as follows:

Eq. 4.34
$$m = 0.63 + 0.8695\omega$$

Eq. 4.35 $$\zeta_c = 0.255 + 0.12\exp(-2\omega)$$

This modification to the PT EOS is called mPT. Note that these correlations were fitted to data for long-chain n-alkanes, and should not be used for small or polar molecules. The original correlations are used for small molecules. The vapour pressure of n-eicosane has been calculated using the PT EOS with *m* and ζ_c using Eq. 4.34 and Eq. 4.35 (see Figure 4-14 below).

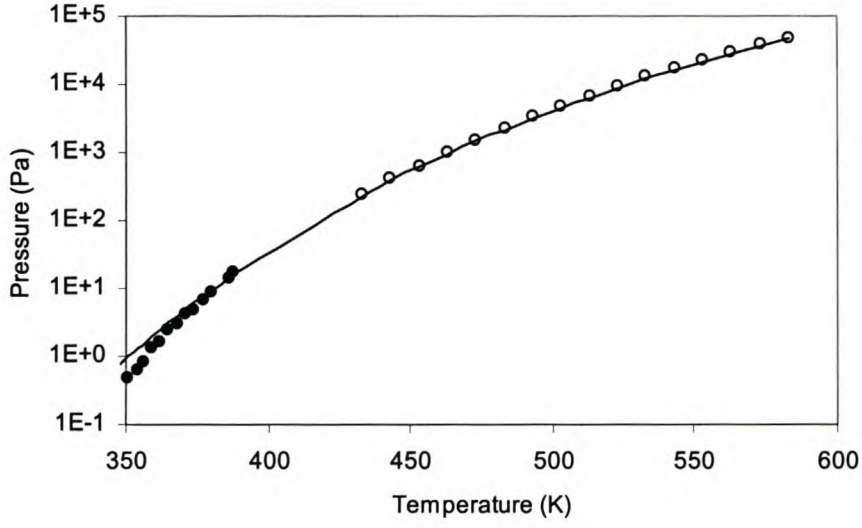

Figure 4-14. Vapour pressure of n-eicosane. — PT EOS using Eq. 4.34 and Eq. 4.35. For symbols see Figure 4-12. RMS error for Piacente et al. data = 60%.

A definite improvement in the low temperature region of the vapour pressure curve is observed, but there is still a systematic deviation close to 350 K.

It is possible that the vapour pressure prediction of this EOS can be further improved by an alpha function (Eq. 4.30) with a more complex temperature dependence. Numerous alpha functions with several adjustable parameters have been proposed (e.g. (Mathias and Copeman, 1983; Twu et al., 1991; Patel, 1996; Souahi et al., 1998; Gasem et al., 2001)). The following alpha correlations containing two adjustable parameters were selected for correlation of the n-alkane vapour pressure data:

Eq. 4.36 $$\alpha = \left(1+m\left(1-\sqrt{T_r}\right)\right)^2$$ $$m = m_0 + m_1\left(1+\sqrt{T_r}\right)\left(0.7-T_r\right)$$ (Stryjek and Vera, 1986)

Eq. 4.37 $$\alpha = 1+m(1-T_r)+n\left(1-\sqrt{T_r}\right)^2$$ (Soave, 1993)

Eq. 4.38 $$\alpha = T_r^{2(m-1)}\exp\left(n\left(1-T_r^{2m}\right)\right)$$ (Twu, 1988)

The alpha correlation of Twu et al. (Eq. 4.38) proved to be the most flexible, and the *m* and *n* parameters of Eq. 4.38 and ζ_c were fitted to the pure component data in Table 4-3. The pure component parameters were then correlated in terms of acentric factors:

Eq. 4.39 $$m = 0.83216 - 0.08569\omega$$

Eq. 4.40 $$n = 0.1589 + 0.4271\omega$$

Eq. 4.41 $$\zeta_c = 0.255 + 0.1\exp(-2\omega)$$

This modification to the PT EOS is called mPT1. The original PT correlations are used for small molecules. The mPT1 EOS was used to calculate the vapour pressure of n-eicosane (see Figure 1-15). The prediction of n-eicosane vapour pressure greatly improved in the low temperature, while retaining the good fit at higher temperatures. An even better fit of the n-eicosane vapour pressure is obtained when using *m*, *n* and ζ_c parameters fitted directly to the data, but the generalised correlations (Eq. 1.39 to Eq. 1.41) cause a slight decrease in accuracy.

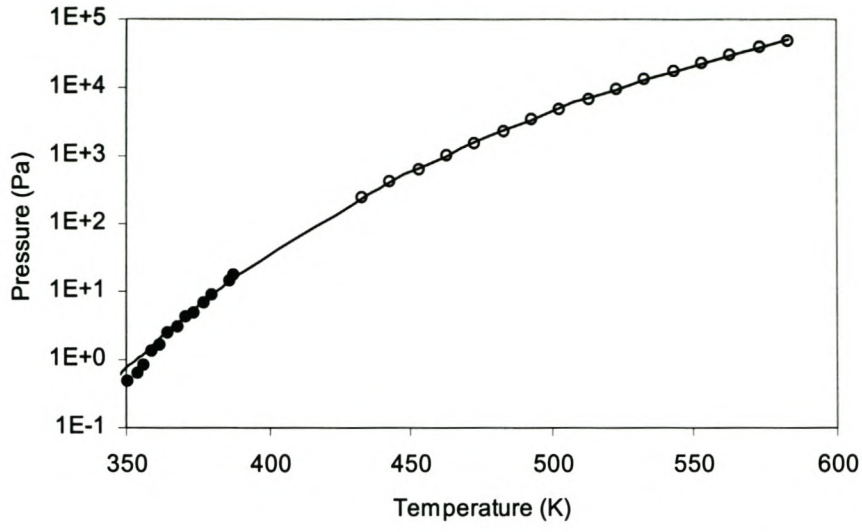

Figure 4-15. Vapour pressure of n-eicosane. — mPT1 EOS. For symbols see Figure 4-12. RMS error for Piacente et al. data = 38%.

Mixture parameters for use in multiphase equilibrium calculations are calculated using quadratic mixing rules for both the *a* and *b* parameters, with a linear mixing rule for the *c* parameter:

Eq. 4.42 $$a_m = \sum_i \sum_j x_i x_j a_{ij}$$

Eq. 4.43 $$b_m = \sum_i \sum_j x_i x_j b_{ij}$$

Eq. 4.44 $$a_{ij} = (1 - k_{ij})\sqrt{a_i a_j}$$

Eq. 4.45 $$b_{ij} = (1 - l_{ij})\frac{(b_i + b_j)}{2}$$

Eq. 4.46 $$c_m = \sum_i x_i c_i$$

The interaction parameters k_{ij} and l_{ij} are fitted to phase equilibrium data, and is used to correct inaccuracies in the underlying equation of state.

4.2.5. Chen equation of state

Walsh and Gubbins (Walsh and Gubbins, 1990) developed an expression for the repulsive compressibility factor of hard bodies of various geometries:

Eq. 4.47 $$z_{rep} = 1 + (2\alpha - 1)\frac{4\eta - 2\eta^2}{(1-\eta)^3} + 2(\alpha - 1)\left(\frac{\eta}{2-\eta} - \frac{3\eta}{1-\eta}\right)$$

with α the nonspherical factor and η the packing fraction. This equation reduces to the Carnahan-Starling expression (Carnahan and Starling, 1969) for hard spheres when α=1. Chen, Chou and Chen (Chen et al., 1996) simplified the repulsive term of Walsh and Gubbins as follows:

Eq. 4.48 $$z_{rep} = \frac{v + K_1 b}{v - K_2 b}$$

where K_1 and K_2 are adjustable parameters fitted to Eq. 4.47 up to a packing fraction of η=0.5, and a range of acentric factors. They further proposed a simple attractive term incorporated with Eq. 4.48 to form their EOS:

Eq. 4.49 $$P = \frac{RT}{v}\left(\frac{v + K_1 b}{v - K_2 b}\right) - \frac{a}{v(v + c)}$$

The constants *a*, *b* and *c* are expressed in terms of the critical constants through use of Eq. 4.2 and Eq. 4.23:

Eq. 4.23 $$\frac{P_c v_c}{RT_c} = \zeta_c$$

Eq. 4.50 $$a = \Omega_a A(T)\frac{R\ T_c^2}{P_c}$$

Eq. 4.51 $$b = \Omega_a B(T)\frac{R\ T_c}{P_c}$$

Eq. 4.52 $$c = \Omega_c \frac{R\,T_c}{P_c}$$

The constants Ω_a, Ω_b and Ω_c are determined as follows:

Eq. 4.53 $$\Omega_c = \frac{\zeta_c^3 - K_1\Omega_b\Omega_c}{K_2\Omega_b}$$

Eq. 4.54 $$\Omega_c = 1 + K_2\Omega_b - 3\zeta_c$$

Ω_b is the smallest positive root of

Eq. 4.55 $$K_2^3\Omega_b^3 + (2K_1K_2 + 2K_2^2 - 3K_2^2\zeta_c)\Omega_b^2 + (K_1 + K_2 - 3K_1\zeta_c - 3K_2\zeta_c + 3K_1\zeta_c^2)\Omega_b - \zeta_c^3 = 0$$

The two parameters K_1 and K_2 are correlated as a function of the nonspherical factor α:

Eq. 4.56 $$K_1 = 4.8319\alpha - 1.5515$$

Eq. 4.57 $$K_2 = 1.8177 - 0.1778\alpha^{-1.3686}$$

The *A(T)* and *B(T)* functions are as follows:

Eq. 4.58 $$A(T) = \left[1 + F_1 \ln T_r + F_2\left(1 - \sqrt{T_r}\right)^2\right]^2$$

Eq. 4.59 $$B(T) = \left[1 + F_3 \ln A(T)\right]^2$$

Eq. 4.60 $$F_1 = -0.6525 - 2.1911\omega + 4.7537\omega^2 - 11.3392\omega^3 + 8.6979\omega^4$$

Eq. 4.61 $$F_2 = -2.1278 - 7.8507\omega + 29.846\omega^2 - 74.902\omega^3 + 59.089\omega^4$$

Eq. 4.62 $$F_3 = 1.0542 + 0.4905\omega - 0.8984\omega^2 + 4.0568\omega^3 + 2.9448\omega^4$$

The α factor and the empirical critical compressibility factor were correlated with the acentric factor:

Eq. 4.63 $$\alpha = 1.2946 + 4.5671\omega - 4.6784\omega^2 + 6.2596\omega^3$$

Eq. 4.64 $$\zeta_c = 0.291 - 0.08\omega$$

For fluid mixtures the following mixing rules were used:

Eq. 4.65 $$\alpha_m = \sum_i x_i \alpha_i$$

Eq. 4.66 $$a_m = \sum_i \sum_j x_i x_j a_{ij}$$

Eq. 4.67 $$b_m = \sum_i \sum_j x_i x_j b_{ij}$$

Eq. 4.68 $$a_{ij} = (1 - k_{ij})\sqrt{a_i a_j}$$

Eq. 4.69 $$b_{ij} = (1 - l_{ij})\frac{(b_i + b_j)}{2}$$

Eq. 4.70 $$c_m = \sum_i x_i c_i$$

Both the *a* and *b* parameters are complex functions of temperature and acentric factor, which makes the EOS quite flexible. In Figure 4-16 the saturation pressure-volume curve and volumes along the 350 K isotherm are calculated with this equation, for ethane and carbon dioxide.

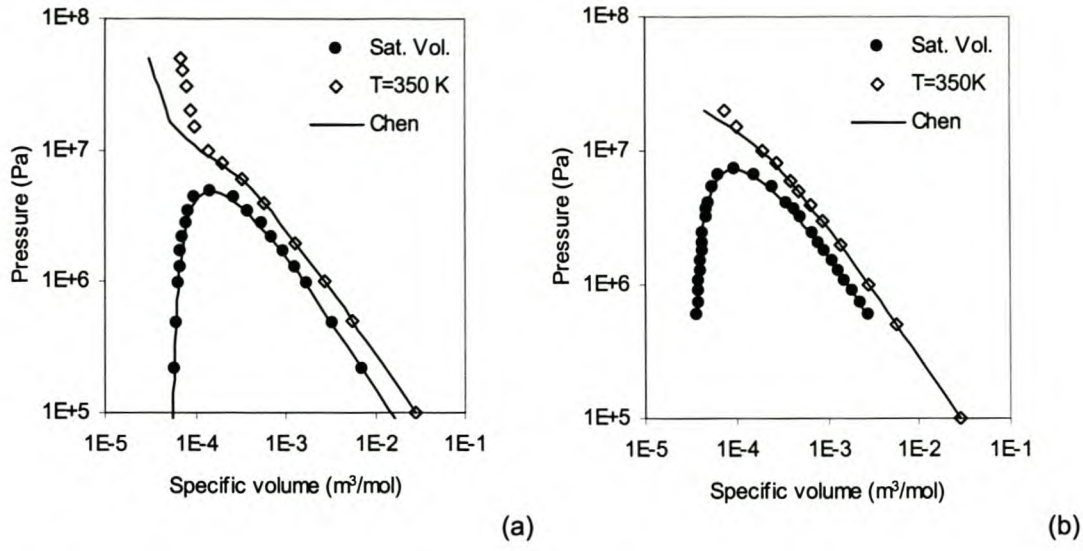

Figure 4-16. Plot of experimental volumes (symbols) compared with calculated volumes (curves) from the Chen EOS. a) Ethane (RMS errors: P^{sat} = 0.4%, V_l^{sat} = 3.2%). b) Carbon dioxide (RMS errors: P^{sat} = 0.4%, V_l^{sat} = 1.6%). Experimental data compiled by Liley (Liley, Thomas et al., 1997).

It is clear that this EOS predicts saturation pressures and volumes very accurately. The fluid volumes for the 350 K isotherm is predicted accurately below the critical pressure, but deviates considerably when the pressure is above the critical pressure of the pure component. This was observed for both ethane and carbon dioxide. The Chen EOS was used to calculate the vapour pressure of n-eicosane. In Figure 4-17 this calculated vapour pressures are compared with experimental values. It was found that the Chen EOS gave a fair prediction of vapour pressures above 450 K, but systematic errors at lower temperatures were observed. The liquid volume predictions of the Chen EOS for n-eicosane deviates by an average of 20% from the pure component correlation.

It appears as if this EOS cannot be used to extrapolate over wide ranges of temperatures and pressures not used in the regression of the parameters. Only saturated properties (T_R < 1) were used during the regression of this EOS, which might explain the deviations between experimental and calculated specific volumes of the 350 K isotherm (T_R = 1.15). The poor performance of the Chen EOS for the n-eicosane data might be due to the fact that n-eicosane was not used during the regression of the EOS parameters. The *a* and *b* parameters of this EOS are complex functions of temperature and acentric factor (see Eq. 4.58 - Eq. 4.62), which might not extrapolate reliably.

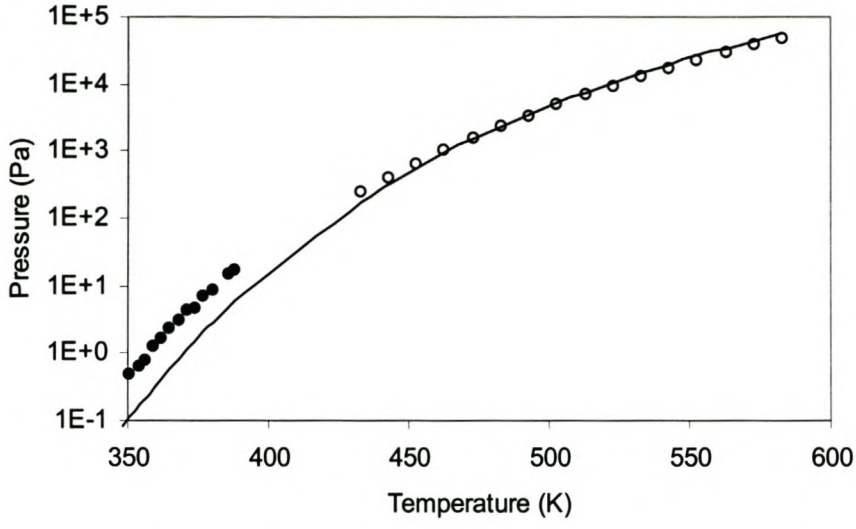

Figure 4-17. Vapour pressure of n-Eicosane. — Chen EOS. Experimental data from Piacente et al. (Piacente, Fontana et al., 1994) (•) and Morgan et al. (Morgan and Kobyashi, 1994) (o). RMS error for Piacente et al. data = 50%.

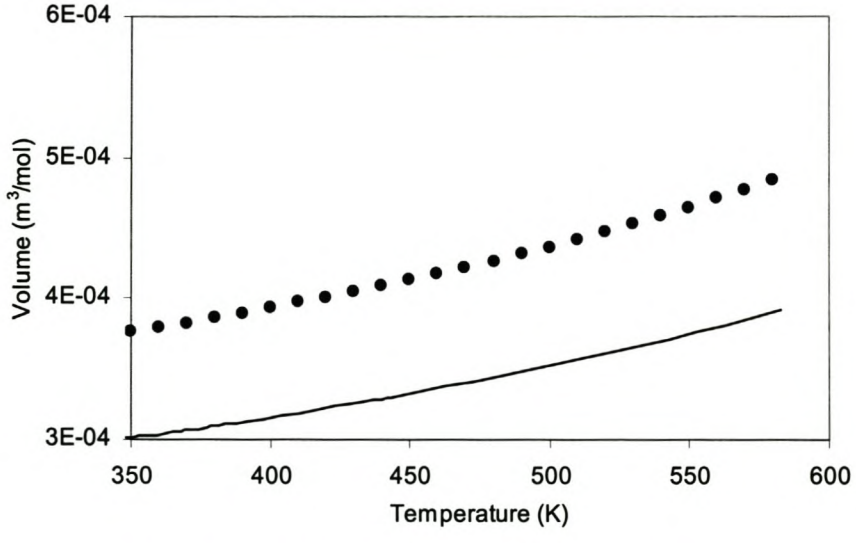

Figure 4-18. Saturated liquid volume of n-eicosane. — Chen EOS. Data points (•) calculated from the correlation tabulated by Thomas (Liley, Thomas et al., 1997). RMS error = 19%.

4.2.6. The PC-SAFT equation

The Perturbed-Chain SAFT (Gross, 2000; Gross and Sadowski, 2000) equation of state adopts a hard-sphere chain fluid as a reference fluid. The

equation of state consists of a reference hard-chain equation of state and a perturbation contribution

Eq. 4.71 $$\frac{A}{NkT} = \frac{A^{hc}}{NkT} + \frac{A^{pert}}{NkT}$$

Eq. 4.72 $$z = z^{hc} + z^{pert}$$

where z is the compressibility factor, A is the Helmholtz free energy, N is the total number of molecules, k is the Boltzmann constant, and superscripts *hc* and *pert* denote the hard-sphere chain reference equation of state, and the perturbation contribution, respectively. In this terminology the reference equation of state reduces to ideal-gas behaviour at the zero-density limit.

Based on Wertheim's thermodynamic perturbation theory Chapman et al. (Chapman et al., 1988) developed an equation of state, which for hard-sphere chains comprising m segments is given by

Eq. 4.73 $$\frac{A^{hc}}{NkT} - \frac{A^{ideal}}{NkT} = m\frac{A^{hs}}{NkT} - \sum_i x_i (m_i - 1) \ln g_{ii}^{hs}(\sigma_{ii})$$

Eq. 4.74 $$z^{hc} = 1 + m(z^{hs} - 1) - \sum_i x_i (m_i - 1)\rho \frac{\partial \ln g_{ii}^{hs}}{\partial \rho}$$

Eq. 4.75 $$m = \sum x_i m_i$$

where x_i is the mole fraction of chains of component i, m_i is the number of segments in a chain of component i, ρ is the total number density of molecules, g_{ii}^{hs} is the radial pair distribution function for segments of component i in the hard sphere system, and superscript *hs* indicates quantities of the hard-sphere system. Expressions of Boublik (Boublik, 1970) and Mansoori et al. (Mansoori et al., 1971) are used for mixtures of the hard-sphere reference system in Eq. 4.73 and Eq. 4.74, given by

Eq. 4.76 $$\frac{A^{hs}}{NkT} = \frac{1}{\zeta_0}\left[\frac{3\zeta_1\zeta_2}{1-\zeta_3} + \frac{\zeta_2^3}{\zeta_3(1-\zeta_3)^2} + \left(\frac{\zeta_2^3}{\zeta_3^2} - \zeta_0\right)\ln(1-\zeta_3)\right]$$

Eq. 4.77 $$z^{hs} = \frac{1}{(1-\zeta_3)} + \frac{3\zeta_1\zeta_2}{\zeta_0(1-\zeta_3)^2} + \frac{3\zeta_2^3 - \zeta_3\zeta_2^3}{\zeta_0(1-\zeta_3)^3}$$

Eq. 4.78 $$g_{ii}^{hs} = \frac{1}{(1-\zeta_3)} + \left(\frac{d_i d_j}{d_i + d_j}\right)\frac{3\zeta_2}{(1-\zeta_3)^2} + \left(\frac{d_i d_j}{d_i + d_j}\right)^2 \frac{2\zeta_2^2}{(1-\zeta_3)^3}$$

where

Eq. 4.79 $$\zeta_m = \frac{\pi}{6}\rho\sum_i x_i m_i d_i^m \qquad m = \{0,1,2,3\}$$

with d_i being a temperature dependent segment diameter of component i , according to

Eq. 4.80 $$d_i = \sigma_{ii}\left(1 - 0.12\exp\left(-3\varepsilon_{ii}/kT\right)\right)$$

In the above equations m_i, σ_{ii}, and ε_{ii} are the pure component parameters (segment number, segment diameter, and interaction-energy parameter).
The packing fraction η is defined by

Eq. 4.81 $$\eta = \zeta_3$$

The second-order perturbation theory of Barker and Henderson was extended to chain molecules. The perturbation contribution is the sum of the first- and second-order term, according to

Eq. 4.82 $$\frac{A^{pert}}{NkT} = \frac{A_1}{NkT} + \frac{A_2}{NkT}$$

Van der Waals one fluid mixing rules are adopted here to extend the perturbation terms to mixtures.

Eq. 4.83 $$\frac{A_1}{NkT} = -2\pi\rho I_1(\eta, m)\sum_i\sum_j x_i x_j m_i m_j \frac{\varepsilon_{ii}}{kT}\sigma_{ij}^3$$

Eq. 4.84 $$\frac{A_2}{NkT} = -\pi\rho m\left(z^{hc} + \rho\frac{\partial z^{hc}}{\partial\rho}\right)^{-1} I_2(\eta, m)\sum_i\sum_j x_i x_j m_i m_j \left(\frac{\varepsilon_{ii}}{kT}\right)^2 \sigma_{ij}^3$$

Conventional mixing rules are employed to determine the parameters between a pair of unlike segments:

Eq. 4.85 $$\sigma_{ij} = \frac{1}{2}(\sigma_{ii} + \sigma_{jj})$$

Eq. 4.86 $$\varepsilon_{ij} = (1 - k_{ij})\sqrt{\varepsilon_{ii}\varepsilon_{jj}}$$

The one-fluid mixing concept is used to obtain the compressibility term of the second order perturbation term:

Eq. 4.87 $$\left(z^{hc} + \rho\frac{\partial z^{hc}}{\partial\rho}\right) = 1 + m\frac{8\eta - 2\eta^2}{(1-\eta)^4} + (1-m)\frac{20\eta - 27\eta^2 + 12\eta^3 - 2\eta^4}{[(1-\eta)(2-\eta)]^2}$$

In these equations, the integrals over the radial pair distribution function of chain-molecules are replaced by 6th order power series in density:

Eq. 4.88 $$I_1(\eta, m) = \sum_{i=0}^{6} a_i(m)\eta^i$$

Eq. 4.89 $$I_2(\eta, m) = \sum_{i=0}^{6} b_i(m)\eta^i$$

where $a_i(m)$ and $b_i(m)$ are coefficients of the power series in density, each depending upon segment number. The dependence of each of the power series coefficients on segment number are described with the following relation:

Eq. 4.90 $$a_i(m) = a_{0i} + \frac{m-1}{m} a_{1i} + \frac{(m-1)(m-2)}{m^2} a_{2i}$$

These model constants a_{0i}, a_{1i}, and a_{2i} as well as b_{0i}, b_{1i}, and b_{2i} were fitted to thermophysical properties of pure n-Alkanes. They are given in Table 4-4 below.

Table 4-4. Constants used in Eq. 4.90.

i	a_{0i}	a_{1i}	a_{2I}	b_{0i}	b_{1i}	b_{2I}
0	0.79198281	-0.62311554	-0.06777556	0.79198281	-0.62311554	-0.06777556
1	1.07148651	0.48573437	0.02837411	2.14297303	0.97146874	0.05674823
2	0.91474661	1.12485267	0.09612281	2.74423982	3.37455809	0.28836841
3	-7.81060651	-2.09485016	0.06815027	-31.2424260	-8.37940062	0.27260110
4	25.7855977	9.45049823	0.05980187	128.927988	47.2524911	0.29900933
5	-56.9822877	-17.1027262	0.28660979	-341.893726	-102.616357	1.71965874
6	41.9308941	7.77610281	-0.74701698	293.516259	54.4327197	-5.22911885

The compressibility factor is given by

Eq. 4.91 $$z^{pert} = z_1 + z_2$$

and the perturbation terms of first- and second-order are given by

Eq. 4.92 $$z_1 = -2\pi\rho \frac{\partial(\eta I_1)}{\partial \eta} \sum_i \sum_j x_i x_j m_i m_j \frac{\varepsilon_{ii}}{kT} \sigma_{ij}^3$$

with

Eq. 4.93 $$\frac{\partial(\eta I_1)}{\partial \eta} = \sum_{j=0}^{6} a_j(m)(j+1)\eta^j$$

and

Eq. 4.94 $$z_2 = -\pi\rho m C_1 \left[\frac{\partial(\eta I_2)}{\partial \eta} - C_2 \eta I_2(\eta, m) \right] \sum_i \sum_j x_i x_j m_i m_j \left(\frac{\varepsilon_{ii}}{kT} \right)^2 \sigma_{ij}^3$$

where

Eq. 4.95 $$\frac{\partial(\eta I_2)}{\partial \eta} = \sum_{j=0}^{6} b_j(m)(j+1)\eta^j$$

C_1 and C_2 are abbreviations defined as

Eq. 4.96 $$C_1 = \left(1 + m\frac{8\eta - 2\eta^2}{(1-\eta)^4} + (1-m)\frac{20\eta - 27\eta^2 + 12\eta^3 - 2\eta^4}{[(1-\eta)(2-\eta)]^2}\right)^{-1}$$

Eq. 4.97 $$C_2 = C_1\left(m\frac{8 + 20\eta - 4\eta^2}{(1-\eta)^5} + (1-m)\frac{40 - 48\eta + 12\eta^2 + 2\eta^3}{[(1-\eta)(2-\eta)]^3}\right)$$

This equation has a strong theoretical framework, and it is claimed to accurately predict phase equilibria in a wide variety of systems (Gross, 2000). The PE computer program developed by Phfol et al. (Pfohl et al., 2000) was used to generate pure component properties for the PC-SAFT EOS, shown in Figure 4-19 to Figure 4-21.

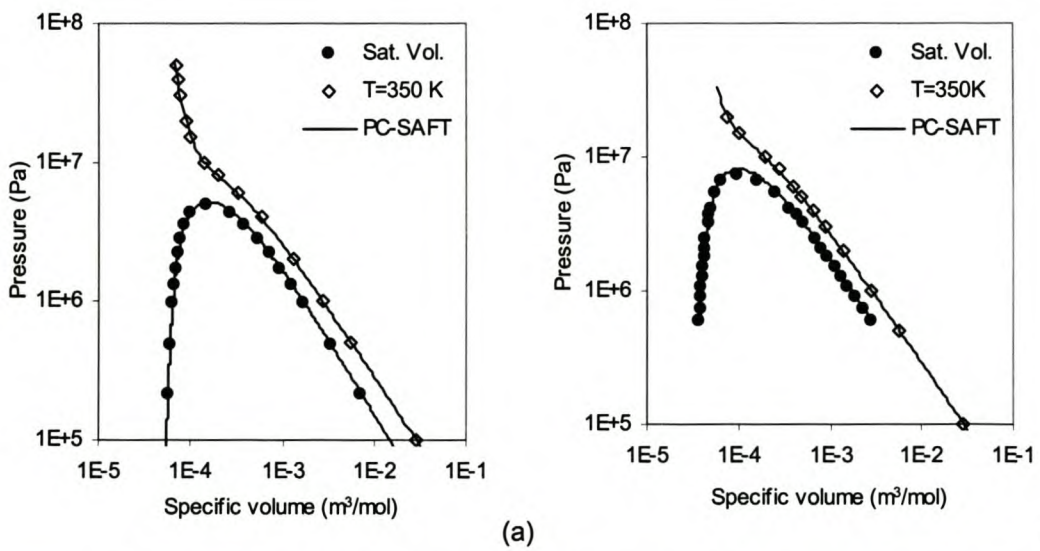

Figure 4-19. Plot of experimental volumes (symbols) compared with calculated volumes (curves) from the PC-SAFT EOS. a) Ethane (RMS errors: P^{sat} = 0.6%, V_l^{sat} = 6.5%). b) Carbon dioxide (RMS errors: P^{sat} = 0.2%, V_l^{sat} = 6.6%). Experimental data compiled by Liley (Liley, Thomas et al., 1997).

PC-SAFT gives a very good prediction of the P*v*T properties of both ethane and CO_2 in both the saturation and supercritical region.

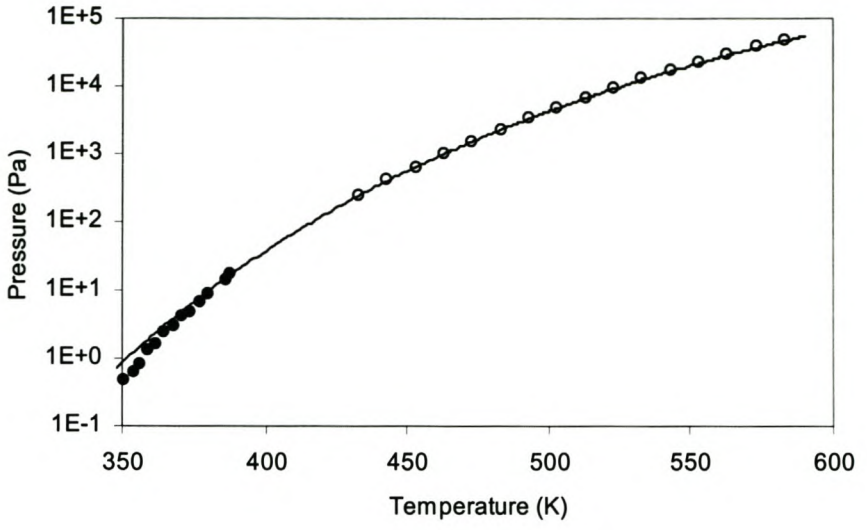

Figure 4-20. Vapour pressure of n-Eicosane. — PC-SAFT EOS. Experimental data from Piacente et al. (Piacente, Fontana et al., 1994) (•) and Morgan et al. (Morgan and Kobyashi, 1994) (o). RMS error for Piacente et al. data = 51%.

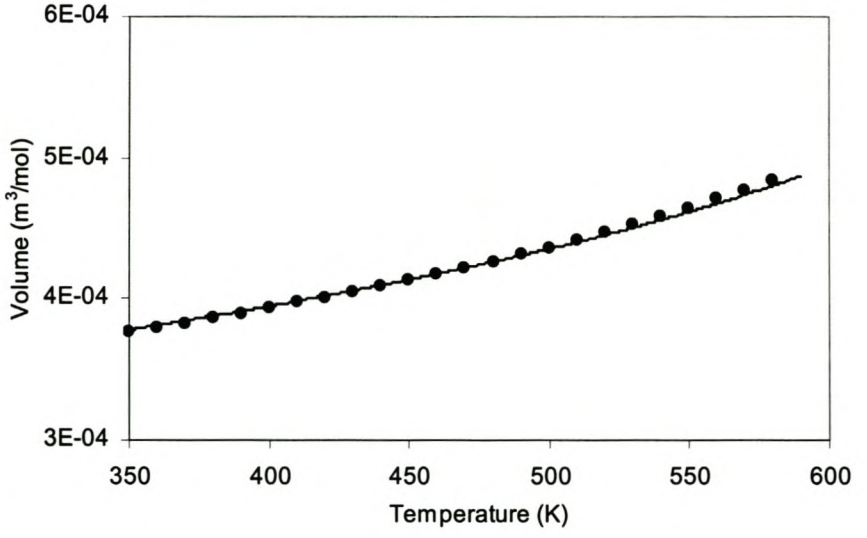

Figure 4-21. Saturated liquid volume of n-eicosane. — PC-SAFT EOS. Data points (•) calculated from the correlation tabulated by Thomas (Liley, Thomas et al., 1997). RMS error = 0.5%.

Vapour pressure calculations for n-eicosane with PC-SAFT are fairly accurate, although a systematic deviation close to 350 K can be seen. This is not as

accurate as the vapour pressure predictions of the SRK EOS. The liquid volume prediction of the PC-SAFT EOS is excellent, the best of all the equations investigated.

4.2.7. Simplified perturbed hard chain theory

The simplified perturbed hard-chain theory (SPHCT EOS) belongs to the family of perturbed hard-chain theory (PHCT) EOS first developed by Beret and Praunsnitz (Beret and Prausnitz, 1975) and Donohue and Prausnitz (Donohue and Prausnitz, 1978). The compressibility factor of the PHCT EOS is given by

Eq. 4.98 $$z = 1 + cz^{rep} + z^{attr}$$

with *c* being Prigogine's parameter (Prigogine, 1957) which represents one third of the total number of density dependent degrees of freedom. The repulsive term was given by Carnahan and Starling (Carnahan and Starling, 1969)

Eq. 4.99 $$z^{rep} = \frac{4\eta - 2\eta^2}{(1-\eta)^3}$$

Eq. 4.100 $$\eta = \frac{\tau v}{v^*}$$

The attractive portion of the compressibility factor, z^{attr}, was obtained from Alder et al. (Alder et al., 1972)

Eq. 4.101 $$z^{attr} = \sum_i \sum_j \frac{A_{ij}}{(\bar{v})^j} \frac{1}{(\bar{T})^i}$$

The constants A_{ji} is listed by Beret et al. (Beret and Prausnitz, 1975). The reduced volume $\bar{v}$ and the reduced temperature $\bar{T}$ is defined as:

Eq. 4.102 $$\bar{v} = \frac{v}{v^*} = \frac{v\sqrt{2}}{N_A s \sigma^3}$$

and

Eq. 4.103 $$\bar{T} = \frac{T}{T^*} = \frac{ckT}{\varepsilon q}$$

The theory assumes that a molecule consists of a number of segments, *s*, having a segmental diameter of σ. The surface area of a segment is *q*, and the surface energy of the segment is ε. Kim et al. (Kim et al., 1986) replaced the z^{attr} term of Alder with a simple expression based on the local composition model of Lee et al. (Lee et al., 1985). For mixtures the attractive term is written as:

Eq. 4.104 $$z^{attr} = -Z_m \frac{\langle cvY \rangle}{v + \frac{\langle cvY \rangle}{c}}$$

where Z_m is the maximum co-ordination number, equal to 36. The mixing rules for the properties are given below:

Eq. 4.105 $$v^* = \sum_i x_i v_i^*$$

Eq. 4.106 $$c = \sum_i x_i c_i$$

Eq. 4.107 $$\langle cvY \rangle = \sum_i \sum_j x_i x_j c_i v_{ji}^* \left[\exp\left(\frac{\varepsilon_{ij} q_i}{2 c_i kT} \right) - 1 \right]$$

Eq. 4.108 $$v_{ij}^* = \frac{N_A s \sigma_{ij}^3}{\sqrt{2}}$$

Eq. 4.109 $$T_{ij}^* = \frac{\varepsilon_{ij} q_i}{c_i k}$$

Eq. 4.110 $$\sigma_{ij} = (1 - l_{ij}) \frac{\sigma_i + \sigma_j}{2}$$

Eq. 4.111 $$\varepsilon_{ij} = (1 - k_{ij}) \sqrt{\varepsilon_{ii} \varepsilon_{jj}}$$

The values of ε and σ were evaluated from the *T**, *v** and *c* parameters for n-alkanes by Kim et al. (Kim, Vimalchand et al., 1986) as follows:

Eq. 4.112 $$\frac{\varepsilon}{k} = 62.5 \quad K$$

Eq. 4.113 $$\frac{N_A s \sigma^3}{\sqrt{2}} = 8.667 \times 10^{-6} \; m^3 / mol$$

Pure component parameters reported by Kim et al. were used for ethane and CO_2. Generalised parameter correlations for *v** and *c* for n-alkanes, developed by Gasem and Robinson (Gasem and Robinson, 1990), were used for the heavy n-alkanes. A simple exponential function in terms of carbon number was used to correlate Gasem and Robinson's *T** values, since their correlation appears to be inconsistent with their reported values:

Eq. 4.114 $$T^* = 215.4 - 81.46 \exp\left(-0.349799(CN - 1)^{0.7462}\right)$$

SPHC gives a good prediction of the P*v*T properties of CO_2, although errors between calculated and experimental liquid volumes for ethane are large close to the critical point.

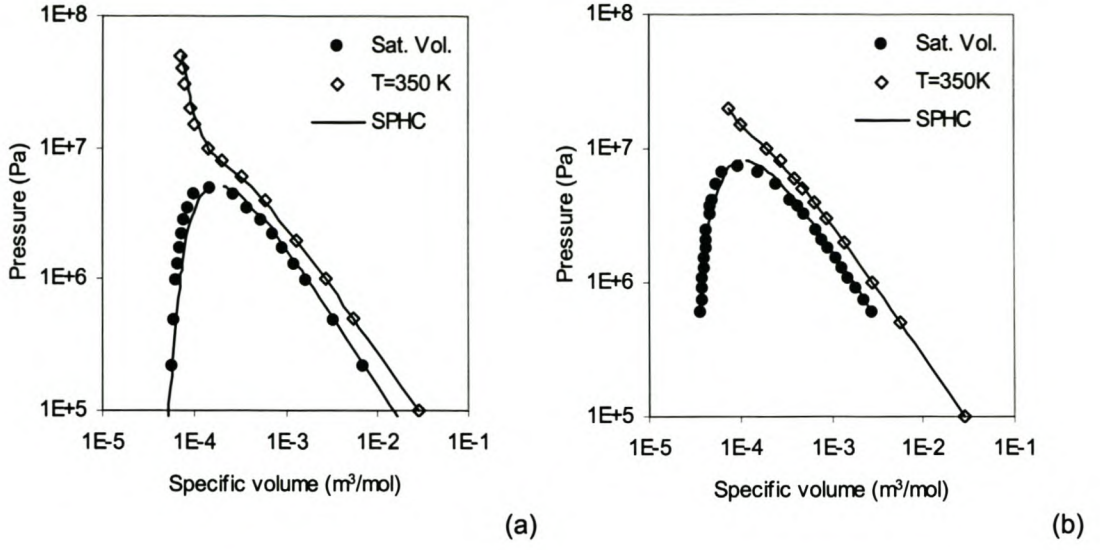

Figure 4-22. Plot of experimental volumes (symbols) compared with calculated volumes (curves) from the SPHC EOS. a) Ethane (RMS errors: P^{sat} = 5.1%, V_l^{sat} = 9.9%). b) Carbon dioxide (RMS errors: P^{sat} = 2.8%, V_l^{sat} = 7.3%). Experimental data compiled by Liley (Liley, Thomas et al., 1997).

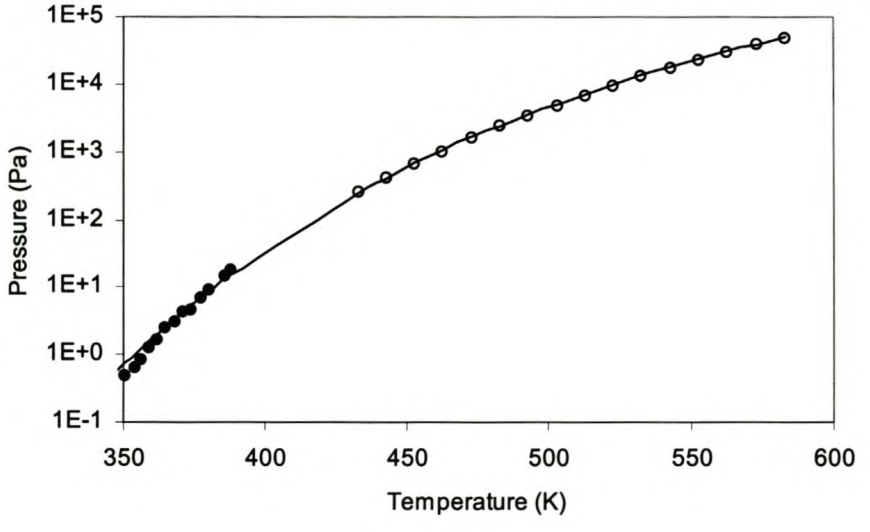

Figure 4-23. Vapour pressure of n-Eicosane. — SPHC EOS. Experimental data from Piacente et al. (Piacente, Fontana et al., 1994) (•) and Morgan et al. (Morgan and Kobyashi, 1994) (o). RMS error for Piacente et al. data = 35%.

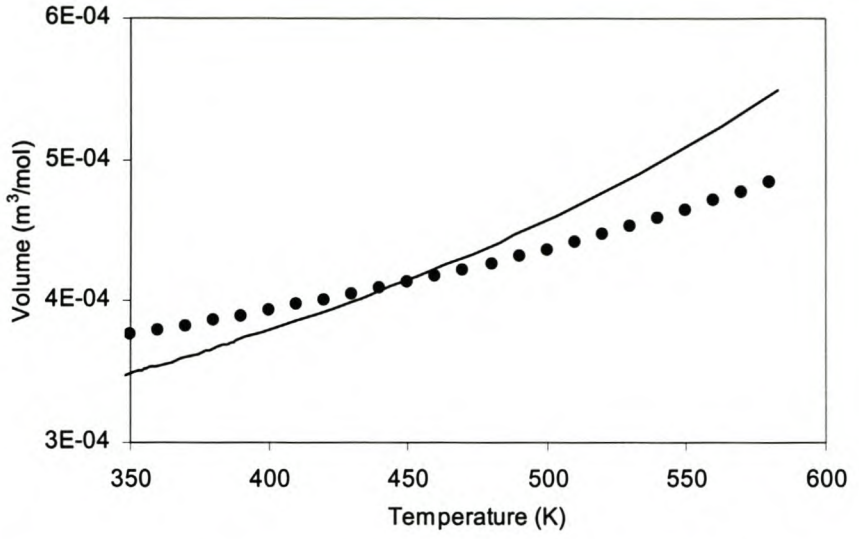

Figure 4-24. Saturated liquid volume of n-eicosane. — SPHC EOS. Data points (•) calculated from the correlation tabulated by Thomas (Liley, Thomas et al., 1997). RMS error = 7%.

The SPHC EOS gives a very good prediction of the vapour pressure of n-eicosane (see Figure 4-23), comparable with the SRK EOS. The liquid volume prediction for n-eicosane is also very good (Figure 4-24).

4.2.8. Cubic simplified perturbed hardsphere chain theory

Following the work of Kim et al. (Kim, Vimalchand et al., 1986), Wang and Guo (Wang and Guo, 1993) modified the attractive portion of the SPHC by reformulation of the coordination number model for mixtures. The attractive term reduces to the SPHC form for pure components, but for mixtures the mixing rule for the energy parameter differs. The repulsive compressibility factor is given by:

Eq. 4.115 $$z_{rep} = \frac{c Z_m a}{v + a}$$

with c the average external degrees of freedom in a molecule, Z_m is the maximum coordination number (Z_m = 36) and

Eq. 4.116 $$a = \sum_i \sum_j x_i x_j v_{ij}^* \left[\exp\left(\frac{\langle T^* \rangle_j}{2T} \right) - 1 \right]$$

Eq. 4.117 $$\left\langle T^{*}\right\rangle_{j}=\frac{\sum_{j} x_i c_i T_{ij}^{*}}{\sum_{j} x_i c_i}$$

v_{ij}^{*} and T_{ij}^{*} are calculated by Eq. 4.108 and Eq. 4.109, using the mixing rules of Eq. 4.110 and Eq. 4.111.

Wang and Guo (Wang and Guo, 1993) also simplified the Carnahan-Starling repulsive term to the following expression:

Eq. 4.118 $$z^{rep}=\frac{4 d_1 \eta}{1-4 d_2 \eta}$$

The values of d_1 and d_2 were determined as 1.11574 and 0.44744 respectively. This simplification reduced this EOS to a cubic polynomial in volume, which can be solved analytically. The original SPHC EOS reduced to a 5th order polynomial in volume, which has to be solved with iterative techniques.

The pure component parameters for ethane and CO_2 were taken from the original publication (Wang and Guo, 1993), while the published correlations were used for the longer chain n-alkanes.

PvT of ethane and CO_2 are compared with predicted values calculated with the CSPHC EOS in Figure 4-25. The errors are similar to that of the SPHC EOS. The vapour pressure of n-eicosane is calculated with the CSPHC EOS and compared with experimental data in Figure 4-26. The CSPHC EOS consistently under-predicts the vapour pressure over the whole temperature range shown.

Experimental liquid volumes of n-eicosane are compared with liquid volumes calculated with the CSPHC EOS in Figure 4-27. Even though the CSPHC EOS poorly represents the vapour pressure of n-eicosane, the liquid volumes are predicted quite accurately.

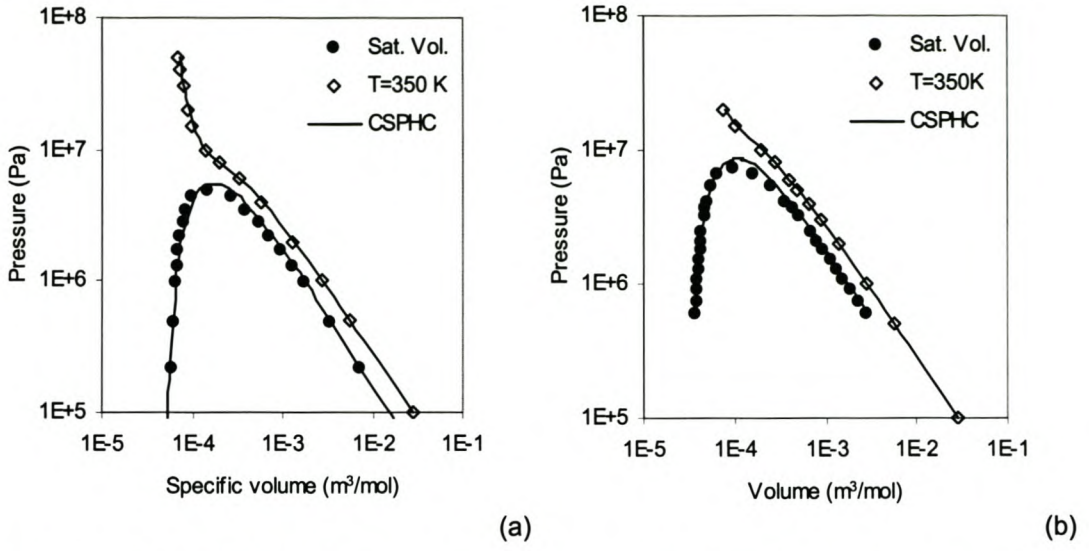

Figure 4-25. Plot of experimental volumes (symbols) compared with calculated volumes (curves) from the CSPHC EOS. a) Ethane (RMS errors: P^{sat} = 3.3%, V_l^{sat} = 8.2%). b) Carbon dioxide (RMS errors: P^{sat} = 0.8%, V_l^{sat} = 7.5%). Experimental data compiled by Liley (Liley, Thomas et al., 1997).

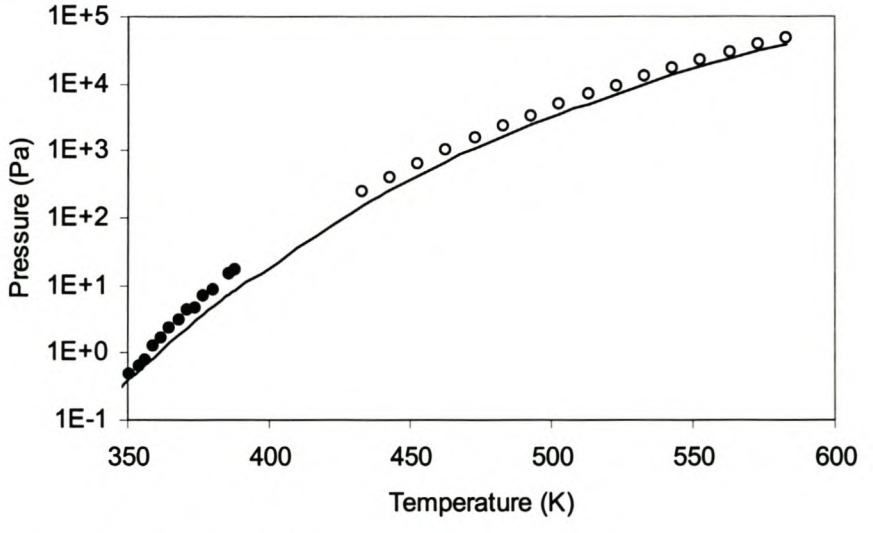

Figure 4-26. Vapour pressure of n-Eicosane. — CSPHC EOS. Experimental data from Piacente et al. (Piacente, Fontana et al., 1994) (•) and Morgan et al. (Morgan and Kobyashi, 1994) (o). RMS error for Piacente et al data = 36%.

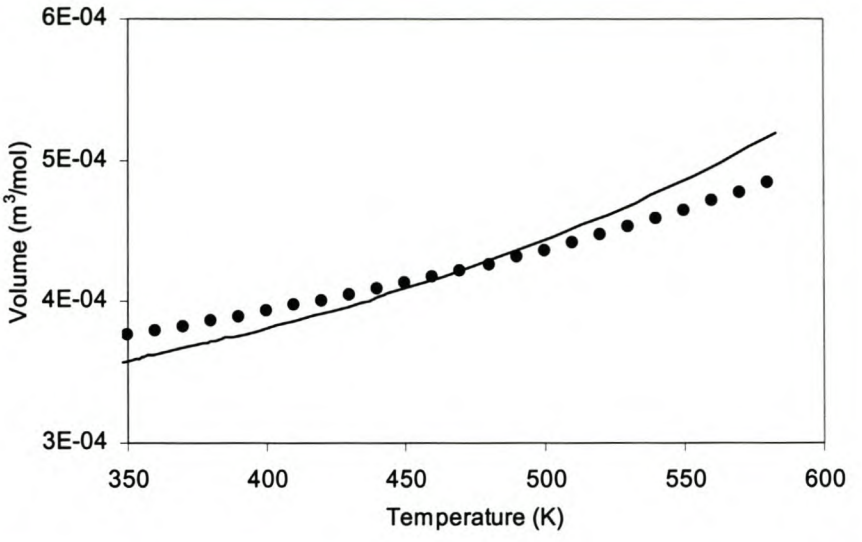

Figure 4-27. Saturated liquid volume of n-eicosane. (—) CSPHC EOS. Data points (•) calculated from the correlation tabulated by Thomas (Liley, Thomas et al., 1997). RMS error = 4%.

4.2.9. Sako equation of state

Sako et al. (Sako et al., 1989) used the generalised van der Waals theory with the Soave-Redlich-Kwong form to decribe the potential field of a molecule. Following Prigogene (Prigogine, 1957), the partition function is factored in an internal and external part, where the external rotational and vibrational degrees of freedom are considered as equivalent translational dgrees of freedom. The resulting equation of state is:

Eq. 4.119 $$P = \frac{RT(v-b+bc)}{v(v-b)} - \frac{a}{v(v+b)}$$

where 3c is the total number of external degrees of freedom per molecule. If parameter c = 1, Eq. 4.119 reduces to the SRK EOS. Parameter c extends the applicability of Eq. 4.119 to large molecules. Parameters a and b are evaluated as follows, using Eq. 4.2:

Eq. 4.120 $$a = a_c \alpha(T)$$

Eq. 4.121 $$a_c = \frac{R^2 T_c^2 (1 + 2D_0 + 2cD_0 + D_0^2 - cD_0^2)(1 + D_0)^2}{3P_c (1 - D_0)^2 (2 + D_0)}$$

Eq. 4.122 $$b = \frac{D_0 R T_c}{3 P_c}$$

D_0 is the smallest positive root of the following function:

Eq. 4.123 $$D_0^3 + (6c - 3)D_0^2 + 3D_0 - 1 = 0$$

Eq. 4.124 $$\alpha(T) = \frac{\alpha_0 (1 - T_r^2) + 2T_r^2}{1 + T_r^2}$$

T_r is the reduced temperature, and α_0 is correlated with the van der Waals volume V_w (cm^3/mol) (calculated using the method of Bondi (Bondi, 1968)) as follows:

Eq. 4.125 $$\alpha_0 = 1.192 + 0.1106 \ln(V_w) + 0.00030734 V_w$$

Values of parameter c for n-alkanes are given by Sako et al. (Sako, Wu et al., 1989). For use in this work, the c values for n-alkanes were successfully correlated using the molar weight, M_r:

Eq. 4.126 $$c = 0.8041 + 0.0122 M_r$$

This c value correlation was also used for carbon dioxide, but α_0 for carbon dioxide was regressed from saturated liquid volume and pressure data, with a value of α_0 =1.71598.

The Sako EOS ability to predict the saturation curve and compressed fluid volumes of ethane and carbon dioxide was investigated as an indication of this equation's suitability to predict solvent properties at conditions close to that encountered in this work. In Figure 4-28 it can be seen that the Sako EOS gives an equally good prediction of the saturation curve and the compressed fluid volume isotherm for both ethane and carbon dioxide. The saturated liquid volume errors however increase close to the critical point.

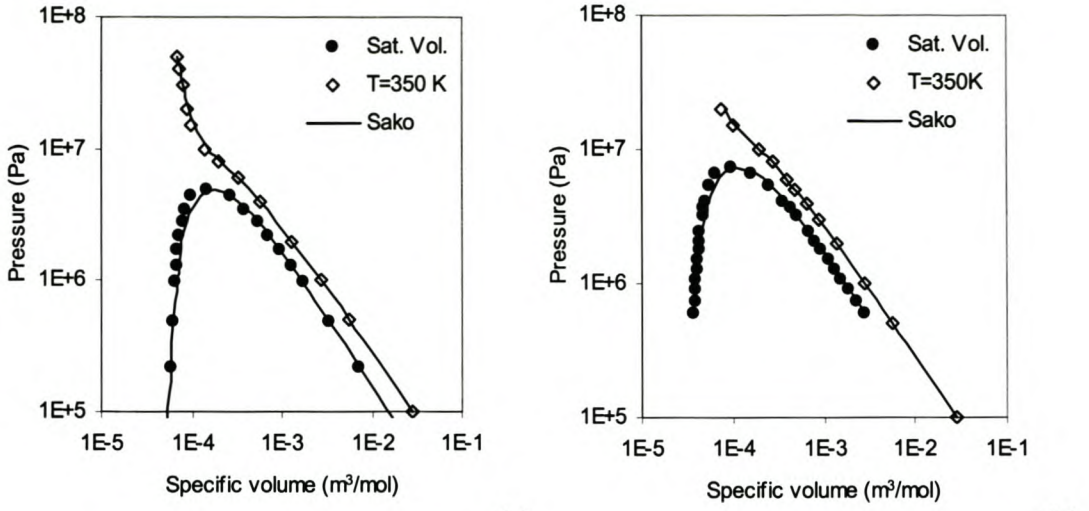

Figure 4-28. Plot of experimental volumes (symbols) compared with calculated volumes (curves) from the Sako EOS. a) Ethane (RMS errors: P^{sat} = 1.9%, V_l^{sat} = 12%). b) Carbon dioxide (RMS errors: P^{sat} = 1.7%, V_l^{sat} = 10%). Experimental data compiled by Liley (Liley, Thomas et al., 1997).

The vapour pressure of n-eicosane, calculated with the Sako EOS, is compared with experimental values in Figure 4-29. Similar to other cubic EOS such as PR or PT, the Sako EOS overestimates the vapour pressure at low temperatures.

The liquid volumes of n-eicosane are compared with calculated liquid volumes using the Sako EOS in Figure 4-30. The liquid volume predictions of the Sako EOS are very accurate.

For fluid mixtures the mixture parameters are calculated as follows:

Eq. 4.127 $$a_m = \sum_i \sum_j x_i x_j a_{ij}$$

Eq. 4.128 $$b_m = \sum_i \sum_j x_i x_j b_{ij}$$

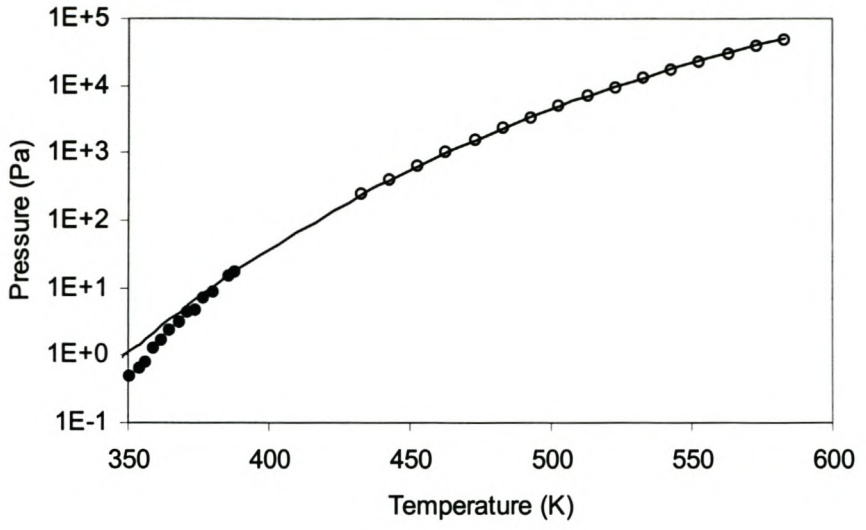

Figure 4-29. Vapour pressure of n-Eicosane. (—) Sako EOS. Experimental data from Piacente et al. (Piacente, Fontana et al., 1994) (•) and Morgan et al. (Morgan and Kobyashi, 1994) (o). RMS error for Piacente et al. data = 83%.

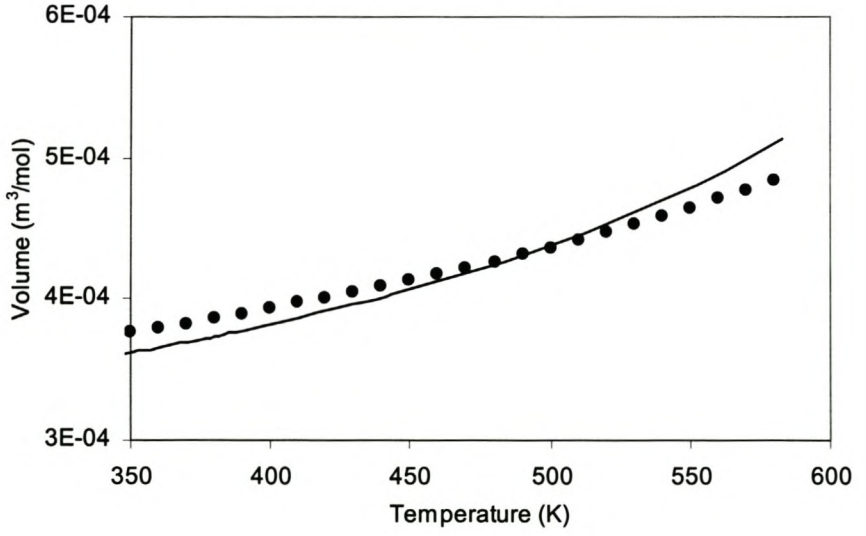

Figure 4-30. Saturated liquid volume of n-eicosane. — Sako EOS. Data points (•) calculated from the correlation tabulated by Thomas (Liley, Thomas et al., 1997). RMS error = 3%.

Eq. 4.129 $$a_{ij} = (1 - k_{ij})\sqrt{a_i a_j}$$

Eq. 4.130 $$b_{ij} = (1 - l_{ij}) \frac{(b_i + b_j)}{2}$$

Eq. 4.131 $$c_m = \sum_i x_i c_i$$

4.3. EOS modelling results of binary phase equilibrium data

During the phase equilibrium modelling stage it was attempted to force the EOS predictions to match the n-alkane solubility in the solvent phase, and to correctly predict compositions close to the mixture critical region, if sufficient data are available. This was done with the aim to predict accurately the composition and solubility of n-alkanes in the extract phase at the expense of less accurate predictions for the solvent solubility in the wax phase.

Initially the interaction parameters of the various EOSs were fitted using a least squares Levenberg-Marquardt algorithm (Levenberg, 1944; Marquardt, 1963) that minimises the error between the experimental and calculated phase compositions. This approach did not always fit the data in the regions of interest; it gave an overall good fit that did not always give a good prediction in the mixture critical region. After a data set was fitted with an EOS using the Levenberg-Marquardt algorithm, the obtained binary interaction parameters were fine-tuned manually to fit the phase equilibria better in the regions of interest.

It was found that the ethane – n-alkane equilibrium data were easier to correlate than the CO_2 – n-alkane data, probably because the ethane is chemically similar to the heavier n-alkanes, while the CO_2 had a strong quadrupole moment. Preliminary tests of the ability of the various equations of state to predict supercritical phase equilibria were done on the system ethane – n-C_{16} at 60 °C.

The following EOS could not fit the phase equilibrium data to the degree of accuracy desired:

- Chen
- PC-SAFT
- SPHC
- CSPHC
- Sako

The quality of the calculated phase boundaries of these equations of state is shown below in Figure 4-31 to Figure 4-35, for various values of the interaction parameters. The Chen EOS could not reproduce the experimental data (Figure 4-31), probably caused by extrapolation of the complex temperature dependence of the *a* and *b* terms of the EOS. This could also explain the deviation of the calculated pure component volumes of ethane and CO_2 for supercritical (350 K) isotherm in Figure 4-16.

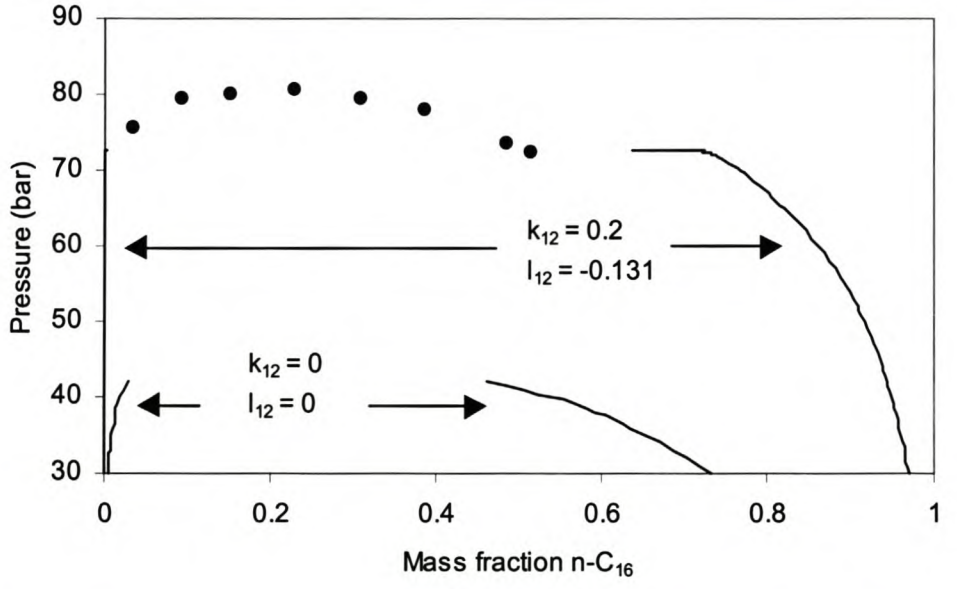

Figure 4-31. Phase equilibrium data (•) for ethane – n-C_{16} (60°C) (du Rand, 2000), with calculated phase boundaries by Chen EOS (—) for different interaction parameter values.

The perturbed chain type EOS (PC-SAFT, SPHC and CSPHC) probably lack accurate enough mixing rules to describe the mixture critical region, with all the perturbed chain EOSs except CSPHC overshooting the mixture critical pressure (see Figure 4-32 to Figure 4-34).

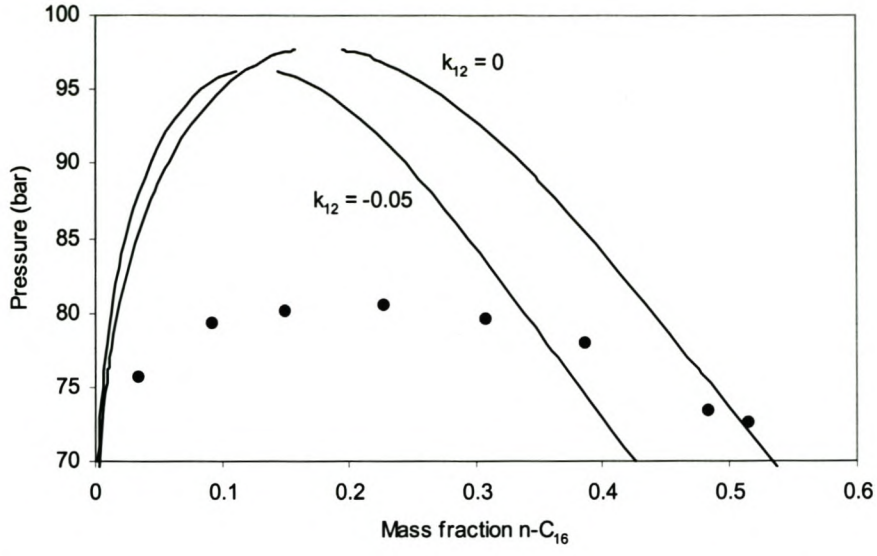

Figure 4-32. Phase equilibrium data (•) for ethane – n-C_{16} (60°C) (du Rand, 2000), with calculated phase boundaries by PC-SAFT EOS (—) for different interaction parameter values.

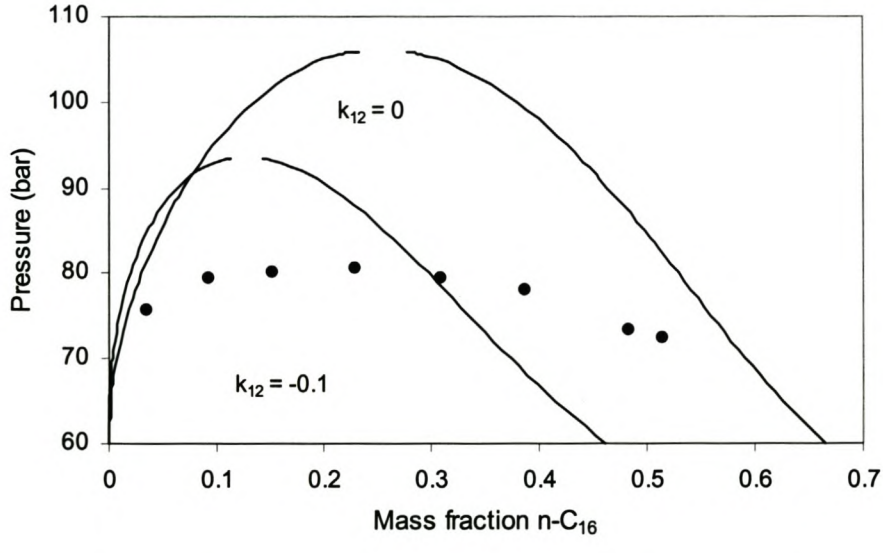

Figure 4-33. Phase equilibrium data (•) for ethane – n-C_{16} (60°C) (du Rand, 2000), with calculated phase boundaries by SPHC EOS (—) for different interaction parameter values.

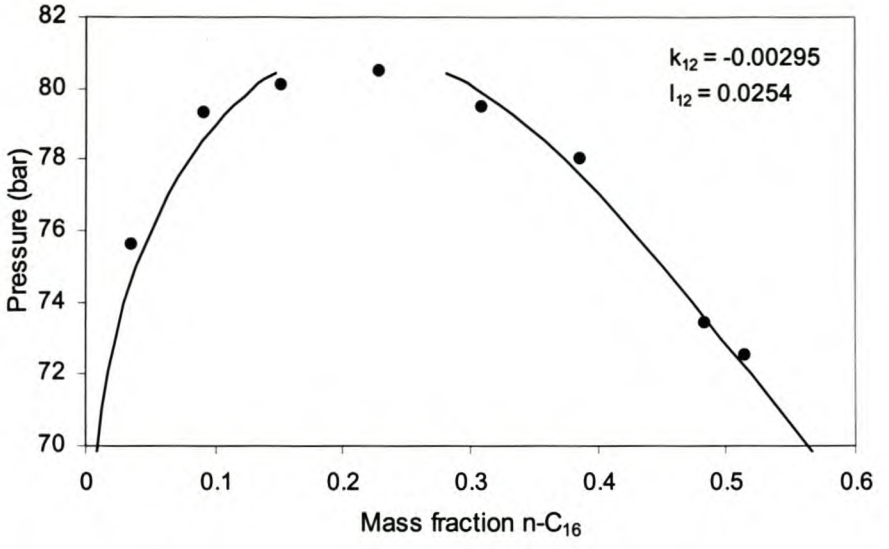

Figure 4-34. Phase equilibrium data (•) for ethane – n-C_{16} (60°C) (du Rand, 2000), with calculated phase boundaries by CSPHC EOS (—).

Although the CSPHC EOS gives a good qualitative description of the phase equilibrium data shown, phase equilibria at 50°C are not correlated satisfactorily. The CSPHC EOS also cannot be used for highly asymmetrical systems such as ethane – n-C_{28}.

Gasem et al. (Gasem and Robinson, 1990) and Peters (Peters et al., 1989) have also commented on the inaccuracy of the SPHC EOS in the vicinity of the mixture critical point. This is unfortunate, since these EOSs have two attractive properties: accurate density predictions, and good phase equilibrium predictions far from the mixture critical point.

Another reason for the poor performance of the perturbed chain type EOS in the mixture critical region can be explained in terms of long-range density fluctuations. A supercritical solvent has a large compressibility and small changes in pressure can cause large changes in density (see Figure 1-6). The large compressibility leads to the presence of long-range fluctuations in density (Sengers, 1994). The extent of these fluctuations increase as a pure component or mixture critical point is approached. Classical EOS based on mean-field approximations, perturbation theory or integral-equation theory perform well away from critical points where the range of the density fluctuations are comparable with the intermolecular distance (Lue and Prausnitz, 1998; Jiang and Prausnitz, 2000), but give poor results close to the critical point. Several researchers have studied the use of renormalised group theory (Wilson, 1983) to correct classical EOS behaviour in the critical region (see e.g. (Lue and Prausnitz, 1998; Fornasiero et al., 1999; Jiang and

Prausnitz, 2000). Very promising results have been obtained, but the methods are numerically intensive and not well suited to engineering applications.

Phase equilibrium data for ethane – n-C_{16} are compared with calculated phase envelopes using the Sako EOS in Figure 4-35.

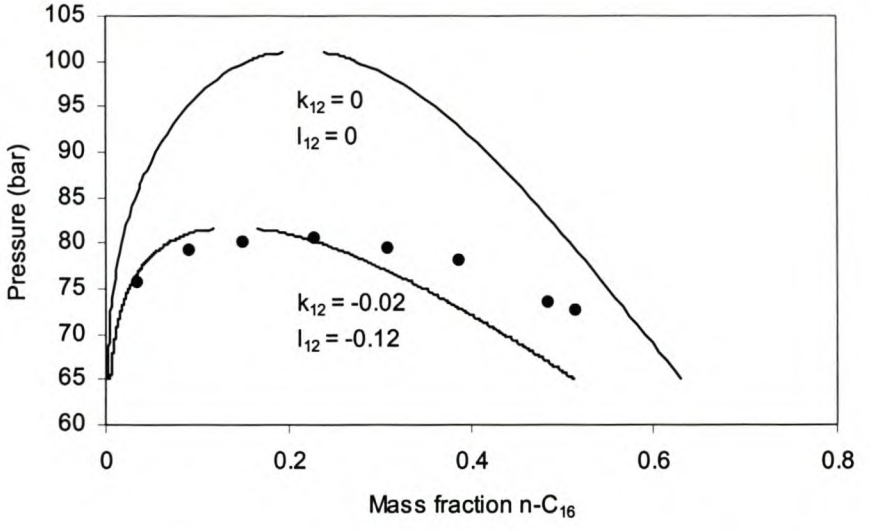

Figure 4-35. Phase equilibrium data (•) for ethane – n-C_{16} (60°C) (du Rand, 2000), with calculated phase boundaries by Sako EOS (—) for different interaction parameter values.

When no binary interaction parameters are used, pressures are overestimated by up to 20 bar. The use of two binary interaction parameters greatly reduces the errors, but still does not give a good fit over the measured composition range.

The following cubic EOS correlated the experimental data for the ethane – n-C_{16} system fairly well: PRSV, PR, SRK and PT. The correlated phase boundaries are shown in Figure 4-36. All four of these EOS correlated the vapour side (low n-C_{16} concentration) quite well, while the PT EOS gave the best liquid side correlation of the data. Even though the PT EOS does not predict vapour pressure quite as accurately as SRK, it gives a marginally better fit of the data. The PT EOS has been modified to better predict vapour pressure (section 4.2.4). These modifications of the PT EOS are compared with experimental data in Figure 4-37.

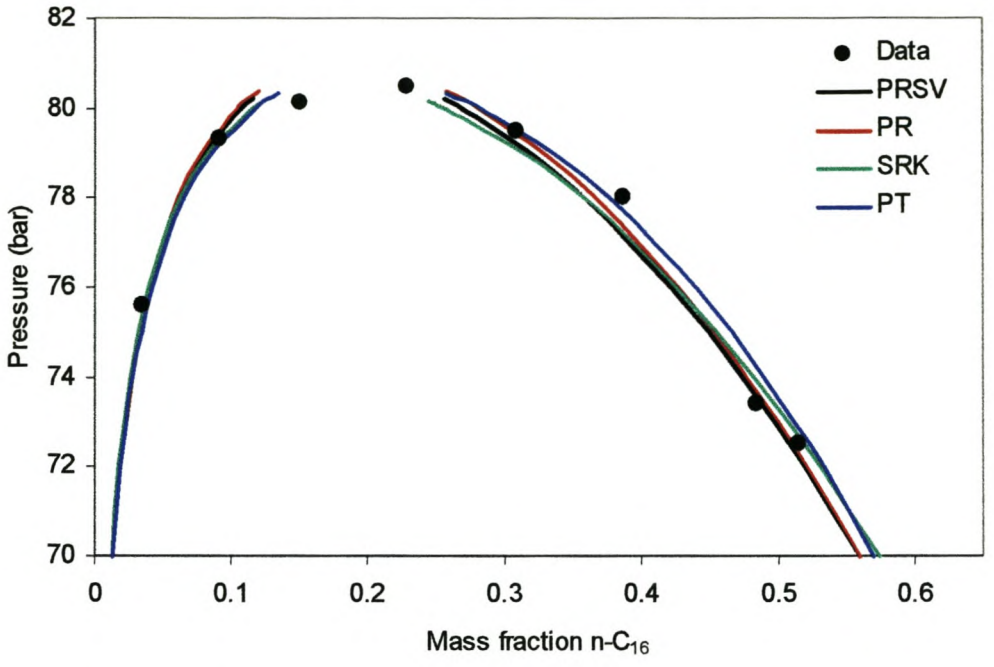

Figure 4-36. Phase equilibrium data (•) for ethane – n-C_{16} (60°C) (du Rand, 2000), with correlated phase boundaries of various EOS.

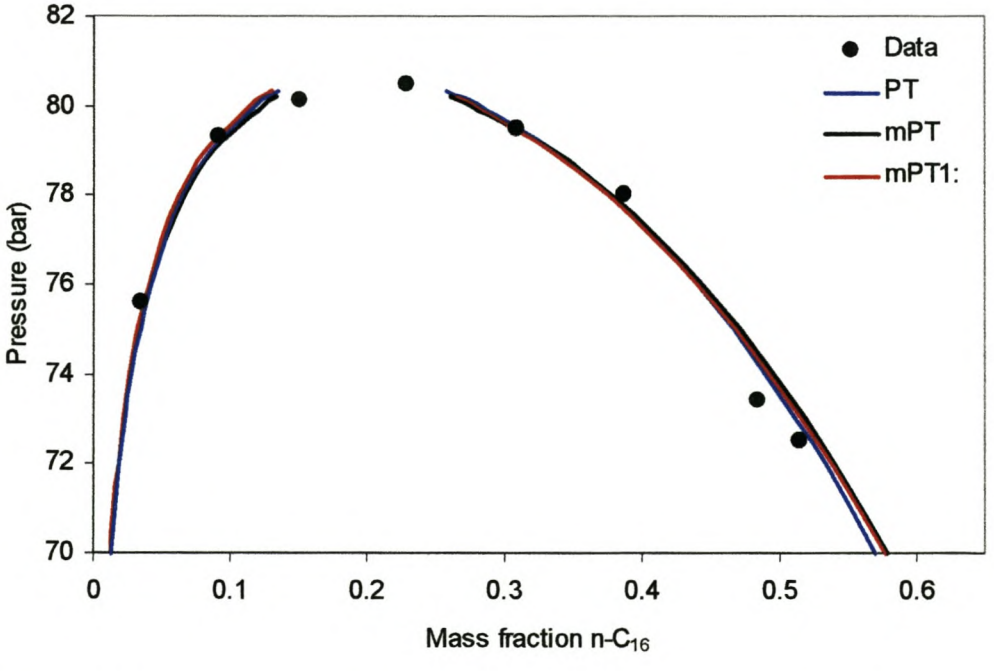

Figure 4-37. Phase equilibrium data (•) for ethane – n-C_{16} (60°C) (du Rand, 2000), with correlated phase boundaries for PT and modified PT EOSs.

Although the three versions of the PT EOS give different vapour pressure results at the temperature of interest, all three versions can be forced to predict virtually identical phase boundaries by adjusting the k_{ij} and l_{ij} interaction parameters. This indicates that a van der Waals type cubic EOS with van der Waals one-fluid mixing rules is a powerful, flexible correlating tool. Neither of the SRK, PR or PT EOSs conform to the non-classical behaviour (Sengers, 1994) observed near critical points, but the parameters in these EOSs are constrained to fit pure component critical temperatures and pressures (see Eq. 4.2). This, together with the flexibility given by using two interaction parameters enables the correlation of phase equilibrium data. It must be remembered that due to the inherent limitations of these EOSs, limited success is expected when extrapolating beyond the data used to develop the interaction correlations.

The interaction parameters used to generate Figure 4-36 and Figure 4-37 are shown in Table 4-5.

Table 4-5. Interaction parameters for the system ethane(1) – n-C_{16}(2) at 60°C.

EOS	k_{12}	l_{12}
PRSV	0.018	-0.045
PR	0.0205	-0.035
SRK	0.027	-0.058
PT	-0.02	-0.015
mPT	-0.022	-0.025
mPT1	-0.03	-0.03

The PT EOS and its two modifications are selected to correlate the ethane and CO_2 phase equilibrium data because 1) The PT EOS and its modifications give more accurate density predictions and 2) The other cubic EOSs do not improve on the phase equilibrium correlation capability of the PT EOS.

4.3.1. Correlation of ethane – n-alkane phase equilibrium data

The PT, mPT and mPT1 EOSs have been used to correlate the ethane – n-alkane equilibrium data listed in Table 4-1. Inspection of the interaction coefficients fitted to the experimental data indicated that the mPT EOS interaction parameters followed a clearer trend, compared with the PT and mPT1 EOSs. Note that this does not imply that the SRK or PR EOSs were

unable to correlate the data, only that the interaction parameters of the mPT EOS were easier to correlate. Correlation of the interaction parameters was performed in three steps: First interaction parameters were fitted to each isothermal data set individually. These interaction parameters were then plotted against carbon number and temperature. It appeared as if the k_{ij} parameters were temperature independent, and related to the carbon number of the n-alkanes. A smooth function in terms of carbon number of the solute was then fitted through the k_{ij} values. Using this k_{ij} correlation, l_{ij} values were refitted to each isotherm. The resulting l_{ij} values were then correlated in terms of carbon number and temperature. The resulting correlations are:

Eq. 4.132 $$k_{ij} = -1.03\times10^{-4}\left(M_r - 30.069\right) - 9.2\times10^{-8}\left(M_r - 30.069\right)^2$$

Eq. 4.133 $$l_{ij} = \frac{-0.2112 + 8.47\times10^{-4} M_r + (T - 333.15)\Delta_T}{1 + 0.5\exp\left(39.6 - 0.2M_r\right)}$$

Eq. 4.134 $$\Delta_T = 0.01098 - 5.6038\times10^{-5} M_r + 7.2355\times10^{-8} M_r^2$$

M_r is the molar mass of the n-alkane, and Δ_T is the component dependent temperature gradient of parameter l_{ij}. The denominator in Eq. 4.133 ensures that the l_{ij} parameter switches from 0 for small molecules to linear behaviour for long-chain molecules. During the generalisation of the interaction parameters greater weight was given to parameters fitted to systems close to the 50 – 60 °C temperature interval, since most of the supercritical extraction pilot plant runs were done in this interval.

The phase boundaries for the ethane – n-alkane systems calculated with the PT EOS using this generalised binary interaction parameters are shown below in Figure 4-38 to Figure 4-40.

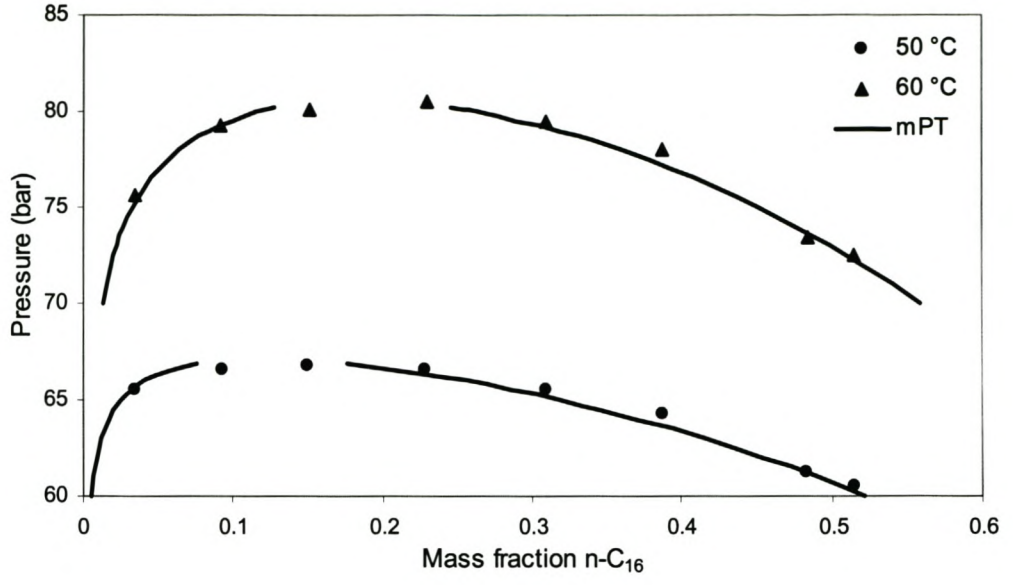

Figure 4-38. Phase boundaries plot of PT EOS (curves) and experimental data (symbols) for ethane - n-C_{16} from (du Rand, 2000).

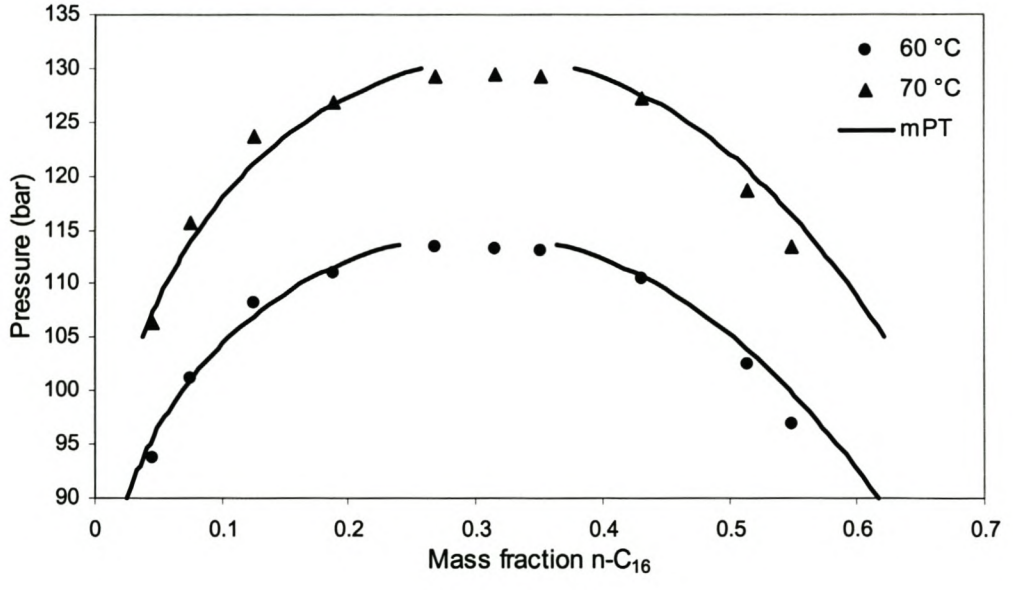

Figure 4-39. Phase boundaries plot of PT EOS (curves) and experimental data (symbols) for ethane - n-C_{24} from (du Rand, 2000).

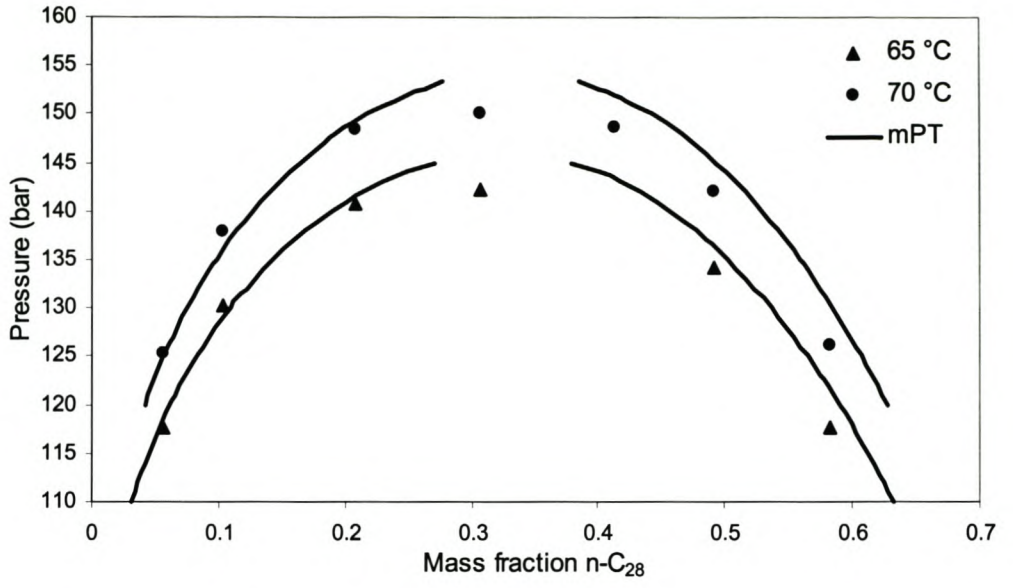

Figure 4-40. Phase boundaries plot of PT EOS (curves) and experimental data (symbols) for ethane - n-C_{28} from (du Rand, 2000).

From the above figures it can be seen that a fairly good correlation of the experimental data was obtained. The ethane – n-C_{20} equilibrium data of (Peters and de Roo, 1987) were not used during above the interaction parameter correlation procedure. The fluid-liquid phase diagram of this system is constructed using the mPT EOS with interaction parameters estimated using Eq. 4.132 and Eq. 4.134 and compared with experimental data in Figure 4-41. It can be seen that the predicted and experimental phase boundaries are in excellent agreement, both in the mixture critical region and in the low-pressure region.

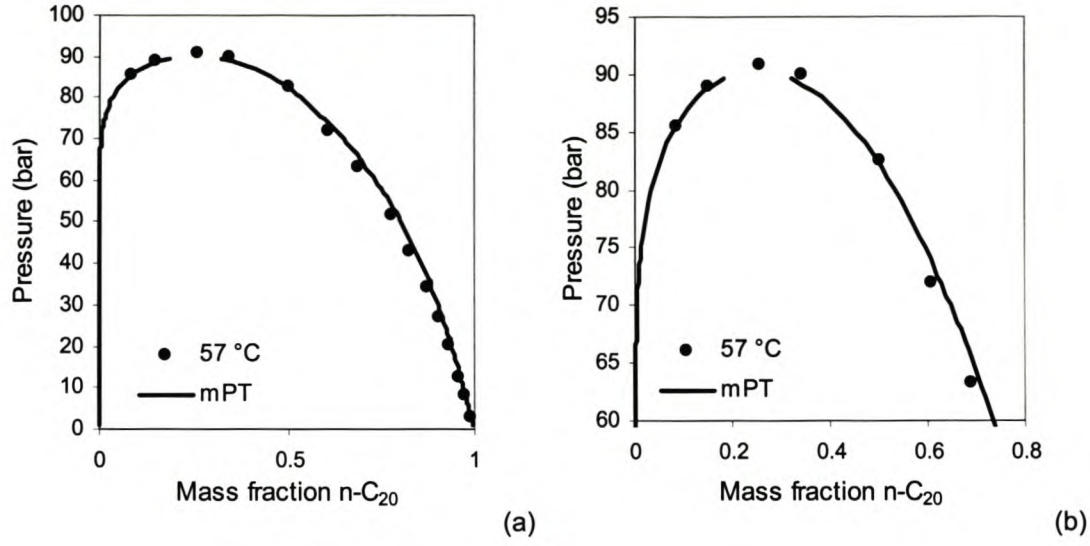

Figure 4-41. Comparison of ethane – n-C_{20} phase equilibrium data from (Peters and de Roo, 1987) with mPT EOS. a) All data. b) Mixture critical region.

4.3.2. Correlation of CO_2 – n-alkane phase equilibrium data

Phase equilibrium data for the CO2 – n-alkane systems listed in Table 4-1 were fitted using the mPT EOS. The interaction parameters were correlated using the procedure described in section 4.3.1. The generalised interaction parameter correlations for the CO_2 – n-alkanes systems are given below:

Eq. 4.135 $$k_{ij} = 0.0586 + 2.003 \times 10^{-5} M_r - 2.902 \times 10^{-7} M_r^2$$

Eq. 4.136 $$l_{ij} = 0.0547 + \frac{0.023}{0.5 + \exp(16.0122 - 0.07071 M_r)}$$

It is interesting to note that both the k_{ij} and l_{ij} parameters do not display any significant temperature dependence over the temperature range of the data.

The mPT EOS with the generalised interaction parameters for the CO_2 – n-alkane systems given above were used to plot the phase boundaries for some of the systems listed in Table 4-1. The resulting graphs are shown below in Figure 4-42 to Figure 4-46. The mPT EOS with binary interaction parameters (Eq. 4.135 and Eq. 4.136) gave an acceptable prediction of the phase boundaries of the CO_2 – n-alkane systems, with the exception of the mixture

critical region of the CO_2 – n-C_{16} and CO_2 – n-C_{20} systems. The maximum extraction pressure for the CO_2 – n-alkane extraction runs were however below 150 bar, a region where the predicted n-alkane solubility in the solvent phase is still quite accurate. The overall correlation between experimental data and calculated phase boundaries are qualitatively worse for the CO_2 systems than for the ethane systems, probably caused by the large quadropole moment of CO_2 which is not explicitly incorporated in the original PT EOS.

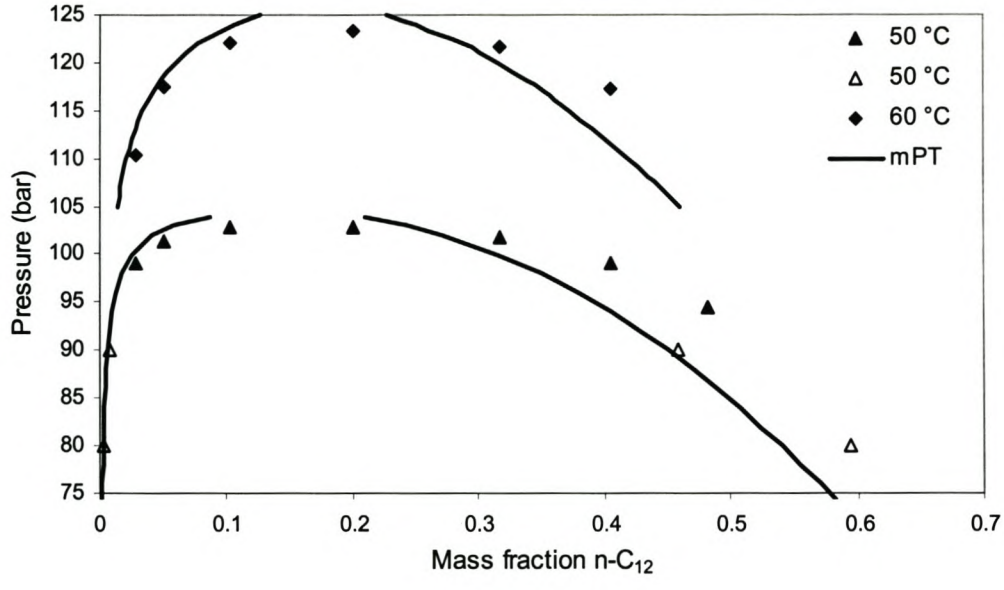

Figure 4-42. Phase boundaries plot of mPT EOS (curves) and experimental data for CO_2 - n-C_{12} from (du Rand, 2000) (solid symbols) and (de Haan, 1991) (open symbols).

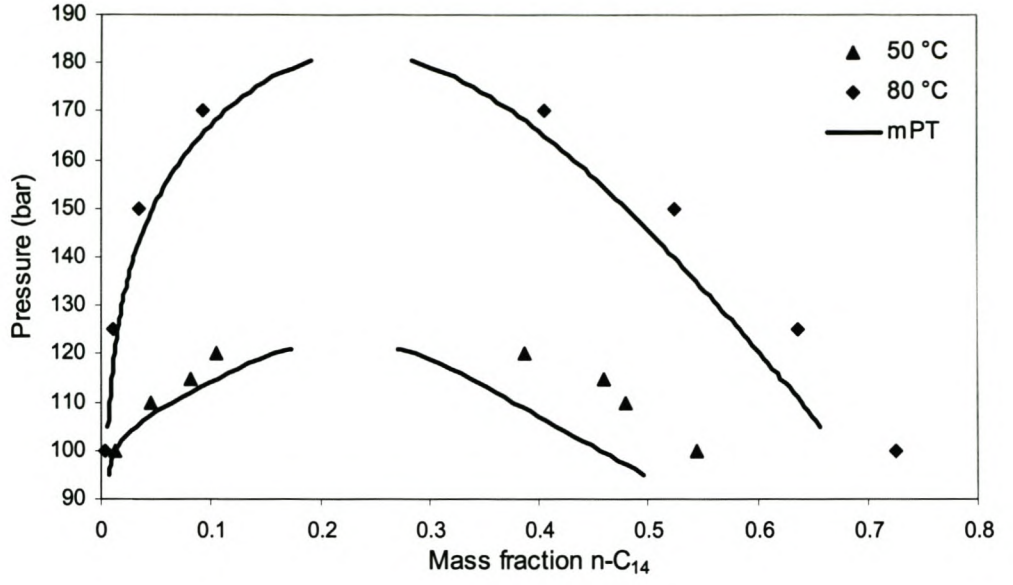

Figure 4-43. Phase boundaries plot of mPT EOS (curves) and experimental data (symbols) for CO_2 - n-C_{14} from (de Haan, 1991).

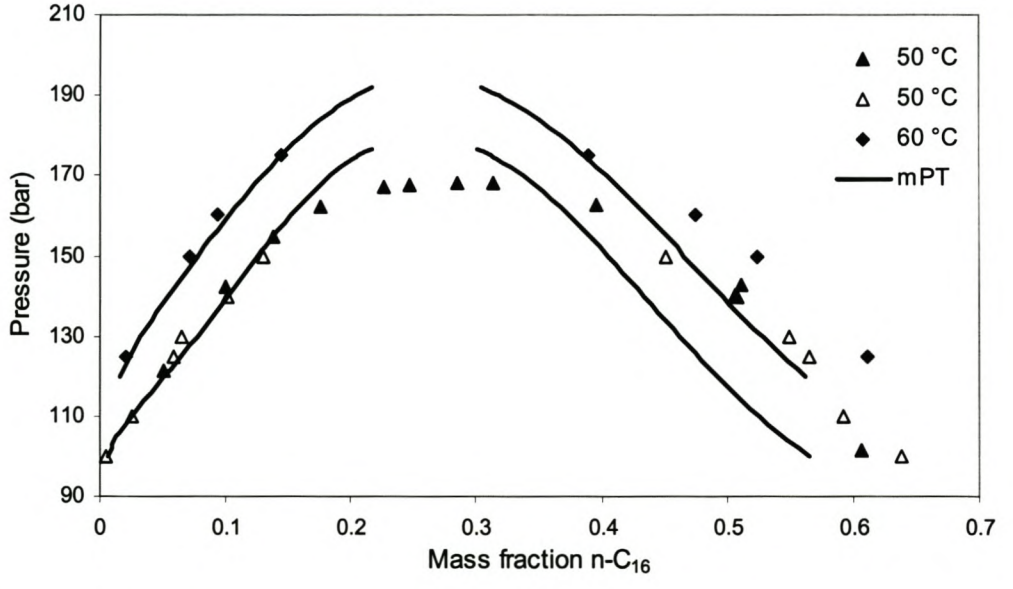

Figure 4-44. Phase boundaries plot of mPT EOS (curves) and experimental data for CO_2 - n-C_{16} from (du Rand, 2000) (solid symbols) and (de Haan, 1991) (open symbols).

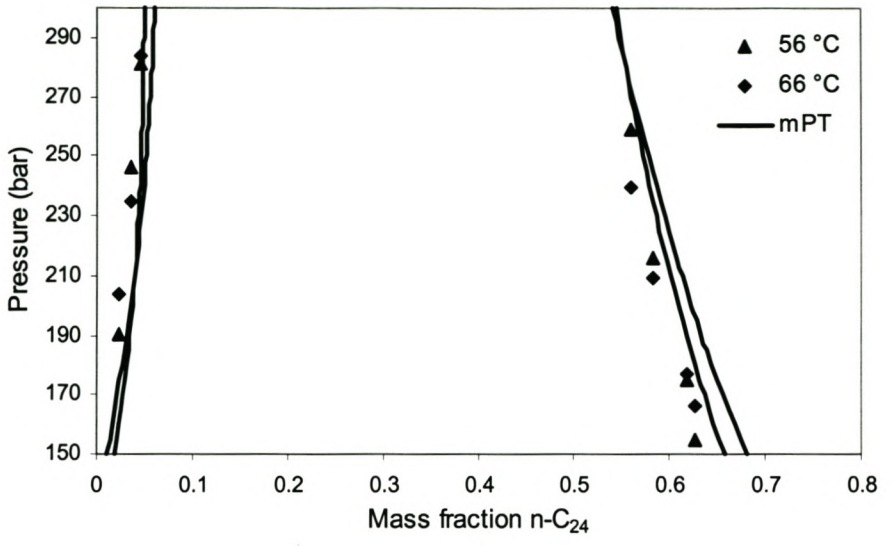

Figure 4-45. Phase boundaries plot of mPT EOS (curves) and experimental data (symbols) for CO_2 - n-C_{24} from (du Rand, 2000).

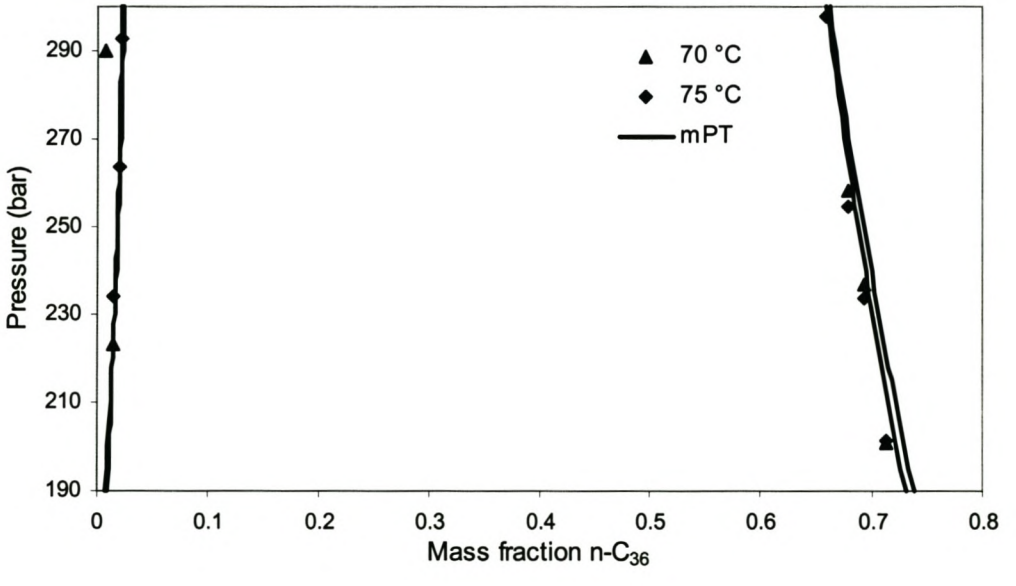

Figure 4-46. Phase boundaries plot of PT EOS (curves) and experimental data (symbols) for CO_2 - n-C_{36} from (du Rand, 2000).

4.4. Low pressure solubility of CO_2 and ethane in n-alkanes

Operating conditions in the separator, where the solvent and wax extract is separated, differ considerably from the conditions in the extraction column. In order to achieve a separation between the solvent and the extract, the temperature in the separator can be higher than the temperature in the extraction column, or the pressure in the separator can be lower than the extraction pressure, or a combination of the two conditions. In this work the separator conditions were chosen such that the pressure was below the critical pressure of the solvent, and the temperature above the critical temperature of the solvent, and sometimes higher than the extraction temperature. Under these conditions the solubility of the n-alkanes was very low in the gaseous solvent, and only the solubility of the solvent in the extract needs to be calculated accurately.

4.4.1. Solubility of ethane in n-alkanes

The correlation of the solubility for ethane – n-alkane systems has been investigated by Peters et al. (Peters et al., 1988) and Gasem and Robinson (Gasem and Robinson, 1990). Both investigations used the SPHC EOS to correlate published solubility data using one interaction parameter (see Eq. 4.111). The SPHC EOS, using one interaction parameter per system, has been used to correlate published solubility data for several ethane – n-alkane systems (see Table 4-2). The interaction parameters were found to vary with n-alkane and temperature. These variations have been correlated with a linear correlation:

Eq. 4.137 $$k_{ij} = 0.00373 + 5.2\times10^{-5} M_r - 8.4\times10^{-5}\left(373.2 - T\right)$$

Eq. 4.137 is compared with the optimum fitted parameters determined for the systems listed in Table 4-2 in Figure 4-47. The scatter is very little, considering the simple form of Eq. 4.137.

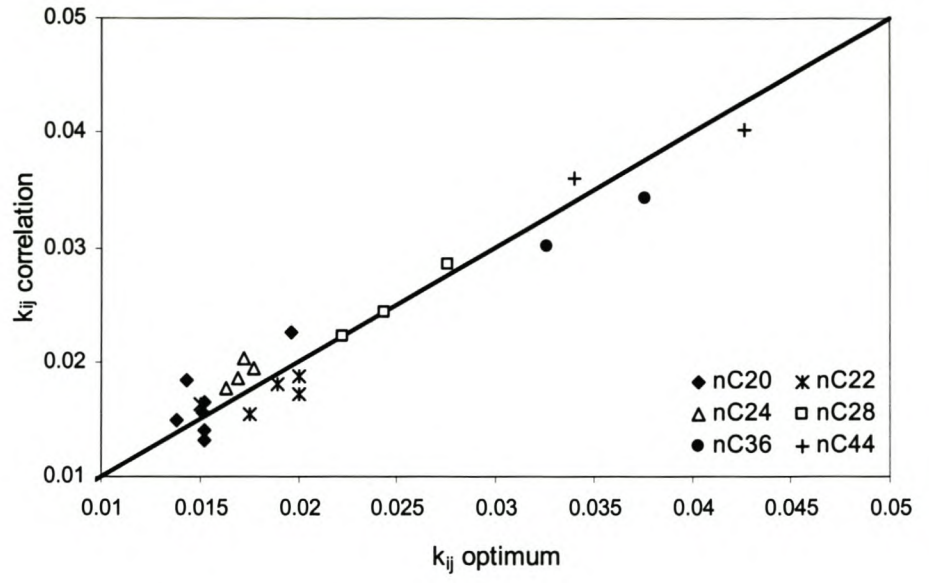

Figure 4-47. Parity plot of optimum fitted and correlated (Eq. 4.137) SPHC EOS interaction parameters.

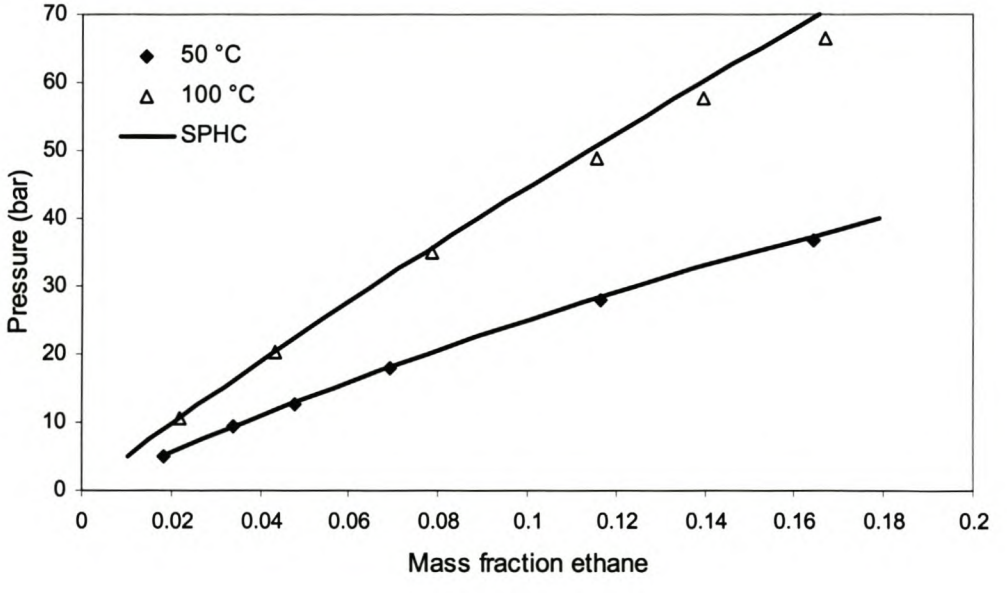

Figure 4-48. Solubility of ethane in n-C_{20} (data points from (Gasem, Bufkin et al., 1989)) calculated with SPHC EOS. k_{ij} calculated with Eq. 4.137.

The solubility of ethane in n-C_{20} was calculated with the SPHC EOS and Eq. 4.137 and compared with experimental data in Figure 4-48. The calculated and experimental solubilities agree very well. The bubble point pressures of the system ethane – n-C_{16} (not used to obtain Eq. 4.137) calculated with SPHC EOS and Eq. 4.137 are shown in Figure 4-49. The maximum error in

the calculated bubble point pressure is 5%, indicating that the SPHC EOS with interaction coefficient from Eq. 4.137 is quite capable of predicting the ethane – n-alkane system equilibria at low pressure.

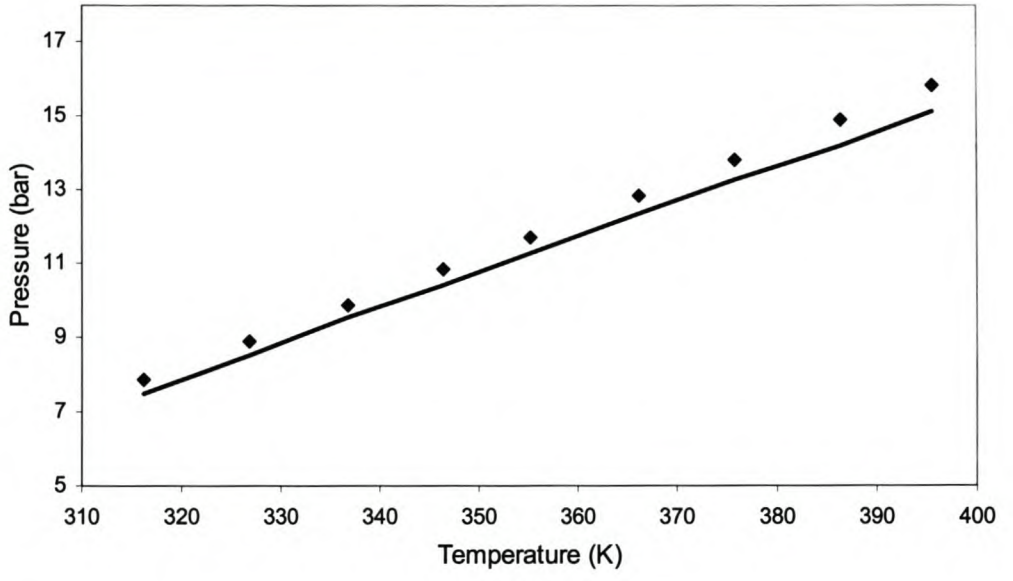

Figure 4-49. Bubble point pressures (data from (Breman et al., 1994)) for the ethane – n-C_{16} isopleth ($x_{mol\ ethane}$ = 0.2) predicted with SPHC EOS and Eq. 4.137.

4.4.2. Solubility of CO_2 in n-alkanes

Ponce-Ramirez et al. (Ponce-Ramirez et al., 1991) tested the applicability of using the SPHC EOS to correlate vapour liquid equilibria for several classes of CO_2 – hydrocarbon systems and obtained very satisfactory results. They also published interaction parameters for some CO_2 – n-alkane systems, but unfortunately the interaction parameters were obtained from data sets where the experimental temperatures are outside the range of interest in this work (50 °C ≤ T ≤ 100 °C). The SPHC EOS was used to correlate low-pressure solubility data from the literature (see Table 4-2) using one binary interaction parameter, k_{ij}.

The interaction coefficients for all the systems correlated showed weak temperature dependence and also depended to some extent on the chain length of the n-alkane. The interaction coefficients were correlated as follows:

Eq. 4.138 $$k_{ij} = 0.54 + 5 \times 10^{-5} M_r - 0.08463 \ln(T)$$

Solubility data of CO_2 in n-C_{20} at 50 °C and 100 °C are compared with calculated solubilities using the SPHC EOS with the k_{ij} interaction parameter calculated from Eq. 4.138. An excellent correlation between the experimental and calculated solubilities is evident. Similar results were obtained for most of the systems used to develop Eq. 4.138.

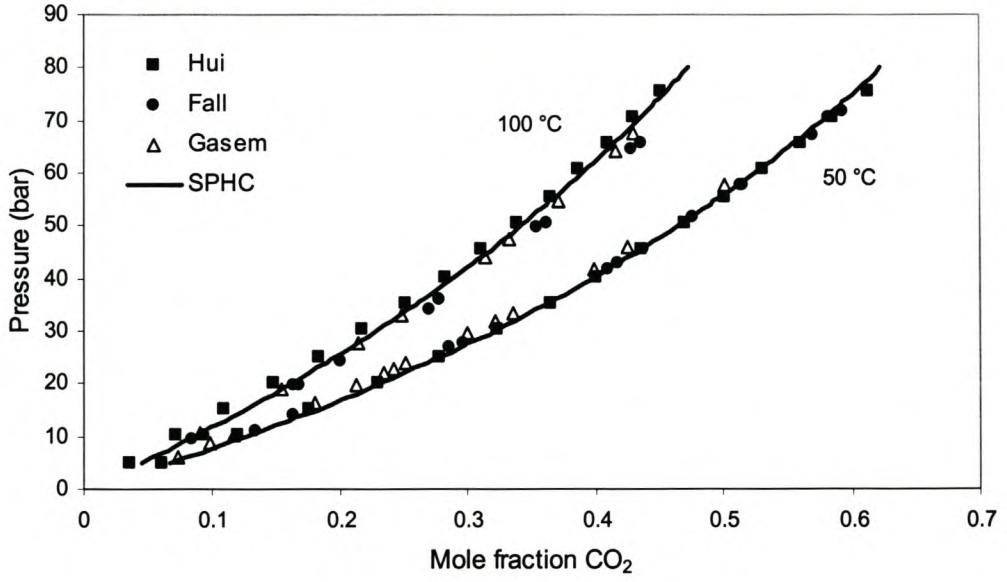

Figure 4-50. Comparison of experimental and calculated solubility data of CO_2 in n-C_{20} using the SPHC EOS.

The bubble point pressures of the system CO_2 – n-C_{16} (not used to obtain Eq. 4.138) calculated with SPHC EOS and Eq. 4.138 are shown in Figure 4-51. The maximum error in the calculated bubble point pressure is about 10%.

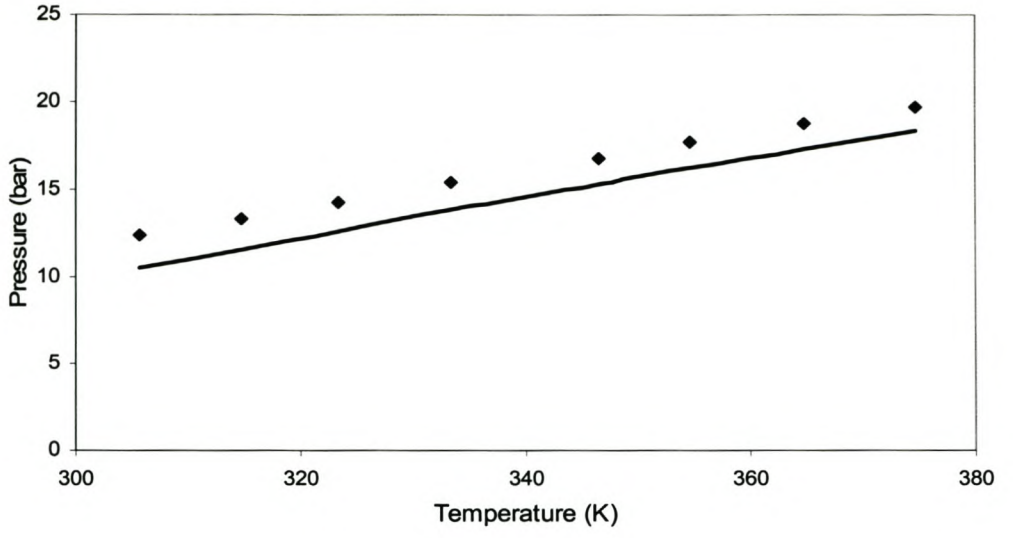

Figure 4-51. Bubble point pressures (data from (Breman, Beenackers et al., 1994)) for the CO_2 – n-C_{16} isopleth (x_{mol} = 0.14) predicted with SPHC EOS and Eq. 4.138.

The SPHC EOS has also been used to calculate bubble point pressures for the ternary system CO_2 – n-C_{11} – n-C_{12} published by (Shariati et al., 1998). An excellent correlation between the calculated and experimental bubble point pressures can be seen in Figure 4-52.

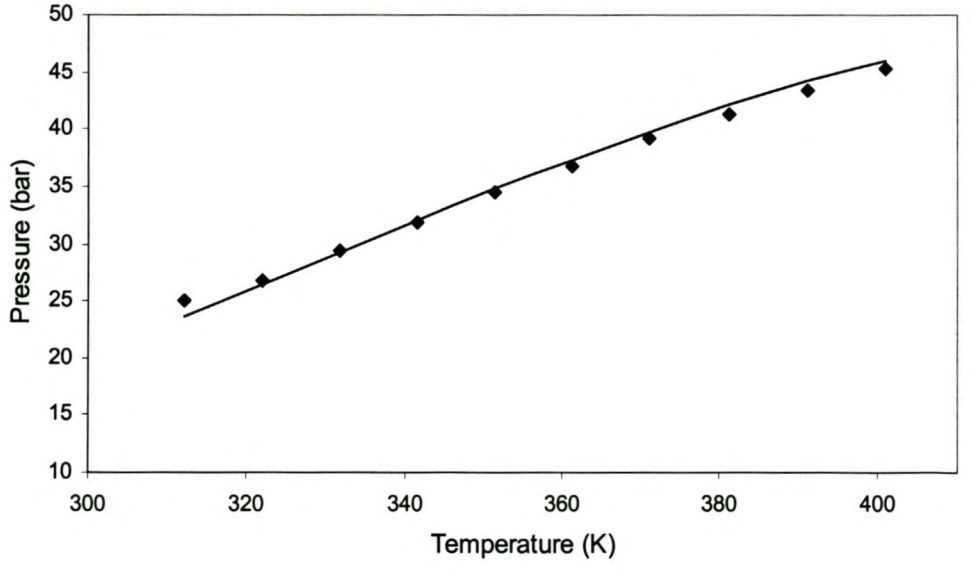

Figure 4-52. Bubble point calculations using SPHC and Eq. 4.138 compared with experimental values from (Shariati, Peters et al., 1998). Mixture molar composition: x_{CO2} = 0.251, $x_{n\text{-}C11}$ = 0.3404, $x_{n\text{-}C12}$ = 0.4086.

4.5. Concluding remarks

In this chapter phase equilibrium modelling for ethane – n-alkane and CO_2 – n-alkane systems has been investigated. Several equations of state have been evaluated for their suitability in correlating and predicting phase equilibria at conditions relevant to supercritical extraction of paraffin waxes. It was found that the more empirical van der Waals type cubic equations of state (SRK, PR and PT) could be used to correlate high pressure phase equilibria up to very close to the mixture critical point. The PT EOS has been modified by fitting the apparent critical volume (ζ_c) and slope of the alpha function (m) to vapour pressure and liquid volume data of long-chain n-alkanes. This modification of the PT EOS (mPT) was used to successfully correlate high–pressure phase equilibria for systems of ethane or CO_2 with n-alkanes. Separate correlations for the interaction parameters k_{ij} and l_{ij} for ethane and CO_2 with the n-alkanes are given. These correlations will be used in the next chapter to calculate phase equilibria in supercritical fluid extraction of paraffin waxes.

Solubility data of ethane and CO_2 in n-alkanes at low to moderate pressure were correlated using the SPHC EOS with one interaction parameter, k_{ij}, per system. The resulting interaction parameters were correlated in terms of the molecular weight of the n-alkane and temperature. Separate correlations for the interaction parameter k_{ij} for ethane and CO_2 with the n-alkanes are given. These correlations will be used in the next chapter to calculate phase equilibria for the separation of extracted n-alkanes from the solvent after supercritical extraction.

4.6. Symbols

A	Helmholtz energy
a	EOS parameter
b	EOS parameter
c	PT EOS parameter
k	Boltzmann's constant
k_{ij}	Interaction parameter
l_{ij}	Interaction parameter
m	Parameter in Eq. 4.5
m	Segment number
N	Number of molecules
P	Pressure
q	Surface area
R	Ideal gas constant

RMS error $= \sqrt{\frac{1}{n}\sum\left(1-\frac{P_{calc}}{P_{\exp}}\right)^2}$

T	Temperature
v	Specific volume
v^*	Close-packed volume
x	Mole fraction
z	Compressibility factor
α	Temperature dependent correction to EOS parameter a
α	Non-spherical parameter
ε	Interaction energy
η	Packing fraction
ρ	Molar density
σ	Segment diameter
τ	Hard-sphere packing fraction ($=\pi\sqrt{2}/6$)
ω	Acentric factor
ζ_c	PT EOS parameter

Subscripts

c	Critical property
m	Mixture property
r	Reduced property

Superscripts

HC	Hard chain
pert	Perturbation

CHAPTER 5. SUPERCRITICAL FLUID EXTRACTION PLANT

In this chapter the fractionation and deoiling of n-paraffin wax will be investigated. Experimental results are reported and compared with simulation results based on an equilibrium stage model of the extraction process. Phase equilibrium calculations needed for the simulations are performed using equation of state models developed in the previous chapter.

Previous studies related to the supercritical fractionation of wax were done by de Haan (de Haan, 1991) (fractionation of liquid hydrocarbons), and Nieuwoudt (Nieuwoudt, 1994) (fractionation high molecular weight n-alkanes). In these studies the extractions were done with countercurrent flow in packed columns. Other investigations done include the extraction of paraffin wax from crude oil (Oschmann et al., 1998), fractionation of petroleum pitch (Hutchenson, Roebers et al., 1991), fractionation of crude wax (Braun and Schmidt, 1984). A patent ((Yoshihisa, 1992) has also been filed describing the fractionation of solid wax by extraction with a supercritical fluid, followed by step-wise precipitation by pressure reduction. These studies employed a batch technique that yields only qualitative results.

5.1. Pilot plant

The extraction column (see Figure 5-1) used in this work is 5 m in height, with an inside diameter of 28 mm. The design pressure is 300 bar and design temperature is 150 °C. The column contains two 2.16 m high sections packed with Sulzer DX packing (see Table 5-1 for technical detail). This is a gauze type packing woven from stainless steel wire.

Table 5-1. Sulzer DX packing data

Geometric information	Value
Crimp height	3 mm
Channel base	6.5 mm
Channel side	4.4 mm
Surface area#	900 m^2/m^3
Void fraction	77 %
Channel angle with horizontal	60°

not including the column wall area of 140 m^2/m^3.

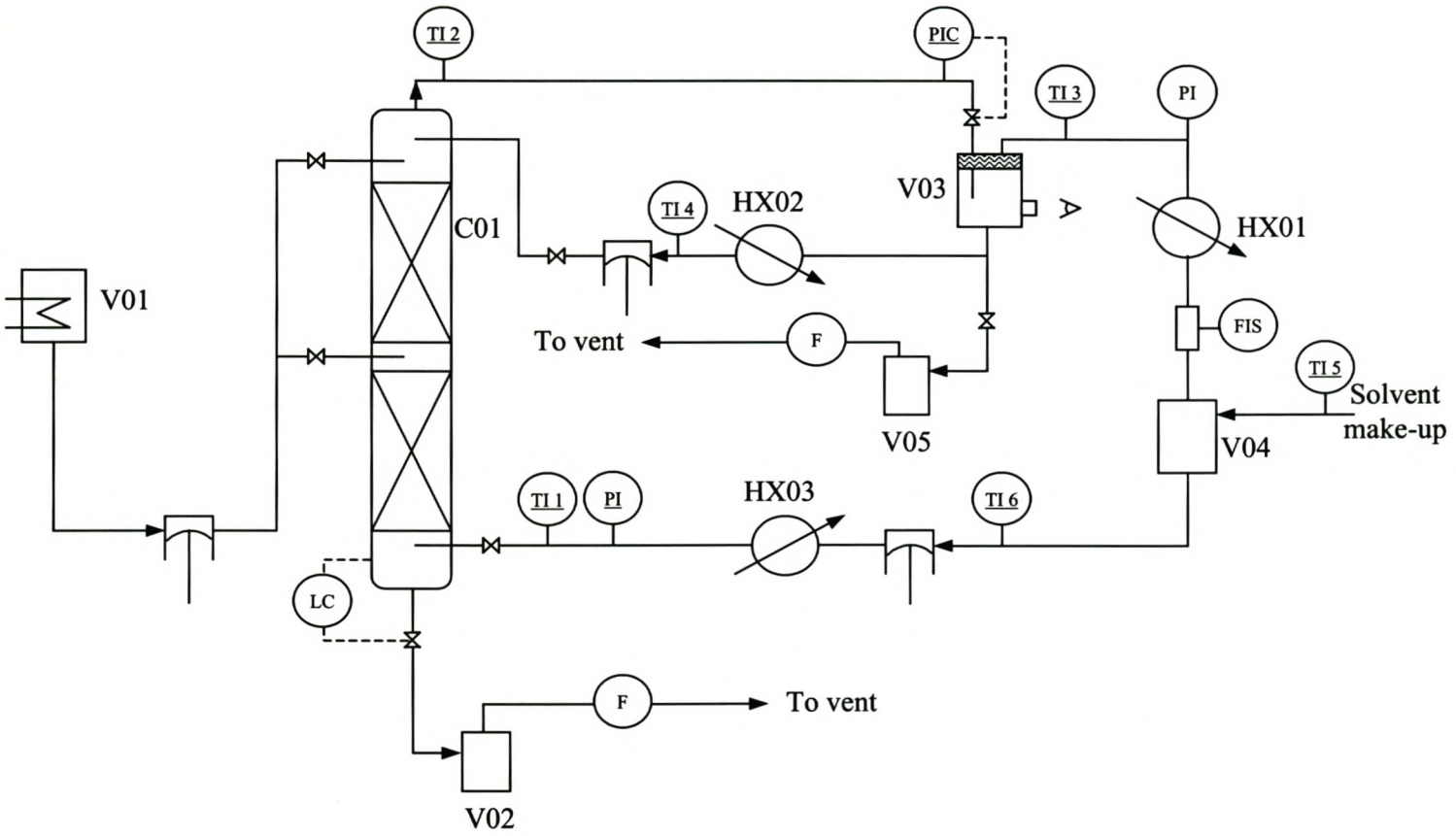

V01 - Feed vessel
V02 - Residue product vessel
V03 - Separator vessel
V04 - Solvent buffer
V05 - Extract product vessel
C01 - Extraction column
HX01 - Solvent condenser
HX02 - Reflux heat exchanger
HX03 - Solvent heater

Figure 5-1. Pilot plant PFD

A process flow diagram of the supercritical fluid extraction plant used in this work is shown in Figure 5-1. The wax feed is heated in the feed vessel (V01), capacity 8 L, and pumped to the extraction column (C01) with a variable stroke length diaphragm pump (Dosapro from Milton Roy) with maximum ratings of 2 L/h at 260 bar. The wax feed can enter the column at the top or the middle of the extraction column, depending on the mode of operation. The extraction column is jacketed, and heated with circulating water.

The wax residue collects at the bottom of the extraction column, where the interface is controlled with an optical interface sensor (from Phönix Analytec). The residue leaving the column expands to atmospheric pressure over the bottom valve, and the residue is collected in a residue vessel (V02). Dissolved solvent liberated from the wax residue by the pressure release flows through a rotating vane gas meter and is vented.

Liquid solvent from the solvent buffer vessel (V04) is pumped to the extraction column with a variable stroke length diaphragm pump (Dosapro from Milton Roy) with maximum rating of 29 L/h at 260 bar. The solvent is heated to the extraction column temperature in heat exchanger HX03 and enters at the bottom of the extraction column.

No distributors were used inside the extraction column; the solvent and the wax feed entered the column through tubes that protruded to the centre of the column. Wetting tests with a paraffin mixture (n-C_{10} – n-C_{13}) showed that a packing segment (54 mm in height) was completely wetted from a single drip point.

The solvent-rich extract phase exits the top of the extraction column and expands over a pressure control valve, which controls the operating pressure. The solvent's solvent power is greatly reduced by the change in pressure and virtually all the dissolved wax precipitates from the solvent phase. The precipitated wax and gaseous solvent is separated in a separator vessel (V03), equipped with a demisting device packed with Goodloe knitted packing. The separator vessel is equipped with a heating jacket heated by circulating water.

The gaseous solvent leaving the separator vessel is condensed in heat exchanger HX01. The condensed solvent flows through a mass flow meter (Danfoss) and collects in the solvent buffer V04. The separator vessel, solvent condenser and solvent buffer vessel operates very close to the

solvent vapour pressure at ambient temperature, since the solvent buffer is connected to a solvent supply cylinder.

Wax extract collected in the separator vessel is drained through a hand-operated valve into the extract vessel (V05). The liquid level inside the separator vessel is visually monitored through a sight glass. Solvent gas liberated from the wax extract flows through a rotating vane flow meter before being vented.

Wax extract from the separator vessel can also be returned to the extract column as reflux. If the column is operated in reflux mode, the separator vessel temperature is controlled at a temperature 5 – 10 °C higher than the extraction column temperature. Extract leaving the separator is then cooled to the extraction column temperature by a double pipe heat exchanger (HX02). This ensures that the reflux pump feed is sufficiently below its bubble point that cavitation does not occur. The reflux pump (Lewa) is a double diaphragm type pump with adjustable stroke length and a maximum capacity of 8 L/h and a maximum discharge pressure of 300 bar. The pump motor speed is controlled with a frequency inverter (Danfoss VLT 2800) to extend the low flow range of the pump.

PT100 RTD's were used to measure temperatures, with an estimated accuracy of ± 0.1 °C (checked against a reference thermometer). The extraction column pressure was measured with a Wika pressure gauge with an accuracy of ± 2 bar, tested against a dead weight gauge.

All piping, valves and pumps in the wax-containing streams were traced with copper tubing heated with hot water. The solvent buffer vessel is jacketed and cooled with chilled water. The solvent line from the solvent buffer, and the solvent pump is traced with copper tubing cooled with chilled water. This prevents possible cavitation at the solvent pump.

Two heating baths from Tool-Temp provide recirculating hot water, and a chiller (Sam Chin Cold Water Machines Ltd.) provides chilled water.

Since ethane is a highly flammable gas, precautions were taken to prevent accumulation of ethane gas in the vicinity of the extraction plant. An extractor fan was used to continuously displace the air close to the extraction plant. All pump motors and instrumentation are flameproof, while all other non-flameproof electrical equipment such as the heating and cooling baths and the process control computer are purged with compressed air.

5.2. Experimental procedure

The extraction plant was kept under pressure (vapour pressure) with the solvent gas used. Care was taken during the initial solvent loading of the plant to ensure that no air was trapped inside the column or other vessels by filling and purging the column with gaseous solvent several times. Feed wax was first melted in an electrically heated oven and then transferred to the feed vessel.

An experiment was initiated by starting the solvent feed pump and setting an operating pressure. Next, the wax feed pump is started and the flow rate is set. If reflux is to be returned to the extraction column, the column is first operated in countercurrent mode until some extract has accumulated in the separator vessel. The reflux pump is then started and a reflux flow rate set. The run is left undisturbed for at least 3 hours after the temperatures and pressure in the extraction column have reached steady values.

After at least 3 hours since the last disturbance has occurred, extract and residue samples are collected for a period of 1–2 hours. The following readings are logged during or after the samples collection period:

- Solvent inlet temperature to extraction column
- Extract temperature exiting the extraction column
- Solvent pressure at the extraction column inlet
- Separator pressure
- Reflux pump inlet temperature
- Solvent flow rate
- Residue and extract mass
- Volume gaseous solvent liberated from residue and extract

The wax samples are analysed as described in 2.3.

5.3. Equilibrium stage modelling of SCFE

A process model is a useful tool for analysing and predicting the effect of process variables such as reflux ratio, number of separation stages etc. on the separation achievable (Brunner, 1998). Shortcut methods such as those of McCabe-Thiele, Ponchon-Savarit and Jänecke can be used to determine the number of theoretical stages (Seader and Henley, 1998) for a separation. Unfortunately these methods can only be applied to (pseudo) binary or ternary systems. For a system with many components a more rigorous multicomponent method is preferred.

The multicomponent equilibrium stage modelling of SCFE can be done in a very simple way if the energy balance requirements can be removed from the overall mathematical description of a stage. Since SCFE is sensitive to temperature and pressure variations (with regard to extraction to feed ratio), SCFE columns should have tight control on these variables. It seems reasonable to assume that an SCFE column would operate isothermally rather than adiabatically. If it can then be assumed that the temperature profile in the column is known, only the mass balance and equilibrium conditions need to be calculated for a stage. This approach leads to a tridiagonal matrix formulation of the problem, which can be solved in a straightforward manner (see e.g. (Kister, 1992) and (Seader and Henley, 1998)) using the Thomas algorithm.

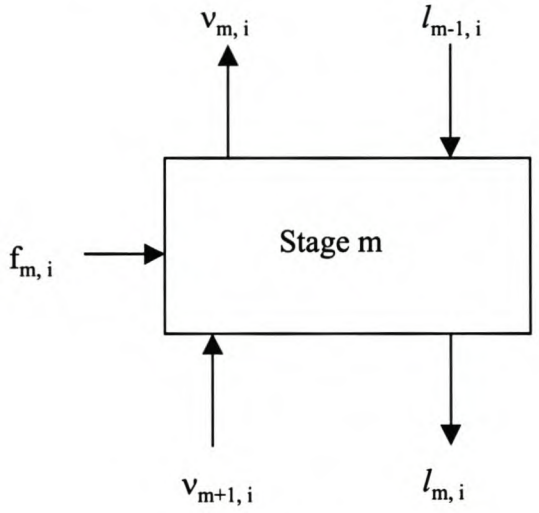

Figure 5-2. Equilibrium stage model

A mass balance for component *i* over stage *m* gives (see Figure 5-2):

Eq. 5.1 $$v_{m+1,i} - v_{m,i} + l_{m-1,i} - l_{m,i} = -f_{m,i}$$

with $v_{m,i}$ and $l_{m,i}$ the vapour and liquid molar flow rates respectively of component *i* from stage *m*. $f_{m,i}$ is the molar feed rate of component *i* to stage *m*. Eq. 5.1 can be transformed to

Eq. 5.2 $$A_{m-1,i} v_{m-1,i} - (1 + A_{m,i}) v_{m,i} + v_{m+1,i} = -f_{m,i}$$

with $A_{m,i}$ defined as:

Eq. 5.3 $$A_{m,i} = \frac{L_m}{K_{m,i} V_m}$$

$K_{m,i}$ is the K-value of component *i* on stage *m*. The K-value is defined as the ratio of the vapour to liquid fractions of component *i*:

Eq. 5.4 $$K_i = \frac{y_i}{x_i}$$

K-values can be calculated from equations of state by noting that at equilibrium between to phases, the component fugacities in each phase must be equal:

Eq. 5.5 $$\hat{f}_i^{\,l} = \hat{f}_i^{\,l}$$

By defining a fugacity coefficient:

Eq. 5.6 $$\hat{\phi}_i^{\,l} = \frac{\hat{f}_i^{\,l}}{x_i P}$$

the equilibrium condition can be expressed as follows:

Eq. 5.7 $$\hat{\phi}_i^{\,l} x_i = \hat{\phi}_i^{\,l} y_i$$

Eq. 5.7 can be rearranged to obtain the K-value:

Eq. 5.8 $$\frac{\hat{\phi}_i^{\,v}}{\hat{\phi}_i^{\,l}} = \frac{y_i}{x_i} = K_i$$

Fugacity coefficients can be calculated from equations of state, see e.g. (Smith, van Ness et al., 1996) and (Tassios, 1993). The correlation of phase

equilibria using equations of state has been discussed in the previous chapter. The total liquid and vapour flow rates are calculated by:

Eq. 5.9 $$L_m = \sum_{i=1}^{C} l_{m,i}$$

and

Eq. 5.10 $$V_m = \sum_{i=1}^{C} v_{m,i}$$

The summations are performed up to the number of components, *c*, in the phase. The liquid and vapour flow rates of a component leaving an equilibrium stage are related by the following relation:

Eq. 5.11 $$A_{m,i} v_{m,i} = l_{m,i}$$

Using the Thomas algorithm, Eq. 5.2 can be written as:

Eq. 5.12 $$v_{m,i} + p_{m,i} v_{m+1,i} = q_{m,i}$$

with $p_{m,i}$ and $q_{m,i}$ defined as:

Eq. 5.13 $$p_{m,i} = \frac{-1}{1 + A_{m,i} + A_{m-1,i} p_{m-1,i}}$$

Eq. 5.14 $$q_{m,i} = \frac{f_{m,i} + A_{m-1,i} q_{m-1,i}}{1 + A_{m,i} + A_{m-1,i} p_{m-1,i}}$$

The matrix of equations formed by Eq. 5.12 over an extraction column can be solved with back substitution by noting that for the last stage in the column (solvent feed stage, *s*):

Eq. 5.15 $$v_{s,i} = q_{s,i}$$

The solution algorithm used to solve Eq. 5.2 - Eq. 5.15 depends on the specifications given, and the unspecified variables to be calculated. In this work the following variables are selected as specifications:

- Column temperature and pressure.
- Feed composition, flow rate and location.
- Solvent composition and flow rate.
- Number of stages.
- Reflux ratio.
- Separator temperature and pressure.

The following unspecified variables must then be solved using an iterative scheme:

- Liquid and vapour component flow rates per stage ($l_{m,i}$ and $v_{m,i}$).
- Component K values per stage ($K_{m,i}$).

Since $l_{m,i}$ and $v_{m,i}$ are related by Eq. 5.11, only 2 independent variables remain to be solved ($v_{m,i}$. and $K_{m,i}$). For supercritical extraction the K values are dependent on both liquid and vapour composition. It is therefore necessary to separate (tear) the variables $v_{m,i}$. and $K_{m,i}$ to obtain an algorithm that gives stable convergence. In this work an equation of state is used to calculate component K values. Since this can be a time-consuming step, it was decided to select the K values as tear variables to solve the set of equations derived above.

The method followed for solving the set of equations is summarised in Table 5-2 and Figure 5-3.

Table 5-2. Solution algorithm for the model equations.

1. User enters temperatures, pressures, number of stages, reflux ratio, feed and solvent flow rate.
2. Algorithm generates initial estimates for $v_{m,i}$, $l_{m,i}$ and $K_{m,i}$ by flashing the wax and solvent feed at the column conditions. Each stage is initialised with the same values.
3. Assume fixed $K_{m,i}$-values, calculate $A_{m,i}$, $p_{m,i}$ and $q_{m,i}$ values.
4. Solve Eq. 5.12 using the Thomas algorithm to obtain new $v_{m,i}$ values.
5. Recalculate $l_{m,i}$, L_i and V_i values.
6. Recalculate $A_{m,i}$, $p_{m,i}$ and $q_{m,i}$.
7. Repeat steps 3 – 6 until V_i values converge.
8. Calculate x_i and y_i values for each stage.
9. Calculate new $K_{m,i}$-values using new x_i and y_i values.
10. Repeat steps 4 - 9 until $K_{m,i}$-values converge.

The convergence criterion for step 7 (Table 5-2) is as follows:

Eq. 5.16 $$\sum_{i=1}^{N}\left|V_i^k - V_i^{k-1}\right| < 10^{-10} N$$

where superscript *k* indicates the current iteration value, and *k-1* indicates the previous iteration value. N is the number of stages. It was found that the algorithm sometimes exhibits unstable behaviour if the inner loop was iterated until Eq. 5.16 was satisfied. This instability could be prevented by limiting the number of iterations allowed in the inner loop. It was found that limiting the number of inner loop iterations to N + 10 iterations resulted in better convergence in most cases. As the solution is approached, the inner loop converges faster, and this limitation on number of iterations does not affect attainment of the convergence specification.

The convergence criterion for step 10 (Table 5-2) is given by:

Eq. 5.17 $$\sum_{i=1}^{C}\sum_{j=1}^{N}\left|K_{j,i}^k - K_{j,i}^{k-1}\right| < 10^{-10} \times N \times C$$

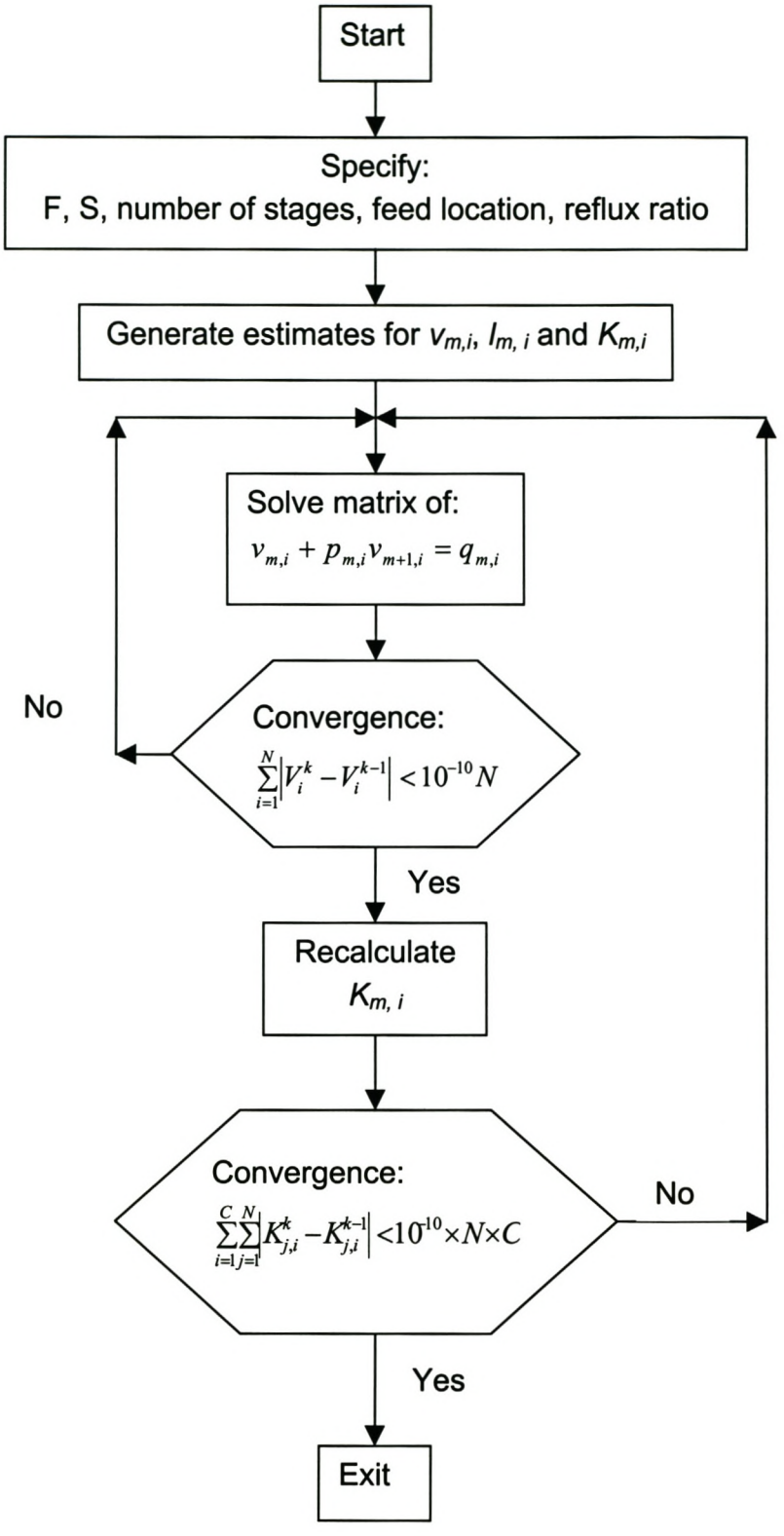

Figure 5-3. Algorithm for solving equilibrium stage model for SCFE.

When the K-values are sensitive to changes in composition, or when a large number of separation stages are being simulated, it is necessary to damp the molar vapour flow rates ($v_{i,j}$) obtained from Eq. 5.12 between iterations to prevent oscillation:

Eq. 5.18 $$v_{i,j}^{k+1} = d \times v_{i,j}^{k+1} + (1-d) \times v_{i,j}^{k}$$

The damping factor, d, is usually chosen between 0.5 and 1.

The algorithm described above has some similarities to the Tsuboka-Katayama algorithm as described by (Seader and Henley, 1998). The main difference between the algorithms is the choice of the tear variable; Tsuboka and Katayama selected V_m as the tear variable. This selection of the tear variable results in the calculation of the K values and liquid compositions in the inner loop. The approach of the Tsuboka-Katayama algorithm is not appropriate for SCFE modelling, due to the computational effort required to evaluate K-values using an EOS and to stability problems.

5.4. Experimental results

Several supercritical extraction runs were done using either carbon dioxide or ethane as supercritical solvent. These extraction runs were performed at various temperatures, pressures and solvent: wax feed ratios and reflux ratios. The purpose of the experiments was two-fold: it was used to explore feasible regions for supercritical fluid extraction and the results of the experiments were compared with simulation results. The conditions of the various extraction runs are shown in Table 5-3 - Table 5-5. The product compositions of the various extraction runs are presented in Appendix D.

The wax feed used for these runs is Gatsch wax from Sasol, consisting of mostly n-alkanes from n-C_{11} to n-C_{30}. The Gatsch also contained small amounts of iso paraffins and alkenes. A typical feed analysis is shown below in Figure 5-4, with the iso alkanes and alkenes lumped with the n-alkanes. The feed composition varied only slightly between runs.

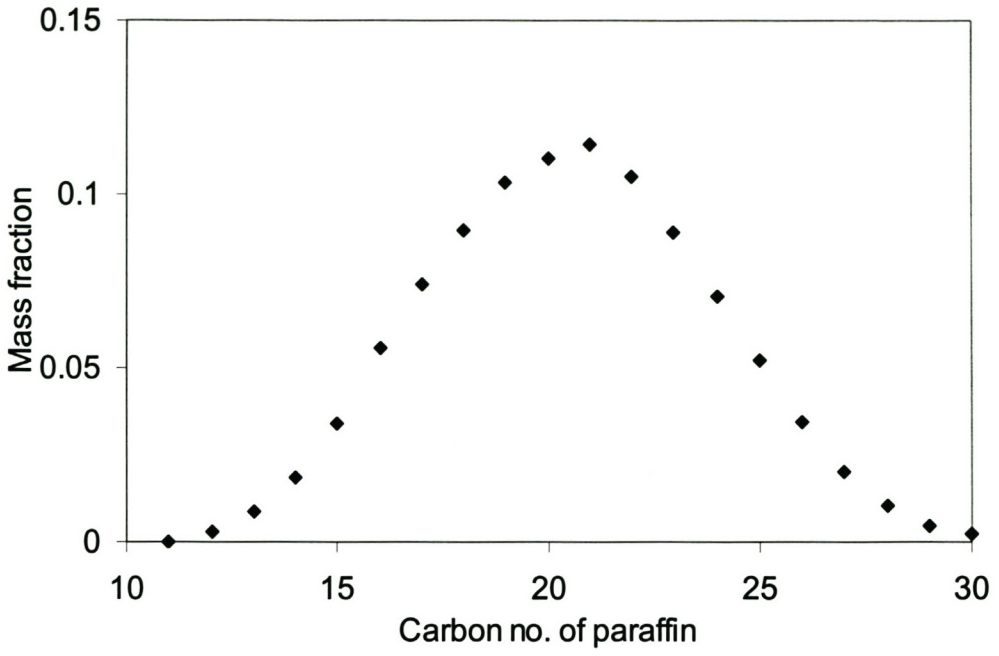

Figure 5-4. Typical wax feed composition used in SCFE runs.

Table 5-3. CO_2 countercurrent extraction conditions.

Run	Extract / Feed	T column °C	P column bar A	P separator bar A	Solvent kg/h	Feed kg/h	S R# kg/h	S E# kg/h
CO_2C1	0.088	55	101	56	5.49	0.295	*	*
CO_2C2	0.269	55	118	52	4.9	0.323	*	*
CO_2C3	0.4	55	130	52	5.6	0.416	*	*
CO_2C4	0.686	55	141	52	4.7	0.268	*	*
CO_2C5	0.06	60	109	50	5.12	0.335	*	*
CO_2C6	0.137	60	118	52	4.65	0.282	*	*
CO_2C7	0.159	65	125	50	4.35	0.163	*	*
CO_2C8	0.546	65	145	50	4.25	0.145	*	*
CO_2C9	0.34	60	125	70	14.5	0.224	0.059	*
CO_2C10	0.33	50	110	66	14.8	0.267	0.073	*
CO_2C11	0.401	48	109	52	13.1	0.263	0.062	0.034

* Not measured

Solvent liberated from raffinate and extract respectively

Table 5-4. CO_2 refluxed extraction conditions.

Run	Extract/Feed	T column °C	P column bar A	T sep °C	P sep bar A	Reflux L/h	S/F	Solvent kg/h	Feed kg/h	S R# kg/h	S E# kg/h	Reflux ratio
CO_2R1	0.377	49	110	54	52	0.20	54.2	14.5	0.267	0.066	0.016	1.4
CO_2R2	0.305	49	111	54	52	0.36	56.2	14.9	0.266	0.074	0.014	3.1
CO_2R3	0.213	49	111	54	52	0.56	53.7	14.4	0.268	0.086	0.010	6.8
CO_2R4	0.316	49	120	54	52	0.52	55.6	14.2	0.255	0.072	0.015	4.4
CO_2R5	0.267	49	121	54	52	1.03	53.9	13.5	0.251	0.078	0.012	10.8
CO_2R6	0.221	49	123	54	53	1.10	53.2	13.3	0.249	0.082	0.011	13.7
CO_2R7	0.252	49	123	54	55	1.16	59.1	14.6	0.246	0.077	0.013	12.7
CO_2R8	0.362	49	131	54	50	0.97	52.4	12.4	0.236	0.064	0.014	7.9
CO_2R9	0.51	49	138	54	52	0.97	64.6	13.6	0.211	0.042	0.017	6.3
CO_2R10	0.384	49	131	54	52	1.15	41.1	12.5	0.304	0.080	0.021	6.8
CO_2R11	0.409	49	131	54	48	1.08	55.4	16.2	0.293	0.072	0.020	6.3
CO_2R12	0.459	49	131	54	50	1.42	47.9	17.9	0.374	0.080	0.029	5.8

Solvent liberated from raffinate and extract respectively

Table 5-5. Ethane countercurrent and reflux extraction runs.

Run	Extract/Feed	P column bar A	T column °C	P sep bar A	T sep °C	Reflux L/h	Solvent kg/h	Feed kg/h	S R# kg/h	S E# kg/h	Reflux ratio
EC 1	0.778	66	45	38	36	0	4.23	0.656	0.12	0.16*	0
EC 2	0.0975	70	60	38	46	0	4.18	0.390	0.22	0.01*	0
EC 3	0.123	81	60	36	61	0	3.99	0.449	0.27	0.12	0
ER 1	0.551	88	60	35	70	0.628	8.36	0.287	0.08	0.024	2.5
ER 2	0.36	88	60	42	70	1.036	8.7	0.472	0.2	0.035	3.6
ER 3	0.378	88	60	42	70	0.930	7.68	0.405	0.17	0.029	3.7
ER 4	0.382	88	60	40	70	0.808	6.44	0.340	0.14	0.024	3.8
ER 5	0.362	88	60	39	70	1.049	9.24	0.454	0.19	0.029	3.9
ER 6	0.333	87	60	40	70	1.186	10.14	0.537	0.24	0.033	4
ER 7	0.321	87	60	40	70	1.268	7.98	0.337	0.14	0.019	7.2

* Not measured, estimated from SPHC EOS

Solvent liberated from raffinate and extract respectively

Several wax extraction runs were done in both countercurrent and countercurrent + reflux mode. The feed and product compositions of a typical countercurrent extraction run are shown in Figure 5-5.

Although some fractionation of the feed wax was achieved, the cut sharpness is poor, with both the extract and raffinate having a large polydispersity. Large overlap between the extract and raffinate products exists, indicating poor separation efficiency.

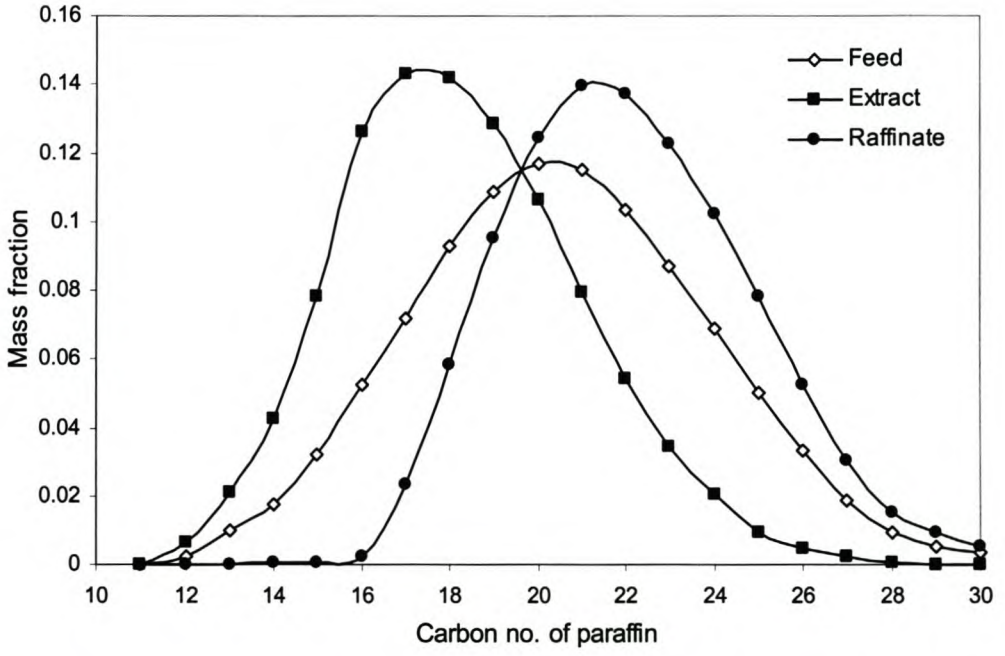

Figure 5-5. Wax feed and solvent-free product compositions for run CO_2C11. (The curves connect the compositions of a wax analysis).

It was found that returning some of the extract to the extraction column as reflux resulted in a much improved fractionation of the wax feed, as can be seen in Figure 5-6. Little overlap between the extract and raffinate products exists, indicating a much better separation efficiency. Since the feed compositions and the wax fraction extracted are very similar for the two runs, the extract compositions of runs CO_2C11 and CO_2R11 are compared in Figure 5-7. It is clear that far more light paraffins are extracted and much less paraffins heavier than n-C_{20} is extracted in run CO_2R11 compared with CO_2C11. This confirms that the use of reflux can dramatically increase separation performance in SCFE.

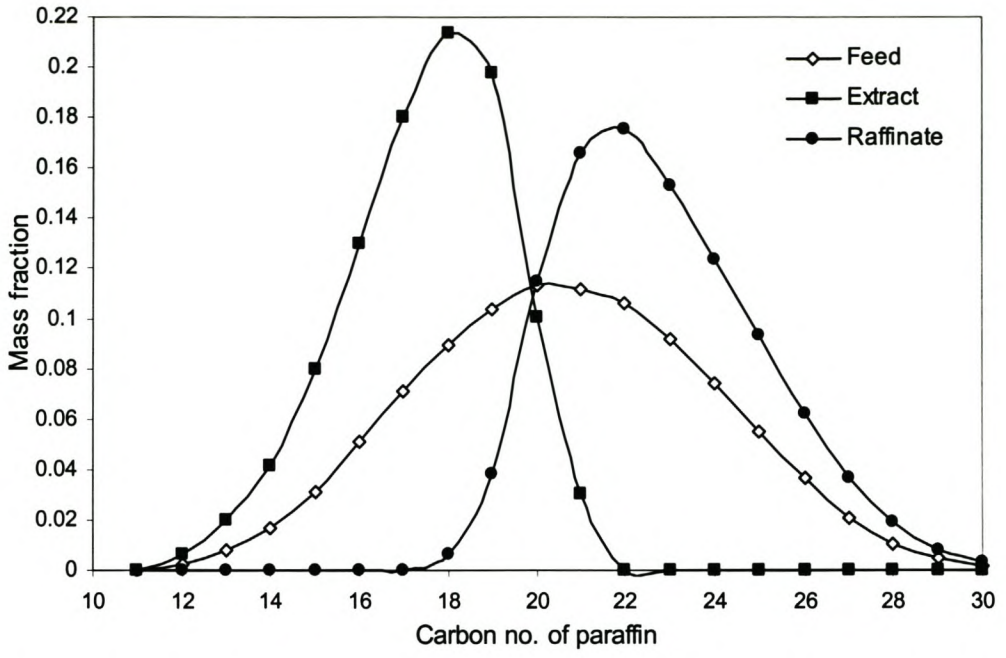

Figure 5-6. Wax feed and solvent-free product compositions for run CO_2R11. The curves connect the compositions of a wax analysis.

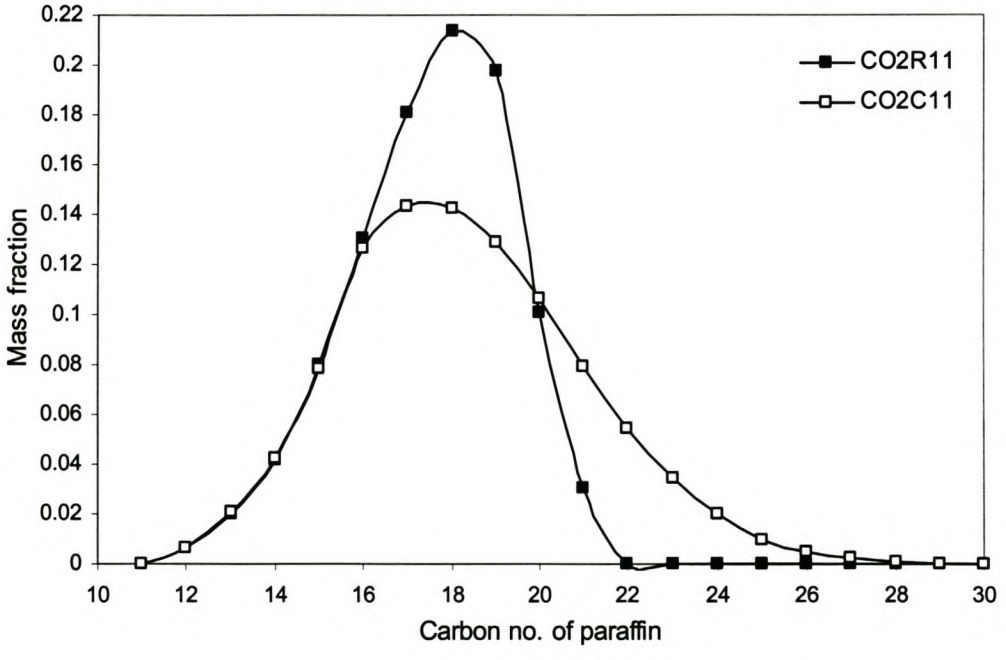

Figure 5-7. Comparison between countercurrent (CO_2C11) and reflux (CO_2R11) experimental extract compositions. (The curves connect the compositions of a wax analysis).

5.5. Modelling results

The experimental results obtained were simulated with the equilibrium stage model discussed in section 5.3 and the modified Patel-Teja equation of state discussed in chapter 4. Thermodynamic modelling of the CO_2 and ethane systems was discussed in chapter 4. Flow rates and temperatures were specified as the experimental values, while the extraction column pressure and number of stages were varied in order to match the simulated solvent-free extract / feed ratio and extract composition respectively. The extraction pressure was chosen as an adjustable parameter since the accuracy of the pressure measurements is about ± 2 bar. The wax feed plate position was fixed as the top stage in the extraction column for countercurrent extraction, and for extraction with reflux it was fixed as the middle stage in the column.

The simulated number of stages and simulated extraction pressures are shown in Table 5-6. The simulated number of theoretical stages varied between 2 – 20 stages. In general the number of stages obtained for countercurrent extraction is less than for countercurrent extraction + reflux. This is most probably caused by pinching of the operating and equilibrium lines, which has also been observed for the ternary system CO_2 – n-C_{16} – 2-methylnaphthalene (Crause and Nieuwoudt, 2000).

Inaccuracies in the calculated phase equilibria can also have a large influence in the number of stages needed during simulation to reach the experimental composition. If an extraction is simulated with calculated relative selectivities lower than actual selectivities, more theoretical stages will be required to match the experimental product composition. The opposite is also possible, where higher calculated selectivities will lead to less theoretical stages required to simulate an experiment.

The HETP calculated for the CO_2 runs are generally better (lower values) than for the ethane runs. The difference between the CO_2 and ethane HETP can be attributed to differences in the accuracy of the phase equilibrium models for the two systems. Data for eight different binary systems were used to fit generalised interaction parameters for the CO_2 – n-alkanes system, while only three different binary systems were used to develop the ethane – n-alkanes interaction parameter correlation. The accuracy of the phase equilibrium models can be tested by comparing the simulated and experimental compositions of countercurrent extraction runs done at low solvent : feed ratios. Figure 5-8 indicates that the CO_2 model predicts less sharp separation than observed, while Figure 5-11 indicates that the ethane model predicts a sharper separation than observed.

Table 5-6. Simulated extraction pressure and number of theoretical stages.

Run	P_{sim} barA	$P_{sim} - P_{exp}$ bar	Stages	HETP m
CO_2C1	103.9	2.9	*	*
CO_2C2	119.3	1.3	*	*
CO_2C3	128	2	*	*
CO_2C4	134	-7	14	0.31
CO_2C5	109.3	0.3	*	*
CO_2C6	118.4	0.4	*	*
CO_2C7	121.3	-3.7	*	*
CO_2C8	140.9	-4.1	*	*
CO_2C9	115.3	-9.7	*	*
CO_2C10	104.5	-5.5	*	*
CO_2C11	104	-5	*	*
CO_2R1	110	0	8	0.55
CO_2R2	110.5	0.5	12	0.37
CO_2R3	111.2	0.2	14	0.31
CO_2R4	114	-6	18	0.24
CO_2R5	122.9	1.9	18	0.24
CO_2R6	122.2	0.8	18	0.24
CO_2R7	122.2	0.8	22	0.2
CO_2R8	131	0	17	0.26
CO_2R9	138	0	17	0.26
CO_2R10	136	5	20	0.22
CO_2R11	129.7	0.3	19	0.23
CO_2R12	142	11	12	0.37
EC1	69.6	3.6	6	72
EC2	73.6	3.6	*	*
EC3	78.3	2.7	*	*
ER1	87.3	-0.7	7	0.63
ER2	87.5	-0.5	6	0.72
ER3	88.1	0.1	6	0.72
ER4	88.2	0.2	6	0.72
ER5	87.4	0.6	6	0.72
ER6	87.3	0.3	6	0.72
ER7	87.2	0.7	8	0.55

* Simulation indicates a pinch, therefore number of calculated theoretical stages not significant.

Another reason might be due to the differences in density between the two systems (which can influence hydrodynamics): the densities of the wax and solvent phases for CO_2 are twice that for ethane.

In Figure 5-8 – Figure 5-10 the simulated and experimental extract compositions of three CO_2 SCFE runs with different reflux ratios are shown. It can be seen that there is a very good correlation between the experimental and simulated extract compositions of the various runs. Similar results were obtained for the other CO_2 SCFE runs. It can also be noted that the simulated extract compositions are mostly slightly less sharp than the experimentally obtained extracts. From a process design point of view this is not a problem, if a SCFE plant is designed using the models developed in this work it is expected that the separation efficiency of the plant will be at least as good as simulated.

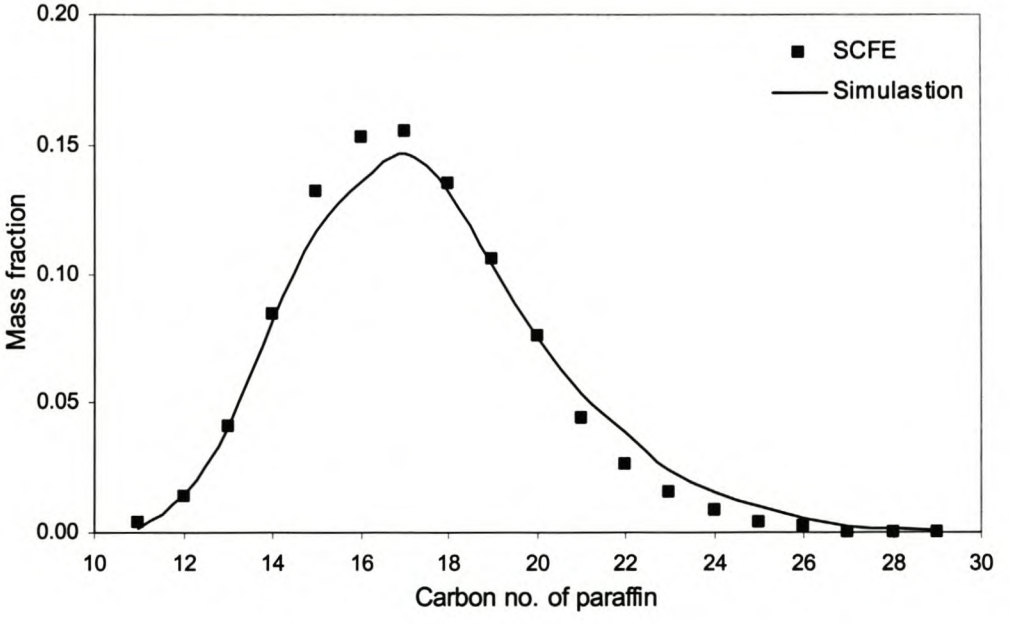

Figure 5-8. Experimental and simulated extract composition of run CO_2C2 (no reflux).

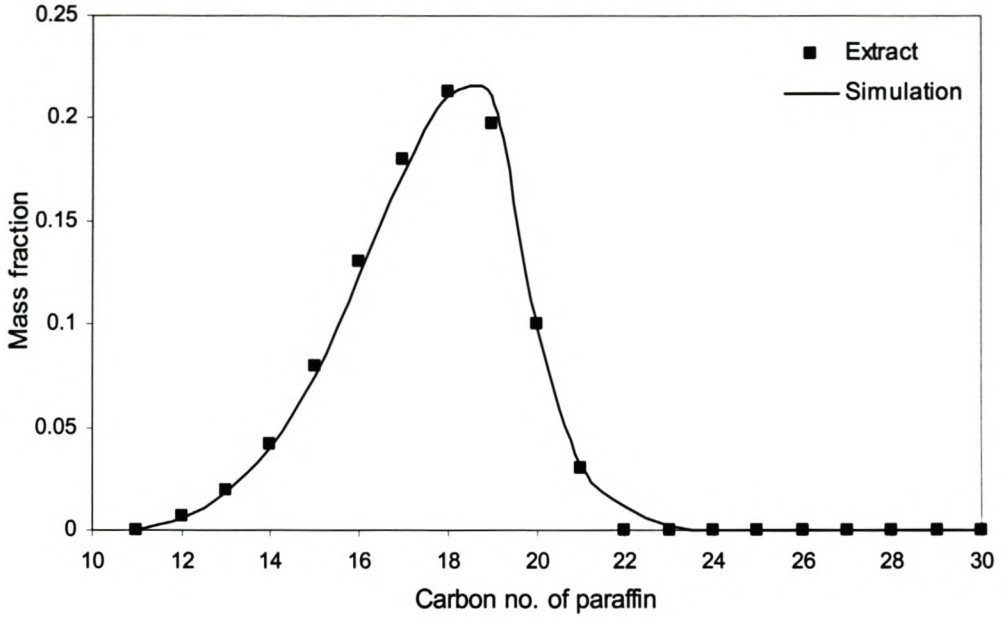

Figure 5-9. Experimental and simulated extract composition of run CO_2R11 (reflux ratio = 6.3).

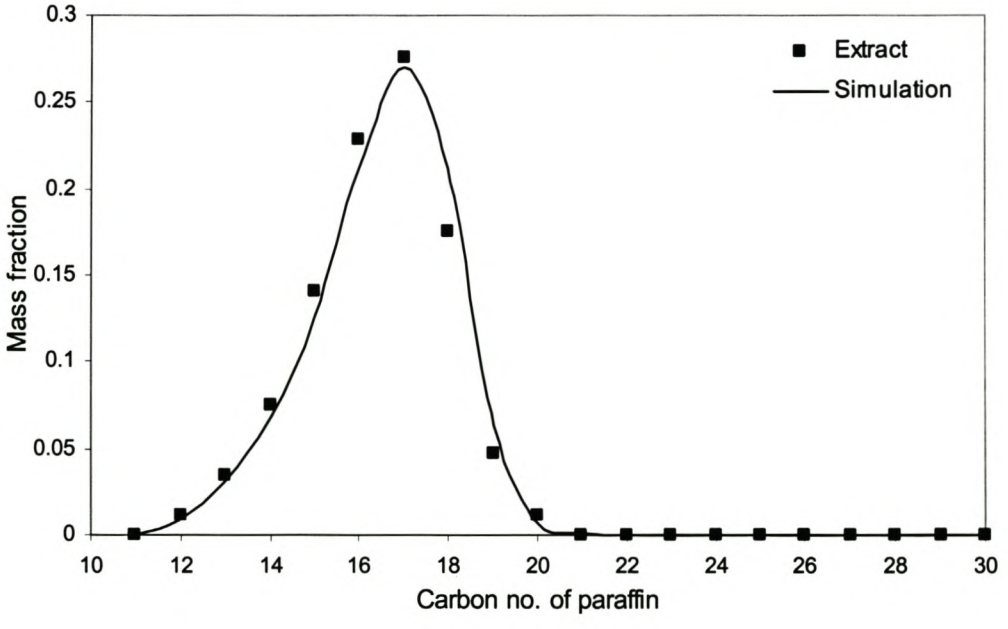

Figure 5-10. Experimental and simulated extract composition of run CO_2R7 (reflux ratio = 12.7).

Experimental and simulated extract compositions of two ethane SCFE runs are shown below in Figure 5-11 and Figure 5-12. The compositions of the

ethane SCFE extracts are accurately predicted. Similar results for the other runs were obtained.

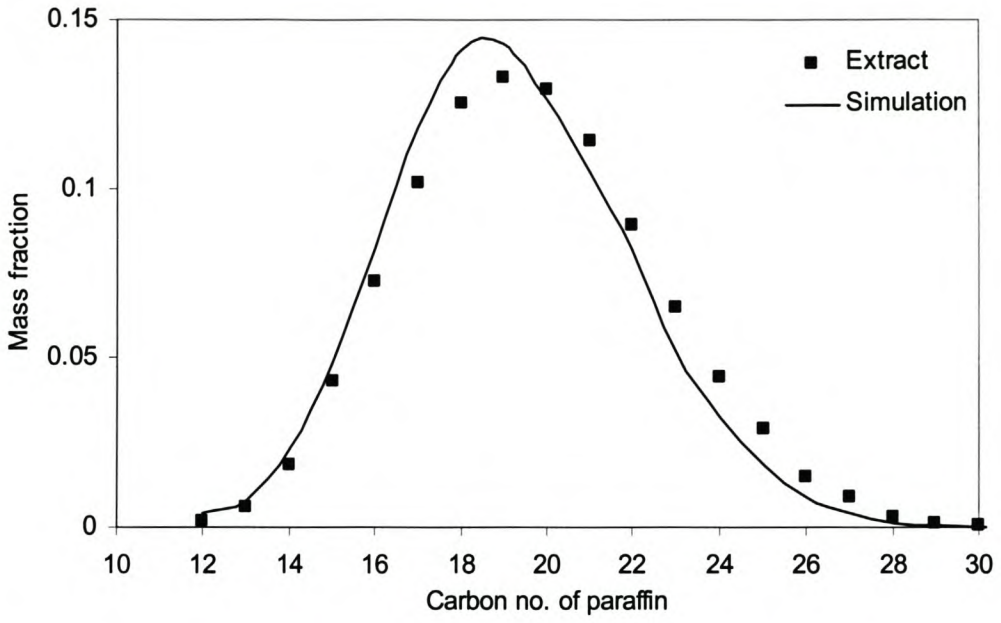

Figure 5-11. Experimental and simulated extract composition of run EC3 (reflux ratio = 0).

Although the modelled and experimental extract compositions are in good agreement, the amount of residual oil in the raffinate (bottoms) product is of more importance in the wax industry. Normally the solvent gets recycled after passing through the separator vessel to save on solvent costs. This recycled solvent still contains small amounts of light wax and oil, which can be detrimental to the quality of the wax product due to the large solvent to feed ratios typically used. Correct simulation of this phenomenon will depend on the ability of the EOS used to accurately predict the wax concentration in the solvent leaving the separator vessel.

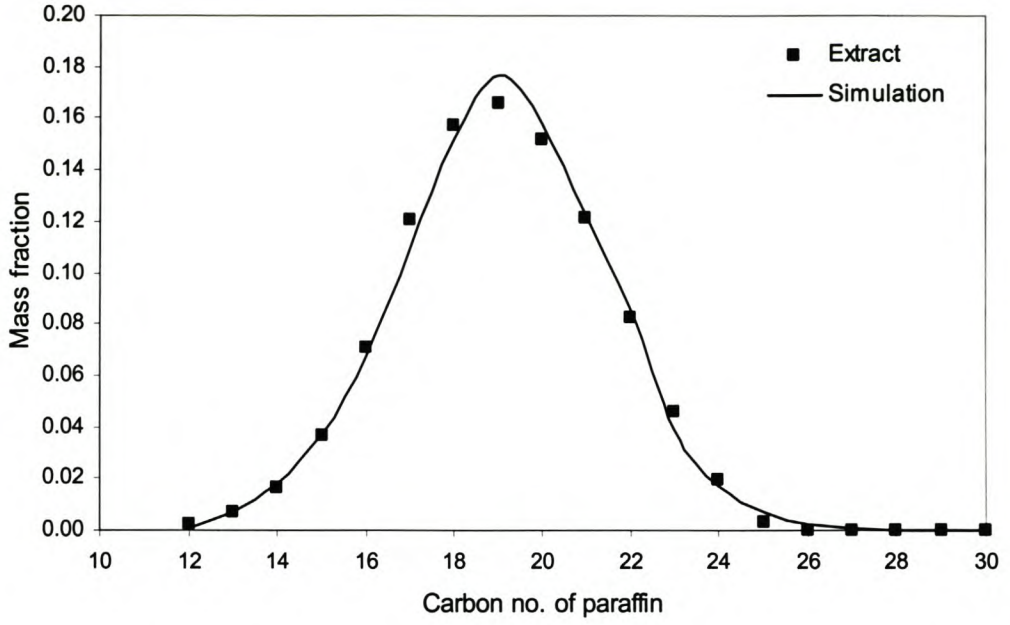

Figure 5-12. Experimental and simulated extract composition of run ER5 (reflux ratio = 4).

The residue composition of run ER7 is shown in Figure 5-13, with simulated residue compositions calculated with and without solvent recirculation. Although the accuracy of the wax analysis for mass fractions below 0.1% is poor, it still appears as if the experimentally observed composition of the light paraffins are below the simulated composition. This indicates that the SPHC EOS used to calculate phase equilibrium in the separator vessel over predicts the amount of wax dissolved in the solvent recycled to the extraction column. This should not be seen as an inconsistency in the SPHC EOS, but rather caused by the fact that the interaction parameters of this EOS were fitted to solubility data of the solvent in n-paraffin liquids only.

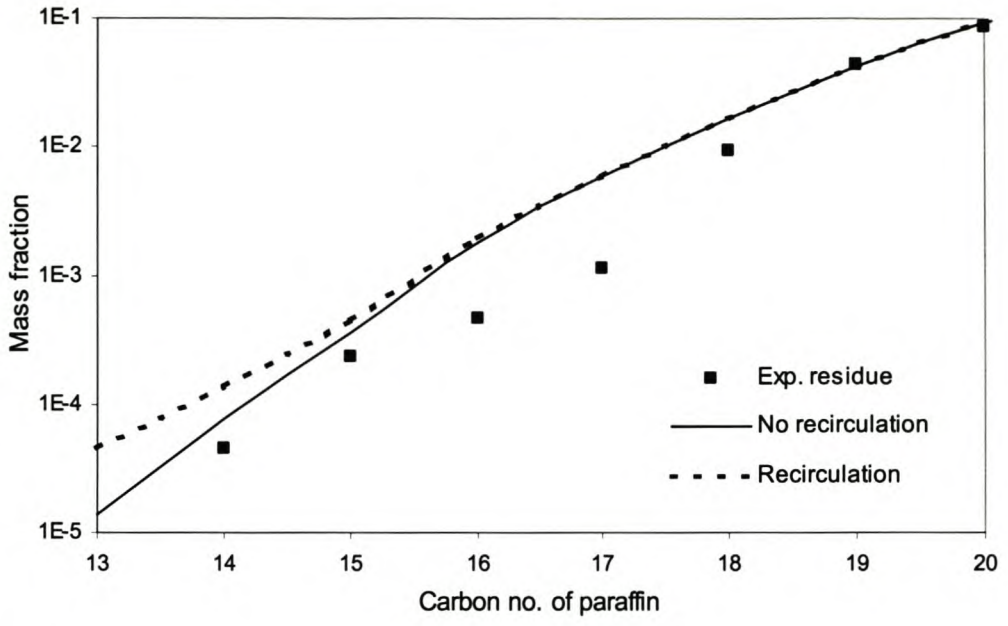

Figure 5-13. Comparison between experimental extract composition (ER7) and extract composition simulated with and without solvent recirculation.

5.6. Comparison of ethane and CO_2 separation efficiency

Direct comparison of the experimental separation efficiencies of ethane and CO_2 is not possible since no two runs have matching operating conditions. Since the equilibrium stage model seems to predict experimental separation performance with reasonable accuracy, the equilibrium stage model will be used to simulate a case study for direct comparison between the separation efficiency of ethane and CO_2. The specifications for the comparison are:

- Extraction temperature = 60 °C.
- Solvent : feed ratio = 30.
- Reflux ratio = 10.
- Solvent free extract to feed ratio = 0.15.

The number of theoretical stages calculated from experimental results (in the same extraction column) differs between ethane and CO_2. The average number of theoretical stages for ethane is taken as 7, while 15 theoretical stages are used for the CO_2 simulation. This corresponds to packed columns of approximately equal height for the two simulations. The extraction pressure is adjusted to obtain the desired extract : feed ratio. A pressure of 77.9 bar was calculated for the ethane extraction simulation, while a pressure

of 138.3 bar was calculated for the CO2 simulation. The two extract products of the two simulations are shown in Figure 5-14.

Based on the specifications set for the simulation, it seems that SCFE using CO_2 as solvent will result in higher separation efficiency. This does not imply that extraction using CO_2 results in a higher selectivity than ethane. If comparative simulations between CO_2 and ethane extractions are done with the same number of stages, the ethane extraction results show higher separation efficiency for the same number of stages than CO_2. This can be seen in Figure 5-15 shown below. It is possible that the pinching observed in the simulation of the CO_2 countercurrent extraction results is caused by conservative phase equilibria calculations. If this is the case, then the number of theoretical stages calculated in Table 5-6 is higher than the actual number of theoretical stages, which can also explain some of the difference between the CO_2 and ethane HETP results.

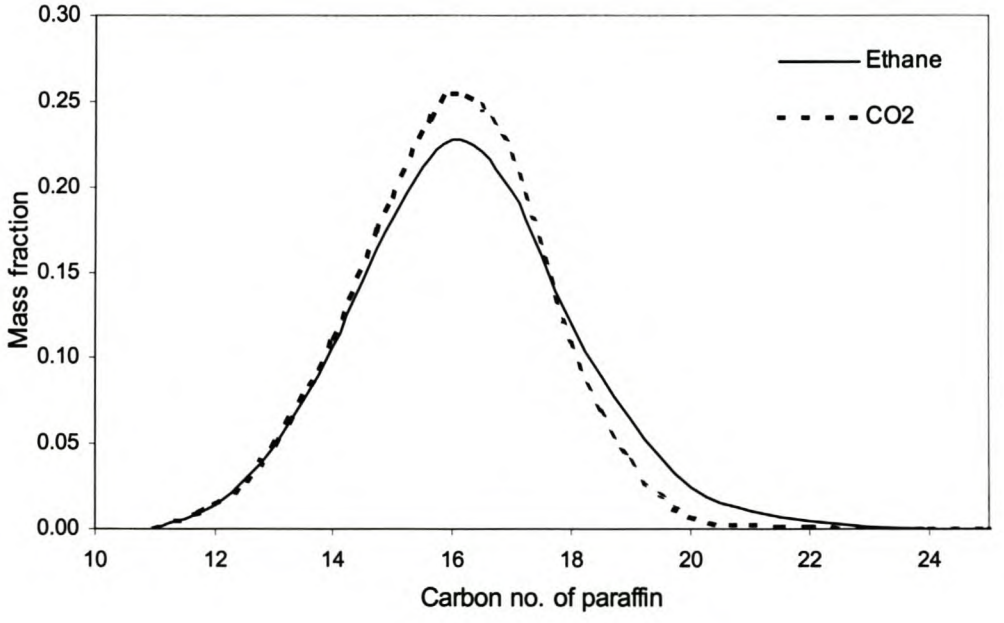

Figure 5-14. Comparison between simulated extract compositions using CO_2 or ethane as solvent (P_{CO2} = 138.3 bar, P_{ethane} = 77.9 bar, 15% of feed extracted at 60 °C, solvent : feed ratio = 30, reflux ratio = 10).

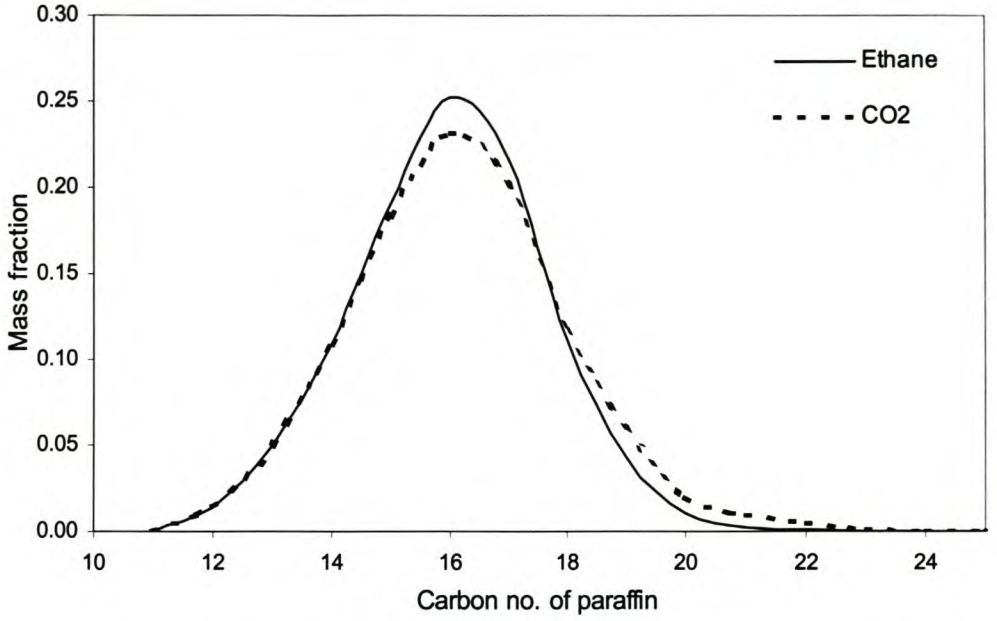

Figure 5-15. Comparison of extract products for SCFE using CO_2 or ethane as solvent. (P_{CO2} = 140 bar, P_{ethane} = 77.7 bar, 15% of feed extracted at 60 °C, solvent : feed ratio = 30, number of stages = 10, reflux ratio = 10).

Although SCFE using CO_2 should result in improved separation efficiency compared with ethane, selecting the most suitable solvent for wax fractionation/deoiling is not straightforward. When choosing between ethane and CO_2 as candidate solvent for SCFE fractionation of n-paraffin waxes, the following factors will determine which solvent will be most suitable:

- The density of both sub- and supercritical ethane is much less (about ½) than the density of CO_2, therefore the process equipment for ethane must be larger than for CO_2.
- The solubility of n-paraffin wax is higher in ethane than in CO_2 hence an ethane SCFE column will operate at a lower pressure than a CO_2 SCFE column.
- CO_2 – n-alkane systems exhibit density inversion at high pressure ((Charoensombut-Amon, Martin et al., 1986)), which might make an SCFE column difficult to control in certain regions.

5.7. Concluding remarks.

Experimental results for the supercritical fractionation of a Fischer-Tropsch wax using ethane or CO_2 as solvent have been reported. It was found that the fractionation efficiency of the SCFE process is increased when returning some reflux to the extraction column.

The experimental data have been modelled using an equilibrium stage based model using a modified Patel-Teja equation of state described in a previous chapter. This model could predict extract compositions with fairly good accuracy, provided the number of stages and the extraction pressures were adjusted somewhat.

The SCFE model developed and tested in this chapter will be used in subsequent chapters to simulate deoiling of a mixed paraffin wax, and to compare the economics of a SCFE deoiling plant with other deoiling technologies.

CHAPTER 6. THE DE-OILING OF PETROLEUM WAX

Up to now only the fractionation and deoiling of Fischer-Tropsch n-paraffin waxes have been considered in this work. A large portion of paraffin wax feedstock (called slack wax) is obtained from the dewaxing of lubricating oil (Sequeira, 1994; Engstler, Stepanski et al., 2000) and can contain, in addition to n-paraffins, various amounts of branched paraffins, naphthenes and some aromatics (Bennett, 1963; McMahon and Wood, 1963; WolfMeier, Schmidt et al., 1996).

The physical properties (such as melting point, ductility, elasticity, seal strength or blocking tendency) of a paraffin wax are greatly influenced by the presence of non-normal paraffins and oil. Brown (Brown et al., 1963) reported that the seal strength of mixtures of n-paraffin and isoparaffin (branched paraffin) waxes are not as good as either the pure n-paraffin or isoparaffin wax (seal strength is a measure of the force necessary to tear two sheets of paper, bonded by wax, apart (Noll and Grogan, 1963)). Removal of the oil and non-normal paraffins from a paraffin wax increases the quality and value of the wax. The relatively high commercial value of deoiled paraffin wax is a strong incentive to upgrade low value waxes containing branched paraffins and oil.

Schuemann-Sasol uses a static crystallisation process to deoil slack waxes. Although static crystallisation can process slack waxes with higher oil content than sweat deoiling (Engstler, Stepanski et al., 2000), problems are experienced with waxes containing large amounts of oil and branched paraffins (Meyer, 2001)). Typical problems associated with deoiling these slack waxes are:

- The wax cake formed tends to bind oil in the wax cake structure.
- The wax cake sometimes detaches from the internal support surfaces and drops into the runoff oil collector.

Solvent extraction of wax flakes using chlorinated solvents can be used for deoiling (Meyer, 2001), but low selectivity results in low yields. Solvent crystallisation is also undesirable due to high energy costs associated with the solvent recovery step, and residual solvent in the wax product.

In this chapter the deoiling of 3 low n-paraffin content petroleum waxes (EMS, SMS and PMR) using short path distillation and supercritical extraction is investigated. The low n-paraffin content of these waxes, coupled with technical difficulties, makes them economically unfeasible to process (Meyer, 2001). Experimental results are presented and modelled using models developed earlier in the thesis. The simulation of wax crystallisation will also be investigated.

6.1. Analysis of the wax feed

Due to the availability of specialised equipment and infrastructure, all petroleum wax analyses were performed in the laboratories of Schuemann-Sasol. An analysis of one of the waxes, EMS, is shown in Figure 6-1. The carbon numbers of the n-paraffins are determined by comparison with an n-paraffin standard. The GC peaks between two n-paraffin peaks are lumped and labelled isoparaffins. The carbon numbers of these isoparaffins are not determined directly from a standard. The carbon numbers assigned to the isoparaffins are assumed the same as the n-paraffin peak following these isoparaffin peaks. It is also important to note that the structures of the non-normal paraffins are also unknown, and may contain cyclic paraffins, highly branched material and even unsaturated hydrocarbons.

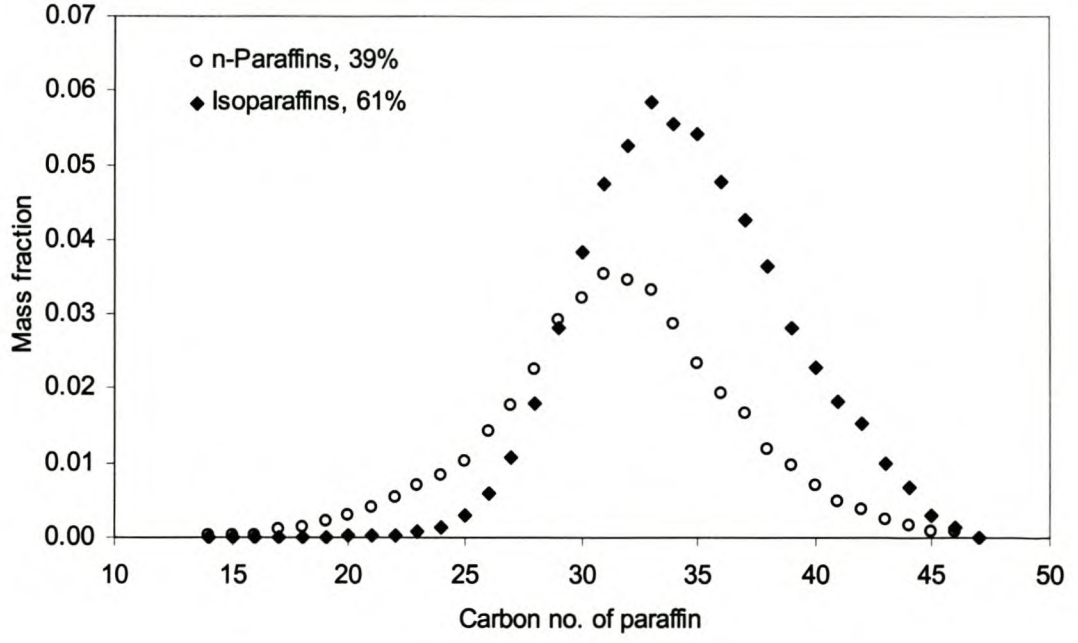

Figure 6-1. Composition of EMS wax.

6.2. Deoiling of EMS wax using SPD

6.2.1. Experimental

The experimental set-up is described in chapter 2. A single SPD run at 200°C and 30 Pa was done. The wax flow rate for the run was 12.45 g/min and the distillate was 10.9% of the feed. Higher distillate recoveries would have been desirable, but the maximum heating temperature was limited by the heating bath and the absolute pressure was limited by the operating limit of the vacuum pump. The composition of the distillate fraction is shown below in Figure 6-2. The complete analyses of the feed and products are available in Appendix E.

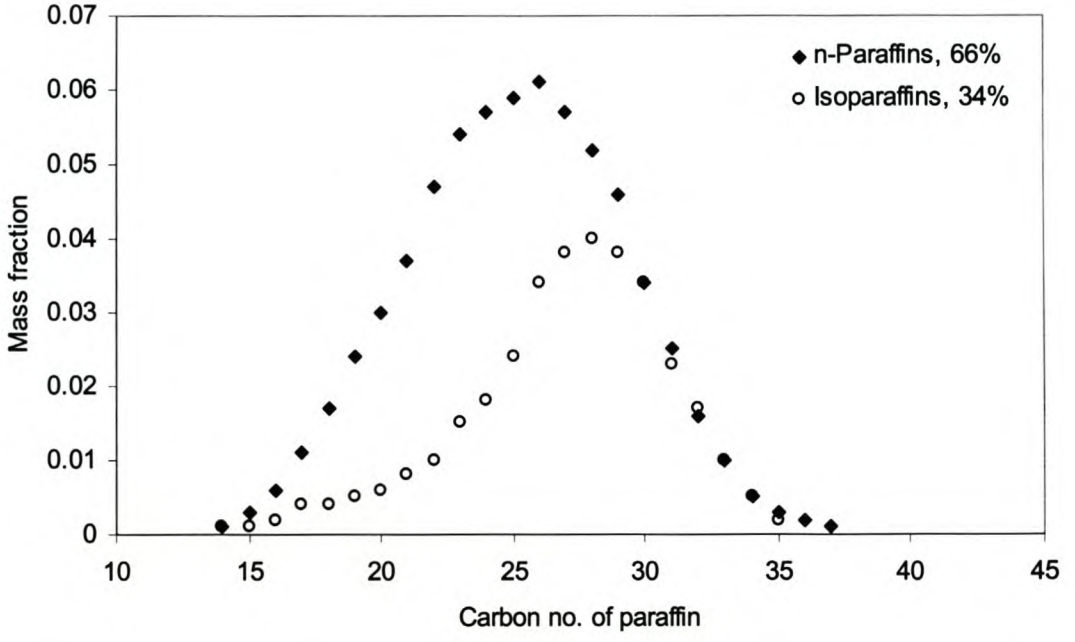

Figure 6-2. Composition of distillate for SPD fractionation of wax EMS.

The SPD run indicates that SPD is not a suitable method for the selective removal of isoparaffins from petroleum wax. The removal of the isoparaffins from the wax is very poor; in fact the n-paraffins concentration in the distillate is even higher than in the feed, indicating that the isoparaffins are concentrating in the bottoms product. The concentration of n-paraffins in the distillate (66% in distillate compared with 39% in feed) is caused by the distributions of the n- and isoparaffins: at low carbon numbers (C_{15} – C_{29}) more n-paraffins are present than isoparaffins. The low carbon number material is evaporated in the SPD unit; hence the distillate will reflect the composition of the low carbon number paraffins of the feed.

Another problem of SPD is the high operating temperatures necessary to distil long chain paraffins. The SPD temperatures for the shorter chain Fischer-Tropsch wax (peak concentration at nC_{20}) is about 130 – 150 °C (see appendix), compared with the SPD temperature of 200°C for the EMS wax (peak concentration between C_{30} and C_{32}). High SPD temperatures also have a negative impact on the economics of a SPD plant, as discussed in section 7.5. SPD deoiling will therefore not be an option for waxes with peak concentrations higher than approximately C_{40} - C_{45}.

The physical properties of the feed wax and SPD bottoms product are shown in Table 6-1. The higher non-normal paraffins concentration in the bottoms cause an increase in the oil content while removal of the shorter chain wax leads to an increase in the congealing point. The needle penetration stayed approximately constant.

Table 6-1. Wax properties of EMS and SPD product.

WAX PRODUCT	Congealing point[1] (°C)	Oil content[2] (%)	Penetration[3] (0.1 mm)	n-Paraffin content[4] (%)
EMS feed	58.5	12.8	98	38.9
EMS SPD Bottoms	59.5	17.6	93	36.8
EMS SPD Distillate	46.5	12.4	131	65.9

1. ASTM D938
2. ASTM D721
3. ASTM D1321
4. GC analysis

6.2.2. Modelling of SPD

The modelling of SPD is discussed in detail in chapter 2, where it was found that the separation could be calculated using a simple flash calculation. The only physical properties needed to model SPD are the molar mass and vapour pressure of each component in the feed. The vapour pressure correlation of Twu (Twu et al., 1994) as modified in appendix (physical properties), are used for n-alkanes. The components in the isoparaffin fraction are not resolved, and as a first approximation the vapour pressure correlation of Twu (Twu, Coon et al., 1994), as modified in appendix (physical properties), are used for this fraction. The acentric factors needed for the vapour pressure correlation are calculated from the 2-methyl alkane correlation shown in appendix (physical properties). The modification of Twu's vapour pressure correlation (Twu, Coon et al., 1994) were done to force the correlation through the low vapour pressure data of (Piacente, Fontana et al., 1994). The acentric factor correlation for the 2-methyl alkanes

were modelled as a perturbation from the n-alkane values, which vanish for long chain lengths. Details of the correlations are given in Appendix A.

The SPD distillation experiment of the EMS wax is simulated by fixing the total pressure at the experimental pressure, and varying the temperature until the simulated and experimental distillate to feed ratios are matched. This is needed due to the fact that one cannot measure the temperature at the evaporating surface of the continuously stirred film. The result is shown in Figure 6-3. The simulated total n-paraffins mass fraction in the distillate is 59%, compared with 66% obtained from the experiment. The small discrepancy between the simulated and experimental n-paraffin fractions in the distillate is quite good, considering the fact that the isoparaffin fractions are approximated as 2-methyl alkanes. The GC-peaks are also not that well resolved – which means that the experimental values are also only accurate to a few percent.

The simulated temperature is 204°C, compared with the heating oil temperature of 200°C. It is expected that the actual liquid surface temperature in the SPD unit should be lower than the temperature of the heating medium. This was also observed in chapter 2 for the n-paraffin deoilng results for n-paraffin wax. The higher simulated temperature for this experiment is probably due to the inaccuracy of the vapour pressure correlation to predict vapour pressures accurately at very low pressure Twu (Twu, Coon et al., 1994).

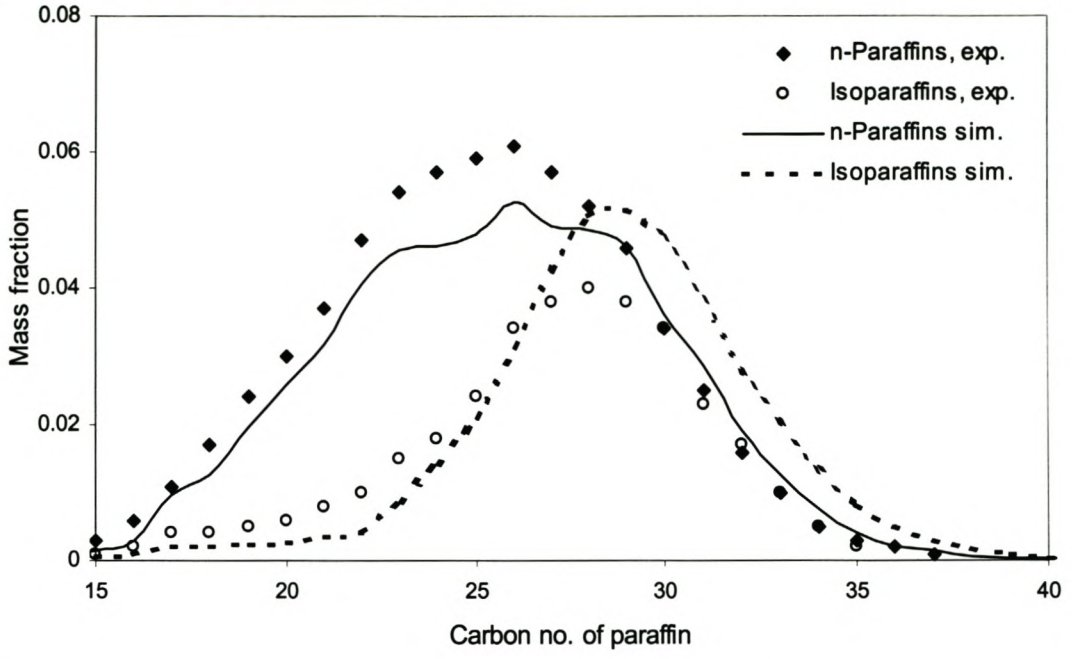

Figure 6-3. Comparison of experimental and simulated distillate compositions for run EMS SPD.

6.3. Deoiling of slack wax using SCFE

The same experimental set-up as described in chapter 5 is used to fractionate the EMS wax. The experimental parameters are shown in Table 6-2 and the product compositions are reported in Appendix E. Ethane and CO_2 were used as solvents.

Table 6-2. Supercritical fluid extraction conditions for deoiling of EMS wax.

Run	Solvent	P (bar)	T (°C)	Feed (g/h)	S/F#	E/F*	Reflux Ratio
EMS R1C	CO_2	165	62	255	52.5	0.081	8.7
EMS R1E	Ethane	110	65	258	32.6	0.304	2.5
EMS R2E	Ethane	110	65	260	32.1	0.257	3.3
EMS R3E	Ethane	115	70	259	32.6	0.236	4.1
SMS R1C	CO_2	200	64	171	68.4	0.211	21.1
SMS R1E	Ethane	112	65	259	33.9	0.138	5.4
SMS R2E	Ethane	122	65	302	27.5	0.406	2.1
SMS R3E	Ethane	123	70	236	33.7	0.157	6.8
PMR R1C	CO_2	200	64	302	43.7	0.172	17.2
PMR R1E	Ethane	130	65	305	21.3	0.282	3.6
PMR R2E	Ethane	125	65	313	16.5	0.163	5.0
PMR R3E	Ethane	111	64	257	29.1	0.226	3.0

Solvent : feed ratio

* Extract : feed ratio

Some of the extract compositions of these SCFE runs are shown below in Figure 6-4 - Figure 6-7. In general the n-paraffin content of the extract increases as the extract to feed ratio increases. This follows from the n-paraffin – isoparaffin distribution in the feed (see Figure 6-1), where the n-paraffin / isoparaffin ratio is larger than 1 at low carbon numbers, and decreases to less than 1 at higher carbon numbers. As more wax is extracted, more of the higher carbon number material is extracted, resulting in a lower total n-paraffin percentage in the extract. This is clearly shown in Figure 6-8 for the three waxes studied.

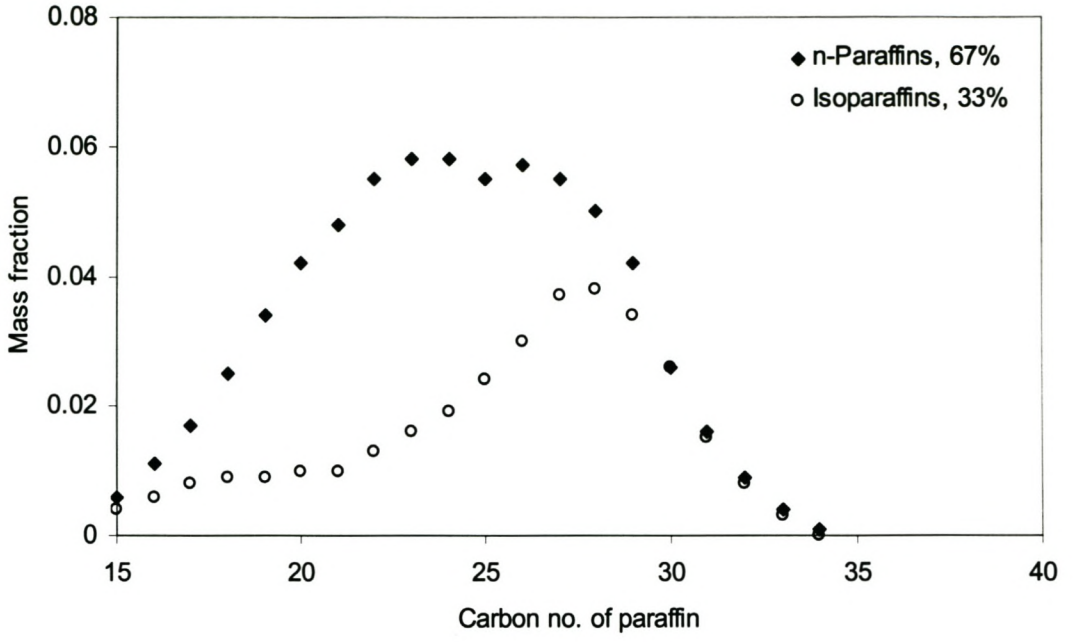

Figure 6-4. Experimental extract composition for SCFE run EMS R1C.

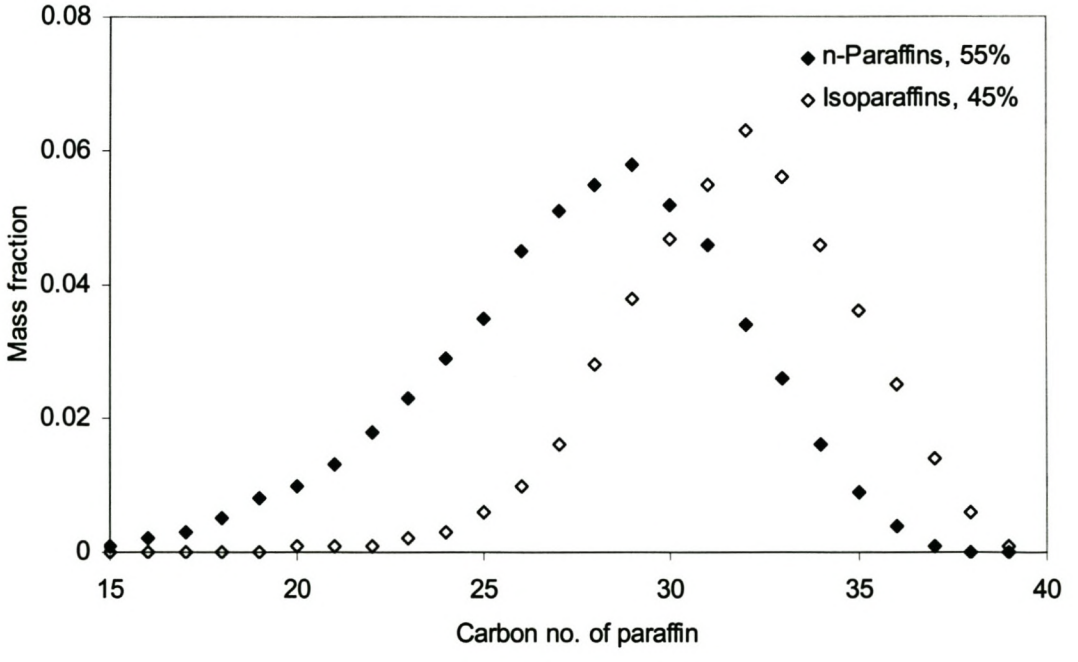

Figure 6-5. Experimental extract composition for SCFE run EMS R1E.

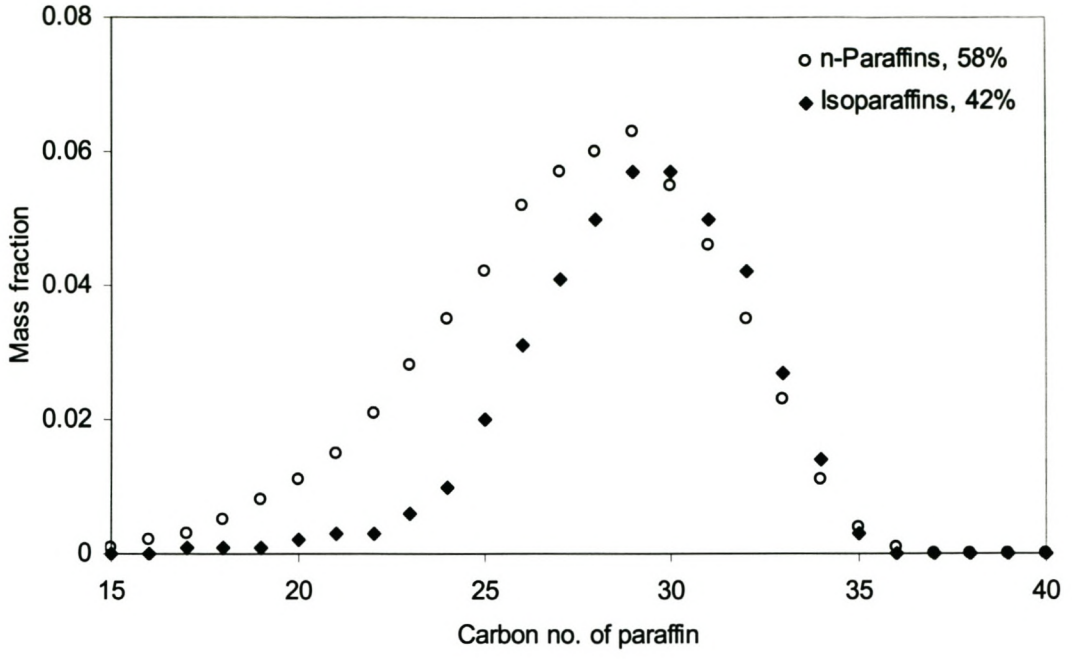

Figure 6-6. Experimental extract composition for SCFE run EMS R2E.

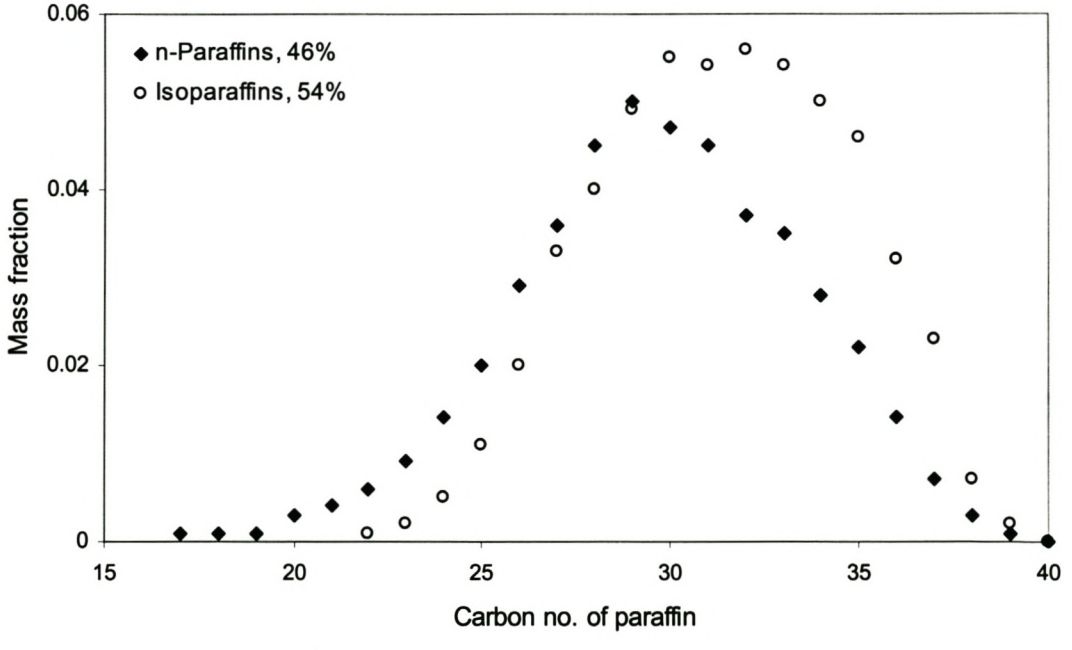

Figure 6-7. Experimental extract composition for SCFE run SMS R1E.

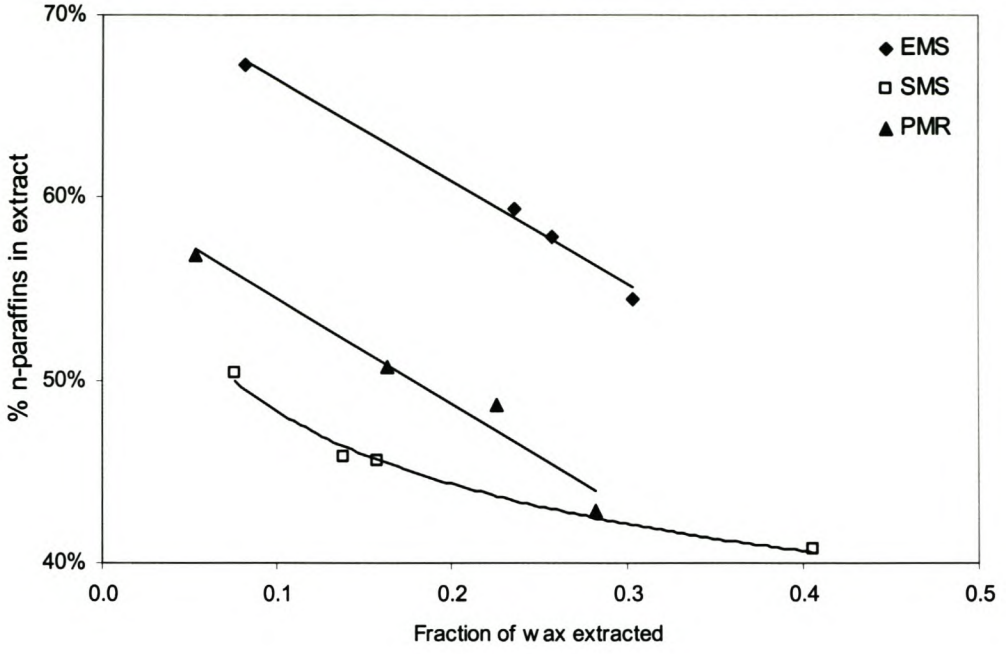

Figure 6-8. Percentage n-paraffins in extract vs. fraction extract/feed fraction (lines indicate trends only).

The characteristics of the SCFE products are compared with the feed wax properties in Table 6-3. Extracting some of the low molecular weight alkanes from the EMS and SMS waxes leads to an increase in congealing point of about 0.5 – 2 °C, and a slight decrease in oil content. This is expected, since low molecular weight alkanes have higher MEK solubilities (higher oil character) and lower melting points. However the needle penetration values increase slightly (wax gets softer), which can be attributed to the lower n-paraffin content of the SCFE product waxes.

Table 6-3. SCFE wax product properties.

Wax product	Congealing point[1] (°C)	Oil content[2] (%)	Penetration[3] (0.1 mm)	n-Paraffin content[4] (%)
EMS feed	58.5	12.8	98	38.9
EMS R1C Residue	60	12.1	88	36
EMS R1C Extract	45	20	186	67
EMS R1E Residue	62	11.9	99	33
EMS R1E Extract	52	17	92	54.6
EMS R2E Residue	61	11.7	101	32.2
EMS R2E Extract	51	17.1	94	57.9
EMS R3E Residue	61	12	95	32.8
EMS R3E Extract	51.5	16.5	103	59.2
SMS feed	65	17.9	86	29
SMS R1C Residue	65.5	16.8	85	28
SMS R1C Extract	51.5	28.4	83	51
SMS R1E Residue	65	18.1	93	27.8
SMS R1E Extract	55.5	26.3	82	46
SMS R2E Residue	67	16.1	90	23.7
SMS R2E Extract	57.5	24.9	83	40.9
SMS R3E Residue	66.4	15.7	100	24.8
SMS R1C Extract	57	26.7	75	45.6
PMR feed	63	3.9	71	38
PMR R1C Residue	64	3.6	71	34
PMR R1C Extract	53.5	8.2	59	58
PMR R1E Residue	64	3.6	71	34
PMR R1E Extract	58	4.7	56	50
PMR R2E Residue	63.5	3.8	72	35
PMR R2E Extract	57.5	4.2	51	51
PMR R3E Residue	63.5	3.6	72	35
PMR R3E Extract	57.5	4.7	55	49

1. ASTM D938
2. ASTM D721
3. ASTM D1321
4. GC analysis

6.4. Modelling of slack wax SCFE

The equilibrium stage model for SCFE is discussed in detail in chapter 5. The Patel-Teja equation of state is used, as discussed in section 4.3, to model phase equilibrium between the solvent and wax phases. The pure component properties needed are obtained from Appendix A and the binary interaction parameters are calculated with equations 4.125 – 4.129. The non-normal paraffin fractions are assumed to be 2-methyl alkanes, using the 2-methyl

alkane correlations for T_c, P_c and ω to calculate phase equilibria with the mPT EOS. The solvent – 2-methyl alkane interaction parameters of the mPT EOS are calculated using the correlations fitted to n-alkane phase equilibria (chapter 5).

The experiments were simulated by specifying the operating temperature, solvent and feed rates, and reflux ratio. The simulations were done with 10 equilibrium stages, with the feed entering on stage 6. This is the approximate number of stages determined from the simulation of the results of supercritical fluid extraction of Fischer-Tropsch wax (see chapter 5). The total pressure was adjusted until the simulated and experimental extract to feed ratio was obtained. A comparison between the experimental and simulated pressures and n-paraffins content of the extract is given below in Table 6-4.

Table 6-4. Comparison between experimental and simulated results.

Run	Pressure (bar)		n-Paraffins in extract (%)	
	Experiment	Simulated	Experiment	Simulated
EMS R1C	165	156	67	57
EMS R1E	110	112.3	55	54
EMS R2E	110	110.6	58	53
EMS R3E	115	116.3	59	54
SMS R1C	200	194.4	50	48
SMS R1E	112	114	46	51
SMS R2E	122	129	41	42
SMS R3E	123	125.6	46	48
PMR R1C	200	185	57	46
PMR R1E	130	130.2	50	43
PMR R2E	125	125.4	51	44
PMR R3E	111	115.4	49	45

The simulated extraction pressures for all the experiments, except runs EMS R1C and PMR R1C, are in close agreement with the experimental value. The agreement between the experimental and simulated n-paraffins fraction in the extract is within about 10%, which is quite good.

The simulated composition profiles of the extracts (Figure 6-9 - Figure 6-12) are in qualitative agreement with the experimental composition profiles. In general the amount of short chain n-paraffins is correctly predicted, but the amount of long chain n-paraffins are under-predicted. The shape of the

simulated isoparaffin distribution curve follows the general trend of the experimental distribution, but the simulated peak isoparaffin concentration is consistently higher than observed.

The zigzags in the simulated n-paraffin distribution for run EMS R1E (see Figure 6-9) are probably caused by the acentric factor values used for the n-alkanes. The acentric values for the n-alkanes up to n-C_{30} + n-C_{32} and n-C_{36} were taken from the Pro/II database, which do not lie on a smooth curve. Small errors in the wax analyses might also account for these uneven bumps in the n-paraffin distributions. The n-alkane acentric values were smoothed using a low order polynomial function, which resulted in smooth simulated extract composition profiles. All subsequent results were calculated using the smoothed acentric factors for n-alkanes.

The discrepancy between the experimental and simulated extract compositions are most likely caused the following factors:

1. The interaction coefficient correlation was tuned to shorter chain n-alkane paraffin data and does not extrapolate reliably.
2. The isoparaffin fraction is approximated by 2-methyl paraffins.
3. The 2-methyl alkane correlations are extrapolated over a large carbon number range.
4. The wax analyses are not very accurate.

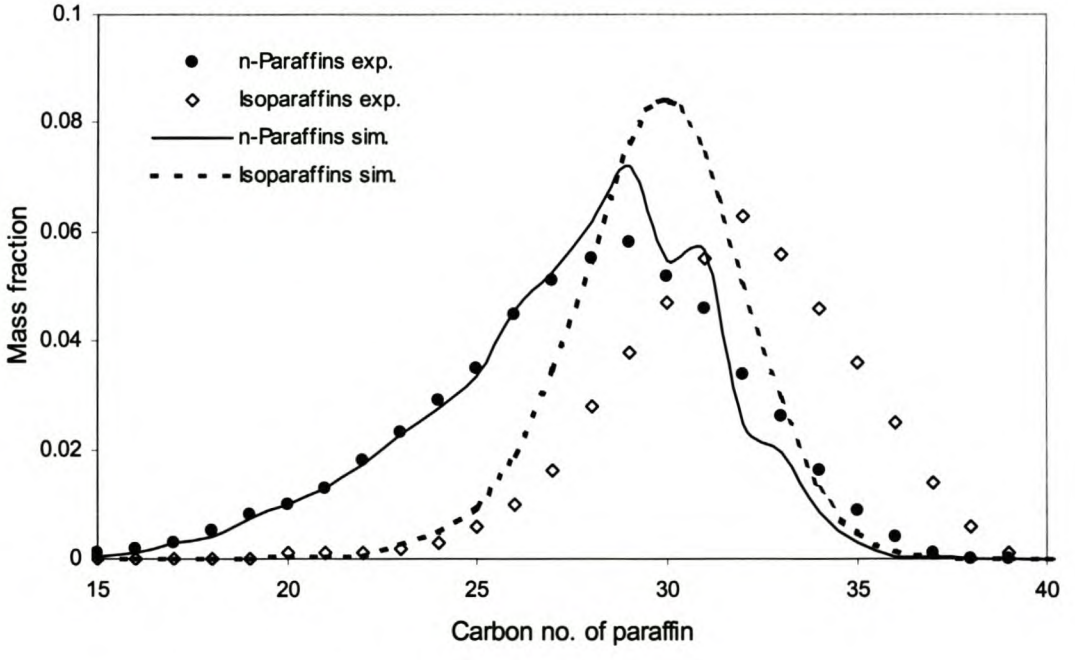

Figure 6-9. Simulation of EMS R1E extract composition.

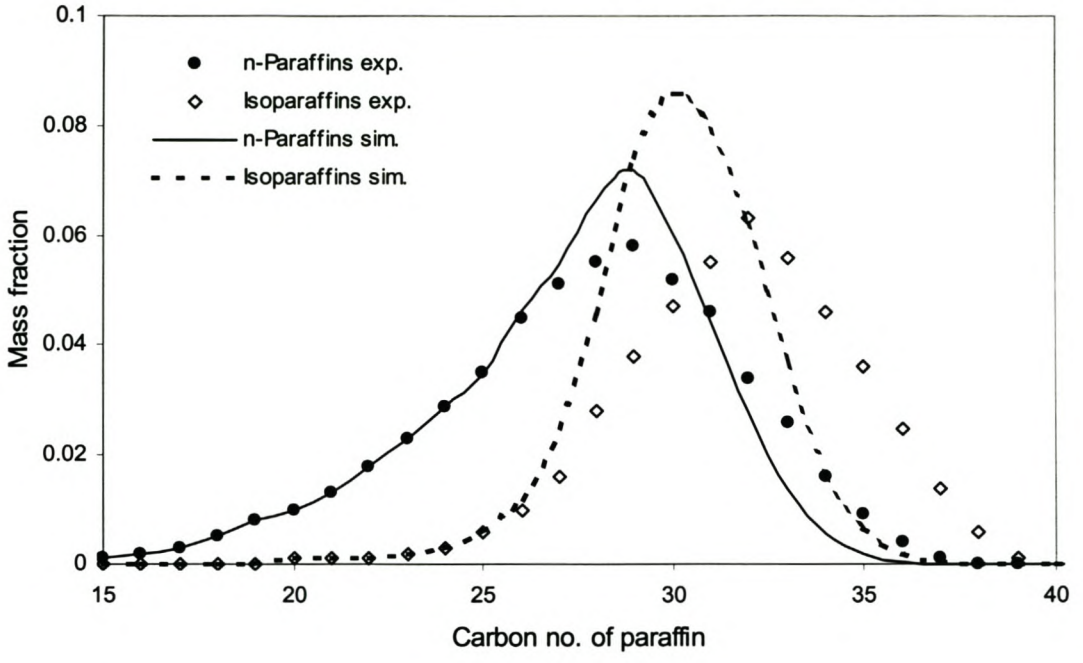

Figure 6-10. Simulation of EMS R1E using smoothed acentric factors for the n-alkanes.

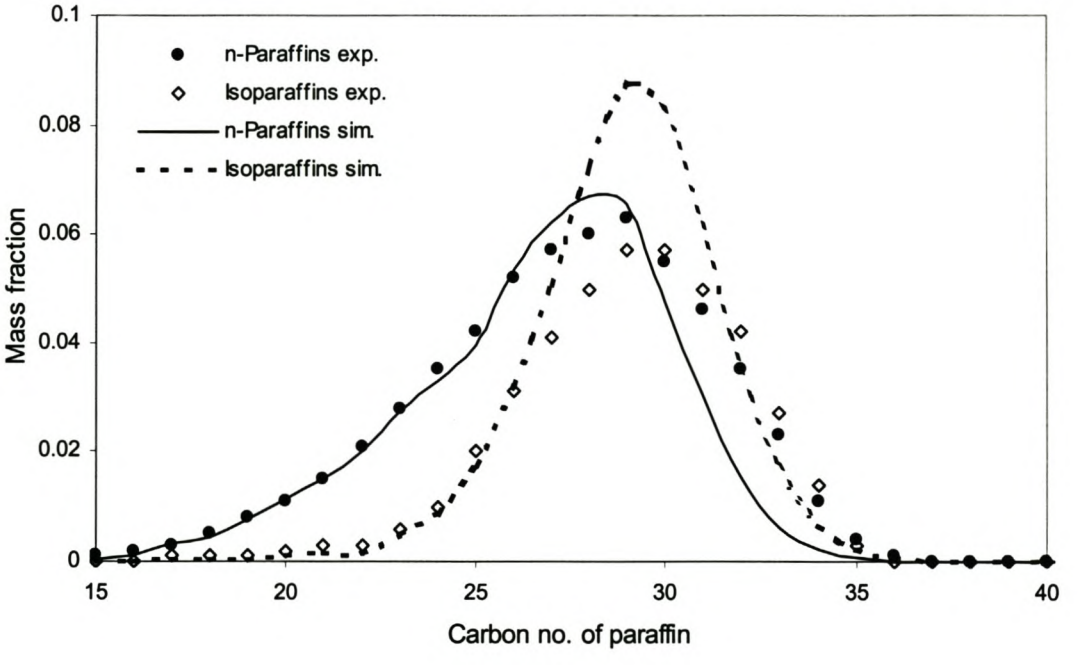

Figure 6-11. Simulation of EMS R2E extract composition using smoothed acentric factors for the n-alkanes.

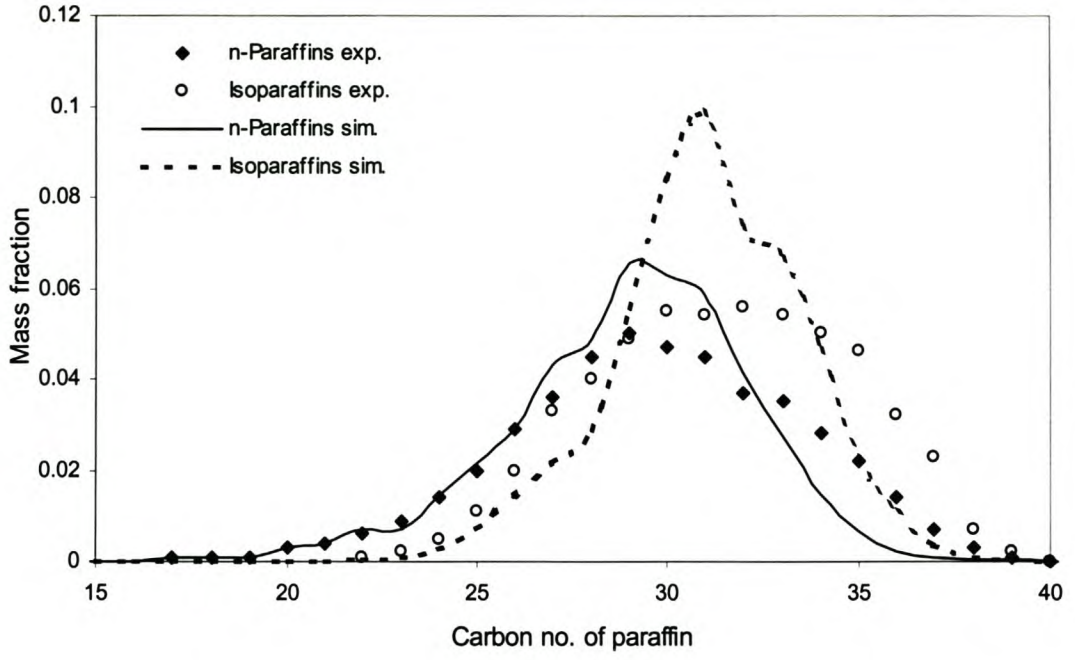

Figure 6-12. Simulation of SMS R1E extract composition using smoothed acentric factors for the n-alkanes.

Examination of Figure 6-9 to Figure 6-12 shows that the long-chain fraction is consistently under-predicted in the extract, which explains the relative high peaks in the simulated extract distribution, compared with the experimental paraffin distribution. Since the interaction parameter correlations were fitted to data obtained for ethane - n-alkanes up to n-C_{28}, the calculated interaction parameters may not be accurate for the long-chain paraffins. The l_{ij} interaction parameter correlation of the ethane – n-alkane system predicts interaction parameters that increase linearly as the chain-length of a paraffin increases. This may result in unrealistic behaviour. It was found that placing an upper limit of 0.14 on the l_{ij} parameter improved the SCFE ethane extraction simulations considerably.

The extract compositions of two SCFE extractions are show below in Figure 6-13 and Figure 6-14, where a qualitative improvement in especially the isoparaffin distribution can be seen.

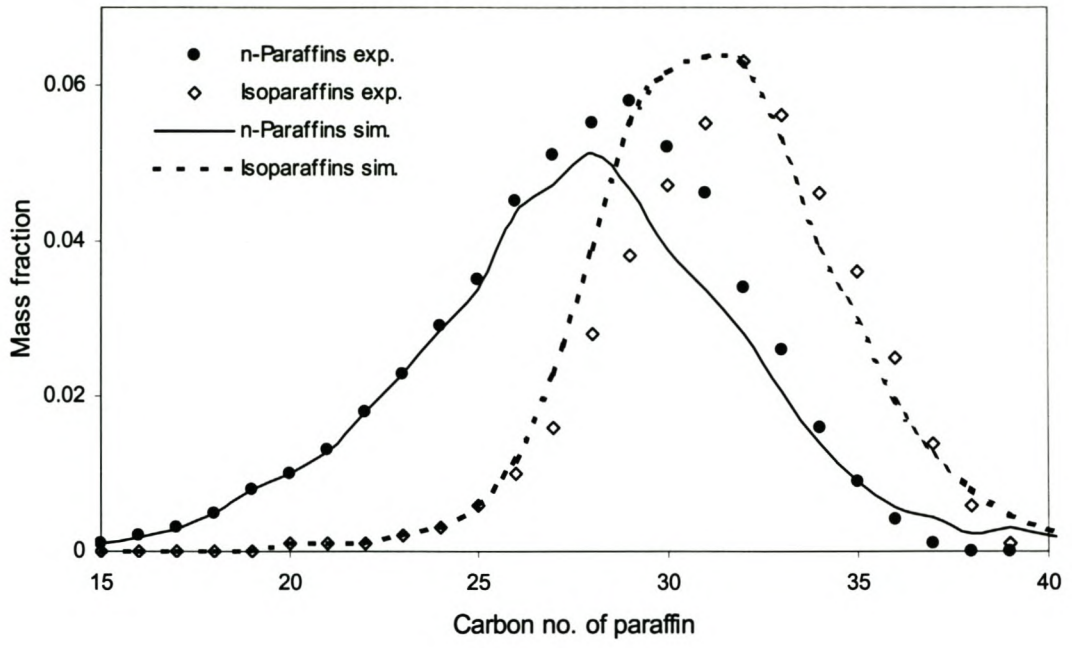

Figure 6-13. Simulation of run EMS R1E extract composition with the l_{ij} interaction parameter capped to 0.14 in value.

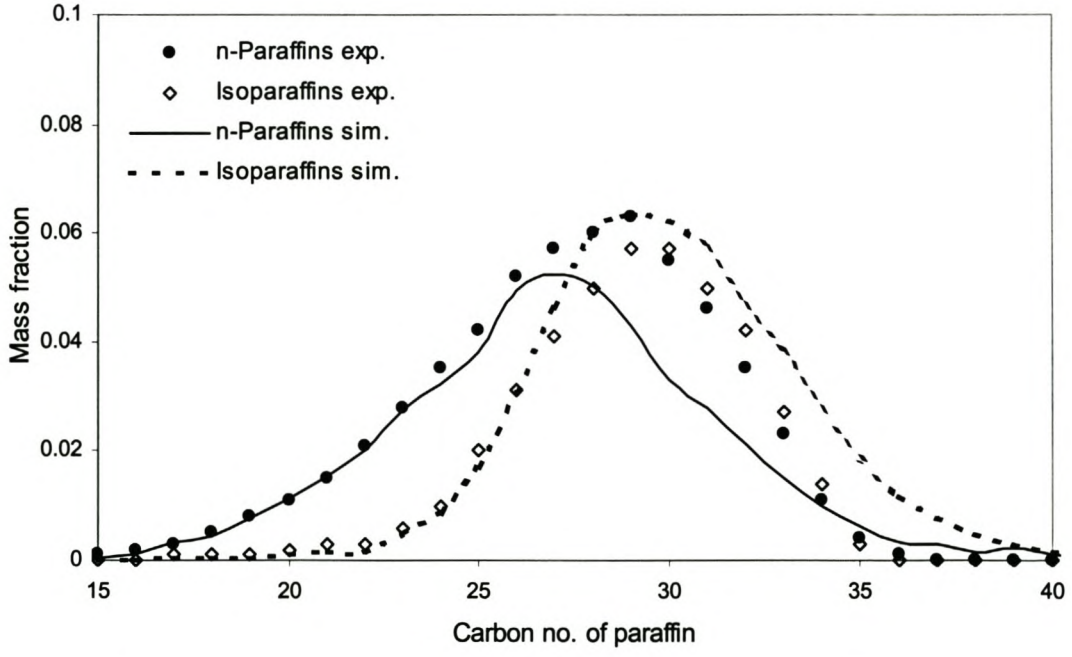

Figure 6-14. Simulation of run EMS R2E extract composition with the l_{ij} interaction parameter capped to 0.14 in value.

6.5. Deoiling of slack wax using wax crystallisation

The deoiling of a mixture of normal and branched paraffins (EMS wax) has been investigated using short path distillation and supercritical extraction. It was shown that it is not possible to selectively separate the normal and branched paraffins. Although practical problems (separation of wax cake and oil) impede the use of static crystallisation, solvent crystallisation can be used to deoil EMS wax. In this section some of the modelling issues of wax crystallisation will be discussed.

6.5.1. Modelling

The modelling of wax crystallisation is discussed in detail in chapter 3. The equilibrium distribution ratio of component *i*, K_i, is calculated from eq. 3.14:

Eq. 3.14

$$K_i^S = \frac{x_i}{s_i} = \frac{\gamma_i^S}{\gamma_i^L} \exp\left[-\frac{\Delta H_i^m}{RT}\left(1 - \frac{T}{T_i^m}\right) - \frac{\Delta H_i^t}{RT}\left(1 - \frac{T}{T_i^t}\right) + \frac{\Delta Cp_i^m}{R}\left(\frac{T_i^m}{T} - 1 - \ln\left(\frac{T_i^m}{T}\right)\right)\right]$$

The solid phase activity coefficients can be calculated using local composition models such as Wilson or NRTL (see chapter 3). The calculation of interaction energies for components with differing molecular structures is not straightforward, therefore an ideal solid phase will be assumed for calculation purposes. It is further assumed that a single solid solution will form. Liquid phase activity coefficients are also assumed ideal, to simplify the solid-liquid equilibrium calculations. This is contrary to the n-alkane modelling done previously, where local composition models such as Wilson and NRTL were used to model non-idealities. Evaluation of the interaction energies between normal and branched alkanes is not as straightforward as the model proposed for n-alkanes, and was not attempted here. The general trends simulated should however still give a qualitative indication of the separation achieved.

The pure component properties (T_i^m, ΔH_i^m, ΔCp_i, ΔH_i^t) for n-alkanes are given in Appendix C. The exact composition of the non-normal alkanes in the wax is not known and two methods are used to calculate the needed physical properties: the non-normal alkanes are assumed to consist of 2-methyl alkanes, and empirical correlations developed to model wax precipitation from crude oil will be used ((Brown et al., 1994; Lira-Galeana, Firoozabadi et al., 1996)). Correlations for the temperature of melting and enthalpy of melting for 2-methyl alkanes are given in Appendix C. Several correlations for melting

temperature and melting enthalpy of non-normal alkanes have been published, e.g. (Hansen et al., 1988; Brown, Niessen et al., 1994; Lira-Galeana, Firoozabadi et al., 1996). The following sets of correlations were used to calculate solid-liquid equilibria for wax mixtures of n-alkane and non-normal alkanes:

This work. Properties of n-alkanes calculated from correlations given in Appendix C. 2-Methyl alkane melting points and melting enthalpies calculated from correlations in appendix. Heat capacity difference for 2-methyl alkanes calculated with n-alkanes correlation, while solid-phase transitions are ignored for the 2-methyl alkanes.

Lira-Galeana (Lira-Galeana, Firoozabadi et al., 1996). N-alkane correlations:

Eq. 6.1 $$T^m = 374.5 + 0.02617 M_r - \frac{20172}{M_r}$$

Eq. 6.2 $$\Delta H^m = 0.597 M_r T^m$$

Eq. 6.3 $$\Delta Cp = 1.27 M_r + 1.94 \times 10^{-3} M_r T^m$$

Non-normal paraffin correlations:

Eq. 6.4 $$T^m = 333.46 - 419.01 \exp(-0.008546 M_r)$$

Eq. 6.5 $$\Delta H^m = 0.221 M_r T^m$$

ΔCp for the non-normal alkanes is also calculated using Eq. 6.3. Solid phase transition effects were ignored.

Brown (Brown, Niessen et al., 1994). N-alkane correlations:

Eq. 6.1 $$T^m = 374.5 + 0.02617 M_r - \frac{20172}{M_r}$$

Eq. 6.6 $$\Delta H^m = 0.682 M_r T^m$$

Non-normal alkane correlations:

Eq. 6.7 $$T^m = T^m(n-alkane) - 90 + \frac{80CN}{100 + CN}$$

The enthalpy of melting of the non-normal alkanes is calculated using Eq. 6.6, while solid phase transition effects and heat capacity effects are ignored.

The above model and physical properties correlations are used to simulate the separation performance of an equilibrium stage crystallisation of EMS wax. The fraction wax precipitated was specified as 70% (mass). Results for the different models are shown below.

It is clear that the physical property correlations used in the calculation of the solid-liquid equilibria have a large influence on the results. The calculated fraction n-paraffins left in the liquid phase varies from 34% (correlations from this work) to 0.3% (correlations of Brown), indicating that the n-alkane / isoalkane separation is either very difficult or very easy. It is known that the EMS wax can be deoiled using solvent extraction of the wax flakes, therefore the results predicted by using 2-methyl alkane properties are too pessimistic (Figure 6-15). On the other hand the separation is not as easy as indicated by the correlations of Brown (Figure 6-17). These results indicate that the correlations used to describe the non-paraffin fraction are very important, and that qualitatively wrong results can be obtained if the non-normal paraffin fraction is characterised incorrectly.

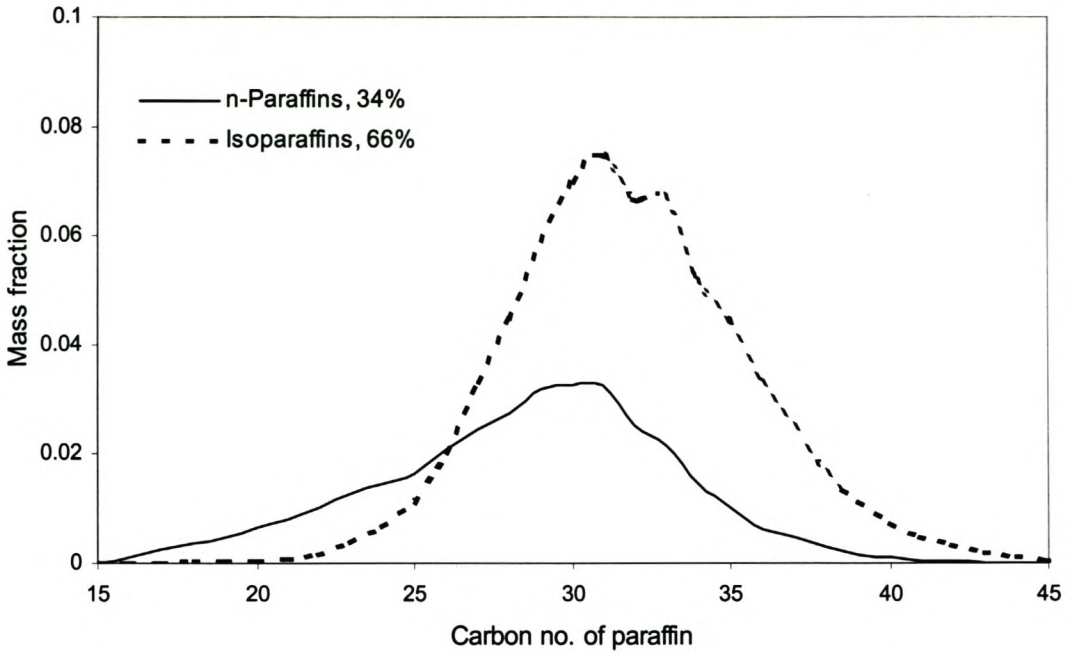

Figure 6-15. Calculated composition of oil for 70% crystallisation of EMS wax using physical properties of this work. T = 64.1 °C.

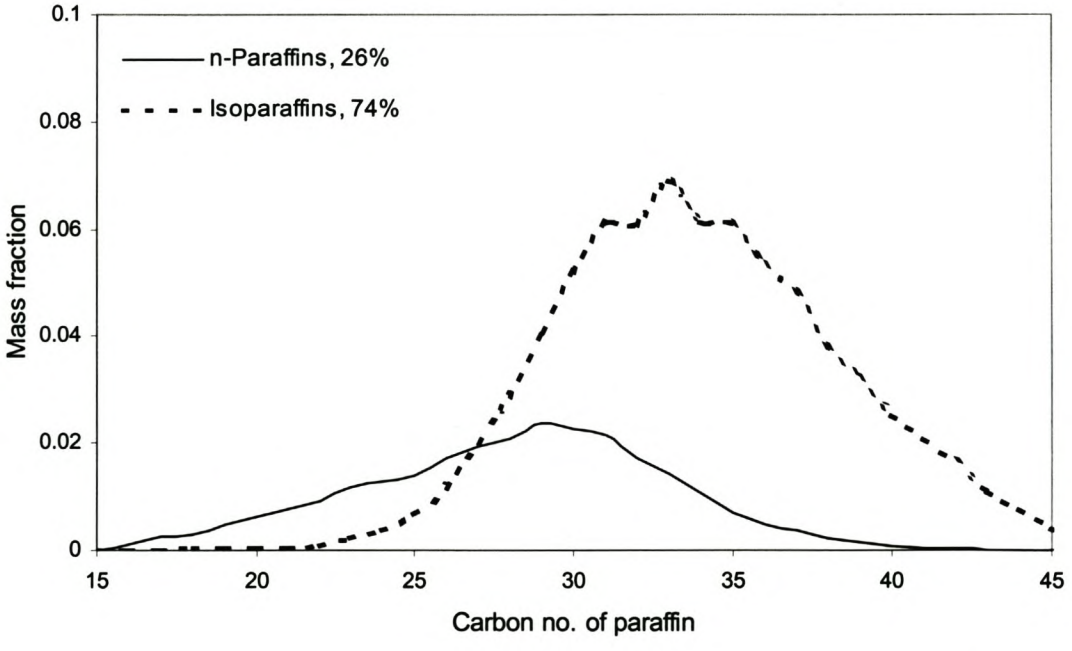

Figure 6-16. Calculated composition of oil for 70% crystallisation of EMS wax using physical properties of Lira-Galeana (Lira-Galeana, Firoozabadi et al., 1996). T = 59.1 °C.

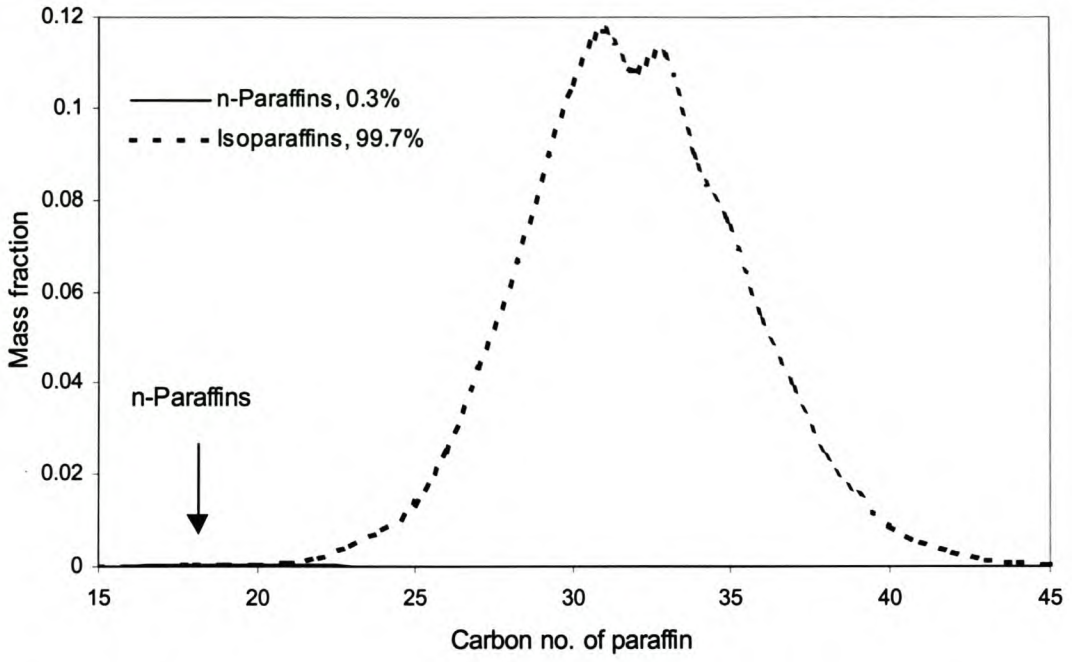

Figure 6-17. Calculated composition of oil for 70% crystallisation of EMS wax using physical properties of Brown (Brown, Niessen et al., 1994). T = 7 °C.

The separation predicted using correlations given by Lira-Galeana is probably nearer to the actual behaviour of the EMS wax (74% isoparaffins in oil vs. 61% in feed), which would require a multistage countercurrent crystalliser set-up for deoiling.

The degree of branching of a paraffin has a large influence on the melting point of the component, e.g. the melting point of n-C_{28} is 61.2°C, while the melting point of 10-nonylnonadecane ($C_{28}H_{58}$) is only –5°C (Warth, 1956). The thermodynamics of crystallisation is strongly influenced by the melting points of components, and a more detailed analysis of the wax is needed (together with accurate property correlations for the individual components) to give more accurate crystallisation simulations.

6.6. Conclusions

In this chapter the deoiling of a mixed paraffin wax, EMS, has been investigated. Experiments showed that separation of the normal and non-normal paraffins in the wax is not possible using either short path distillation or supercritical fluid extraction. The experimental results have been simulated by extending models previously applied to n-paraffin waxes and qualitative agreement between the simulations and experiments were obtained. This was done by treating the non-normal paraffins as 2-methyl paraffins.

It is known that this wax can be deoiled using solvent extraction of the wax flakes, albeit with a low yield. Using a solid-liquid equilibrium model, it was shown that using 2-methyl alkane properties for the non-normal fraction showed poor separation between normal and non-normal paraffins – although it is significantly better than SPD or SCFE. Other correlations for the non-normal paraffin fraction indicated that an easy separation is possible. This indicates that the analysis of the non-normal fraction is very important for accurate modelling of crystallisation.

Deoiling through crystallisation appears to be the only option currently for waxes with high non-normal paraffin content. The use of solvent deoiling is more energy intensive and therefore more expensive than static crystallisation. If the deoiling of this type of wax is to be economical compared with waxes having higher n-paraffin content, the practical problems currently experienced with static crystallisation have to be overcome.

Supercritical extraction can be further investigated as a possible deoiling process for petroleum waxes by using alternative solvents such as halogenated alkanes (Nieuwoudt, 2001) or branched chain entrainers such as isobutane. The halogenated alkanes might increase the extraction selectivity of polarisable molecules such as alkenes and aromatics, while a branched chain entrainer might increase the extraction selectivity with regards to branched alkanes.

CHAPTER 7. N-PARAFFIN WAX FRACTIONATION: STATE OF THE ART VS. SCFE.

In chapters 2 and 3 models have been developed to describe the separation efficiency of the current state-of-the-art wax deoiling and fractionation processes (solvent recrystallisation, wax sweating and short path distillation (SPD)). Supercritical fluid extraction (SCFE) was investigated as an alternative wax deoiling and fractionation technology. In chapter 4 supercritical fluid – n-paraffin phase equilibrium data are correlated using a cubic equation of state approach, which is used in chapter 5, together with an equilibrium stage extraction model, to simulate SCFE. All these models were tested against experimental or published data, and were found to give satisfactory results.

In this chapter the deoiling of a synthetic n-paraffin wax mixture will be simulated using crystallisation, SPD and SCFE processes. The cost effectiveness of these processes will then be compared, based on capital and running costs. Models describing the separation efficiency of these processes have been tested in previous chapters, and will be used to calculate the simulated number of separation stages necessary to achieve the required separation.

7.1. Case study description

A wax feed consisting of n-paraffins must be deoiled to obtain a product containing less than 0.5% by mass of n-paraffins with a molar mass less than that of n-C_{20}. This specification was chosen, rather than an oil content (percentage of wax soluble in MEK at –32°C) of say 0.5%, since the oil content of a wax cannot be accurately calculated. An additional constraint is that 70% by mass of the feed must be recovered, since high recovery of wax has a high priority due to economic reasons.

The feed wax consists of n-paraffins from n-C_{11} to n-C_{36}. The composition profile of the feed wax is shown in Figure 7-1. Although this wax composition does not correspond to any particular wax feed, the n-paraffin distribution should qualitatively correspond to a soft wax cut from Sasol's Fischer-Tropsch wax stream.

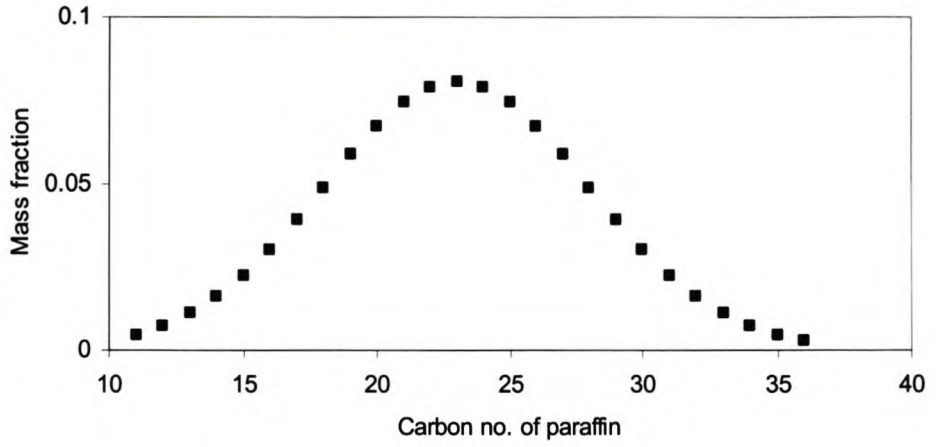

Figure 7-1. Composition of the n-paraffin wax feed used in the case studies.

Flow sheets for static crystallisation, SPD and SCFE are proposed that can achieve both the specified product purity and recovery. Detailed cash flow analyses of these plants are done to compare their profitability. The cash flow analysis of a plant is based on the assumptions listed in Table 7-1 (Nieuwoudt, 1994).

Table 7-1. Cash flow analysis details.

The working capital consist of two weeks inventory of final products, debtors equal to eight weeks sales, creditors equal to four weeks production costs.
Feedstock price = R 1000/ton, combined extract + residue value = R 2000/ton
The cost of process materials per year = 0.5% of the plant capital cost.
The cost of maintenance materials per year = 1.5% of the plant capital cost.
Annual labour cost equals R 981 000.
Annual overheads on labour equals 60% of the labour cost.
An annual overhead on capital amounts to 2% of the capital.
The cost of marketing amounts to 2% of sales.
Straight-line depreciation of capital is calculated over 5 years.
Tax rate = 42%.
Plant capacity = 60 000 ton wax / year.
Feed wax available at battery limits as liquid at 60 °C.
Assume plant will be running 300 days / year.
Cash flow analyses are done assuming a 1 year construction time, 1 year production at 50% capacity and 15 years of full production.
No scrap value is assigned to the plant after production is stopped.

The internal rate of return (IRR) and net present value (NPV), calculated at 13%, and the pay pack time for each plant is calculated. These figures are then used to determine the relative profitability of the different plants. The costs associated with utilities are listed in Table 7-2.

Table 7-2. Cost of utilities at battery limit of process (from (Turton et al., 1998)).

Utility	$/GJ[2]	R/GJ[3]
Low pressure steam (160°C)	3.17	26.29
Medium pressure steam (184°C)	3.66	30.35
Electricity	16.80	139.33
Cooling water[1]	0.16	1.33
Refrigeration (5°C)	20.00	165.86

1. Based on 10°C change in cooling water temperature.
2. Basis 1996.
3. Basis 2001.

7.2. Static crystallisation

In an effort to replace solvent based wax deoiling processes, Sulzer Chemtech and Schuemann Sasol jointly developed a static crystallisation deoiling process (Jans and Stepanski, 1999; Engstler, Stepanski et al., 2000; Meyer and Hildebrand, 2000). The advantages of wax deoiling by static crystallisation, compared to wax sweating and solvent based deoiling processes are:

- Low energy consumption
- High yield
- No residual solvent in product

Due to these advantages of static crystallisation over processes such as solvent recrystallisation and wax sweating, static crystallisation is chosen as the preferred state-of-the-art modern crystallisation process.

7.2.1. Simulation of static crystallisation plant

As a first approximation the separation efficiency of a static crystallisation unit will be simulated as an equilibrium stage. Although the crystalliser units are designed to operate as differential crystallisers, which would result in separation efficiency slightly better than an equilibrium crystallisation, practical problems such as inclusion of residual oil in the solid wax should decrease the actual separation efficiency achieved with a unit.

The modelling of wax crystallisation is discussed in chapter 3, where several models were identified that could give reasonable predictions of wax precipitation experiments. It was found that using solid phase models such as NRTL and Wilson gave a better temperature prediction of the amount of wax crystallised from a solution, while free volume type models accounted for liquid phase non-idealities. The Wilson and Flory-FV models are selected for use in this case study, since it predicts more optimistic separation efficiencies than the NRTL or ideal models.

The composition of the wax product from a single stage crystalliser is calculated using a flash algorithm, with the temperature adjusted to obtain the desired wax fraction. The wax product of this single stage crystallisation is shown in Figure 7-2. From this figure it is clear that the total fraction of the wax product below n-C_{20} amounts to 10% of the total composition, well above the specified value of 0.5%.

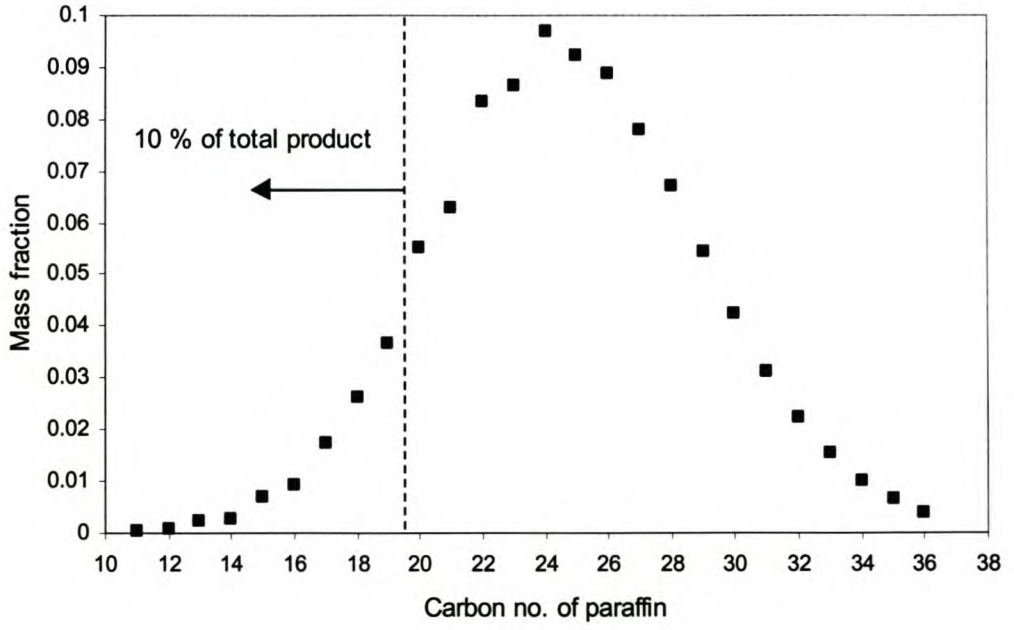

Figure 7-2. Simulated wax product composition for a single stage crystallisation. Dotted line indicates cut-off carbon number below which not more than 0.5% wax is desired. Simulated temperature = 30.9°C.

Since a single stage crystalliser cannot achieve the product specification, a multistage static crystallisation plant will be necessary to achieve the recovery and purity specifications. This is similar to the Schuemann Sasol deoiling plant, where five static crystallisers in series are used, together with internal

reflux, to achieve both high product purity and high recovery (Meyer and Hildebrand, 2000).

This cascade of separation stages are simulated (see Figure 7-3) using a stage by stage flash algorithm with a constant light oil fraction recovered per stage (analogous to a constant molar vapour flow in distillation). At each stage the required temperature was calculated to produce the specified light oil fraction from the feed to the stage. This procedure is repeated until the calculated stage temperatures have converged.

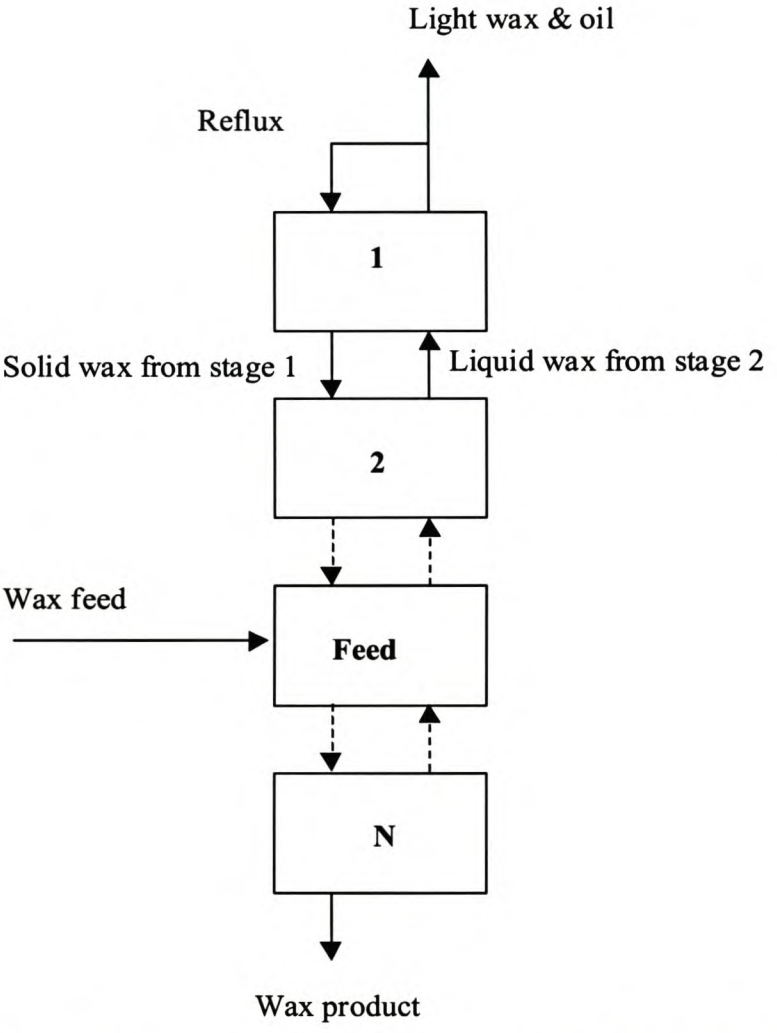

Figure 7-3. Schematic diagram for modelling of crystallisers in series.

7.2.2. Cost estimation of crystalliser plant

The capital costs of the simulated crystalliser plants are based on an existing static wax crystalliser plant of Shuemann-Sasol, build by Sulzer Chemtech AG (Jans and Stepanski, 1999; Engstler, Stepanski et al., 2000). This wax

deoiling plant has a capacity of 100 000 ton/year, with 5 crystalliser units in series to obtain good separation efficiency and high recovery. The installed cost (IC) of the simulated crystalliser plants are calculated as follows:

Eq. 7.1 $$IC = \left(\frac{C}{C_{ref}}\right)^{0.7} \left(\frac{N_{units}}{N_{units,ref}}\right) \times IC_{ref}$$

C is the capacity of the simulated plant, and N_{units} is the number of crystalliser units in the plant. Subscript *ref* refers to the reference plant of Schuemann-Sasol (C_{ref} = 100 000 ton/a, $N_{units,ref}$ = 5, IC_{ref} = DM 6×10^7, 1998 (Nieuwoudt, 2001)). The internal flow through a stage is affected by the amount of reflux used, which would affect the size of the crystallisers. The effect of reflux is not included in the capital cost calculation, since not enough detail of the Schuemann-Sasol plant is available.

The cooling duty required is calculated as the energy needed to crystallise a certain fraction of wax per stage, while the heating duty is calculated as the energy needed to melt the crystallised wax again. An average heat of fusion of 236 kJ/kg wax was used for these calculations. The stage temperatures are between 20 and 40 °C, so low-pressure steam will be used for heating. It is further assumed that the molten wax is heated to 5°C above the operating temperature of the stage to prevent wax precipitation during transfer between stages. An average C_p value of 2.4 kJ/kg.K for the liquid wax is used. The pumping cost for transferring the wax from stage to stage is assumed to be negligible.

7.2.3. Economic evaluation of static crystalliser plants

To determine the number of crystalliser stages, feed stage and reflux ratio that would lead to the most economical plant design, the following strategy was used:

1. A fixed number of crystalliser stages are selected.
2. The feed stage is selected.
3. The reflux ratio is adjusted to match the required purity and recovery specifications.
4. Repeat steps 2 and 3 until the optimum feed stage is located for the chosen number of stages.
5. Repeat steps 1 – 4 until the optimum total number of stages is determined.

The optimum plant design is chosen as the design leading to the highest internal rate of return (IRR) and the shortest payback period (PBP). The results for different number of crystalliser stages are shown below in Table 7-3.

Table 7-3. Cash flow analysis for different crystalliser plant designs.

Number of stages (feed)	Reflux ratio	Capital cost R million	IRR[1] %	PBP[2] years	NPV[3] R million	Energy cost R /ton feed
5 (3)	4.2	176	15	5.2	17.6	62
6 (3)	1.5	211	12.4	6	-5.5	46
7 (4)	1.1	247	10.1	7	-31.6	43

1. Internal (or interest) rate of return.
2. Payback period.
3. Net present value after 16 years of production, discounted by 13%.

From Table 7-3 it is clear that a static crystalliser plant with 5 crystalliser units will result in the highest return based on a cash flow analysis. This is also the minimum number of stages that can obtain the desired product specifications. If the number of crystallisation units is increased, the required reflux ratio drops, but the total energy usage increases. This increase in energy usage is due to the fact that the total energy usage is proportional to the product of the energy used per stage and the total number of stages. It must be noted that the liquid loading for the plant with 5 stages is double that of the plant with 6 stages. The effect of internal liquid loading on the size (and cost) of the crystalliser units are not reflected in the present analysis, since not enough detail of the reference plant is known.

The simulated composition of the wax product of the 5 stage crystalliser plant is shown in Figure 7-4. The flow and temperature profiles of the simulations in Table 7-3 are shown in Appendix F.

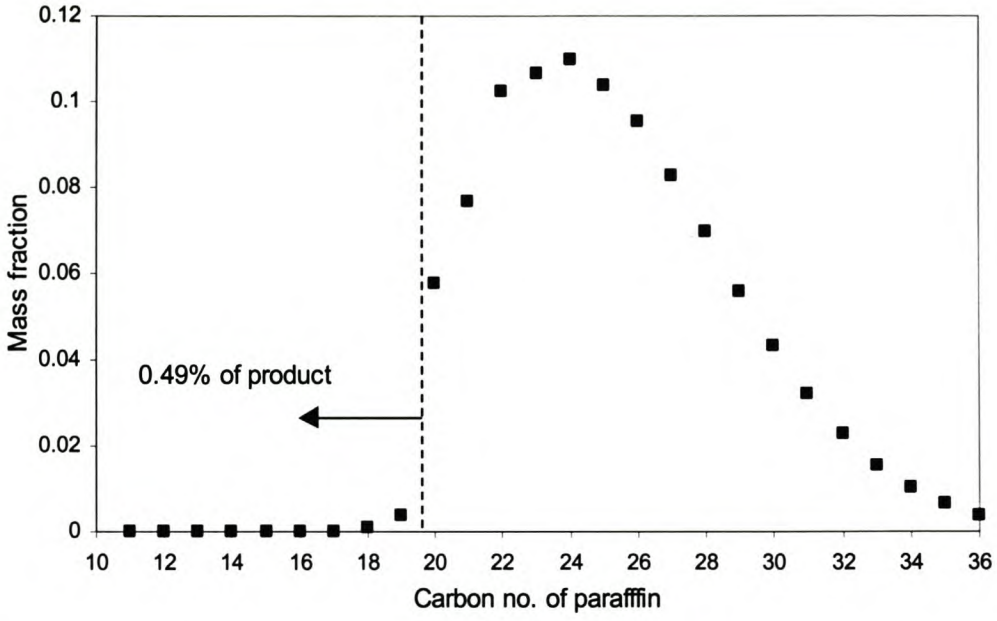

Figure 7-4. Simulated product composition of 5 stage static crystalliser plant.

7.3. Short path distillation

Short path distillation (SPD) is commonly used to separate or recover low volatility or heat labile components from liquid mixtures. Typical uses include (Fischer and Bethge, 1992; Fischer, 2000; Pope, 2000):

- Recovery and concentration of edible oils and vitamins such as vitamin E, carotene and polyunsaturated fatty acids from plant and animal oils.
- Polymer devolatilization and monomer stripping from di-isocyanites.
- Wax fractionation.
- Solvent recovery.
- Pharmaceutical and biomaterial concentration.

SPD is typically used to fractionate hard waxes, as opposed to vacuum distillation, since an SPD unit can operate at very low pressures (10^{-1} - 10 Pa). It is necessary to operate at these low pressures to prevent high temperatures that might lead to thermal degradation of the wax.

7.3.1. Simulation of SPD plant

The separation efficiency of a SPD unit was investigated in chapter 2. It was found that experimental results could be simulated as a single stage flash using ideal liquid phase activity and assuming ideal vapour phase behaviour.

The composition of the wax product from a single stage SPD unit is calculated using a flash algorithm, with the temperature adjusted to obtain the desired wax fraction. The operating pressure is kept constant at 40 Pa, and the temperature is adjusted to obtain the desired (bottoms) wax recovery. The wax product of this single stage crystallisation is shown in Figure 7-5.

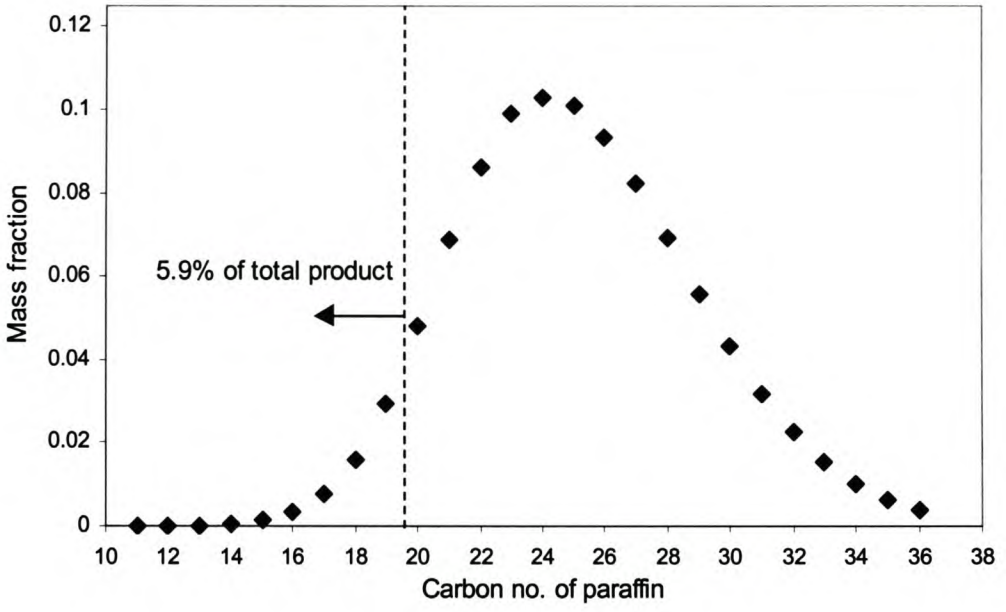

Figure 7-5. Simulated product composition for a single stage SPD separation. Pressure = 40 Pa, temperature = 137.5 °C.

From this figure it can be seen that the total fraction of the wax product below n-C_{20} amounts to 5.9% of the total composition, well above the specified value of 0.5%. It is clear that one SPD unit can not produce a product that meets the required purity and recovery. Similar to the wax crystalliser plant, several SPD units in cascade are needed to achieve the required wax purity and recovery.

This cascade of separation stages ise simulated (see Figure 7-3) using a stage by stage flash algorithm with a constant molar vapour flow between stages. At each stage the required temperature was calculated to produce the specified vapour from the feed to the stage, with the total pressure kept constant at 40 Pa. This procedure is repeated until the calculated stage temperatures have converged.

7.3.2. Cost estimation of SPD plant

The capital cost of the simulated SPD plants is based on an existing SPD wax fractionation plant of Sasol (Nieuwoudt, 2001). The installed cost (IC) of the simulated SPD plants are calculated as follows:

Eq. 7.2
$$IC = \left(\frac{C \times (V/F)}{C_{ref} \times (V/F)_{ref}} \right)^{0.7} \left(\frac{N_{units}}{N_{units,ref}} \right) \times IC_{ref}$$

C is the capacity of the simulated plant, and N_{units} is the number of SPD units in the plant. IC is the installed cost of a plant. Subscript *ref* refers to the reference plant of Sasol (C_{ref} = 30 000 ton/a, $N_{units,ref}$ = 5, IC_{ref} = DM 6×10^7, $(V/F)_{ref}$ = 0.75, basis = 1998 (Nieuwoudt, 2001)). The size of a SPD unit is determined by the required evaporation rate. This is accounted for by the V/F term; with V the average vapour flow per SPD unit and F the feed rate to the plant.

The heating duty of the SPD plant consists of two contributions: energy required for evaporating wax, and energy required for heating up wax flowing into a unit. The energy used to evaporate wax per stage is calculated as the vapour flow rate from that stage, multiplied by the heat of vaporisation. An average value of 370 kJ/kg wax is used for the heat of vaporisation. It is further assumed that the distillate of an SPD unit is subcooled by 40 °C to ensure good separation efficiency and high capacity, since high condenser temperatures will lead to re-evaporation of the distillate. When the distillate from a SPD unit flows to the nest SPD unit in the cascade, this distillate must then be heated to the operating temperature again. An average C_p value of 2.4 kJ/kg.K for the liquid wax is used.

The SPD units are heated with recirulating heating oil, which in turn is heated using steam or electricity. The highest process side temperature is about 156 °C, therefore medium pressure steam (184 °C) is used. The cooling duty is assumed to be the same as the heating duty. The pumping cost for transferring the wax between stages is calculated assuming an elevation change of 5 m. This cost is negligible compared with the heating and cooling costs.

7.3.3. Economic evaluation of SPD plants

To determine the number of SPD units, feed stage and reflux ratio that would lead to the most economical plant design, the following strategy was used:

1. A fixed number of SPD units are selected.
2. The feed stage is selected.
3. The reflux ratio is adjusted to match the required purity and recovery specifications.
4. Repeat steps 2 and 3 until the optimum feed stage is located for the chosen number of SPD units.
5. Repeat steps 1 – 4 until the optimum total number of units are located.

The optimum plant design is chosen as the design leading to the highest internal rate of return (IRR) and the shortest payback period (PBP). The results for different number of SPD units are shown below in Table 7-4. Stage profiles for temperatures, flow rates and heating/cooling duties are presented in Appendix F.

Table 7-4. Cash flow analysis for different SPD plant designs.

Number of stages (feed)	Reflux ratio	Capital cost R million	IRR[1] %	PBP[2] years	NPV[3] R million	Energy cost R / ton feed
4 (2)	1.4	137	23.8	3.9	71.1	47
5 (2)	0.23	107	25.4	3.7	77.3	30
6 (1)	0	113	20.0	4.3	51.2	30

1. Internal (or interest) rate of return.
2. Payback period.
3. Net present value after 16 years of production, discounted by 13%.

From Table 7-4 it is clear that a 5 unit SPD plant will result in the highest return based on cash flow analysis. It is interesting to note that the capital cost for a 5 unit SPD plant is less than a 4 unit SPD plant. When fewer SPD units are used, more reflux is required to obtain the same wax product. More reflux implies a higher evaporation rate per unit, which increases the required surface area of a SPD unit.

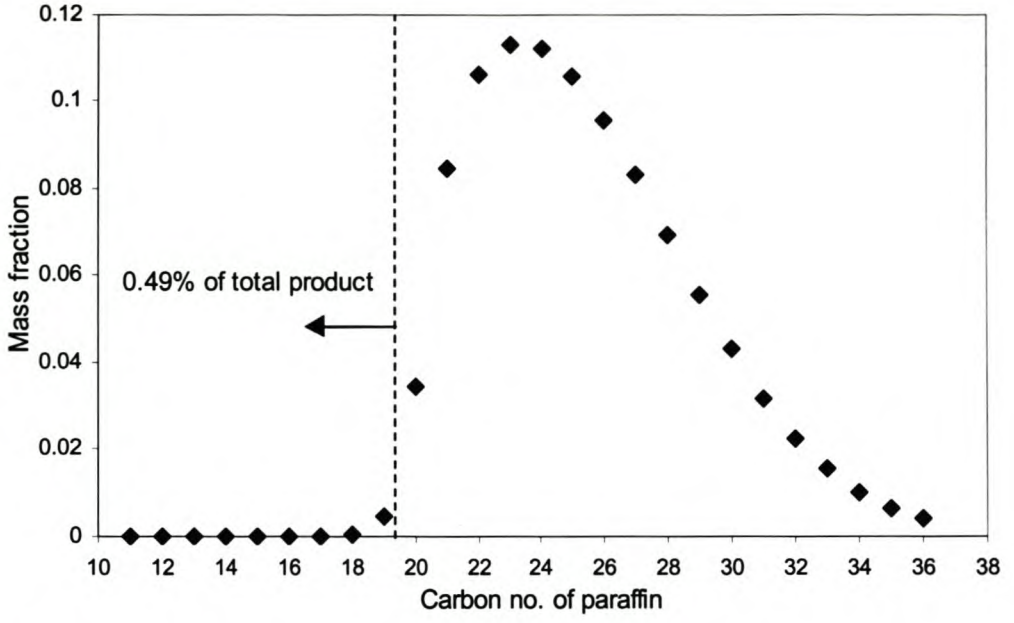

Figure 7-6. Simulated product composition of run SPD 5.

7.4. Supercritical fluid extraction

Near critical fluid processing of petroleum using technologies such as the propane deasphalting process, ROSE, DEMEX and Solvahl-Asvahl processes is widely known and has been in commercial use for decades (see section 1.3.1). Supercritical processes such as decaffeination of coffee and tea, spice and hop flavour extraction and polymer processing have also been commercialised for several decades. In this work SCFE is investigated as a possible fractionation/deoiling process, using CO_2 or ethane as solvent. Phase equilibrium modelling were done in chapter 4, while experimental fractionation data and process simulations were covered in chapter 5. The economic aspects of SCFE will be discussed below.

7.4.1. Process conditions and process flow diagram

Several possible sets of SCFE conditions exist that would meet the specified recovery and purity specifications. Either ethane or CO_2 can be used as the solvent. The higher density of CO_2 would lead to a smaller diameter extraction column, compared with ethane at the same flow rate. CO_2 is also non-flammable, while ethane is flammable. Ethane is, however, preferred as the solvent due to the following reasons:

- CO_2 has lower solvent power than ethane at the same pressure. A higher extraction pressure is required to extract the same amount of wax with CO_2, compared with ethane.
- The higher density of the solvent phase results in a smaller density difference between the wax and solvent phases, which can lead to premature flooding in the extraction column.
- There is a possibility of density inversion at high pressures (Charoensombut-Amon, Martin et al., 1986; du Rand, 2000).
- Ethane is normally available on a Fischer-Tropsch plant.

The extraction column conditions were chosen as 70 °C and ± 100 bar. At this temperature and pressure there is an acceptable balance between the capacity of the solvent (ethane) and the density difference between the wax and solvent phases. Simulations were done with 25, 30, 35 and 40 theoretical stages in the extraction column. The pressure, solvent to feed ratio (S/F) and reflux ratio for a simulation was adjusted to attain the specified wax product purity and recovery.

The extraction column pressure, S/F ratio and reflux ratio were selected to ensure a minimum density difference of 120 kg/m^3 between the solvent and wax phases through the extraction column. This was done to prevent premature flooding caused by too small a density difference in the extraction column. Brunner (Brunner, 1998) recommends a value of 100 kg/m^3 (based mostly on CO_2 data), but a 20% safety factor is included to compensate for possible errors resulting from the use of the PT EOS for calculation of phase density.

To minimise solvent cost, the solvent is recycled after the separator vessel. The recycled solvent contains trace amounts of wax, which contaminates the bottoms product. In section 4.6 it was shown that the amount of light wax contaminating the wax product is over predicted if the solvent feed to the column is taken as the solvent from the separator vessel. This is most likely due to the SPHC EOS over-predicting the concentration of light wax dissolved in the solvent. It was therefore decided to simulate the SCFE plant with pure solvent (i.e. with no solvent recirculation). The total allowable concentration of paraffins below n-C_{20} in the wax product was however lowered from 0.5 % to 0.4 % to allow for possible contamination of the wax product with light wax dissolved in the solvent stream.

The solubility of wax in the solvent phase decreases with a decrease in separator pressure, but decreasing the separator pressure leads to an increase in energy required to recycle the solvent. A separator pressure of

about 55 bar was chosen as a compromise between energy usage and residual wax solubility in the solvent. The separator temperature, which minimises the wax solubility in the solvent at this pressure, is about 56 °C. The effect of different separator pressures on the economic feasibility of SCFE will be investigated later in this chapter.

The operating conditions were selected to minimise the solvent : feed (S/F) ratio, while conforming to the product recovery and purity specifications, and the minimum density difference requirement. This was done as follows:

1. Specify S/F ratio and feed location for fixed number of stages.
2. Adjust reflux ratio and extraction pressure to obtain required product purity and recovery.
3. If the minimum density difference is larger than specified increase S/F ratio, else decrease S/F ratio. Repeat step 2 until minimum density difference is approached.
4. Adjust feed location and repeat 2 – 3 until minimum S/F ratio is obtained.

The following trends were observed during simulation (pressure was adjusted to maintain a fixed raffinate to feed fraction):

- Increasing the reflux ratio (at constant S/F) decreases light fraction in raffinate and decrease density difference between wax and solvent phases.
- Increasing S/F (at constant reflux ratio) decreases light fraction in raffinate and increase density difference between wax and solvent phases.

The sets of operating conditions, determined from simulations, that satisfy the required product specifications for the different number of equilibrium stages are shown in Table 7-5 below.

Table 7-5. Extraction column operating conditions for different number of equilibrium stages (at 70 °C).

Number of stages	Feed stage	Solvent : feed ratio	Reflux ratio	Pressure [bar]
25	9	21.5	12	99.1
30	10	19.9	11	99.0
35	10	19.1	10.5	99.1
40	11	18.55	10.2	99.1

Several possible flow schemes exist for the solvent recycle circuit, and three alternatives will be investigated. The first flow scheme, PFD1, is shown in Figure 7-7. This flow diagram can be split in two conceptual circuits: a wax

circuit and a solvent recycle circuit. The solvent circuit can be configured in many different ways, but the wax circuit is kept the same for all the different flow diagrams and will be discussed only for the PFD1 flow diagram.

The feed wax is pumped to the extraction column through pump P1 and heated to the extraction temperature with heat exchanger HX1. Some of the wax extract from the separator, SEP1, is returned to the extraction column as reflux through pump P2 and heated to the extraction column temperature with heat exchanger HX2. The rest of the wax extract is collected in vessel V1. The wax residue from the extraction column is collected in vessel V2. The product vessels V1 and V2 have internal heating elements to heat the wax to 60 °C to liberate dissolved solvent from the wax.

These heating elements mean that the liquid (and the gas liberated from the liquid) only is heated to the higher temperature. The bulk of the gas that enters will thus not be heated. It can be modelled as an adiabatic flash on the whole stream followed by an isothermal (60°C) flash on the liquid only. The gases from the adiabatic flash and the isothermal flash are mixed to determine the final temperature of the gas leaving the vessel. It is important to conserve energy in this solvent recovery step, since it amounts to 20 – 40 % of the total electricity usage.

These vessels operate at atmospheric pressure. Using the SPHC EOS, the residual ethane dissolved in the wax at these conditions is calculated as about 0.31 % by mass. Solvent gas from V1 and V2 are compressed to 55 bar with multistage compressor CMP1, cooled to 55 °C with air cooler HX3 and returned to the solvent recycle circuit.

Description of PFD1.

The solvent stream from the extraction column is first expanded over an expansion valve to the separator pressure, then heated to the separator temperature by heat exchanger HX4. Due to the lowered solvent power of the solvent at the separator conditions, the wax extract drops out of solution in the separator vessel. The solvent from the separator vessel is condensed in heat exchanger HX5, using cooling water. The exit temperature of the solvent from HX5 is about 28 °C. This liquid is pumped to the extraction column with positive displacement pump P3 and heated to the extraction temperature with heat exchanger HX6, using low-pressure steam.

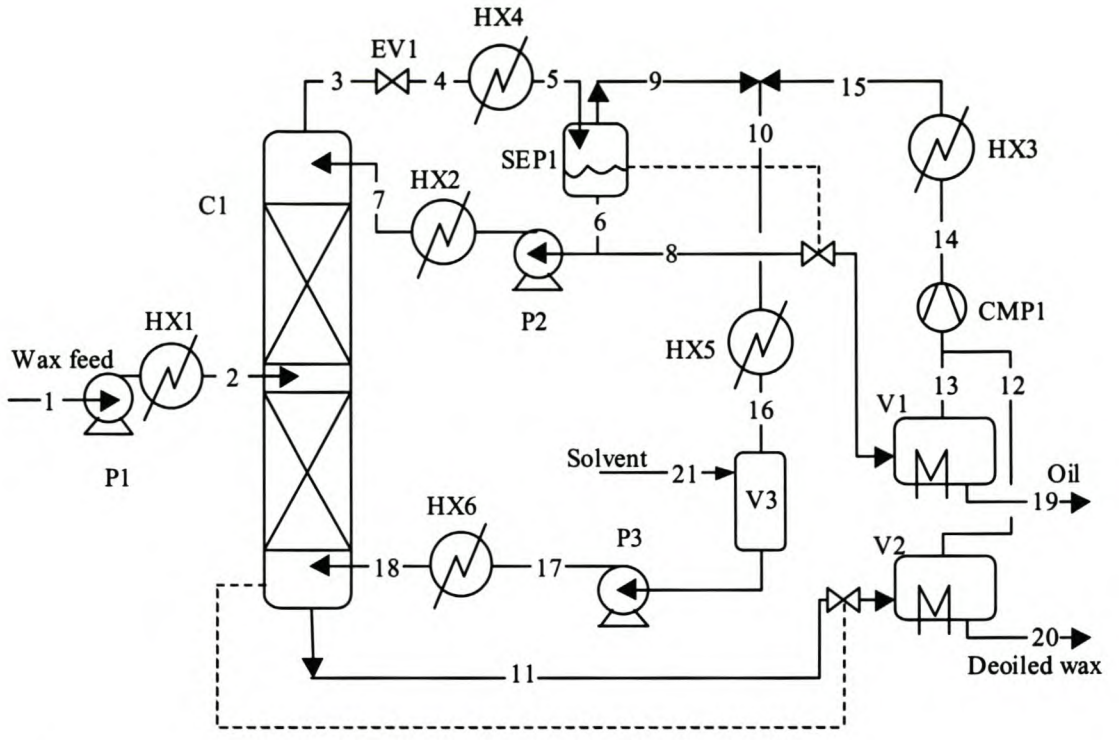

Figure 7-7. Flow diagram PFD1, SCFE with liquid solvent recycle.

Description of PFD2.

The energy demand of the PFD1 flow diagram is very high and can be decreased by heat integration. King et al. (King et al., 1990) discuss a flow diagram for near critical extraction where heat integration is used. This concept is adapted to the SCFE processing of this work, as shown in Figure 7-8.

The solvent from the extraction column is expanded over expansion valve (EV1). The solvent stream from EV1 is heated to the separator temperature in heat exchanger HX4. The gaseous solvent from the separator SEP1 is compressed to the extraction pressure with vapour compressor CMP2. The hot vapour from the compressor is cooled with the vapour stream from the expansion valve in HX4. The temperature of the compressed solvent stream from HX4 is cooled further to the extraction temperature with heat exchanger HX5 using cooling water.

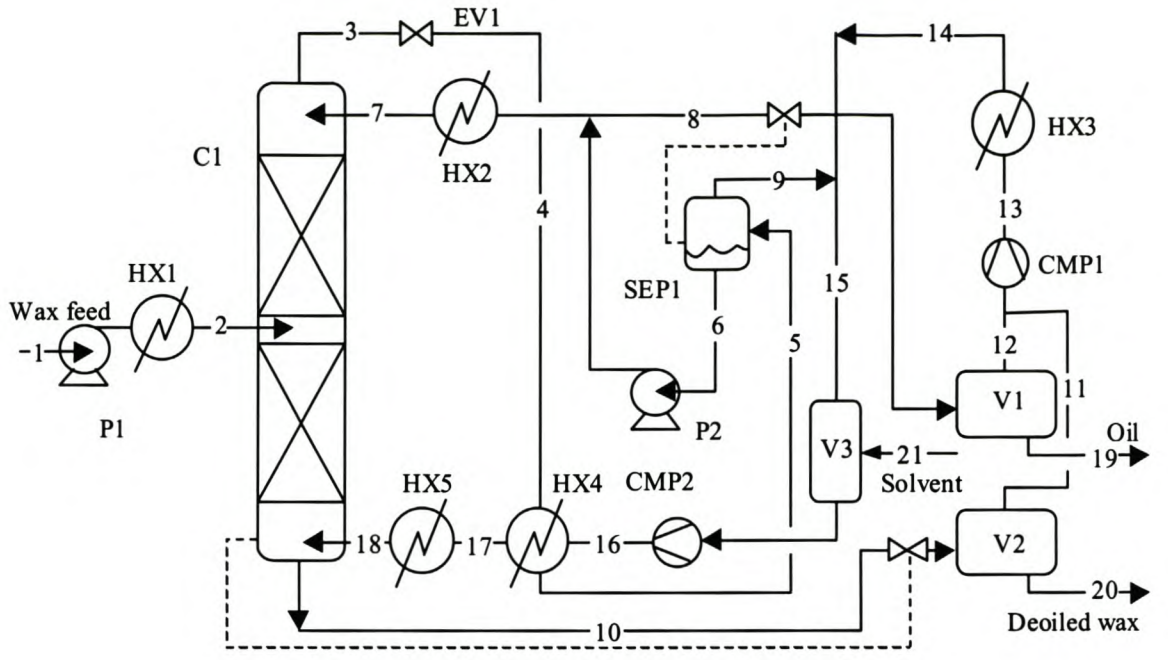

Figure 7-8. Flow diagram PFD2, SCFE with solvent expansion over valve and vapour compression.

Description of PFD3.

It is possible not only to do heat integration, but also to integrate the work done by the compressor. In the 3rd flow diagram, the expansion valve is replaced with an expander to recover mechanical work from the solvent expansion step, which is used to drive the compressor. This flow diagram is shown in Figure 7-9.

The pressure of the solvent stream from the extraction column is reduced to the separator pressure in two steps over expanders EXP1 and EXP2. This two-step pressure reduction with heating is used to prevent isentropic expansion temperatures below the congealing temperature of the extracted wax.

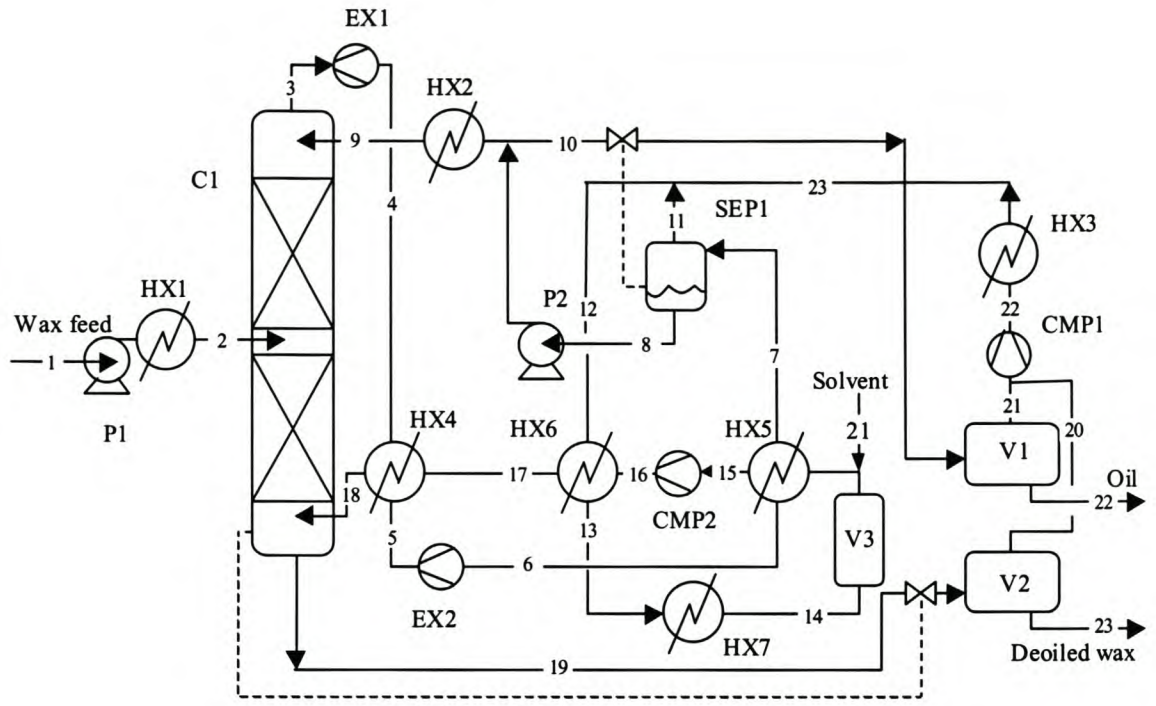

Figure 7-9. Flow diagram PFD3, SCFE with solvent expansion through expanders, and vapour compression.

The effect of different outlet pressures on the flow sheet calculations is shown in Table 7-6. The power requirement of the flow sheet increases as the outlet pressure of EXP1 decreases. There is, however, an upper limit to the outlet pressure of EXP1 where the outlet temperature of EXP2 enters the two-phase region. To protect the turbines and to prevent possible congealing of the extracted wax, the outlet pressure of EXP1 is chosen as 90 bar. The solvent stream pressure is reduced to 55.5 bar and the temperature to 42.5 °C through expander EXP2. The outlet from expander EXP2 is heated to the separator temperature with heat exchanger HX5. Compressor CMP2 compresses the solvent vapour to the extraction column pressure. The hot outlet from CMP2 is cooled by heat exchanger HX6 using the separator outlet stream. The solvent vapour from HX6 is cooled down to 73 °C with heat exchanger HX7 using cooling water. The solvent stream from HX7 is used to heat the solvent stream going to the separator in HX5, and then goes to CMP2. The hot stream from CMP2 is cooled to the extraction column temperature in heat exchangers HX6 and HX4, by exchanging heat with colder streams.

Table 7-6. Effect of EXP1 outlet pressure on flow sheet.

EXP1 P_{out} bar	EXP2 Outlet T °C	SEP1 T °C	HX7 outlet °C	Energy required* kW
92	37.1#	54.8	72.6	670
91	42.2	54.6	73.3	692
90	42.5	55.3	74	697
89	42.9	56	74.7	702

Outlet stream in two-phase region.

* Difference between CMP1 power consumption and EXP1 + EXP2 power output.

7.4.2. Equipment design

Extraction column

The design of the extraction column are done similar to that of (de Haan, 1991) and (Nieuwoudt, 1994). Sulzer BX gauze packing will be used as packing for the extraction column, since it has a greater capacity than the SULZER DX packing used in the pilot plant tests of this work does. (de Haan, 1991) calculated height equivalent to a theoretical plate (HETP) values (BX packing) between 0.4 - 0.7 m for the fractionation of liquid paraffins with CO_2, while (Nieuwoudt, 1994) also calculated HETP values (BX packing) between 0.4 - 0.7 m for the fractionation of paraffin wax using LPG as solvent. Brunner (Brunner, 1998) reported average HETP values for the CO_2 fractionation of fatty acid ethyl esthers of 0.22 m (Sulzer EX) and 0.27 m (Sulzer CY).

HETP values using Sulzer DX packing were calculated from experimental work in chapter 5. HETP values of 0.2 – 0.5 m were obtained for CO_2 – wax and 0.5 – 0.7 m for ethane – wax systems. Since HETP values are system-dependent (Brunner, 1998), values for paraffin systems will be used to estimate the expected HETP of the ethane – wax system using Sulzer BX packing.

The HETP for the Sulzer BX packing is expected to be higher than for the DX packing used in the pilot plant column, since the surface area of the BX packing is 500 m^3/m^2, compared with 900 m^3/m^2 for DX packing. The HETP value of the BX packing is estimated to be 60% more than the DX packing. The average HETP value obtained for the ethane – wax separation (with reflux) is 0.68 m, resulting in an HETP value of 1.1 m for the BX packing. The total height of the extraction column is calculated as 1.25 times the packed height. The extra 25% unpacked space in the column is used as disengagement space at the top and bottom of the column, and for fluid-liquid distributors through the column.

The diameter of the extraction column is determined by calculating the flooding velocity. The design velocity is then taken as 70% of the flooding velocity. No flooding data is available for the ethane – wax system for Sulzer BX packing, so a flooding correlation is needed to predict flooding conditions. General flooding correlations for distillation conditions have been developed (see e.g. (Fair and Bravo, 1990) and (Stichlmair et al., 1989)). Another method used to predict pressure drop and flooding in distillation is the so called Generalised Pressure Drop Correlation (GPDC) (Kister, 1992). No general flooding correlation valid for supercritical extraction conditions are available (Stockfleth and Brunner, 2001).

Stockfleth and Brunner (Stockfleth and Brunner, 2001) published flooding data for selected random and structured packing using supercritical CO_2. They correlated flooding data for Sulzer CY packing for the system CO_2 – water using coordinates originally proposed by Sherwood (Sherwood et al., 1938). This approach is analogous to the GPDC method used in distillation. Packing factors for use with the GPDC correlation are reported by (Kister, 1992) for several different packing types, including Sulzer BX and CY packings. The correlation given by (Stockfleth and Brunner, 2001) for Sulzer CY packing is compared with the GPDC correlation in Figure 7-10. The GPDC curve for 1.23 kPa/m (1.5 inches H_2O / ft) pressure drop is used, and the viscosity correction is ignored. The resulting curves are relatively close, and coincide in the flow regime found in the SCFE column. In the region of interest the difference between the two correlations is less than the deviation reported by (Stockfleth and Brunner, 2001). Based on this "validation", the GPDC method will be used to predict flooding velocities for the Sulzer BX packing.

The abcissa of the GPDC method is called the flow parameter:

Eq. 7.3 $$FP = \frac{L}{G}\left(\frac{\rho_g}{\rho_\ell}\right)^{0.5}$$

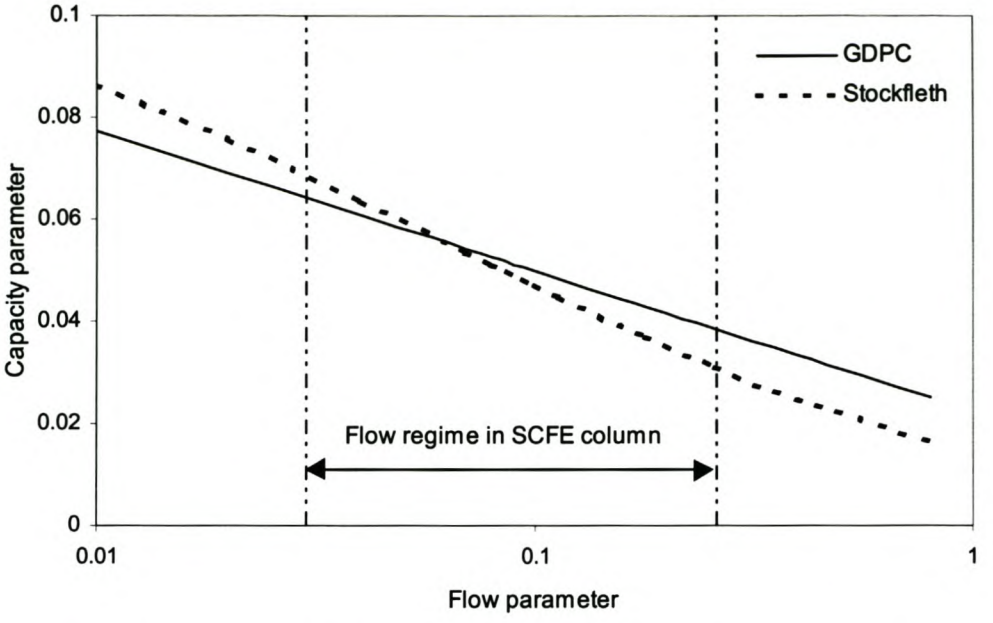

Figure 7-10. Comparison of the GPDC and Stockfleth correlations for predicting flooding.

L and *G* are the liquid and gas mass flow rate respectively, with ρ_ℓ and ρ_g the density of the liquid and gas phases. The ordinate is the capacity parameter:

Eq. 7.4 $$CP = C_s F_p^{0.5} \nu^{0.05}$$

F_p is an empirical packing factor, with a value of 21 ft^{-1} for Sulzer BX packing. ν is the kinematic viscosity of the liquid in centistoke.

C_s (in ft/s) is the superficial gas velocity corrected for liquid and gas densities:

Eq. 7.5 $$C_s = u_s \sqrt{\frac{\rho_g}{\rho_\ell - \rho_g}}$$

The design velocity was taken as 70% of the flooding velocity. The superficial velocity, *u* (ft/s), used in the design of the extraction column diameter was calculated as follows (ignoring the viscosity correction term):

Eq. 7.6 $$u = \frac{CP}{F_p^{0.5}} \sqrt{\frac{\rho_\ell - \rho_g}{\rho_g}} \times 0.7$$

The GDPC (SP) curve for 1.5 inches H_2O/ft pressure drop was correlated with the following empirical correlation:

Eq. 7.7 $$CP = 0.6108 - 0.3214 \ln(FP)$$

Vessels

The diameter of the separator vessel, SEP1, is designed using the following equation (Sinnott, 1997) for the maximum gas velocity, *u*:

Eq. 7.8 $$u = 0.035 \sqrt{\frac{\rho_\ell}{\rho_g}}$$

The total height of the separator vessel is determined by adding the liquid height and the vapour disengagement height. The liquid height is determined to give a liquid hold-up of 15 minutes. The vapour disengagement height is taken equal to the diameter of the vessel. The separator vessel should also be equipped with a demisting section.

The wax product vessels, V1 and V2, are sized to provide a liquid hold-up of 40 minutes when half full. The vessels are equipped with demisting sections, and internal heating elements to evaporate solvent from the liquid wax.

The solvent feed/buffer vessel, V3, is sized to hold the total ethane inventory of the plant.

Pumps, compressors, expanders and heat exchangers

The hydraulic calculations of the flow diagrams were done using the simulation package Pro/II of Simulation Science Inc. The solvent circuit was simulated using pure ethane, the wax feed stream using n-C_{24}, and the reflux stream using a mixture of ethane and n-C_{24}. All thermodynamic calculations were done using the Peng-Robinson EOS. The performance of the compressors and expanders was simulated assuming an adiabatic efficiency of 90%. The duties of the pumps were calculated assuming 100% efficiency, since the PR EOS over-predicts the liquid volume used to calculate the duties of the pumps.

All heat exchangers were sized using the rigorous shell and tube heat exchanger model of the Pro/II simulation package, except heat exchanger HX3. The area of air-cooled exchanger HX3 was calculated assuming an overall heat transfer coefficient of 1 $W/m^2.K$ (70 $Btu/h.ft^2.°F$ from (Nieuwoudt, 1997)) and an average temperature driving force of 80 °C.

All piping must be heat traced. The extraction column and vessels V1, V2 and SPE1 must be jacketed to prevent heat loss and possible congealing of the wax.

7.4.3. Economic evaluation of SCFE

The costs associated with utility consumption are calculated using the utilities costs listed in Table 7-2. The cost of make-up solvent is calculated assuming an average residual solvent level of 0.32 mass %, calculated using the SPHC EOS. The FOB cost of ethane is given as R 350/ton (CAN$23.33 /bbl) by (Ashton et al., 2001). Since the synthetic wax will always be within a Fischer-Tropsch complex where ethane will definitely be available, the price of ethane is taken as R 400/ton.

The capital costs of the proposed flow diagrams are show in Appendix G. The capital cost estimations were done with the CapCost capital cost estimation program (Turton, Bailie et al., 1998). The CapCost values are given in 1996 US$. The Chemical Engineering journal's Plant Cost Index (CEPCI) are used to adjust costs to present values (CEPCI(1996) = 386, CEPCI(2001) = 396). The 2001 Rand/dollar exchange rate was taken as $1 = R8.

The results of the cash flow analyses are shown in Table 7-7. In general the capital cost of a plant based on the PFD2 flow diagram is cheapest, closely followed by the cost of a plant based on PFD1. Plants based on PFD3 flow diagrams are about 10-15% more expensive. Increasing the number of stages in the extraction column from 35 to 40 stages increases the capital cost by ± 1%. The reduced solvent/feed ratio causes this small increase in capital cost required for the separation.

Table 7-7. Cash flow analyses for different SCFE plants.

Number of stages	Capital cost (R million)	IRR[1] (%)	PBP[2] (Years)	NPV[3] (R million)	Energy cost R / ton feed
PFD1					
25	110.2	19.8	4.40	41.6	202
30	109.9	20.2	4.34	44.3	189
35	113.0	19.9	4.38	43.1	183
40	114.1	19.8	4.39	43.1	179
PFD2					
25	108.5	21.7	4.15	53.2	148
30	107.9	22.0	4.11	55.4	139
35	109.7	21.8	4.13	54.8	135
40	111.9	21.5	4.17	53.7	132
PFD3					
25	124.2	21.6	4.15	58.69	58
30	122.7	21.9	4.11	60.47	54
35	124.0	21.7	4.13	59.81	53
40	126.1	21.4	4.17	58.46	51

1. Internal (or interest) rate of return.
2. Payback period.
3. Net present value after 16 years of production, discounted by 13%.

Based on the internal rate of return (IRR) and payback period (PBP) values, the following plants appear to be the more economical alternatives: PFD2-30 and PFD3-30. Of these two flow sheets, PFD3-30 is the plant with the highest NPV. It is interesting to note that the energy cost per ton of feed is about the same for PFD1 and PFD2, even though PFD2 is designed with heat integration. This is caused by the fact that most of the energy supplied in PFD1 is in the form of steam, while only electricity is supplied to PFD2. Even though the energy requirements for PFD2 is lower than for PFD1, the higher cost of electricity (compared with steam) negates the cost effectiveness of heat integration. The capital cost of PFD2 is however less than PFD1.

It is clear that plants based on both flow sheets PFD2 and PFD3 result in significant economic improvements compared with plants based on flow sheet PFD1. The number of theoretical separation stages leading to the best economic performance for flow sheets PFD2 and PFD3 are 30. Deciding between flow sheet PFD2 or PFD3 for a design will depend on several factors:

- Available capital. If capital is in short supply, flow sheets based on PFD2 must be considered, since the required capital is lowest for this flow sheet.
- Complexity. A plant based on PFD3 contains more equipment, will require more advanced control strategies, and will possibly be more expensive to maintain.
- Energy expenditure. Plants based on flow sheet PFD3 will consume 2.5 times less energy than plants based on flow sheet PFD2.

The separator pressure (and temperature) determines the residual level of wax returned to the extraction column with the solvent recycle stream. Since no experimental solubility data of n-alkanes in ethane at the separator conditions are available, the separator pressure was fixed at a pressure considered low enough to prevent excessive contamination of the wax product. Since there is some uncertainty with regards to the optimum separator pressure, the effect of different separator pressures on the economics of SCFE was investigated. The three proposed flow sheets were simulated with the optimum number of stages (30) at 50 and 60 bar (separator pressure). The results are shown in Table 7-8. The separator temperatures that minimise the amount of wax dissolved in the ethane are 42°C @ 50 bar and 64°C @ 60 bar.

The energy cost for PFD1 decreases as the separator pressure decreases. The temperature of the solvent stream after the expansion valve is below 40°C, and must be heated to the separator temperature. Since lower separator pressures lead to lower separator temperatures, less energy is required to heat the solvent stream to the separator temperature.

The opposite is observed for the PFD2 and PFD3 flow sheets. A higher separator pressure implies that less energy is required to recompress the solvent vapour to the extraction pressure. In general the IRR increases with an increase in separator pressure. It is obvious that higher separator pressures will reduce the overall energy consumption and increase the profitability of SCFE. However, higher pressures were not investigated due to a lack of experimental data to compare with. Higher separator pressures will be feasible for wax feeds containing less low-molecular weight components.

Table 7-8. Effect of separator pressure on economics of SCFE.

$P_{separator}$ bar	Capital cost (R million)	IRR[1] (%)	PBP[2] (Years)	NPV[3] (R million)	Energy cost R / ton feed
PFD1-30					
50	114.3	20.1	4.36	44.7	169
55	109.9	20.2	4.34	44.3	189
60	106.7	20.5	4.30	45.2	197
PFD2-30					
50	111.3	21.2	4.21	51.5	146
55	107.9	22.0	4.11	55.4	139
60	99.8	24.2	3.87	65.3	120
PFD3-30					
50	134.4	19.8	4.38	49.1	68
55	122.7	21.9	4.11	60.47	54
60	112.7	23.6	3.91	68.4	52

7.5. Discussion

An economic comparison for the more economical plants based on wax recrystallisation, SPD and SCFE are shown below in Table 7-9.

Table 7-9. Economic comparison of wax recrystallisation, SPD and SCFE plants.

Type of plant	No. units or stages	Capital cost (R million)	IRR %	NPV (R million)	Energy cost (R/ton wax)
Wax cryst.	5	176	15	17.6	62
SPD	5	107	25.4	77.3	30
SPD (electr)[#]	5	107	22.4	57.6	132
SCFE, PFD1	30	110	20.2	44.3	189
SCFE, PDF2	30	108	22	55.4	139
SCFE, PFD3	30	123	21.9	60.5	54

[#] SPD unit with steam heating replaced with electrical heating.

* Electric drive of compressor replaced with steam turbine (efficiency = 65%)

Wax recrystallisation is an expensive technology with the highest capital cost. Wax deoiling using SPD is marginally more economical than SCFE technology based on the assumptions made during the simulation of the SPD plant and the accuracy of the capital cost estimation method. This might not be true for the fractionation of higher molecular weight waxes, where thermal degradation is likely.

Wax deoiling using SCFE is slightly more expensive compared with SPD, but still much cheaper than wax recrystallisation. The SCFE plants simulated in this chapter does not necessarily correspond to the optimum configured column and some cost savings are possible. The number of theoretical separation stages were not optimised rigorously, only selected at fixed intervals. Further saving is possible if the separator pressure is increased. The separator pressure was chosen based on extrapolation of pilot plant runs at lower separator pressures, therefore some uncertainty remains as to the maximum separator pressure to be used. It is important that a globally acceptable optimisation (for wax deoiling in general) cannot be done since several different grades of wax are marketed, each with different specifications.

Even though SPD appears to be the wax deoiling plant with the best economic potential, it is limited to processing short chain length n-paraffin waxes. The distillation temperature rises steeply as the wax chain length increases, e.g. the boiling point at 40 Pa of n-C_{24} and n-C_{32} are 166 °C and 225 °C respectively. At temperatures higher than about 200 °C electricity has to be used as heating medium, which is very expensive compared with medium pressure steam (about 4x as expensive, see Table 7-2). When the wax distillate's molecular weight becomes too high, normal cooling water will cause congealing of the distillate. To prevent this a tempered cooling water system should be used, which is an added expense. With SCFE the extraction temperature can be regulated by manipulating the extraction pressure or using a solvent with a higher molar mass, which makes SCFE a potential candidate for wax fractionation of medium and heavy n-paraffin waxes.

The work in this chapter is based on an n-paraffin wax mixture, similar to a low molecular weight Fischer-Tropsch type wax. Wax from crude oil contains a mixture of different paraffins in addition to n-paraffins, such as iso- and cyclo-paraffins. The branched and cyclo-paraffins have lower melting points than the corresponding n-paraffins and thus have a larger influence on the oil content of a wax. Deoiling of such petroleum based wax mixtures presents other technical challenges and were considered in chapter 6.

CHAPTER 8. CONCLUSIONS AND RECOMMENDATIONS

Supercritical extraction has been investigated for deoiling and fractionation of paraffin waxes. Two state-of-the-art technologies, short path distillation (SPD) and static crystallisation, were modelled and used as benchmarks for the performance of SCFE.

Experimental SPD fractions were produced and simulated using a differential flash method and a simple flash. The experiments were best described using a simple flash calculation, which gave very good results. The generalised vapour pressure equation proposed by Twu (Twu, Coon et al., 1994) was modified to predict recently published low pressure data.

Wax crystallisation was modelled in two steps: first solubility data of pure n-alkanes in solvents were predicted using free volume liquid activity coefficient methods such as Flory-FV and chain-FV. The solubility of n-alkane mixtures in solvents were then modelled using the Wilson and NRTL local composition models. Good results were obtained when calculating the solubility of wax in solvents, but only qualitative agreement on the phase compositions were obtained. Correlations for melting and solid transition temperatures and enthalpies were developed for n-alkanes and 2-methyl alkanes based on values reported in literature. The Wilson (solid phase) and Flory-FV (liquid phase) models are recommended for calculating solid-liquid equilibria in n-alkane wax systems.

Supercritical phase equilibrium data for ethane – n-alkane and CO_2 – n-alkane systems close to the mixture critical region have been obtained from literature, and several equations of state have been investigated to correlate the equilibrium data. Statistical mechanical equations of state failed to correlate the data close to the mixture critical region. It was found that simple cubic equations of state such as Soave-Redlich-Kwong, Peng-Robinson and Patel-Teja could correlate the data using two interaction parameters, probably because they are very flexible correlating tools rather than fundamentally accurate. The Patel-Teja EOS was modified by fitting it to predict low vapour pressure data for long-chain n-alkanes. This modified Patel-Teja EOS was then fitted to the phase equilibria by adjusting two interaction parameters per binary system. It was found that most equations of state do not accurately predict saturated vapour pressures in the low pressure region (<10 Pa). This should be investigated further, since it may have an influence on the

predictive capability of equations of state at the temperatures of interest in this work.

A supercritical fluid extraction column was constructed and used to produce wax fractions from a low molecular weight Fischer-Tropsch wax. The results were simulated using an equilibrium stage model for the extraction column, with equilibrium relations predicted using the modified Patel-Teja equation of state. A solution algorithm for the equilibrium stage model has been proposed that converges in a stable manner for most conditions. This algorithm also reduces the number of K-value evaluations compared with other algorithms.

The deoiling of petroleum waxes containing large fractions of non-normal paraffins was investigated. SPD and SCFE could not deoil the wax to the desired extent. Solvent extraction and static crystallisation can be used to deoil these waxes, but technical problems and low yields prevent their commercial use.

The economics of deoiling an n-paraffin wax using static crystallisation, SPD and SCFE has been investigated. SPD appears to be the more economical deoiling method for the low molecular weight wax used. SCFE should however be the choice for the deoiling/fractionation of longer chain waxes, due to the high temperatures required in SPD processing. The higher SPD temperatures can only be achieved by using electricity as heating medium, which is far more expensive than the medium pressure steam used for the fractionation of low molecular weight n-alkanes. Longer chain waxes can however be processed with SCFE without greatly increasing the temperature. This can be done by either higher extraction pressures or by using a higher molecular weight solvent.

Several aspects were identified that need closer inspection:

- Current models do not yet accurately predict the compositions of both solvent and solid phases in crystallisation of n-alkanes. More work is needed to improve this situation. The equilibrium stage crystallisation model should also be tested against crystallisation plant data to verify the equilibrium stage assumption.
- The correlation of supercritical phase equilibria in the mixture critical region is not very satisfactory, the models cannot yet be used to extrapolate with confidence. Renormalised group theory appears to correct classical equations of state for near-critical density fluctuations, but this theory is very cumbersome to implement currently. Another option is to investigate the use of more complex mixing rules such as excess Gibbs energy type mixing rules for the correlation of interaction parameters.

- The separator pressure plays an important role in the economics of SCFE, and the amount of wax in the solvent stream returned to the extraction column. The modelling of the vapour phase concentration of wax in the separator needs more attention. No literature data is available for the conditions in this work.
- Flooding data for supercritical extraction are scarce, and no general flooding correlation exists to predict flooding velocities for design puposes.

CHAPTER 9. REFERENCES

Alder, B.J., Young, D.A. and Mark, M.A. (1972). *Studies in molecular dynamics. I: Corrections to the augmented van der Waals theory for square-well fluid.* **J. Chem. Phys.,** 56, 3013.

Andrews, T. (1875-76). *The Bakerian lecture - On the state gaseous of matter.* **Proc. R. Soc. London,** 24, 455. Qouted in McHugh and Krukonis, 1993.

Ashton, B., Ashton, A., Jenkins, J. and Mann, R. (2001). **Table 1, Ashton Jenkins Mann, Price Forecast 2001 04, Base Case Forecast Effective April 1, 2001.** http://www.ajma.net/PriceTable.htm

Basarova, P. and Svoboda, V. (1995). *Prediction of the enthalpy of vaporization by the group contribution method.* **Fluid Phase Equilibria,** 105, 27-47.

Batistella, C.B. and Maciel, M.R.W. (1996). *Modeling, simulation and analysis of molecular distillators: centrifugal and falling film.* **Computers and Chemical Engineering,** 20 (Supplement), S19-S24.

Bennett, H. (1963). **Industrial waxes.** New York, Chemical Publishing Company.

Beret, S. and Prausnitz, J.M. (1975). *Perturbed hard-chain theory: an equation of state for fluids containing small or large molecules.* **American Chemical Engineering Journal,** 21, 1123-1132.

Bhat, N.V. (1996). **Phase transformation and crystallization of paraffin mixtures under non-isothermal condition.** Calgary, Canada, University of Calgary.

Bogdanic, G. and Fredenslund, A. (1994). *Revision of the group-contribution Flory equation of state for phase equiilbria calculations in mixtures with polymers. 1. Prediction of vapor-liquid equilibria for polymer solutions.* **Industrial & Engineering Chemistry Research,** 33, 1331-1340.

Bondi, A. (1968). **Physical properties of molecular crystals, liquids, and glasses.** New York, John Wiley.

Boublik, T. (1970). *Hard-Sphere Equation of State.* **J. Chem. Phys.,** 53, 471.

Braun, G. and Schmidt, H. (1984). *High pressure extraction of crude Montan wax.* **Ber. Bunsenges. Phys. Chem.,** 88, 891-894.

Breman, B.B., Beenackers, A.A.C.M., Rietjens, E.W.J. and Stege, R.J.H. (1994). *Gas-liquid solubilities of carbon monoxide , carbon dioxide, hydrogen, water, 1-alcohols ($1 \leq n \leq 6$), and n-paraffins ($2 \leq n \leq 6$) in hexadecane, octacosane, 1-hexadecanol, phenanthrene, and tetraethylene glycol at pressures up to 5.5 MPa and temperatures from 293 to 553 K.* **J. Chem. Eng. Data,** 39, 647-666.

Brignole, E.A., Andersen, P.M. and Fredenslund, A. (1987). *Supercritical fluid extraction of alcohols from water.* **Industrial & Engineering Chemistry Research,** 26, 254-261.

Broadhurst, M.G. (1962). *An analysis of the solid phase behaviour of normal paraffins.* **J. Res. Nat. Bureau Standards,** 66A (3), 241-249.

Brown, D.S., Lewis, W.E. and Smith, A.C. (1963). *Commercial paraffin waxes - How composition affects competence.* **ASTM-TAPPI symposium on petroleum waxes - Characterization, performance and additives.**, New York, Mack Printing Company. 135-145.

Brown, T.S., Niessen, V.G. and Erickson, D.D. (1994). *The effects of light ends and high pressure on paraffin formation. SPE 28505.* **SPE 69th Annual Technical Conference and Exhibition.**, New Orleans, LA. 415-430.

Brunner, G. (1994). **Gas extraction.** Darmstadt, Steinkopff.

Brunner, G. (1998). *Industrial process development countercurrent multistage gas extraction (SFE) processes.* **Journal of Supercritical Fluids,** 13, 283-301.

Buchowski, H., Ksiazczak, A. and Pietrzyk, S. (1980). *Solvent activity along a saturation line and solubility of hydrogen-bonding solids.* **J. Phys. Chem.,** 84, 975-979.

Budich, M., Heilig, S., Wesse, T., Leibkuchler, V. and Brunner, G. (1999). *Countercurrent deterpenation of citrus oils with supercritical CO_2.* **Journal of Supercritical Fluids,** 14, 105-114.

Burrows, G. (1960). **Molecular distillation.** Oxford, Oxford University Press.

Butler, R.M. and MacLeod, D.M. (1961). *Solid-liquid equilibria in wax crystallization.* **Canadian Journal of Chemical Engineering,** 39, 53-63.

Cagniard de la Tour, C. (1822). *Effect obtained by simulations application of heat and pressure on certain liquids.* **Ann. Chim.,** 22, 410. Qouted in McHugh and Krukonis, 1993.

Carnahan, N.F. and Starling, K.E. (1969). *Equation of state for non-attracting rigid spheres.* **J. Chem. Phys,** 51, 635.

Chapman, W.G., Jackson, G. and Gubbins, K.E. (1988). *Phase equilibria of associating fluids. Chain molecules with multiple bonding sites.* **Mol. Phys.,** 65 (5), 1057.

Charoensombut-Amon, T., Martin, R.J. and Kobyashi, R. (1986). *Application of a generalized multiproperty apparatus to measure phase equilibrium and vapor phase densities of supercritical carbon dioxide in n-hexadecane systems up to 26 MPa.* **Fluid Phase Equilibria,** 31, 89-104.

Chen, F., Fredenslund, A. and Rasmussen, P. (1990). *Group-contribution Flory equation of state for vapor-liquid equilibria in mixtures with polymers.* **Industrial & Engineering Chemistry Research,** 29, 875-882.

Chen, S.-F., Chou, Y.-L. and Chen, Y.-P. (1996). *A new cubic simplified perturbed hard-body equation of state.* **Fluid Phase Equilibria,** 118, 201-219.

Chevallier, V., Provost, E., Bourdet, J.B., Bouroukba, M., Petitjean, D. and Dirand, M. (1999). *Mixtures of numerous different n-alkanes: 1. Structural studies by X-ray diffraction at room temperature - Correlation between the crystallographic long c parameter and the average composition of multi-alkane phases.* **Polymer,** (40), 2121-2128.

Chihara, K., Oomori, K., Oono, T. and Mochizuki, Y. (1997). *Supercritical CO_2 regeneration of activated carbon loaded with organic adsorbates.* **Water Science and Technology,** 35 (7), 261-268.

Chou, G.F. and Prausnitz, J.M. (1989). *A phenomenological correction to an equation of state for the critical region.* **American Chemical Engineering Journal,** 35 (9), 1487-1496.

Cocero, M.J., Alonso, E. and Torio, R. (2000). *Supercritical water oxidation (SCWO) for polyethylene terephthalate (PET) industry effluents.* **Proceedings of the 5th International Symposium on Supercritical Fluids**, Atlanta, GA, USA

Cottle, J.E. (1963). **Supercritical polymerization.** USA, Patent no. US3294772

Coutinho, J.A.P. (1999). *Predictive local composition models: NRTL and UNIQUAQ and their application to model solid-liquid equilibrium of n-alkanes.* **Fluid Phase Equilibria,** 158-160, 447-457.

Coutinho, J.A.P., Andersen, S.I. and Stenby, E.H. (1995). *Evaluation of activity coefficient models in prediction of alkane solid-liquid equilibria.* **Fluid Phase Equilibria,** 103, 23-39.

Coutinho, J.A.P., Andersen, S.I. and Stenby, E.H. (1996). *Solid-liquid equilibrium of n-alkanes using the Chain Delta Lattice Parameter model.* **Fluid Phase Equilibria,** 117, 138-145.

Coutinho, J.A.P., Knudsen, K., Andersen, I. and Stenby, E.H. (1996). *A local composition model for paraffinic solid solutions.* **Chemical Engineering Science,** 51 (12), 3273-3282.

Coutinho, J.A.P. and Ruffier-Meray, V. (1997). *Experimental measurements and thermodynamic modeling of paraffinic wax formation in undercooled solutions.* **Industrial & Engineering Chemistry Research,** 36, 4977-4983.

Coutinho, J.A.P. and Stenby, E.H. (1996). *Predictive local composition models for solid/liquid equilibrium in n-alkane systems: Wilson equation for multicomponent systems.* **Industrial & Engineering Chemistry Research,** 35, 918-925.

Crause, J.C. and Nieuwoudt, I. (2000). *The fractionation of paraffin mixtures.* **Industrial & Engineering Chemistry Research,** 39 (12), 4871-4876.

Crooker, P.J., Ahluwalia, K.S. and Fan, Z. (2000). *Operatic results from supercritical water oxidation plants.* **Proceedings of the 5th International Symposium of Supercritical Fluids**, Atlanta, GA, USA

Cvengroš, J. (1995). *Three-stage wiped-film molecular evaporator: design and application.* **Chemical Engineering Technology,** 18, 49-58.

Cvengroš, J. and Lutišan, J. (1995). *Mean free path of molecules on molecular distillation.* **Chemical Engineering Journal,** 56, 39-50.

Cvengroš, J., Lutišan, J. and Micov, M. (2000). *Feed temperature influence on the efficiency of molecular evaporation.* **Chemical Engineering Journal,** 78, 61-67.

de Haan, A.B. (1991). **Supercritical fluid extraction of liquid hydrocarbon mixtures.** Faculty of Chemical Technology and Materials Science. Delft, Delft University of Technology.

de Sant' Ana, H.B., Ungerer, P. and de Hemptinne, J.C. (1999). *Evaluation of an improved volume translation for the prediction of hydrocarbon volumetric properties.* **Fluid Phase Equilibria,** 154, 193-204.

Debenedetti, P.G. (1994). *Supercritical fluids as particle formation media.* **Supercritical fluids.** E. Kiran and J. M. H. Levelt Sengers. Dordrecht, Kluwer Academic Publishers: 719-729.

Dernini, S. and de Santias, R. (1976). *Solubility of solid hexadecane and tetracosane in hexane.* **Canadian Journal of Chemical Engineering,** 54, 369-370.

Dickson, N.L. and Meyers, J.M. (1952). *Solexol fractionation of menhaden oil.* **J. Am. Oil Chem. Soc.,** 29, 235-239.

Donohue, M.D. and Prausnitz, J.M. (1978). *Perturbed hard-chain theory for fluid mixtures: thermodynamic properties for mixtures in natural gas and petroleum technology.* **American Chemical Engineering Journal,** 24, 849-860.

Dorset, D.L. (1990). *Chain length and the cosolubility of n-paraffins in the solid state.* **Macromolecules,** 23, 623-633.

du Rand, M. (2000). **High pressure fluid phase equilibria.** Dept. Chemical Engineering. Stellenbosch, University of Stellenbosch.

Elbro, H.S., Fredenslund, A. and Rasmussen, P. (1990). *A new simple equation for the prediction of solvent activities in polymer solutions.* **Macromolecules,** 23, 4707-4714.

Engstler, H., Stepanski, M., Jans, B.J., Lippuner, F., Hildebrand, G., Richter, F. and Matzat, N. (2000). **Process for obtaining paraffin or paraffin fractions.** USA, Patent no. US6074548

Erickson, D.D., Niesen, V.G. and Brown, T.S. (1993). *Thermodynamic measurement and prediction of paraffin precipitation in crude oil.* **SPE 26604, 66th Annual technical conference and exhibition of the Society of Petroleum Engineers.**, Houston, TX.

Esquivel, M.M., Ribeiro, M.A. and Bernardo-Gil, M.G. (1999). *Supercritical extraction of savory oil: study of antioxidant activity and extract characterization.* **Journal of Supercritical Fluids,** 14, 129-138.

Fair, J.R. and Bravo, J.L. (1990). *Distillation columns containing structured packing.* **Chemical Engineering Progress,** 86, 19-29.

Fall, D.J., Fall, J.L. and Luks, K.D. (1985). *Liquid-liquid-vapor immiscibility limits in carbon dioxide + n-paraffin mixtures.* **J. Chem. Eng. Data,** 60, 82-88.

Fall, D.J. and Luks, K.D. (1984). *Phase equilibria behaviour of the systems carbon dioxide + n-dotriacontane and carbon dioxide + n-docosane.* **J. Chem. Eng. Data,** 29, 413-417.

Finke, H.L., Gross, M.E., Waddington, G. and Huffman, H.M. (1954). *Low-temperature thermal data for the nine normal hydrocarbons from octane to hexadecane.* **J. Am. Chem. Soc.,** 76, 333-341.

Fischer, W. (2000). **Application of short-path distillation in the production of edible oil and fat.** http://www.uic-gmbh.de/e/prospfre.html

Fischer, W. and Bethge, D. (1992). *Short path distillation.* **Distillation and adsorption '92**, Birmingham A403-A414.

Flory, P.J. (1953). **Principles of polymer chemistry.** London, Cornell University Press.

Flory, P.J. (1970). *Thermodynamics of polymer solutions.* **Discuss. Faraday Soc.,** 49, 7-29.

Fong, W.S. (1989). **Supercritical fluid processing.** Menlo Park, SRI International

Fornasiero, F., Lue, L. and Bertucco, A. (1999). *Improving cubic EOSs near the critical point by a phase-space cell approximation.* **American Chemical Engineering Journal,** 45 (4), 906-915.

Francis, A.W. (1954). *Ternary systems of liquid carbon dioxide.* **Journal of Physical Chemistry,** 58, 1099-1114. Qouted in McHugh and Krukonis, 1993.

Gasem, K.A.M., Bufkin, B.A., Raff, A.M. and Robinson, R.L. (1989). *Solubilities of ethane in heavy normal paraffins at pressures to 7.8 MPa and temperatures from 348 to 423 K.* **J. Chem. Eng. Data,** 34, 187-191.

Gasem, K.A.M., Dickson, K.B., Dulcamara, P.B., Nagarajan, N. and Robinson, R.L. (1989). *Equilibrium phase compositions, phase densities, and interfacial tensions for CO_2 + hydrocarbon systems: 5. CO_2 + n-tetradecane.* **Journal of Chemical Engineering Data,** 34, 191-195.

Gasem, K.A.M., Gao, W., Pan, Z. and Robinson, R.L. (2001). *A modified temperature dependence for the Peng-Robinson equation of state.* **Fluid Phase Equilibria,** 181, 113-125.

Gasem, K.A.M. and Robinson, R.L. (1985). *Solubilities of carbon dioxide in heavy normal paraffins (C_{20} - C_{44}) at pressures to 9.6 MPa and temperatures from 323 to 423 K.* **J. Chem. Eng. Data,** 30, 53-56.

Gasem, K.A.M. and Robinson, R.L. (1990). *Evaluation of the simplified perturbed hard chain theory (SPHCT) for predictions of phase behaviour of n-paraffins and mixtures of n-paraffins with ethane.* **Fluid Phase Equilibria,** 58, 13-33.

Gmehling, J. and Onken, U. (1977). **Vapor-liquid equilibrium data collection.** Frankfurt am Main, Dechema.

Gross, J. (2000). **Homepage of the Perturbed-Chain SAFT equation of state.** http://pcitr4.fb10.tu-berlin.de/pc-saft/pc-saft-home.html

Gross, J. and Sadowski, G. (2000). *Application of perturbation theory to a hard-chain reference fluid: an equation of state for square-well chains.* **Fluid Phase Equilibria,** 168 (2), 183-199.

Haji-Sheikh, A., Eftekhar, J. and Lou, D.Y.S. (1983). *Some Thermophysical Properties of Paraffin Wax as a Thermal Storage Medium.* **Progress in Astronautics and Aeronautics,** 86, 241-254.

Hannay, J.B. and Hogarth, J. (1879). *On the solubility of solids in gases.* **Proc. R. Soc. London,** 29, 324. Qouted in McHugh and Krukonis, 1993.

Hansen, J.H., Fredenslund, A., Pedersen, K.S. and Ronningsen, H.P. (1988). *A thermodynamic model for predicting wax formation in crude oils.* **American Chemical Engineering Journal,** 34 (12), 1937-1942.

Hildebrand, J.H. and Scott, R.L. (1964). **The solubility of nonelectrolytes.** New York, Dover.

Hoerr, C.W. and Harwood, H.J. (1951). *Solubilities of high molecular weight aliphatic componds in n-hexane.* **J. Org. Chem.,** 16, 779-791.

Huie, N.C., Luks, K.D. and Kohn, J.P. (1973). *Phase-equilibria behaviour of systems carbon dioxide - n-eicosane and carbon dioxide - n-decane - n-eicosane.* **J. Chem. Eng. Data,** 18 (3), 311-313.

Hunter, E. and Richards, R.B. (1945). **Polymeric fractionation.** USA, Patent no. US2457238

Hutchenson, K.W., Roebers, J.R. and Thies, M.C. (1991). *Fractionation of petroleum pitch with supercritical toluene.* **Journal of Supercritical Fluids,** 4, 7-14.

IFP (2000). **IFP North America - Process lisensor.** http://www.ifpna.com/

Irwin, R.E. and Aufhauser, A. (1975). USA, Patent no. US3926776

Jans, B. and Stepanski, M. (1999). **Solvent-free Deoiling of Paraffin.** Sulzer Tecnical Review. Buchs, Sulzer Chemtech AG

Ji, W.-R. and Lempe, D.A. (1997). *Density improvement of the SRK equation of state.* **Fluid Phase Equilibria,** 130, 49-63.

Jiang, J. and Prausnitz, J.M. (2000). *Phase equilibria of chain-fluid mixtures near to and far from the critical region.* **American Chemical Engineering Journal,** 46 (12), 2525-2536.

Jones, R., Mitchael, M. and al, e. (1991). **Fractionation process for petroleum wax.** USA, Patent no. US5032249

Jung, J. and Perrut, M. (2001). *Particle design using supercritical fluids: Literature and patent survey.* **Journal of Supercritical Fluids,** 20, 179-219.

Katayama, Y. (1992). **Molecular weight fractionation wax from solid wax.** Japan, Patent no. JP4089868

Katayama, Y. (1993). **Producing method of fractionated wax products having different molecular weights from solid wax.** USA, Patent no. US5223122

Kawala, Z. (1992). *Modelling of short-path high vacuum distillation.* **Distillation and Absorption 1992, I. Chem. E. Symp. Series 128.**, Birmingham, Hemisphere Publishing Company. B195-B203.

Kim, C.-H., Vimalchand, P., Donohue, M.D. and Sandler, S.I. (1986). *Local composition model for chainlike molecules: A new simplified version of the perturbed hard chain theory.* **American Chemical Engineering Journal,** 32, 1726-1734.

Kim, Y.J., Carfagno, J.A., McCaffrey, D.S. and Kohn, J.P. (1967). *Partial miscibility phenomena in the ternary system ethane - n-nonadecane - n-eicosane.* **Journal of Chemical Engineering Data,** 12 (3), 289-291.

King, M.B., Catchpole, O.J. and Bott, T.R. (1990). *Energy and economic assessment of near-critial extraction processes.* **Extraction 90, I. Chem. E. Symp. Series 119**

Kiran, E. (1994). *Polymer formation, modifications and processing in or with supercritical fluids.* **Supercritical fluids.** E. Kiran and J. M. H. Levelt Sengers. Dordrecht, Kluwer Academic Publishers: 541-588.

Kister, H.Z. (1992). **Distillation design.** New York, McGraw-Hill.

Kleintjens, L.A. (1994). *Optimizing properties of polymer systems.* **Supercritical fluids.** E. Kiran and J. M. H. Levelt Sengers. Dordrecht, Kluwer Academic Publishers: 589-598.

Kolis, J.W. (2000). *Synthesis and crystal growth of new inorganic materials in supercritical water.* **Proceedings of the 5th International Symposium on Supercritical Fluids**, Atlanta, GA, USA

Kontogeorgis, G.M., Coutsikos, P., Tassios, D.P. and Fredenslund, A. (1994). *Improved models for the prediction of activity coefficients in nearly athermal mixtures. Part I. Empirical modifications of free-volume models.* **Fluid Phase Equilibria,** 92, 35-66.

Kontogeorgis, G.M., Nikolopoulos, G.I., Fredenslund, A. and Tassios, D.P. (1997). *Improved models for the prediction of activity coefficients in nearly athermal mixtures. Part II. A theoretically-based G^e-model based on the van der Waals partition function.* **Fluid Phase Equilibria.,** 127, 103-121.

Kontogeorgis, G.M., Voutsas, E.C. and Tassios, D.P. (1996). *A molecular simulation-based method for the estimation of activity coefficients for alkane solutions.* **Chemical Engineering Science,** 51 (12), 3247-3255.

Kordikowski, A. and Schneider, G.M. (1993). *Fluid phase equilibria of binary and ternary mixtures of supercritical carbon dioxide with low-volatility organic substances up to 100 MPa and 393 K: cosolvency effect and miscibility windows.* **Fluid Phase Equilibria,** 90, 149-162.

Korner, J.-P. (1984). *Supercritical gas extraction.* **Food Engineering International,** (November), 40-42.

Krase, N.W. (1945). **Improvements in or relating to the polymerisation of olefines.** USA, Patent no. US2388160

Krase, N.W. and Lawrence, A.E. (1946). **Process for the preparation of ethylene polymers.** USA, Patent no. US 2396791

Krukonis, V.J. (1984). *Supercritical fluid nucleation of difficult-to-commute solids.* **Paper presented at the AIChE Annual Meeting**, San Francisco, CA, USA

Krukonis, V.J. (1985). *Processing of polymers with supercritical fluids.* **Polymer News,** 11, 7-16.

Larsen, B.L., Rasmussen, P. and Fredenslund, A. (1987). *A modified UNIFAC group contribution model for prediction of phase equilibria and heats of mixing.* **Ind. Eng. Chem. Res.,** 26 (11), 2274-2286.

Lee, K.H., Lombardo, M. and Sandler, S.I. (1985). *The generalized van der Waals partition function. II. Application to square well fluids.* **Fluid Phase Equilibria,** 21, 177.

Levenberg, K. (1944). *A method for the solution of certain non-linear problems in least squares.* **Quart. Appl. Math.,** 2, 164-168.

Liley, P.E., Thomas, G.H., Friend, D.G., Daubert, T.E. and Buck, E. (1997). *Physical and chemical data.* **Perry's chemical engineers' handbook - 7th edition.** R. H. Perry and D. W. Green. New York, NY, USA, McGraw-Hill.

Linstrom, P.J. and Mallard, W.G.E. (2000). **NIST chemistry webbook, NIST standard reference database number 69.** Gaithersburg MD, National Institute of Standards and Technology (http://webbook.nist.gov).

Lira-Galeana, C., Firoozabadi, A. and Prausnitz, J.M. (1996). *Thermodynamics of wax precipitation in petroleum mixtures.* **American Chemical Engineering Journal,** 42 (1), 239-248.

Lue, L. and Prausnitz, J.M. (1998). *Thermodynamics of fluid mixtures near to and far from the critical region.* **American Chemical Engineering Journal,** 44 (6), 1455-1466.

Madras, G., Erkey, M., Orejuela, M. and Akgerman, A. (1993). *Supercritical fluid regeneration of activated carbon loaded with heavy molecular weight organics.* **Industrial & Engineering Chemistry Research,** 32, 1163.

Magoulas, K. and Tassios, D. (1990). *Thermophysical properties of n-alkanes from C1 to C20 and their prediction for higher ones.* **Fluid Phase Equilibria,** 56, 119-140.

Mansoori, G.A., Carnahan, N.F., Starling, K.E. and Leland, T.W. (1971). *Equilibrium Thermodynamic Properties of the Mixture of Hard Spheres.* **J. Chem. Phys.,** 54 (4), 1523-1525.

Marquardt, D.W. (1963). *An algorithm for least-squares estimation of nonlinear parameters.* **J. Soc. Indust. Appl. Math.,** 11 (2), 431-441.

Martin, J.J. (1967). *Equation of state.* **Industrial Engineering Chemistry,** 59, 34-52.

Matheson, R.R. and Smith, P. (1985). *A simple thermodynamic analysis of solid-solution formation in binary systems of homologous extended-chain alkanes.* **Polymer,** 26, 288-292.

Mathias, P.M. and Copeman, T.W. (1983). *Extension of the Peng-Robinson Equation of State to Complex Mixtures.* **Fluid Phase Equilibria,** 13, 91-108.

McHugh, M. and Krukonis, V. (1993). **Supercritical fluid extraction : principles and practice.** Stoneham, Butterworth-Heineman.

McHugh, M.A., Seckner, A.J. and Yogan, T.J. (1984). *High-pressure phase behavior of binary mixtures of octacosane and carbon dioxide.* **Industrial Engineering Chemistry Fundamentals,** 234, 493-499.

McMahon, G.S. and Wood, J.A. (1963). *Identification of some chemical components of waxes and their effect on performance characteristics.* **ASTM-TAPPI symposium on petroleum waxes - Characterization, performance and additives.**, New York, Mack Printing Company. 78-94.

Meyer, G. (2001). **Personal communication.**

Meyer, G. and Hildebrand, G. (2000). *Replacement of solvent deoiling of slack waxes by an environmentally friendly process (in German).* **Erdöl Erdgas Kohle,** 116 (4), 192-195.

Michelsen, M.L. and Kistenmacher, H. (1990). *On composition-dependent interaction coefficients.* **Fluid Phase Equilibria,** 58, 229.

Modell, M., de Filippi, R.P. and Krukonis, V.J. (1978). *Regeneration of activated carbon with supercritical carbon dioxide.* **Paper presented at the ACS Annual Meeting**, Miami

Monnery, W.D., Svrcek, W.Y. and Satyro, M.A. (1998). *Gaussian-like volume shift for the Peng-Robinson equation of state.* **Industrial & Engineering Chemistry Research,** 37, 1663-1672.

Morgan, D.L. and Kobyashi, R. (1994). *Direct vapor pressure measurements of ten n-alkanes in the C_{10}-C_{28} range.* **Fluid Phase Equilibria,** 97, 211-242.

Nasser, W.E. (1999). *Waxes, natural and synthetic.* **Encyclopedia of chemical processing and design**. J. J. McKetta. New York, Marcel Decker, Inc. 67.

Nelson, S.R. and Roodman, R.G. (1985). *ROSE: the energy efficient bottom of the barrel alternative.* **Chemical Engineering Progress,** 81, 63-68.

Nguyen, A.-D. and Le Goffic, F. (1997). *Limits of wiped film short path distiller.* **Chemical Engineering Science,** 52 (16), 2661-2666.

Nieuwoudt, I. (1994). **The fractionation of high molecular weight alkane mixtures with supercritical fluids.** Dept. Chemical Engineering. Stellenbosch, University of Stellenbosch.

Nieuwoudt, I. (1997). **Process design course notes.**, Dept. Chemical Engineering, University of Stellenbosch.

Nieuwoudt, I. (2001). **Personal communication.**

Noll, R.G. and Grogan, P.M. (1963). *An instrument for measuring the seal strength of waxed paper at various separation angles.* **ASTM-TAPPI symposium on petroleum waxes - Characterization, performance and additives.**, New York, Mack Printing Company.

Oschmann, H.J., Prahl, U. and Severin, D. (1998). *Separation of paraffin from crude oil by supercritical fluid extraction.* **Petr. Sci. Tech.,** 16, 133-143.

Pan, C. and Radosz, M. (1999). *Modeling of solid-liquid equilibria in naphthalene, normal-alkane and polyethylene solutions.* **Fluid Phase Eqilibria,** 155, 57-73.

Parkinson, G. and Johnson, E. (1989). *Supercritical processes win CPI acceptance.* **Chemical Engineering,** (July), 36-39.

Passino, H.J. (1949). *The solexol process.* **Industrial Engineering Chemistry,** 41, 280.

Patel, N.C. (1996). *Improvements of the Patel-Teja equation of state.* **Int. J. Thermophysics,** 17 (3), 673-682.

Patel, N.C. and Teja, A.S. (1982). *A new cubic equation of state for fluids and fluid mixtures.* **Chemical Engineering Science,** 37 (3), 463-473.

Patterson, D. (1969). *Fee volume and polymer solubility. A qualitative view.* **Macromolecules,** 2, 672-677.

Pauly, J., Dauphin, C. and Daridon, J.L. (1998). *Liquid-solid equilibria in a decane + multi-paraffins system.* **Fluid Phase Equilibria,** 149, 191-207.

Pedersen, K.S., Skovborg, P. and Ronningsen, H.P. (1991). *Wax precipitation from North-Sea crude oils: 4. Thermodynamic modeling.* **Energy and Fuels,** 5, 924.

Pedersen, W.B., Hansen, A.B., Larsen, E., Nielsen, A.B. and Ronningsen, H.P. (1991). *Wax precipitation from North-Sea crude oils: 2. Solid-phase content as function of temperature determined by pulsed NMR.* **Energy and Fuels,** 5, 908.

Peneloux, A. and Rauzy, E. (1982). *A consistent correction for Redlich-Kwong-Soave volumes.* **Fluid Phase Equilibria,** 8, 7-23.

Peng, D.Y. and Robinson, D.B. (1976). *A new two-constant equation of state.* **Industrial Engineering Chemistry Fundamentals,** 15, 59-64.

Peters, C.J. and de Roo, J.L. (1987). *Measurements and calculations of phase equilibria of binary mixtures of ethane + eicosane. Part I. Vapour + liquid equilibria.* **Fluid Phase Equilibria,** 34, 287-308.

Peters, C.J., de Roo, J.L. and Lichtenthaler, R.N. (1991). *Measurements and calculations of phase equilibria in binary mixtures of ethane + eicosane. Part 3. Three-phase equilibria.* **Fluid Phase Equilibria,** 69, 51-66.

Peters, C.J., de Swaan Aarons, J., Levelt Sengers, J.M.H. and Gallagher, J.S. (1988). *Global phase behaviour of mixtures of short and long n-alkanes.* **American Chemical Engineering Journal,** 34 (5), 834-839.

Peters, C.J., de Swaan Arons, J., Harvey, A.H. and Levelt Sengers, J.M.H. (1989). *On the relationship between the carbon-number of n-paraffins and their solubility in supercritical solvents.* **Fluid Phase Equilibria,** 52, 389-396.

Peters, C.J., Spiegelaar, J. and de Swaan Arons, J. (1988). *Phase equilibria in binary mixtures of ethane + docosane and molar volumes of liquid docosane.* **Fluid Phase Equilibria,** 41, 245-256.

Peters, C.J., van der Kooi, H.J. and de Swaan Arons, J. (1987). *Measurements and calculations of phase equilibria for (ethane + tetracosane) and (p, V_m, T) of liquid tetracosane.* **Journal of Chemical Thermodynamics,** 19, 395-405.

Pfohl, O., Petkof, S. and Brunner, G. (2000). **PE 2000 for Windows.** http://vt2pc8.vt2.tu-harburg.de/HomePage.html

Piacente, V., Fontana, D. and Scardala, P. (1994). *Enthalpies of vaporization of a homologous series of n-alkanes determined from vapor pressure measurements.* **J. Chem. Eng. Data,** 39, 231-237.

Pohler, H., Scheidgen, A.L. and Schneider, G.M. (1996). *Fluid phase equilibria of binary and ternary mixtures of supercritical carbon dioxide with a 1-alkanol and an n-alkane up to 100 MPa and 393 K - cosolvency effect and miscibility windows (Part II).* **Fluid Phase Equilibria,** 115, 165-177.

Polyzou, E.N., Vlamos, P.M., Dimakos, G.M., Yakoumis, I.V. and Kontogeorges, G.M. (1999). *Assessment of activity coefficient models for predicting solid-liquid equilibria of asymmetric binary alkane systems.* **Industrial & Engineering Chemistry Research,** 38, 316-323.

Ponce-Ramirez, L., Lira-Galeana, C. and Tapia-Medina, C. (1991). *Application of the SPHCT model to the prediction of phase equilibria in the CO_2 - hydrocarbon systems.* **Fluid Phase Equilibria,** 70, 1-18.

Pope (2000). **Pope wiped-film molecular stills and evaporators.** http://www.popeinc.com/wiped.htm

Prigogine, I. (1957). **Molecular theory of solutions.** Amsterdam, North-Holland.

Provost, E., Chevallier, V., Bouroukba, M., Petitjean, D. and Dirand, M. (1998). *Solubility of some n-alkanes (C_{23}, C_{25}, C_{26}, C_{28}) in heptane, methylcyclohexane, and toluene.* **J. Chem. Eng. Data,** 43, 745-749.

Rachford, H.H. and Rice, J.D. (1952). *Procedure for use of electronic digital computers in calculating flash vaporization hydrocarbon equilbrium.* **J. Petr. Tech.,** (October), Section 1.19.

Redlich, O. and Kwong, J.N.S. (1949). *On the thermodynamics of solutions.* **Chem. Rev.,** 44, 233.

Reid, R.C., Prausnitz, J.M. and Poling, B.E. (1987). **The properties of liquids and gases.** New York, McGraw-Hill.

Renon, H. and Prausnitz, J.M. (1968). *Local compositions in thermodynamic excess functions for liquid mixtures.* **American Chemical Engineering Journal,** 14 (1), 135-144.

Reverchon, E. (1997). *Supercritical fluid extraction and fractionation of essential oils and related products.* **Journal of Supercritical Fluids,** 10, 1-37.

Riazi, M.R. and Al-Sahhaf, T.A. (1996). *Physical properties of heavy petroleum fractions and crude oils.* **Fluid Phase Equilibria,** 117, 217-224.

Rice, S.F., Wu, B.C. and Winters, S. (2000). *Engineering modeling of the Pine Bluff Arsenal supercritical water oxidation reactor.* **Proceedings of the 5th International Symposium on Supercritical Fluids**, Atlanta, GA, USA

Riha, V. and Brunner, G. (1999). *Phase equilibrium of fish oil ethyl esters with supercritical carbon dioxide.* **Journal of Supercritical Fluids,** 15, 33-50.

Riha, V. and Brunner, G. (2000). *Separation of fish oil ethyl esters with supercritical carbon dioxide.* **Journal of Supercritical Fluids,** 17, 55-64.

Sako, T., Wu, A.H. and Prausnitz, J.M. (1989). *A cubic equation of state for high-pressure phase equilibria of mixtures containing polymers and volatile fluids.* **Journal of Applied Polymer Science,** 38, 1839-1858.

Schaerer, A.A., Busso, C.J., Smith, A.E. and Skinner, L.B. (1955). *Properties of pure normal alkanes in the C_{17} to C_{36} range.* **J. Am. Chem. Soc.,** 77, 2017-2019.

Scott, R.L. (1956). *Corresponding states treatment of nonelectrolyte solutions.* **J. Chem. Phys.,** 25, 193-205.

Seader, J.D. and Henley, E.J. (1998). **Separation process principles.** New York, J. Wiley & Sons.

Sengers, J.V. (1994). *Effects of critical fluctuations on the thermodynamic and transport properties of supercritical fluids.* **Supercritical fluids. Fundamentals for applications.** E. Kiran and J. M. H. Levelt Sengers. Dordrecht, Kluwer Academic Publishers: 231-271.

Sequeira, A. (1994). **Lubricant base oil and wax processing**. New York, Marcel Decker Inc.

Shariati, A., Peters, C.J. and Moshfeghian, M. (1998). *Bubble point pressures of some selected carbon dioxide + synthetic C_{6+} mixtures.* **Journal of Chemical Engineering Data,** 43, 785-788.

Sharma, S.K. and Singh, S. (1979). *Paraffin wax as phase change thermal storage materials*. **National Workshop on Solar Energy Storage**, Chandigarh 133-146.

Sherwood, T.K., Shipley, G.H. and Holloway, F.A. (1938). *Flooding velocities in packed columns.* **Industrial & Engineering Chemistry Research,** 7, 765.

Sinnott, R.K. (1997). **Coulson & Richardson's Chemical engineering Vol. 6: Chemical engineering design.** Oxford, Butterworth-Heinemann Ltd.

Sinowax (2000). **Wax application.** http://www.sinowax.com/maindoc/use/use_wiw_application.htm

Smith, J.M., van Ness, H.C. and Abbott, M.M. (1996). **Introduction to chemical engineering thermodynamics.** New York, McGraw-Hill.

Smith, V.S., Campbell, P.O. and Teja, A.S. (1996). *Solubilities of long-chain hydrocarbons in carbon dioxide.* **Int. J. Thermophysics,** 17 (1), 23-33.

Snyder, R.G., Conti, V.J.P., Strauss, H.L. and Dorset, D.L. (1993). *Thermally-induced mixing in partially microphase segregated binary n-alkane crystals.* **Journal of Physical Chemistry,** 97, 7342.

Soave, G. (1972). *Equilibrium constants from a modified Redlich-Kwong equation of state.* **Chemical Engineering Science,** 27 (6), 1197-1203.

Soave, G. (1993). *Improving the treatment of heavy hydrocarbons by the SRK EOS.* **Fluid Phase Equilibria,** 84, 339-342.

Souahi, F., Sator, S., Albane, S.A., Kies, F.K. and Chitour, C.E. (1998). *Development of a new form for the alpha function of the Redlich-Kwong cubic equation of state.* **Fluid Phase Equilibria,** 153, 73-80.

Spencer, C.F. and Danner, R.P. (1972). *Improved equation for prediction of saturated liquid densities.* **Journal of Chemical Engineering Data,** 17, 236.

Stichlmair, J., Bravo, J.L. and Fair, J.R. (1989). *General model for prediction of pressure drop and capacity of countercurrent gas/liquid packed columns.* **Gas Sep. Purif.,** 3, 19.

Stockfleth, R. and Brunner, G. (2001). *Holdup, pressure drop, and flooding in packed countercurrent columns for the gas extraction.* **Industrial & Engineering Chemistry Research,** 40 (1), 347-356.

Stryjek, R. and Vera, J.H. (1986). *PRSV: an improved Peng-Robinson equation of state for pure compounds and mixtures.* **Canadian Journal of Chemical Engineering,** 64, 323-333.

Suleiman, D., Gurdial, G.S. and Eckert, C.A. (1993). *An apparatus for phase equilibria of heavy paraffins in supercritical fluids.* **American Chemical Engineering Journal,** 39 (7), 1257-1260.

Tassios, D. (1971). *A single-parameter equation for isothermal vapor-liquid equilibrium correlations.* **American Chemical Engineering Journal,** 17 (6), 1367-1371.

Tassios, D.P. (1993). **Applied chemical engineering thermodynamics.** Berlin, Springer-Verlag.

Tomasko, D.L., Hay, K.J., Leman, G.W. and Eckart, C.A. (1993). *Pilot scale study and design of a granular activated carbon regeneration process using supercritical fluids.* **Envirnmental Progress,** 12 (3), 208.

Topliss, R.J., Dimitrelis, D. and Prausnitz, J.M. (1988). *Computational aspects of a non-cubic equation of state for phase-equilibrium calculations. Effect of density-dependent mixing rules.* **Computers and Chemical Engineering,** 12 (5), 483-489.

Tsai, F.-N. and Yau, J.-S. (1990). *Solubility of carbon dioxide in n-tetracosane and in n-dotriacosane.* **Journal of Chemical Engineering Data,** 35, 43-45.

Tsonopoulos, C. and Tan, Z. (1993). *The critical constants of normal alkanes from methane to polyethylene II. Application of Flory theory.* **Fluid Phase Equilibria,** 83, 127-138.

Turton, R., Bailie, R.C., Whiting, W.B. and Shaeiwitz, J.A. (1998). **Analysis, synthesis, and design of chemical processes.** Upper Saddle River, NJ, Prentice Hall.

Twu, C.H. (1988). *A modified Redlich-Kwong equation of state for highly polar, supercritical systems.* **International Symposium on Thermodynamics in Chemical Engineering and Industry.**, Beijing, China

Twu, C.H., Bluck, D., Cunningham, J.R. and Coon, J.E. (1991). *A cubic equation of state with a new alpha function and a new mixing rule.* **Fluid Phase Equilibria,** 69, 33-50.

Twu, C.H., Coon, J.E. and Cunningham, J.R. (1994). *A generalized vapor pressure equation for heavy hydrocarbons.* **Fluid Phase Equilibria,** 96, 19-31.

Vafaie-Sefti, M., Mousavi-Dehghani, S.A. and Bahar, M.M.-Z. (2000). *Modification of multisolid phase model for prediction of wax precipitation: a new and effective solution method.* **Fluid Phase Equilibria,** 173, 65-80.

Villard, P. (1896). *Solibilities of solids and liquids in gas.* **J. Phys.,** 5, 455. Qouted in McHugh and Krukonis, 1993.

Wagner, J.R., MacCaffrey, D.S. and Kohn, J.P. (1968). *Partial miscibility phenomena in the ternary system ethane - n-hexadecane - n-eicosane.* **Journal of Chemical Engineering Data,** 13 (1), 22-24.

Wagner, W. (1973). *New vapor pressure measurements for argon and nitrogen and a new method for establishing a rational vapor pressure equation.* **Cryogenics,** 13, 470-482.

Walsh, J.M. and Gubbins, K.E. (1990). *A modified thermodynamic perturbation theory equation for molecules with fused hard sphere cores.* **Journal of Physical Chemistry,** 94, 5115-5120.

Wang, L.-S. and Gmehling, J. (1999). *Improvement of the SRK equation of state for representing volumetric properties of petroleum fluids using Dortmund Data Bank.* **Chemical Engineering Science,** 54, 3885-3892.

Wang, L.-S. and Guo, T.M. (1993). *A cubic simplified perturbed hard-chain equation of state for fluids with chainlike molecules.* **Canadian Journal of Chemical Engineering,** 71, 591-604.

Warth, A.H. (1956). **The chemistry and technology of waxes**. New York, Reinhold Publishers.

Wax.org (2000). **Application of waxes.** http://www.wax.org/wax1/pages/f_appli.htm

West, T.H. (1985). **Modified deoiling-dewaxing process.** USA, Patent no. US4541917

Wilson, G.M. (1964). *Vapor-liquid equilibrium. XI. A new expression for the excess free energy of mixing.* **J. Am. Chem. Soc.,** 86, 127-130.

Wilson, K.G. (1983). *The renormalisation group and critical phenomena.* **Rev. Mod. Phys.,** 55, 583.

Wilson, R.E., Keith, P.C. and Haylett, R.E. (1936). *Liquid propane: Use in dewaxing, deasphalting and refining heavy oils.* **Industrial Engineering Chemistry,** 28, 1065-1078. Qouted in McHugh and Krukonis, 1993.

WolfMeier, U., Schmidt, H. and al., e. (1996). *Waxes.* **Ullmann's encyclopedia of industrial chemistry**. B. Elvers and S. Hawkins. Weinheim, VCH Verlagsgesellschaft mbH. A28.

Won, K.W. (1986). *Thermodynamics for solid solution-liquid-vapor equilibria: wax phase formation from heavy hydrocarbon mixtures.* **Fluid Phase Equilibria,** 30, 265-279.

Won, K.W. (1989). *Thermodynamic calculation of cloud point temperatures and wax phase compositions of refined hydrocarbon mixtures.* **Fluid Phase Equilibria,** 53, 377.

Wong, K.F. and Eckert, C.A. (1971). *Dilute solution behavior of two cyclic anhydrides.* **Industrial Engineering Chemistry Fundamentals,** 10 (1), 20-23.

Worthy, W. (1981). *Supercritical fluids offer improved separations.* **Chemical & Engineering News,** (August), 16-17.

Yau, J.-S. and Tsai, F.-N. (1993). *Solubilities of heavy n-paraffins in subcritical and supercritical carbon dioxide.* **Journal of Chemical Engineering Data,** 38, 171-174.

Yoshihisa, K. (1992). **Molecular weight fractionation wax from solid wax.** Japan, Patent no. JP4089868

Zhu, J.-Q., Yu, Y.-S. and He, C.-H. (1999). *Calculation of solid's solubilities in mixed liquid solvents by the lh equation using mixing rules.* **Fluid Phase Equilibria,** 155, 85-94.

Zhuang, M.S. and Thies, M.C. (2000). *Extraction of petroleum pitch with supercritical toluene: experiment and prediction.* **Proceedings of the 5th International Symposium on Supercritical Fluids**, Atlanta, GA, USA

Appendix A. Physical properties correlations

A.1. Pure component correlations for n-alkanes

Pure component parameters for all n-alkanes up to n-C_{30}, and n-C_{32} and n-C_{36} were obtained from the Pro/II simulation package's database. The parameters for other n-alkanes were obtained from correlations given below.

T_c, P_c, V_c correlations were taken from (Tsonopoulos and Tan, 1993).

$$T_c = \frac{0.11867}{c_0 + c_1 s^{-1} + c_2 s^{-2}}$$

$$P_c = \frac{17759\left(b_0 + b_1 s^{-1} + b_2 s^{-2}\right)}{\left(a_0 + a_1 s^{-1}\right)^2}$$

$$V_c = 3.5783 \times 10^{-6} s\left(a_0 + a_1 s^{-1}\right)$$

$s = CN + 1$, with *CN* the number of carbon atoms in the n-paraffin.

a_0 =16.00
a_1 = -8.199
b_0 = 74.82
b_1 = 367100
b_2 = -725400
c_0 = 0.1107x10^{-3}
c_1 = 0.9485x10^{-3}
c_2 = -0.5863x10^{-3}

The T_b correlation were taken from (Riazi and Al-Sahhaf, 1996):

$$T_b = 1070 - \exp\left(6.98291 - 0.02013 M_r^{0.6667}\right)$$

The ω correlation were taken from (Magoulas and Tassios, 1990):

$$\omega = 0.194778 + 0.0315382CN + 1.73473 \times 10^{-2} CN^2 - 1.13389 \times 10^{-6} CN^3 + 8.96972 \times 10^{-9} CN^4$$

A.2. Pure component correlations for 2-methyl alkanes

Pure component parameters were only available for 2-methyl alkanes from $2mC_4$ (2-methyl propane) to $2mC_{10}$ (obtained from the NIST web database, http://webbook.nist.gov/chemistry). It appeared as if the P_c and V_c parameters follow the same trend as the n-alkanes:

$$P_{c,2mC} = P_{c,n}$$

$$V_{c,2mC} = V_{c,n}$$

It appear as if the T_c, T_b and ω parameters tend to converge to n-alkane values for longer chain lengths, so the 2-methyl alkane properties were modelled as a perturbation from the n-alkane properties for low carbon numbers, which vanishes at long chain lengths.

$$T_{c,2mC} = \frac{T_{c,n}}{1.022 - 0.022\exp\left(\frac{-86.62}{CN^2}\right)}$$

$$T_{b,2mC} = \frac{T_{b,n}}{1.03 - 0.03\exp\left(\frac{-74}{CN^2}\right)}$$

$$\omega_{b,2mC} = \frac{\omega_{b,n}}{1.15 - 0.15\exp\left(\frac{-30.36}{CN^2}\right)}$$

A.3. Temperature dependent properties

Vapour pressure and liquid molar volume correlations for all n-alkanes up to n-C_{30}, and n-C_{32} and n-C_{36} were obtained from the Pro/II simulation package's database. Other alkane correlations are given below.

The vapour pressure for both n- and 2-methyl alkanes are calculated using a Lee-Kesler type correlation (Twu, Coon et al., 1994):

$$\ln(P_r) = \ln(P_r^0) + \omega\ln(P_r^1)$$

$\ln(P_r^0)$ and $\ln(P_r^1)$ are given, correlated with the Wagner equation (Wagner, 1973). The constants of the $\ln(P_r^1)$ equation have been adjusted slightly to ensure a smooth extrapolation between the Pro/II correlations, low vapour pressure data of (Piacente, Fontana et al., 1994) and the Lee-Kesler type correlation of (Twu, Coon et al., 1994):

$$\ln(P_r^0) = \frac{1}{T_r}\left(-5.96346(1-T_r)+1.17639(1-T_r)^{1.5}-0.559607(1-T_r)^3-1.31901(1-T_r)^6\right)$$

$$\ln(P_r^1) = \frac{1}{T_r}\left(-4.70025(1-T_r)+0.328435(1-T_r)^{1.5}-9.84001(1-T_r)^3-4.98662(1-T_r)^6\right)$$

Liquid molar volumes for both n- and 2-methyl alkanes are calculated using the modified Rackett equation (Spencer and Danner, 1972):

$$V_L = \frac{A}{Z_R^n}$$

$$n = 1+(1-T_r)^B$$

The parameters were fitted to data obtained from Pro/II correlations for n-C_{10} – n-C_{30} over the temperature range 300-580 K, correlated as follows:

$$A = 0.08728\times10^{-3}+0.016059\times10^{-3}\mathrm{M_r}$$

$$Z_R = 3.88487+0.08263\omega$$

$$B = 0.26364+0.0001963\mathrm{M_r}$$

Heat of vaporisation correlations for all n-alkanes up to n-C_{30}, and n-C_{32} and n-C_{36} were obtained from the Pro/II simulation package's database. The heat of vaporisation for other n-alkanes were obtained from the group contribution correlation proposed by (Basarova and Svoboda, 1995):

$$\Delta H^{vap} = A(1-T_R)^B \exp(-BT_R)$$

$$A = 24691+5751(CN-2)$$

To enable smooth extrapolation between the Pro/II and Basarova correlations, parameter B has been adjusted slightly:

$$B = 0.244+0.00393CN$$

Symbol	Description	Units
CN	Carbon number	
ΔH^{vap}	Heat of vaporisation	J/mol
M_r	Molecular weight	g/mol
P	Pressure	Pa
s	CN + 1	
T	Temperature	K
V	Molar volume	m^3/mol
ω	Pitzer's acentric factor	
Z_R	Rackett parameter	

Subscripts

b	Boiling
c	Critical property
2mC	2-methyl alkane
n	n-alkane
r	Reduced property

Appendix B. Short path distillation experimental results.

Table 9-1. Experimental conditions.

Run	T jacket °C	P Pa	Distillate/Feed ratio	Feed rate g/min
SPD1	145	40	0.44	71.8
SPD2	145	50	0.33	112.7
SPD3	145	60	0.17	161.1
SPD4	150	40	0.44	79.9
SPD5	150	50	0.19	151.8
SPD6	150	60	0.12	205.2
SPD7	160	40	0.41	88.5
SPD8	160	50	0.32	126.6
SPD9	160	60	0.19	169.1
SPD10	142	30	0.61	25.6
SPD11	142	40	0.35	41.0
SPD12	142	50	0.19	51.6
SPD13	155	40	0.72	26.1
SPD14	155	50	0.52	46.1
SPD15	155	60	0.42	41.6
SPD16	170	50	0.55	72.4
SPD17	170	60	0.44	91.8
SPD18	170	70	0.39	73.9
SPD19	150	120	0.15	35.9
SPD20	140	85	0.10	54.3
SPD21	170	80	0.54	24.7

Table 2. Composition (mass fraction) of SPD streams.

Component	SPD1			SPD2			SPD3			SPD4		
	Feed	Distillate	Bottoms	Feed	Distillate	Bottoms	Feed	Distillate	Bottoms	Feed	Distillate	Bottoms
n-C_{11}	0	0	0	0	0	0	0	0	0	0	0	0
n-C_{12}	0.0005	0.0012	0	0.0004	0.0017	0	0.0002	0.0019	0	0.0002	0.0009	0
n-C_{13}	0.0018	0.0042	0	0.0019	0.0060	0	0.0012	0.0070	0	0.0013	0.0034	0
n-C_{14}	0.0066	0.0152	0	0.0071	0.0217	0.0005	0.0050	0.0233	0.0011	0.0069	0.0215	0
n-C_{15}	0.0208	0.0460	0.0007	0.0215	0.0630	0.0028	0.0149	0.0630	0.0052	0.0158	0.0374	0.0012
n-C_{16}	0.0493	0.1072	0.0036	0.0495	0.1302	0.0127	0.0371	0.1286	0.0174	0.0376	0.0819	0.0051
n-C_{17}	0.0826	0.1688	0.0155	0.0864	0.1903	0.0377	0.0718	0.1855	0.0492	0.0686	0.1394	0.0182
n-C_{18}	0.1187	0.2125	0.0440	0.1196	0.2082	0.0803	0.1066	0.2004	0.0889	0.1040	0.1866	0.0438
n-C_{19}	0.1402	0.1939	0.0981	0.1422	0.1705	0.1300	0.1315	0.1681	0.1253	0.1323	0.1973	0.0835
n-C_{20}	0.1424	0.1338	0.1483	0.1464	0.1093	0.1632	0.1402	0.1139	0.1450	0.1352	0.1481	0.1265
n-C_{21}	0.1272	0.0713	0.1747	0.1224	0.0582	0.1520	0.1278	0.0575	0.1429	0.1265	0.0955	0.1469
n-C_{22}	0.0990	0.0273	0.1535	0.0973	0.0225	0.1305	0.1085	0.0273	0.1252	0.1094	0.0521	0.1504
n-C_{23}	0.0742	0.0114	0.1245	0.0733	0.0106	0.1010	0.0862	0.0130	0.0981	0.0861	0.0208	0.1307
n-C_{24}	0.0541	0.0047	0.0920	0.0517	0.0048	0.0727	0.0651	0.0064	0.0778	0.0658	0.0094	0.1070
n-C_{25}	0.0365	0.0019	0.0635	0.0355	0.0021	0.0504	0.0473	0.0030	0.0552	0.0478	0.0041	0.0799
n-C_{26}	0.0229	0.0006	0.0396	0.0223	0.0010	0.0323	0.0297	0.0012	0.0352	0.0308	0.0015	0.0522
n-C_{27}	0.0131	0	0.0226	0.0128	0	0.0185	0.0148	0	0.0185	0.0178	0	0.0308
n-C_{28}	0.0061	0	0.0113	0.0058	0	0.0092	0.0073	0	0.0087	0.0078	0	0.0135
n-C_{29}	0.0028	0	0.0047	0.0026	0	0.0037	0.0034	0	0.0044	0.0040	0	0.0069
n-C_{30}	0.0013	0	0.0023	0.0013	0	0.0018	0.0016	0	0.0019	0.0020	0	0.0034

Table 2. continued.

Component	SPD1			SPD2			SPD3			SPD4		
	Feed	Distillate	Bottoms	Feed	Distillate	Bottoms	Feed	Distillate	Bottoms	Feed	Distillate	Bottoms
n-C_{11}	0	0	0	0	0	0	0	0	0	0	0	0
n-C_{12}	0.0001	0.0010	0	0.0001	0.0015	0	0.0001	0.0005	0	0.0001	0.0008	0
n-C_{13}	0.0008	0.0038	0	0.0003	0.0049	0	0.0005	0.0018	0.0003	0.0008	0.0027	0
n-C_{14}	0.0031	0.0124	0.0008	0.0026	0.0168	0.0008	0.0023	0.0061	0.0022	0.0028	0.0087	0
n-C_{15}	0.0102	0.0390	0.0033	0.0089	0.0465	0.0041	0.0080	0.0209	0.0073	0.0097	0.0286	0.0016
n-C_{16}	0.0274	0.0919	0.0112	0.0225	0.0980	0.0129	0.0210	0.0531	0.0194	0.0264	0.0687	0.0068
n-C_{17}	0.0572	0.1511	0.0337	0.0520	0.1593	0.0380	0.0474	0.1049	0.0473	0.0536	0.1254	0.0210
n-C_{18}	0.0926	0.1879	0.0684	0.0911	0.1874	0.0788	0.0820	0.1621	0.0815	0.0896	0.1736	0.0506
n-C_{19}	0.1252	0.1877	0.1093	0.1222	0.1792	0.1135	0.1171	0.2041	0.1148	0.1208	0.1882	0.0892
n-C_{20}	0.1404	0.1448	0.1412	0.1375	0.1312	0.1422	0.1359	0.1742	0.1361	0.1431	0.1691	0.1317
n-C_{21}	0.1314	0.0913	0.1412	0.1353	0.0877	0.1368	0.1406	0.1292	0.1451	0.1370	0.1123	0.1473
n-C_{22}	0.1198	0.0498	0.1366	0.1250	0.0486	0.1356	0.1251	0.0783	0.1250	0.1228	0.0658	0.1493
n-C_{23}	0.0972	0.0214	0.1156	0.0991	0.0214	0.1100	0.1032	0.0377	0.1040	0.0991	0.0332	0.1298
n-C_{24}	0.0744	0.0103	0.0903	0.0766	0.0104	0.0857	0.0811	0.0168	0.0817	0.0716	0.0140	0.0964
n-C_{25}	0.0532	0.0048	0.0651	0.0570	0.0048	0.0639	0.0599	0.0074	0.0600	0.0545	0.0061	0.0774
n-C_{26}	0.0344	0.0019	0.0427	0.0345	0.0021	0.0387	0.0369	0.0028	0.0362	0.0346	0.0022	0.0500
n-C_{27}	0.0172	0.0008	0.0213	0.0187	0.0003	0.0207	0.0202	0.0003	0.0203	0.0178	0.0007	0.0258
n-C_{28}	0.0091	0	0.0114	0.0097	0	0.0106	0.0108	0	0.0109	0.0091	0	0.0135
n-C_{29}	0.0044	0	0.0055	0.0048	0	0.0054	0.0053	0	0.0054	0.0045	0	0.0065
n-C_{30}	0.0019	0	0.0024	0.0021	0	0.0024	0.0024	0	0.0023	0.0021	0	0.0031

Table 2. – continued.

Component	SPD5			SPD6			SPD7			SPD8		
	Feed	Distillate	Bottoms	Feed	Distillate	Bottoms	Feed	Distillate	Bottoms	Feed	Distillate	Bottoms
n-C_{11}	0	0	0	0	0	0	0	0	0	0	0	0
n-C_{12}	0	0	0	0	0	0	0	0	0	0.0001	0.0006	0
n-C_{13}	0.0003	0.0028	0	0.0004	0.0014	0	0.0000	0.0000	0	0.0005	0.0022	0
n-C_{14}	0.0021	0.0098	0	0.0036	0.0062	0.0034	0.0005	0.0013	0	0.0018	0.0079	0
n-C_{15}	0.0082	0.0317	0.0028	0.0109	0.0173	0.0109	0.0021	0.0056	0	0.0063	0.0269	0.0010
n-C_{16}	0.0226	0.0747	0.0101	0.0271	0.0430	0.0271	0.0065	0.0178	0	0.0192	0.0704	0.0053
n-C_{17}	0.0509	0.1308	0.0307	0.0630	0.0980	0.0631	0.0201	0.0526	0.0012	0.0424	0.1325	0.0179
n-C_{18}	0.0867	0.1800	0.0630	0.1034	0.1550	0.1050	0.0435	0.1074	0.0062	0.0773	0.1890	0.0499
n-C_{19}	0.1198	0.1903	0.1015	0.1244	0.1831	0.1244	0.0769	0.1669	0.0247	0.1113	0.1973	0.0914
n-C_{20}	0.1402	0.1546	0.1328	0.1417	0.1879	0.1417	0.1108	0.2016	0.0596	0.1337	0.1604	0.1268
n-C_{21}	0.1384	0.1076	0.1475	0.1334	0.1414	0.1344	0.1329	0.1777	0.1063	0.1450	0.1074	0.1544
n-C_{22}	0.1264	0.0644	0.1439	0.1133	0.0876	0.1137	0.1370	0.1307	0.1407	0.1292	0.0594	0.1471
n-C_{23}	0.1035	0.0296	0.1227	0.0894	0.0454	0.0894	0.1297	0.0776	0.1595	0.1082	0.0258	0.1289
n-C_{24}	0.0771	0.0147	0.0964	0.0717	0.0206	0.0715	0.1093	0.0363	0.1524	0.0847	0.0120	0.1033
n-C_{25}	0.0537	0.0065	0.0617	0.0515	0.0090	0.0506	0.0862	0.0155	0.1278	0.0616	0.0054	0.0759
n-C_{26}	0.0349	0.0024	0.0430	0.0327	0.0031	0.0317	0.0636	0.0068	0.0954	0.0396	0.0020	0.0491
n-C_{27}	0.0186	0	0.0232	0.0181	0.0011	0.0179	0.0418	0.0023	0.0642	0.0205	0.0007	0.0259
n-C_{28}	0.0098	0	0.0122	0.0091	0	0.0091	0.0216	0	0.0342	0.0107	0	0.0135
n-C_{29}	0.0047	0	0.0059	0.0043	0	0.0042	0.0119	0	0.0188	0.0053	0	0.0067
n-C_{30}	0.0020	0	0.0026	0.0020	0	0.0020	0.0057	0	0.0091	0.0024	0	0.0029

Table 2. continued.

Component	SPD5			SPD6			SPD7			SPD8		
	Feed	Distillate	Bottoms	Feed	Distillate	Bottoms	Feed	Distillate	Bottoms	Feed	Distillate	Bottoms
n-C_{11}	0	0	0	0	0	0	0	0	0	0	0	0
n-C_{12}	0	0	0	0.0002	0.0008	0	0.0003	0.0008	0	0	0	0
n-C_{13}	0.0001	0.0004	0	0.0017	0.0032	0	0.0017	0.0038	0	0.0012	0.0021	0
n-C_{14}	0.0019	0.0026	0	0.0062	0.0115	0	0.0055	0.0126	0	0.0049	0.0086	0
n-C_{15}	0.0063	0.0086	0.0008	0.0180	0.0330	0.0006	0.0172	0.0394	0.0007	0.0160	0.0266	0.0018
n-C_{16}	0.0181	0.0240	0.0033	0.0433	0.0776	0.0031	0.0409	0.0877	0.0040	0.0411	0.0660	0.0079
n-C_{17}	0.0461	0.0615	0.0089	0.0772	0.1319	0.0120	0.0743	0.1476	0.0164	0.0748	0.1153	0.0209
n-C_{18}	0.0794	0.1051	0.0204	0.1127	0.1750	0.0366	0.1092	0.1904	0.0452	0.1113	0.1578	0.0488
n-C_{19}	0.1166	0.1493	0.0412	0.1359	0.1806	0.0765	0.1330	0.1885	0.0895	0.1364	0.1746	0.0852
n-C_{20}	0.1388	0.1685	0.0719	0.1436	0.1597	0.1229	0.1422	0.1504	0.1356	0.1440	0.1604	0.1193
n-C_{21}	0.1455	0.1586	0.1154	0.1334	0.1109	0.1563	0.1289	0.0940	0.1557	0.1313	0.1199	0.1461
n-C_{22}	0.1343	0.1320	0.1513	0.1113	0.0649	0.1680	0.1082	0.0493	0.1545	0.1106	0.0791	0.1550
n-C_{23}	0.1103	0.0915	0.1590	0.0845	0.0293	0.1487	0.0851	0.0213	0.1354	0.0874	0.0476	0.1408
n-C_{24}	0.0823	0.0540	0.1546	0.0577	0.0138	0.1119	0.0638	0.0095	0.1067	0.0602	0.0240	0.1090
n-C_{25}	0.0556	0.0262	0.1206	0.0368	0.0055	0.0769	0.0422	0.0035	0.0728	0.0397	0.0115	0.0777
n-C_{26}	0.0332	0.0118	0.0769	0.0204	0.0019	0.0449	0.0247	0.0013	0.0432	0.0216	0.0048	0.0435
n-C_{27}	0.0174	0.0043	0.0422	0.0100	0.0004	0.0232	0.0125	0	0.0223	0.0115	0.0018	0.0242
n-C_{28}	0.0085	0.0015	0.0201	0.0045	0	0.0109	0.0060	0	0.0107	0.0049	0	0.0120
n-C_{29}	0.0039	0	0.0094	0.0021	0	0.0051	0.0029	0	0.0051	0.0023	0	0.0052
n-C_{30}	0.0016	0	0.0038	0.0005	0	0.0023	0.0012	0	0.0023	0.0008	0	0.0024

Table 2. continued.

Component	SPD5			SPD6			SPD7			SPD8		
	Feed	Distillate	Bottoms	Feed	Distillate	Bottoms	Feed	Distillate	Bottoms	Feed	Distillate	Bottoms
n-C_{11}	0.0001	0.0002	0	0	0	0	0	0	0	0	0	0
n-C_{12}	0.0002	0.0008	0	0.0002	0.0010	0	0.0002	0.0029	0	0.0002	0.0039	0
n-C_{13}	0.0015	0.0034	0	0.0016	0.0041	0.0016	0.0024	0.0118	0	0.0023	0.0167	0
n-C_{14}	0.0053	0.0121	0	0.0054	0.0136	0.0054	0.0061	0.0305	0	0.0059	0.0423	0
n-C_{15}	0.0167	0.0363	0.0015	0.0164	0.0388	0.0164	0.0140	0.0632	0.0038	0.0135	0.0828	0.0038
n-C_{16}	0.0395	0.0822	0.0063	0.0403	0.0904	0.0403	0.0263	0.1110	0.0096	0.0267	0.1355	0.0134
n-C_{17}	0.0719	0.1379	0.0205	0.0746	0.1515	0.0745	0.0446	0.1563	0.0231	0.0451	0.1709	0.0299
n-C_{18}	0.1093	0.1835	0.0516	0.1088	0.1904	0.1086	0.0694	0.1761	0.0465	0.0684	0.1727	0.0552
n-C_{19}	0.1300	0.1792	0.0925	0.1323	0.1845	0.1323	0.0941	0.1610	0.0789	0.0932	0.1436	0.0867
n-C_{20}	0.1441	0.1543	0.1372	0.1414	0.1449	0.1414	0.1146	0.1225	0.1108	0.1140	0.1021	0.1148
n-C_{21}	0.1374	0.1063	0.1587	0.1276	0.0937	0.1281	0.1253	0.0786	0.1323	0.1235	0.0621	0.1304
n-C_{22}	0.1116	0.0572	0.1540	0.1092	0.0492	0.1092	0.1236	0.0442	0.1384	0.1225	0.0339	0.1335
n-C_{23}	0.0883	0.0280	0.1353	0.0864	0.0230	0.0864	0.1106	0.0228	0.1306	0.1117	0.0176	0.1247
n-C_{24}	0.0609	0.0126	0.0985	0.0647	0.0097	0.0647	0.0931	0.0115	0.1127	0.0945	0.0094	0.1066
n-C_{25}	0.0393	0.0044	0.0669	0.0435	0.0039	0.0435	0.0723	0.0053	0.0882	0.0734	0.0042	0.0832
n-C_{26}	0.0225	0.0015	0.0388	0.0249	0.0013	0.0253	0.0495	0.0021	0.0602	0.0504	0.0021	0.0571
n-C_{27}	0.0120	0	0.0213	0.0129	0	0.0127	0.0284	0	0.0347	0.0290	0	0.0326
n-C_{28}	0.0057	0	0.0102	0.0061	0	0.0062	0.0145	0	0.0171	0.0147	0	0.0160
n-C_{29}	0.0025	0	0.0045	0.0028	0	0.0027	0.0078	0	0.0097	0.0077	0	0.0087
n-C_{30}	0.0012	0	0.0022	0.0010	0	0.0009	0.0030	0	0.0033	0.0031	0	0.0033

Table 2. – concluded.

Component	SPD21		
	Feed	Distillate	Bottoms
n-C_{11}	0	0	0
n-C_{12}	0	0	0
n-C_{13}	0.0022	0.0029	0
n-C_{14}	0.0065	0.0097	0
n-C_{15}	0.0140	0.0214	0.0019
n-C_{16}	0.0264	0.0419	0.0038
n-C_{17}	0.0450	0.0715	0.0095
n-C_{18}	0.0683	0.1063	0.0182
n-C_{19}	0.0932	0.1406	0.0337
n-C_{20}	0.1138	0.1594	0.0571
n-C_{21}	0.1239	0.1526	0.0907
n-C_{22}	0.1225	0.1204	0.1279
n-C_{23}	0.1115	0.0807	0.1538
n-C_{24}	0.0943	0.0464	0.1574
n-C_{25}	0.0734	0.0250	0.1368
n-C_{26}	0.0540	0.0211	0.1046
n-C_{27}	0.0279	0	0.0602
n-C_{28}	0.0144	0	0.0305
n-C_{29}	0.0070	0	0.0139
n-C_{30}	0.0017	0	0

Appendix C. Correlation of solid transition and melting properties of alkanes.

C.1. Correlations developed for n-alkanes.

C.1.1. Melting temperatures

Data used:
n-C_8 – n-C_{16} : (Finke, Gross et al., 1954)
n-C_{17} – n-C_{30}, n-C_{36} : (Schaerer, Busso et al., 1955)
n-C_{32} : (Polyzou, Vlamos et al., 1999)
n-C_{31}, all data from n-C_{33} : (Broadhurst, 1962)

The data were well correlated (see Figure 1) with the following correlation:

Eq. 9.1 $$T^m = 425.202 - \frac{5230.59}{M_r^{0.67}} + 0.7\ln(M_r)$$

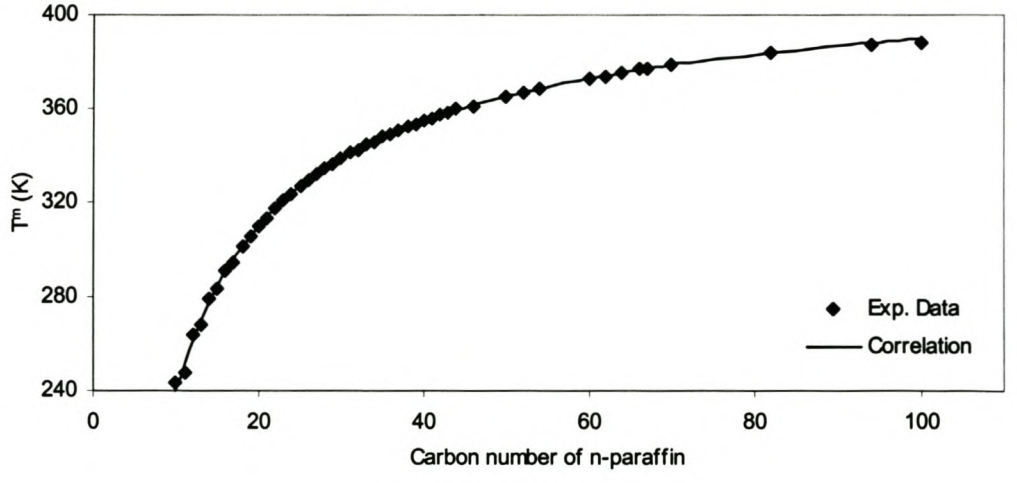

Figure 11. Comparison of equation 1 with experimental melting temperatures.

C.1.2. Melting enthalpies

Data used:
n-C_8 – n-C_{16} : (Finke, Gross et al., 1954)
n-C_{18} – n-C_{29}, n-C_{36} : (Schaerer, Busso et al., 1955)
n-C_{32} : (Polyzou, Vlamos et al., 1999)
n-C_{34} and n-C_{35} : (Broadhurst, 1962)

Eq. 9.2 $$H^m = 0.5 M_r T^m$$

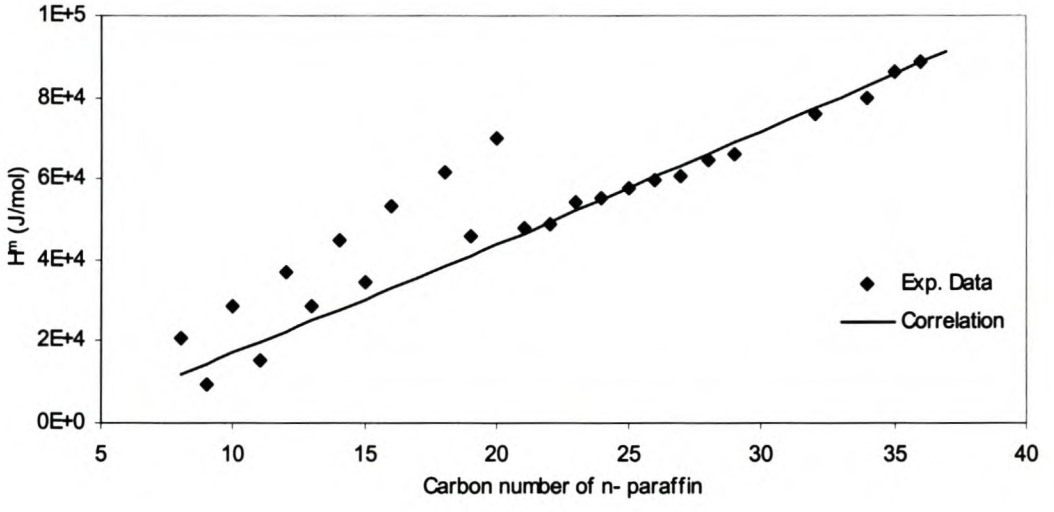

Figure 12. Comparison of eq. 2 with experimental melting enthalpies.

From Figure 2 it is evident that the melting enthalpies of the even numbered n-alkanes below n-C_{22} does not lie on the same curve than the other n-alkanes. This is probably caused by the absence of a solid-solid transition, and these components were not included in the correlation procedure. The difference between the experimentally determined melting enthalpy and Eq. 2 is assumed to correspond to a solid-solid transition occurring at the melting temperature, and will be added to the solid-solid transition correlations below.

C.1.3. Solid-solid transition temperature

Data used:
n-C_9, n-C_{11}, n-C_{13}, n-C_{15} : (Finke, Gross et al., 1954)
n-C_{19}, n-C_{21} - n-C_{28} : (Schaerer, Busso et al., 1955)
n-C_{29} - n-C_{43} : (Broadhurst, 1962)

The transition temperatures for the even n-alkanes n-C_{20} and below were taken as the melting temperatures. From a plot of the data it is clear that two separate correlations are needed to accurately correlate the transition temperatures of both even and uneven numbered n-alkanes.

Eq. 9.3 $$T^t = 389.153 - 175.674\exp(-0.0028\mathrm{M_r})$$ (even n-alkanes)

$$T^t = T^t(even) \; -17.90443\exp(-1.07409\times10^{-5}\mathrm{M_r})$$ (odd n-alkanes)

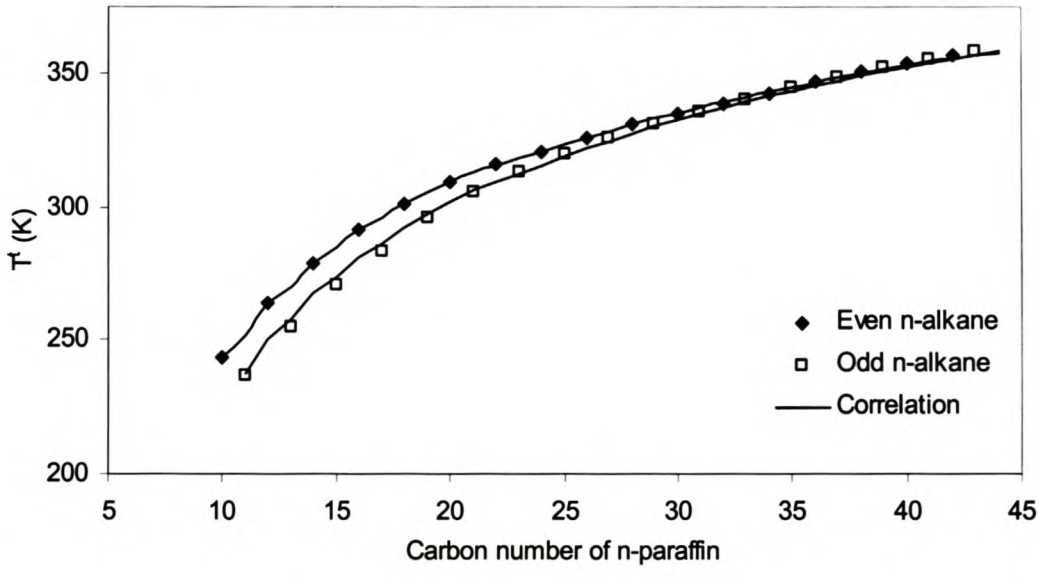

Figure 13. Comparison of experimental transition temperatures with Eq. 9.3.

C.1.4. Heat capacity difference

The heat capacity difference between liquid and solid n-alkanes were correlated with the even alkane data from Finke et al. (Finke, Gross et al., 1954) using the correlation proposed by Pedersen (Pedersen, Skovborg et al., 1991):

Eq. 9.4 $$\Delta Cp = 0.9M_r - 0.002M_rT^m$$

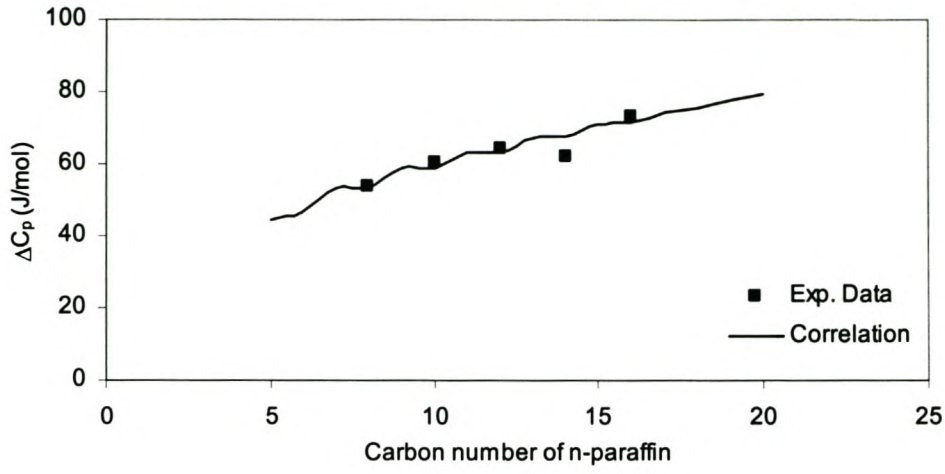

Figure 14. Comparison of experimental ΔC_p values with Eq. 9.4.

C.1.5. Solid-solid enthalpy of transition

Data used:
n-C_9, n-C_{11}, n-C_{13}, n-C_{15} : (Finke, Gross et al., 1954)
n-C_{19}, n-C_{21} - n-C_{28} : (Schaerer, Busso et al., 1955)
n-C_{29} - n-C_{30} : (Broadhurst, 1962)

As described in section C.1.2, pseudo solid-solid transition properties are assumed for the even n-alkanes for n-C_{20} and below. The data for even and odd numbered n-alkanes did not fall on the same general curve, and separate correlations were fitted to the data.

Eq.9.5 $H^t = -59396 + 34.807 M_r + 13362.8 \ln(M_r)$ (even n-alkanes)

$$H^t = H^t(even) - 11691 \exp\left(\frac{-(M_r - 254.23)^2}{15510}\right) \quad \text{(odd n-alkanes)}$$

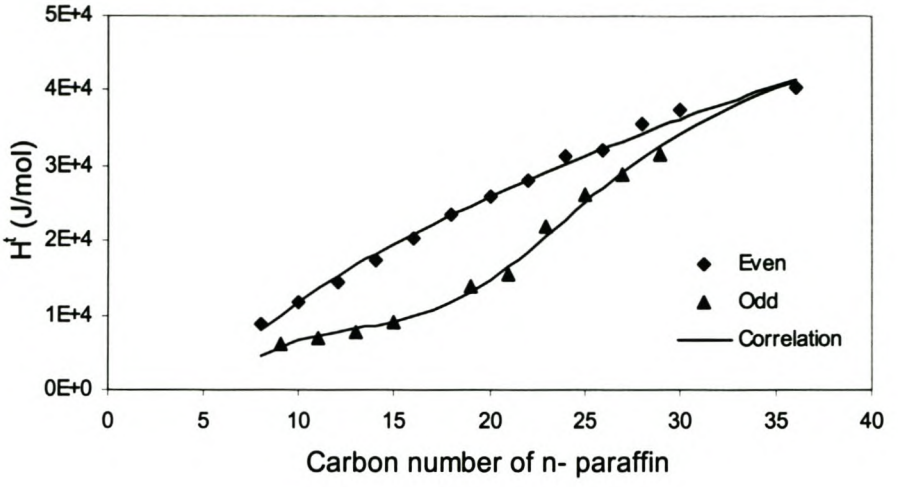

Figure 15. Comparison of Eq.9.5 with experimental solid-solid transition change in enthalpy.

C.2. Correlations for 2-methyl alkanes.

C.2.1. Melting temperature

Data used:
2m-C_4 – 2m-C_{11}: (Linstrom and Mallard, 2000)
2m-C_{24}, 2m-C_{34} – 2m-C_{36}: (Warth, 1956)

The melting temperatures of 2-methyl alkanes appear to converge to that of n-alkanes for long chain lengths. The melting temperatures of the 2-methyl alkanes were therefore modelled as a deviation from the corresponding n-alkane correlation:

Eq.9.6 $$T^m = \frac{T^m(n-alkane)}{1.29 - 0.29\exp\left(\frac{-18895}{M_r^2}\right)}$$

The experimental melting temperatures and Eq. 6. is shown below in Figure 16:

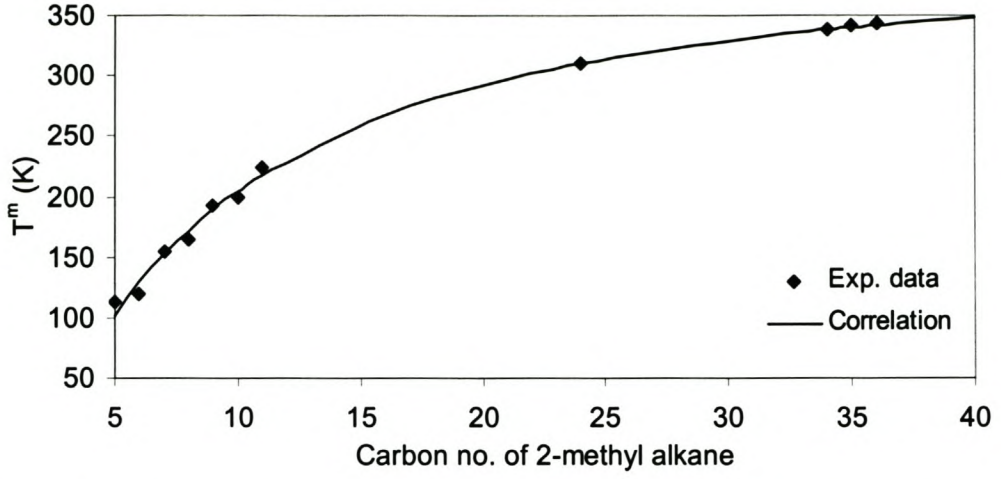

Figure 16. Comparison of experimental melting temperatures with correlation Eq. 6.

C.2.2. Enthalpy of melting

Data used:
2m-C_8, 2m-C_{10}, 2m-C_{11}: (Linstrom and Mallard, 2000)
2m-C_{24}: (Warth, 1956)

The experimental data were successfully correlated as follows:

Eq.9.7 $\Delta H^m = 0.66 M_r T^m$

This correlation is compared with experimental data below:

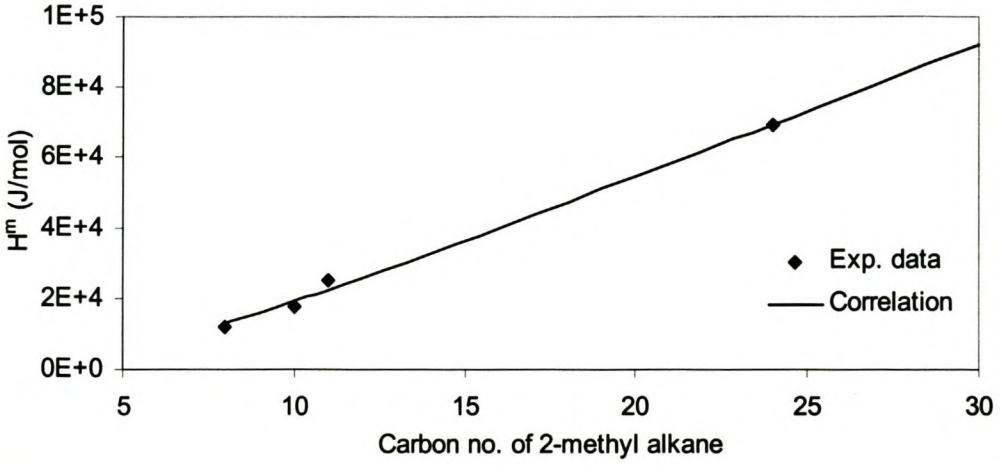

Figure 17. Comparison between experimental enthalpy of melting data with Eq.9.7.

C.2.3. Butler et al correlation.

Butler (Butler and MacLeod, 1961) lumped the enthalpies of melting and solid-solid transition, and presented the following correlation for n-alkanes:

Eq. 9.8 $$H^m = 3409CN$$

CN is the number of carbon atoms in the paraffin molecule.

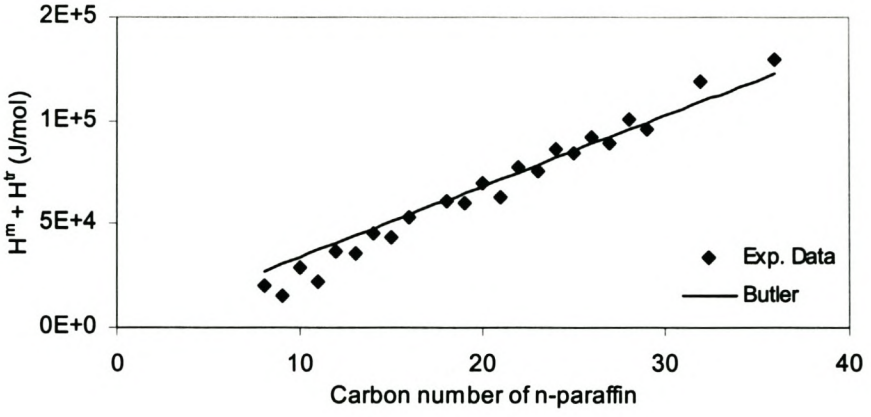

Figure 111. Experimental H^m + H^{tr} data compared with Butler et al. (Butler and MacLeod, 1961) correlation.

Appendix D. SCFE experimental results

Table 9-3. Wax compositions (mass fraction) of countercurrent CO_2 extraction runs.

Component	CO_2C1			CO_2C2			CO_2C3			CO_2C4		
	Feed	Extract	Raffinate	Feed	Extract	Raffinate	Feed	Extract	Raffinate	Feed	Extract	Raffinate
n-C_{11}	0.0032	0.0150	0	0.0006	0.0046	0	0.0008	0.0038	0	0	0	0
n-C_{12}	0.0076	0.0524	0	0.0056	0.0207	0	0.0058	0.0142	0	0.0061	0.0090	0
n-C_{13}	0.0193	0.1013	0.0053	0.0156	0.0532	0.0008	0.0165	0.0411	0	0.0184	0.0272	0
n-C_{14}	0.0423	0.1464	0.0263	0.0329	0.0983	0.0082	0.0345	0.0842	0.0014	0.0382	0.0569	0
n-C_{15}	0.0765	0.1724	0.0681	0.0618	0.1328	0.0356	0.0594	0.1318	0.0104	0.0676	0.1028	0.0009
n-C_{16}	0.1132	0.1632	0.1084	0.0965	0.1441	0.0820	0.0903	0.1533	0.0439	0.1027	0.1451	0.0074
n-C_{17}	0.1416	0.1325	0.1436	0.1229	0.1521	0.1215	0.1165	0.1549	0.0889	0.1290	0.1724	0.0406
n-C_{18}	0.1420	0.0945	0.1533	0.1349	0.1322	0.1367	0.1261	0.1349	0.1261	0.1353	0.1550	0.1029
n-C_{19}	0.1254	0.0570	0.1406	0.1261	0.0965	0.1377	0.1191	0.1058	0.1238	0.1313	0.1172	0.1588
n-C_{20}	0.1125	0.0342	0.1212	0.1072	0.0692	0.1224	0.1081	0.0760	0.1290	0.1104	0.0833	0.1583
n-C_{21}	0.0709	0.0154	0.0759	0.0860	0.0432	0.1021	0.0886	0.0444	0.1195	0.0848	0.0552	0.1460
n-C_{22}	0.0498	0.0082	0.0557	0.0672	0.0256	0.0815	0.0718	0.0263	0.1031	0.0613	0.0339	0.1224
n-C_{23}	0.0378	0.0043	0.0414	0.0492	0.0151	0.0606	0.0539	0.0153	0.0803	0.0442	0.0203	0.0930
n-C_{24}	0.0262	0.0021	0.0281	0.0365	0.0080	0.0444	0.0412	0.0083	0.0640	0.0312	0.0121	0.0682
n-C_{25}	0.0150	0.0011	0.0158	0.0258	0.0035	0.0308	0.0296	0.0038	0.0466	0.0200	0.0063	0.0468
n-C_{26}	0.0091	0	0.0091	0.0164	0.0009	0.0191	0.0192	0.0020	0.0311	0.0117	0.0032	0.0289
n-C_{27}	0.0046	0	0.0049	0.0089	0	0.0100	0.0107	0	0.0179	0.0054	0	0.0162
n-C_{28}	0.0029	0	0.0022	0.0043	0	0.0051	0.0053	0	0.0087	0.0021	0	0.0072
n-C_{29}	0	0	0	0.0015	0	0.0016	0.0023	0	0.0043	0.0004	0	0.0025
n-C_{30}	0	0	0	0	0	0	0.0003	0	0.0010	0	0	0

Table 9-3. -continued

Component	CO_2C5			CO_2C6			CO_2C7			CO_2C8		
	Feed	Extract	Raffinate	Feed	Extract	Raffinate	Feed	Extract	Raffinate	Feed	Extract	Raffinate
n-C_{11}	0	0	0	0.0003	0.0041	0	0.0002	0.0029	0	0	0	0
n-C_{12}	0.0039	0.0103	0.0031	0.0043	0.0240	0.0011	0.0024	0.0147	0	0.0021	0.0027	0
n-C_{13}	0.0132	0.0462	0.0112	0.0130	0.0576	0.0059	0.0072	0.0448	0.0004	0.0072	0.0124	0
n-C_{14}	0.0295	0.0993	0.0276	0.0276	0.0979	0.0164	0.0167	0.0760	0.0055	0.0168	0.0312	0.0005
n-C_{15}	0.0521	0.1413	0.0530	0.0469	0.1334	0.0331	0.0315	0.1036	0.0178	0.0323	0.0560	0.0015
n-C_{16}	0.0797	0.1621	0.0829	0.0719	0.1585	0.0580	0.0560	0.1266	0.0429	0.0560	0.0999	0.0058
n-C_{17}	0.1040	0.1555	0.1109	0.0928	0.1521	0.0822	0.0734	0.1285	0.0631	0.0768	0.1286	0.0179
n-C_{18}	0.1135	0.1301	0.1157	0.1088	0.1280	0.1044	0.0961	0.1308	0.0896	0.0964	0.1353	0.0504
n-C_{19}	0.1187	0.0960	0.1245	0.1132	0.0938	0.1155	0.1044	0.1104	0.1033	0.1059	0.1301	0.0752
n-C_{20}	0.1134	0.0667	0.1169	0.1133	0.0644	0.1216	0.1117	0.0924	0.1147	0.1152	0.1179	0.1092
n-C_{21}	0.0978	0.0410	0.0990	0.0990	0.0385	0.1082	0.1084	0.0642	0.1167	0.1069	0.0956	0.1216
n-C_{22}	0.0823	0.0248	0.0796	0.0880	0.0234	0.0981	0.1013	0.0433	0.1145	0.0992	0.0721	0.1354
n-C_{23}	0.0649	0.0145	0.0606	0.0720	0.0132	0.0813	0.0881	0.0282	0.0997	0.0854	0.0494	0.1293
n-C_{24}	0.0482	0.0076	0.0449	0.0549	0.0071	0.0625	0.0725	0.0179	0.0829	0.0707	0.0319	0.1165
n-C_{25}	0.0326	0.0035	0.0322	0.0372	0.0028	0.0461	0.0547	0.0096	0.0632	0.0540	0.0195	0.0940
n-C_{26}	0.0231	0.0012	0.0203	0.0271	0.0012	0.0312	0.0369	0.0042	0.0424	0.0363	0.0105	0.0667
n-C_{27}	0.0133	0	0.0113	0.0161	0	0.0186	0.0213	0.0020	0.0243	0.0210	0.0048	0.0404
n-C_{28}	0.0065	0	0.0053	0.0082	0	0.0095	0.0108	0	0.0121	0.0110	0.0022	0.0216
n-C_{29}	0.0026	0	0.0012	0.0039	0	0.0041	0.0046	0	0.0053	0.0047	0	0.0101
n-C_{30}	0.0006	0	0	0.0015	0	0.0021	0.0016	0	0.0016	0.0021	0	0.0040

Table 9-3. -concluded

Component	CO_2C9			CO_2C10			CO_2C11		
	Feed	Extract	Raffinate	Feed	Extract	Raffinate	Feed	Extract	Raffinate
n-C_{11}	0	0	0	0	0	0	0	0	0
n-C_{12}	0.0028	0.0081	0	0.0026	0.0068	0.0003	0.0025	0.0062	0
n-C_{13}	0.0095	0.0271	0	0.0080	0.0236	0.0006	0.0101	0.0210	0.0002
n-C_{14}	0.0180	0.0494	0.0013	0.0178	0.0523	0.0013	0.0175	0.0426	0.0003
n-C_{15}	0.0329	0.0913	0.0020	0.0328	0.0964	0.0022	0.0321	0.0784	0.0006
n-C_{16}	0.0537	0.1385	0.0087	0.0526	0.1359	0.0125	0.0527	0.1264	0.0023
n-C_{17}	0.0726	0.1480	0.0323	0.0720	0.1412	0.0380	0.0720	0.1433	0.0233
n-C_{18}	0.0919	0.1392	0.0646	0.0921	0.1387	0.0698	0.0931	0.1420	0.0588
n-C_{19}	0.1072	0.1223	0.0995	0.1080	0.1214	0.1010	0.1086	0.1286	0.0952
n-C_{20}	0.1142	0.0975	0.1251	0.1165	0.0983	0.1252	0.1166	0.1063	0.1249
n-C_{21}	0.1146	0.0708	0.1387	0.1159	0.0722	0.1392	0.1149	0.0793	0.1401
n-C_{22}	0.1031	0.0471	0.1331	0.1035	0.0485	0.1298	0.1035	0.0541	0.1376
n-C_{23}	0.0867	0.0290	0.1176	0.0868	0.0302	0.1136	0.0870	0.0342	0.1231
n-C_{24}	0.0685	0.0166	0.0958	0.0669	0.0176	0.0903	0.0688	0.0203	0.1022
n-C_{25}	0.0506	0.0087	0.0728	0.0506	0.0095	0.0704	0.0504	0.0096	0.0786
n-C_{26}	0.0334	0.0041	0.0491	0.0334	0.0047	0.0472	0.0333	0.0049	0.0529
n-C_{27}	0.0191	0.0017	0.0280	0.0191	0.0019	0.0271	0.0190	0.0021	0.0304
n-C_{28}	0.0100	0.0006	0.0148	0.0100	0.0008	0.0144	0.0092	0.0008	0.0154
n-C_{29}	0.0069	0	0.0105	0.0070	0	0.0105	0.0054	0	0.0091
n-C_{30}	0.0043	0	0.0060	0.0045	0	0.0066	0.0034	0	0.0051

Table 9-4. Wax compositions (mass fraction) of CO_2 extraction runs with reflux.

Component	CO_2R1			CO_2R2			CO_2R3			CO_2R4		
	Feed	Extract	Raffinate	Feed	Extract	Raffinate	Feed	Extract	Raffinate	Feed	Extract	Raffinate
n-C_{11}	0.0003	0.0014	0	0.0003	0.0020	0	0.0002	0.0018	0	0.0003	0.0016	0
n-C_{12}	0.0034	0.0112	0.0001	0.0030	0.0101	0	0.0029	0.0142	0	0.0026	0.0086	0
n-C_{13}	0.0102	0.0218	0.0002	0.0098	0.0299	0.0002	0.0090	0.0440	0.0002	0.0080	0.0264	0
n-C_{14}	0.0174	0.0469	0.0003	0.0181	0.0602	0.0004	0.0189	0.0932	0.0004	0.0173	0.0572	0
n-C_{15}	0.0320	0.0857	0.0007	0.0333	0.1113	0.0007	0.0343	0.1675	0.0011	0.0322	0.1064	0
n-C_{16}	0.0520	0.1338	0.0040	0.0543	0.1727	0.0039	0.0538	0.2355	0.0066	0.0533	0.1727	0.001
n-C_{17}	0.0714	0.1533	0.0237	0.0731	0.1891	0.0221	0.0717	0.2325	0.0281	0.0729	0.2241	0.007
n-C_{18}	0.0912	0.1479	0.0569	0.0928	0.1752	0.0550	0.0850	0.1497	0.0646	0.0890	0.2111	0.036
n-C_{19}	0.1071	0.1298	0.0925	0.1070	0.1382	0.0934	0.0993	0.0539	0.1058	0.1039	0.1386	0.089
n-C_{20}	0.1175	0.1041	0.1252	0.1132	0.0841	0.1259	0.1144	0.0077	0.1430	0.1150	0.0472	0.145
n-C_{21}	0.1149	0.0734	0.1390	0.1132	0.0260	0.1513	0.1187	0	0.1505	0.1125	0.0062	0.159
n-C_{22}	0.1041	0.0467	0.1379	0.1017	0.0014	0.1445	0.1044	0	0.1348	0.1025	0	0.147
n-C_{23}	0.0877	0.0262	0.1242	0.0869	0	0.1250	0.0901	0	0.1141	0.0897	0	0.129
n-C_{24}	0.0692	0.0123	0.1030	0.0692	0	0.0994	0.0712	0	0.0904	0.0716	0	0.103
n-C_{25}	0.0510	0.0042	0.0790	0.0513	0	0.0737	0.0523	0	0.0662	0.0534	0	0.076
n-C_{26}	0.0337	0.0011	0.0535	0.0339	0	0.0491	0.0345	0	0.0439	0.0355	0	0.051
n-C_{27}	0.0191	0.0002	0.0308	0.0195	0	0.0275	0.0198	0	0.0252	0.0203	0	0.029
n-C_{28}	0.0090	0	0.0153	0.0102	0	0.0146	0.0103	0	0.0132	0.0106	0	0.015
n-C_{29}	0.0054	0	0.0087	0.0059	0	0.0086	0.0060	0	0.0075	0.0062	0	0.009
n-C_{30}	0.0035	0	0.0050	0.0033	0	0.0048	0.0033	0	0.0042	0.0033	0	0.005

Table 9-4. – continued.

Component	CO_2R5			CO_2R6			CO_2R7			CO_2R8		
	Feed	Extract	Raffinate	Feed	Extract	Raffinate	Feed	Extract	Raffinate	Feed	Extract	Raffinate
n-C_{11}	0	0	0	0	0	0	0	0	0	0	0	0
n-C_{12}	0.0028	0.0107	0	0.0025	0.0116	0	0.003	0.0113	0	0.0025	0.007	0
n-C_{13}	0.0085	0.0332	0	0.0078	0.0351	0	0.008	0.0343	0	0.0082	0.023	0
n-C_{14}	0.0182	0.0729	0	0.0168	0.0771	0	0.018	0.0750	0	0.0167	0.046	0
n-C_{15}	0.0338	0.1359	0	0.0312	0.1445	0	0.032	0.1407	0	0.0307	0.086	0
n-C_{16}	0.0555	0.2164	0.0017	0.0525	0.2340	0.0025	0.054	0.2287	0.0023	0.0505	0.142	0
n-C_{17}	0.0741	0.2602	0.0103	0.0708	0.2823	0.0124	0.072	0.2759	0.0085	0.0699	0.194	0
n-C_{18}	0.0897	0.2004	0.0495	0.0837	0.1710	0.0567	0.083	0.1753	0.0475	0.0910	0.226	0.0152
n-C_{19}	0.1035	0.0637	0.1136	0.1037	0.0444	0.1193	0.102	0.0476	0.1119	0.1062	0.181	0.0646
n-C_{20}	0.1101	0.0065	0.1441	0.1165	0	0.1489	0.114	0.0113	0.1469	0.1173	0.075	0.1394
n-C_{21}	0.1142	0	0.1515	0.1178	0	0.1517	0.117	0	0.1532	0.1133	0.020	0.1662
n-C_{22}	0.1050	0	0.1410	0.1072	0	0.1375	0.108	0	0.1429	0.1070	0	0.1653
n-C_{23}	0.0891	0	0.1211	0.0904	0	0.1159	0.091	0	0.1220	0.0909	0	0.1420
n-C_{24}	0.0707	0	0.0964	0.0718	0	0.0922	0.074	0	0.0977	0.0722	0	0.1131
n-C_{25}	0.0525	0	0.0718	0.0537	0	0.0690	0.054	0	0.0721	0.0530	0	0.0832
n-C_{26}	0.0347	0	0.0466	0.0345	0	0.0435	0.035	0	0.0466	0.0350	0	0.0548
n-C_{27}	0.0200	0	0.0271	0.0198	0	0.0250	0.020	0	0.0267	0.0198	0	0.0313
n-C_{28}	0.0106	0	0.0145	0.0108	0	0.0140	0.010	0	0.0135	0.0099	0	0.0157
n-C_{29}	0.0047	0	0.0071	0.0055	0	0.0074	0.004	0	0.0057	0.0041	0	0.0062
n-C_{30}	0.0024	0	0.0037	0.0031	0	0.0040	0.002	0	0.0025	0.0018	0	0.0029

Table 9-4. – concluded.

Component	CO_2R9			CO_2R10			CO_2R11			CO_2R12		
	Feed	Extract	Raffinate	Feed	Extract	Raffinate	Feed	Extract	Raffinate	Feed	Extract	Raffinate
n-C_{11}	0	0	0	0	0	0	0	0	0	0	0	0
n-C_{12}	0.0027	0.0056	0	0.0025	0.0071	0	0.003	0.0064	0	0.0027	0.0058	0
n-C_{13}	0.0084	0.0165	0	0.0081	0.0217	0	0.008	0.0198	0	0.0081	0.0174	0
n-C_{14}	0.0171	0.0340	0	0.0173	0.0468	0	0.017	0.0417	0	0.0171	0.0368	0
n-C_{15}	0.0312	0.0643	0	0.0322	0.0876	0	0.031	0.0797	0	0.0309	0.0667	0
n-C_{16}	0.0511	0.1027	0	0.0533	0.1441	0	0.051	0.1300	0	0.0491	0.1050	0
n-C_{17}	0.0697	0.1384	0	0.0746	0.2015	0.0017	0.071	0.1804	0	0.0675	0.1409	0
n-C_{18}	0.0887	0.1700	0.0049	0.0935	0.2285	0.0144	0.089	0.2134	0.0062	0.0867	0.1761	0.0046
n-C_{19}	0.1057	0.1981	0.0085	0.1066	0.1771	0.0658	0.104	0.1976	0.0384	0.1014	0.1838	0.0210
n-C_{20}	0.1125	0.1665	0.0449	0.1128	0.0675	0.1362	0.113	0.1005	0.1146	0.1110	0.1351	0.0760
n-C_{21}	0.1076	0.0790	0.1269	0.1077	0.0180	0.1583	0.112	0.0305	0.1661	0.1101	0.0754	0.1365
n-C_{22}	0.1050	0.0250	0.1819	0.1037	0	0.1611	0.106	0	0.1756	0.1079	0.0371	0.1692
n-C_{23}	0.0918	0	0.1884	0.0895	0	0.1418	0.091	0	0.1530	0.0945	0.0157	0.1679
n-C_{24}	0.0748	0	0.1554	0.0718	0	0.1155	0.074	0	0.1239	0.0769	0.0042	0.1481
n-C_{25}	0.0563	0	0.1196	0.0536	0	0.0871	0.055	0	0.0934	0.0576	0	0.1154
n-C_{26}	0.0376	0	0.0809	0.0355	0	0.0581	0.037	0	0.0625	0.0386	0	0.0785
n-C_{27}	0.0216	0	0.0474	0.0207	0	0.0339	0.021	0	0.0363	0.0222	0	0.0459
n-C_{28}	0.0113	0	0.0250	0.0104	0	0.0165	0.011	0	0.0189	0.0113	0	0.0239
n-C_{29}	0.0050	0	0.0119	0.0043	0	0.0069	0.004	0	0.0077	0.0045	0	0.0091
n-C_{30}	0.0020	0	0.0042	0.0017	0	0.0027	0.002	0	0.0033	0.0020	0	0.0040

Table 9-5. Wax compositions (mass fraction) of ethane extraction runs.

Component	EC1			EC2			EC3			ER1		
	Feed	Extract	Raffinate	Feed	Extract	Raffinate	Feed	Extract	Raffinate	Feed	Extract	Raffinate
n-C_{11}	0	0	0	0	0	0	0	0	0	0	0	0
n-C_{12}	0.0031	0.0040	0	0.0028	0.0124	0.0016	0.0006	0.0015	0.0004	0	0	0
n-C_{13}	0.0081	0.0104	0	0.0077	0.035	0.0049	0.0013	0.0061	0.0004	0.0030	0.0056	0
n-C_{14}	0.0171	0.0220	0	0.0168	0.064	0.0120	0.0043	0.0185	0.0020	0.0076	0.0140	0
n-C_{15}	0.0308	0.0395	0.0002	0.0304	0.093	0.0242	0.0114	0.0430	0.0068	0.0153	0.0281	0
n-C_{16}	0.0496	0.0629	0.0020	0.0484	0.115	0.0417	0.0257	0.0728	0.0185	0.0278	0.0514	0
n-C_{17}	0.0696	0.0870	0.0086	0.0674	0.125	0.0618	0.0467	0.1018	0.0410	0.0464	0.0854	0.0010
n-C_{18}	0.0928	0.1110	0.0289	0.0909	0.126	0.0874	0.0719	0.1251	0.0657	0.0719	0.1274	0.0029
n-C_{19}	0.1053	0.1223	0.0459	0.1060	0.115	0.1061	0.0953	0.1328	0.0907	0.0965	0.1662	0.0106
n-C_{20}	0.1193	0.1272	0.0912	0.1238	0.103	0.1271	0.1172	0.1294	0.1179	0.1155	0.1648	0.0521
n-C_{21}	0.1156	0.1154	0.1159	0.1164	0.076	0.1200	0.1257	0.1140	0.1275	0.1257	0.1387	0.1078
n-C_{22}	0.1053	0.0961	0.1389	0.1057	0.054	0.1109	0.1232	0.0892	0.1292	0.1221	0.0986	0.1478
n-C_{23}	0.0885	0.0731	0.1425	0.0891	0.035	0.0936	0.1106	0.0652	0.1168	0.1074	0.0632	0.1623
n-C_{24}	0.0720	0.0538	0.1349	0.0719	0.023	0.0761	0.0932	0.0441	0.1002	0.0907	0.0355	0.1618
n-C_{25}	0.0521	0.0351	0.1117	0.0522	0.012	0.0561	0.0710	0.0288	0.0743	0.0698	0.0158	0.1372
n-C_{26}	0.0343	0.0209	0.0811	0.0343	0.006	0.0372	0.0454	0.0145	0.0491	0.0479	0.0053	0.1005
n-C_{27}	0.0194	0.0105	0.0507	0.0195	0.003	0.0210	0.0306	0.0090	0.0298	0.0275	0	0.0613
n-C_{28}	0.0104	0.0054	0.0279	0.0102	0.002	0.0110	0.0137	0.0027	0.0155	0.0143	0	0.0316
n-C_{29}	0.0047	0.0023	0.0135	0.0046	0.001	0.0049	0.0073	0.0012	0.0088	0.0074	0	0.0165
n-C_{30}	0.0021	0.0009	0.0061	0.0020	0	0.0022	0.0030	0.0003	0.0033	0.0031	0	0.0067
n-C_{31}	0	0	0	0	0	0	0.0013	0	0.0014			
n-C_{32}	0	0	0	0	0	0	0.0006	0	0.0007			

Table 9-5. – continued.

Component	ER2			ER3			ER4			ER5		
	Feed	Extract	Raffinate	Feed	Extract	Raffinate	Feed	Extract	Raffinate	Feed	Extract	Raffinate
n-C_{11}	0	0	0	0	0	0	0	0	0	0	0	0
n-C_{12}	0.0002	0.0010	0	0.0004	0.0019	0	0.0002	0.0010	0	0.0004	0.0019	0
n-C_{13}	0.0027	0.0068	0	0.0025	0.0058	0	0.0026	0.0058	0	0.0027	0.0068	0
n-C_{14}	0.0070	0.0176	0	0.0070	0.0166	0	0.0068	0.0156	0	0.0068	0.0166	0
n-C_{15}	0.0142	0.0362	0	0.0144	0.0352	0	0.0144	0.0352	0	0.0143	0.0362	0
n-C_{16}	0.0270	0.0707	0.0010	0.0273	0.0687	0.0010	0.0275	0.0707	0	0.0268	0.0707	0
n-C_{17}	0.0456	0.1174	0.0038	0.0460	0.1154	0.0029	0.0467	0.1184	0.0029	0.0460	0.1203	0.0029
n-C_{18}	0.0687	0.1527	0.0192	0.0688	0.1516	0.0163	0.0698	0.1527	0.0182	0.0694	0.1576	0.0183
n-C_{19}	0.0928	0.1615	0.0522	0.0927	0.1605	0.0493	0.0935	0.1635	0.0492	0.0939	0.1654	0.0531
n-C_{20}	0.1131	0.1495	0.0905	0.1143	0.1565	0.0885	0.1132	0.1515	0.0874	0.1147	0.1515	0.0943
n-C_{21}	0.1225	0.1203	0.1225	0.1220	0.1193	0.1215	0.1226	0.1213	0.1223	0.1248	0.1213	0.1293
n-C_{22}	0.1216	0.0836	0.1433	0.1209	0.0846	0.1422	0.1213	0.0846	0.1440	0.1232	0.0825	0.1492
n-C_{23}	0.1101	0.0494	0.1456	0.1100	0.0504	0.1475	0.1099	0.0494	0.1483	0.1113	0.0463	0.1515
n-C_{24}	0.0935	0.0239	0.1350	0.0931	0.0239	0.1369	0.0927	0.0218	0.1377	0.0942	0.0197	0.1400
n-C_{25}	0.0736	0.0063	0.1151	0.0732	0.0063	0.1170	0.0731	0.0053	0.1179	0.0723	0.0031	0.1130
n-C_{26}	0.0535	0.0032	0.0886	0.0537	0.0032	0.0916	0.0535	0.0032	0.0915	0.0505	0	0.0814
n-C_{27}	0.0297	0	0.0480	0.0295	0	0.0490	0.0297	0	0.0500	0.0286	0	0.0449
n-C_{28}	0.0143	0	0.0212	0.0141	0	0.0211	0.0140	0	0.0211	0.0146	0	0.0222
n-C_{29}	0.0066	0	0.0086	0.0065	0	0.0086	0.0068	0	0.0096	0.0038	0	0
n-C_{30}	0.0034	0	0.0055	0.0037	0	0.0065	0.0017	0	0	0.0017	0	0

Table 9-5. – concluded.

Component	ER6			ER7		
	Feed	Extract	Raffinate	Feed	Extract	Raffinate
n-C_{11}	0	0	0	0	0	0
n-C_{12}	0	0	0	0	0	0
n-C_{13}	0.0014	0	0	0.0021	0.0039	0
n-C_{14}	0.0050	0.0068	0	0.0062	0.0147	0
n-C_{15}	0.0119	0.0255	0	0.0135	0.0363	0
n-C_{16}	0.0241	0.0610	0	0.0265	0.0778	0
n-C_{17}	0.0435	0.1155	0.0029	0.0448	0.1345	0
n-C_{18}	0.0674	0.1578	0.0182	0.0680	0.1848	0.0096
n-C_{19}	0.0930	0.1716	0.0521	0.0926	0.1919	0.0436
n-C_{20}	0.1149	0.1617	0.0923	0.1136	0.1660	0.0877
n-C_{21}	0.1253	0.1295	0.1262	0.1240	0.1165	0.1286
n-C_{22}	0.1243	0.0898	0.1460	0.1226	0.0572	0.1554
n-C_{23}	0.1128	0.0505	0.1493	0.1119	0.0144	0.1618
n-C_{24}	0.0952	0.0218	0.1367	0.0953	0.0021	0.1443
n-C_{25}	0.0733	0.0042	0.1108	0.0734	0	0.1112
n-C_{26}	0.0519	0.0032	0.0802	0.0509	0	0.0774
n-C_{27}	0.0294	0.0011	0.0448	0.0289	0	0.0429
n-C_{28}	0.0153	0	0.0232	0.0151	0	0.0223
n-C_{29}	0.0077	0	0.0118	0.0075	0	0.0108
n-C_{30}	0.0035	0	0.0054	0.0031	0	0.0044

Appendix E. Petroleum wax deoiling experimental results

Table 9-6. Run EMS-SPD

Carbon no.	Feed		Bottoms		Dist.	
	n	iso	n	iso	n	iso
14	5E-05	5E-05			0.001	0.001
15	0.0002	5E-05			0.003	0.001
16	0.0003	0.0001			0.006	0.002
17	0.0011	0.0002			0.011	0.004
18	0.0014	0.0002			0.017	0.004
19	0.0023	0.0003			0.024	0.005
20	0.0031	0.0003			0.03	0.006
21	0.0040	0.0004			0.037	0.008
22	0.0055	0.0005	0.001	0	0.047	0.01
23	0.0069	0.0013	0.001	0	0.054	0.015
24	0.008	0.0024	0.002	0.001	0.057	0.018
25	0.01	0.0042	0.004	0.002	0.059	0.024
26	0.0139	0.0076	0.008	0.004	0.061	0.034
27	0.0179	0.0135	0.013	0.01	0.057	0.038
28	0.0223	0.0216	0.019	0.02	0.052	0.04
29	0.029	0.0304	0.027	0.03	0.046	0.038
30	0.0321	0.0401	0.032	0.041	0.034	0.034
31	0.0354	0.0471	0.036	0.048	0.025	0.023
32	0.0353	0.0504	0.039	0.056	0.016	0.017
33	0.0335	0.0553	0.037	0.059	0.01	0.01
34	0.029	0.054	0.032	0.06	0.005	0.005
35	0.0238	0.051	0.026	0.057	0.003	0.002
36	0.0194	0.0462	0.023	0.052	0.002	
37	0.017	0.0424	0.019	0.047	0.001	
38	0.0132	0.0353	0.015	0.04		
39	0.0099	0.0278	0.011	0.032		
40	0.0071	0.0213	0.008	0.023		
41	0.0052	0.0175	0.006	0.018		
42	0.0038	0.0151	0.004	0.016		
43	0.0028	0.0081	0.003	0.007		
44	0.0019	0.0053	0.002	0.004		
45	0.0009	0.0024	0.001	0.002		
46	0.0009	0.001	0.001	0		
Total	0.397	0.603	0.37	0.629	0.658	0.339

Table 9-7. Run EMS R1C (SCFE extraction using CO_2).

Carbon no.	Feed		Bottoms		Dist.	
	n	iso	n	iso	n	iso
14	0.0001	0.0001			0.003	0.003
15	0.0002	0.0002			0.006	0.004
16	0.0004	0.0002			0.011	0.006
17	0.0012	0.0003			0.017	0.008
18	0.0015	0.0004			0.025	0.009
19	0.0024	0.0004			0.034	0.009
20	0.0032	0.0004			0.042	0.01
21	0.0040	0.0004			0.048	0.01
22	0.0052	0.0005	0.001	0	0.055	0.013
23	0.0072	0.0016	0.003	0.001	0.058	0.016
24	0.0087	0.0027	0.005	0.002	0.058	0.019
25	0.0105	0.0044	0.007	0.003	0.055	0.024
26	0.0144	0.008	0.011	0.006	0.057	0.03
27	0.0181	0.0145	0.015	0.013	0.055	0.037
28	0.0222	0.0217	0.02	0.021	0.05	0.038
29	0.0291	0.0302	0.028	0.03	0.042	0.034
30	0.0318	0.0399	0.032	0.041	0.026	0.026
31	0.0347	0.0472	0.035	0.048	0.016	0.015
32	0.0325	0.0496	0.033	0.054	0.009	0.008
33	0.0323	0.0571	0.034	0.062	0.004	0.003
34	0.0292	0.0536	0.032	0.058	0.001	0
35	0.0239	0.0508	0.026	0.055		
36	0.0182	0.0473	0.02	0.053		
37	0.0168	0.0403	0.018	0.041		
38	0.012	0.0359	0.012	0.04		
39	0.0096	0.0282	0.01	0.032		
40	0.0067	0.0229	0.007	0.026		
41	0.0048	0.0191	0.005	0.021		
42	0.0038	0.0144	0.004	0.014		
43	0.0024	0.0078	0.002	0.006		
44	0.0015	0.0058	0.001	0.005		
45	0.001	0.0029	0.001	0.003		
46	0.001	0.0015	0.001	0.001		
Total	0.39	0.61	0.363	0.636	0.673	0.327

Table 9-8. Run EMS R1E (SCFE extraction using ethane).

Carbon no.	Feed		Bottoms		Dist.	
	n	iso	n	iso	n	iso
14	0.0002	0			0.001	0
15	0.0002	0			0.001	0
16	0.0003	0			0.002	0
17	0.001	0			0.003	0
18	0.0013	0			0.005	0
19	0.0022	0			0.008	0
20	0.003	0.0002			0.01	0.001
21	0.004	0.0002			0.013	0.001
22	0.0052	0.0002			0.018	0.001
23	0.007	0.0008			0.023	0.002
24	0.0084	0.0015			0.029	0.003
25	0.0103	0.0029			0.035	0.006
26	0.0142	0.0059	0.001	0.001	0.045	0.01
27	0.0178	0.0108	0.003	0.004	0.051	0.016
28	0.0225	0.0179	0.009	0.009	0.055	0.028
29	0.0292	0.0281	0.017	0.021	0.058	0.038
30	0.0323	0.0383	0.024	0.03	0.052	0.047
31	0.0354	0.0475	0.03	0.042	0.046	0.055
32	0.0347	0.0525	0.036	0.053	0.034	0.063
33	0.0333	0.0586	0.037	0.062	0.026	0.056
34	0.0288	0.0556	0.034	0.062	0.016	0.046
35	0.0235	0.0543	0.029	0.067	0.009	0.036
36	0.0194	0.0477	0.028	0.06	0.004	0.025
37	0.0167	0.0428	0.023	0.055	0.001	0.014
38	0.0117	0.0365	0.015	0.052	0	0.006
39	0.0095	0.0283	0.013	0.042	0	0.001
40	0.007	0.0228	0.01	0.034		
41	0.0049	0.0182	0.007	0.025		
42	0.0037	0.0153	0.005	0.021		
43	0.0025	0.0099	0.003	0.014		
44	0.0017	0.0066	0.002	0.009		
45	0.0008	0.0029	0.001	0.004		
46	0.0008	0.0013	0.001	0.001		
Total	0.393	0.607	0.328	0.672	0.545	0.455

Table 9-9. Run EMS R2E (SCFE extraction using ethane).

Carbon no.	Feed		Bottoms		Dist.	
	n	iso	n	iso	n	iso
14	0.0001	0			0.001	0
15	0.0001	0			0.001	0
16	0.0003	0			0.002	0
17	0.0009	0.0001			0.003	0.001
18	0.0011	0.0001			0.005	0.001
19	0.002	0.0001			0.008	0.001
20	0.0029	0.0003			0.011	0.002
21	0.0039	0.0004			0.015	0.003
22	0.0052	0.0004			0.021	0.003
23	0.0071	0.0013			0.028	0.006
24	0.0085	0.0023			0.035	0.01
25	0.0104	0.0046			0.042	0.02
26	0.0144	0.0084	0.002	0.001	0.052	0.031
27	0.0182	0.0138	0.005	0.004	0.057	0.041
28	0.0224	0.0214	0.01	0.012	0.06	0.05
29	0.0293	0.0305	0.018	0.022	0.063	0.057
30	0.032	0.0396	0.024	0.033	0.055	0.057
31	0.0351	0.0465	0.03	0.04	0.046	0.05
32	0.0345	0.0496	0.035	0.053	0.035	0.042
33	0.0328	0.0543	0.036	0.06	0.023	0.0
34	0.0282	0.0533	0.033	0.066	0.011	0.014
35	0.0229	0.0493	0.028	0.063	0.004	0.003
36	0.0188	0.0442	0.026	0.057	0.001	0
37	0.0163	0.0412	0.021	0.053		
38	0.0117	0.0357	0.014	0.049		
39	0.0095	0.0291	0.012	0.042		
40	0.0068	0.024	0.009	0.035		
41	0.0047	0.0203	0.006	0.029		
42	0.0039	0.0169	0.005	0.024		
43	0.0026	0.0106	0.003	0.015		
44	0.0017	0.0068	0.002	0.009		
45	0.0009	0.0041	0.001	0.007		
46	0.0009	0.0017	0.001	0.002		
Total	0.39	0.61	0.321	0.679	0.58	0.42

Table 9-10. Run EMS R3E (SCFE extraction using ethane).

Carbon no.	Feed		Bottoms		Dist.	
	n	iso	n	iso	n	iso
14	0.0001	0			0.001	0
15	0.0001	0			0.001	0
16	0.0003	0			0.002	0
17	0.0009	0.0001			0.003	0.001
18	0.0011	0.0001			0.005	0.001
19	0.002	0.0001			0.008	0.001
20	0.0029	0.0003			0.011	0.002
21	0.0039	0.0004			0.015	0.003
22	0.0052	0.0004			0.021	0.003
23	0.0071	0.0013			0.028	0.006
24	0.0085	0.0023			0.035	0.01
25	0.0104	0.0046			0.042	0.02
26	0.0144	0.0084	0.002	0.001	0.052	0.031
27	0.0182	0.0138	0.005	0.004	0.057	0.041
28	0.0224	0.0214	0.01	0.012	0.06	0.05
29	0.0293	0.0305	0.018	0.022	0.063	0.057
30	0.032	0.0396	0.024	0.033	0.055	0.057
31	0.0351	0.0465	0.03	0.04	0.046	0.05
32	0.0345	0.0496	0.035	0.053	0.035	0.042
33	0.0328	0.0543	0.036	0.06	0.023	0.0
34	0.0282	0.0533	0.033	0.066	0.011	0.014
35	0.0229	0.0493	0.028	0.063	0.004	0.003
36	0.0188	0.0442	0.026	0.057	0.001	0
37	0.0163	0.0412	0.021	0.053		
38	0.0117	0.0357	0.014	0.049		
39	0.0095	0.0291	0.012	0.042		
40	0.0068	0.024	0.009	0.035		
41	0.0047	0.0203	0.006	0.029		
42	0.0039	0.0169	0.005	0.024		
43	0.0026	0.0106	0.003	0.015		
44	0.0017	0.0068	0.002	0.009		
45	0.0009	0.0041	0.001	0.007		
46	0.0009	0.0017	0.001	0.002		
Total	0.39	0.61	0.321	0.679	0.58	0.42

Table 9-11. Run SMS R1C (SCFE extraction using CO_2).

Carbon no.	Feed		Bottoms		Dist.	
	n	iso	n	iso	n	iso
14						
15	4E-05	0			0.001	0.001
16	4E-05	4E-05			0.002	0.001
17	8E-05	4E-05			0.003	0.001
18	0.0001	4E-05			0.005	0.002
19	0.0002	8E-05			0.007	0.003
20	0.0003	0.0001			0.01	0.004
21	0.0004	0.0002			0.013	0.006
22	0.001	0.0002			0.018	0.008
23	0.0012	0.0003			0.023	0.009
24	0.0019	0.0003			0.031	0.015
25	0.0027	0.0011			0.037	0.024
26	0.0039	0.0024	0.001	0.001	0.047	0.035
27	0.0057	0.0042	0.002	0.003	0.053	0.047
28	0.0074	0.0056	0.004	0.004	0.054	0.051
29	0.0103	0.0092	0.007	0.007	0.052	0.1
30	0.0116	0.0131	0.009	0.0	0.041	0.049
31	0.0131	0.0173	0.011	0.014	0.033	0.048
32	0.0133	0.0173	0.012	0.014	0.024	0.039
33	0.0153	0.0279	0.015	0.029	0.021	0.035
34	0.0162	0.0355	0.016	0.036	0.015	0.027
35	0.0183	0.0437	0.02	0.048	0.009	0.02
36	0.021	0.0579	0.022	0.063	0.003	0.012
37	0.0236	0.0658	0.026	0.07	0.001	0.003
38	0.0231	0.074	0.024	0.082	0	0.001
39	0.0235	0.0686	0.026	0.078	0	0
40	0.0211	0.0687	0.024	0.074	0	0
41	0.0177	0.0591	0.02	0.062	0	0
42	0.0163	0.0534	0.018	0.056	0	0
43	0.0097	0.038	0.009	0.039	0	0
44	0.0072	0.0267	0.008	0.022	0	0
45	0.0043	0.0108	0.005	0.005	0	0
46	0.0024	0.004	0.003	0.001	0	
47	0.001	0	0.001			
Total	0.2939	0.7054	0.282	0.718	0.504	0.494

Table 9-12. Run SMS R1E (SCFE extraction using ethane).

Carbon no.	Feed		Bottoms		Dist.	
	n	iso	n	iso	n	iso
17	0.0001				0.001	
18	0.0001				0.001	
19	0.0001				0.001	
20	0.0004				0.003	
21	0.0006				0.004	
22	0.001	7E-05	0.001		0.006	0.001
23	0.001	0.0001	0.001		0.009	0.002
24	0.002	0.0003	0.002		0.014	0.005
25	0.003	0.001	0.002	0.001	0.02	0.011
26	0.004	0.002	0.004	0.002	0.029	0.02
27	0.006	0.003	0.005	0.003	0.036	0.033
28	0.007	0.004	0.007	0.005	0.045	0.04
29	0.01	0.008	0.01	0.009	0.05	0.049
30	0.011	0.013	0.011	0.0	0.047	0.1
31	0.013	0.018	0.013	0.017	0.045	0.054
32	0.013	0.018	0.014	0.021	0.037	0.056
33	0.015	0.026	0.015	0.027	0.035	0.054
34	0.016	0.035	0.016	0.035	0.028	0.05
35	0.017	0.041	0.017	0.043	0.022	0.046
36	0.021	0.056	0.021	0.056	0.014	0.032
37	0.023	0.066	0.022	0.064	0.007	0.023
38	0.024	0.072	0.019	0.075	0.003	0.007
39	0.023	0.065	0.021	0.072	0.001	0.002
40	0.02	0.069	0.02	0.067	0	0
41	0.017	0.061	0.017	0.061	0	0
42	0.016	0.055	0.015	0.055	0	0
43	0.011	0.04	0.01	0.042	0	0
44	0.007	0.033	0.007	0.032	0	0
45	0.004	0.017	0.004	0.017	0	0
46	0.002	0.007	0.002	0.007	0	0
47	0.001		0.001	0	0	0
Total	0.2884	0.7106	0.276	0.722	0.458	0.54

Table 9-13. Run SMS R2E (SCFE extraction using ethane).

Carbon no.	Feed		Bottoms		Dist.	
	n	iso	n	iso	n	iso
17	0	0				
18	0	0				
19	0.0004	0			0.001	
20	0.0004	0			0.001	
21	0.0008	0			0.002	
22	0.0012	0			0.003	
23	0.002	0.0004			0.005	0.001
24	0.0032	0.0008			0.008	0.002
25	0.0045	0.0024			0.011	0.006
26	0.0069	0.0053			0.017	0.013
27	0.0093	0.0093			0.023	0.023
28	0.0126	0.0122			0.031	0.03
29	0.0168	0.0162	0.001		0.04	0.04
30	0.0176	0.0201	0.001	0.0	0.042	0.0
31	0.0188	0.0239	0.003	0.004	0.042	0.053
32	0.0182	0.0275	0.006	0.01	0.036	0.053
33	0.0196	0.0324	0.009	0.017	0.035	0.055
34	0.0191	0.038	0.011	0.027	0.031	0.054
35	0.0191	0.0467	0.015	0.037	0.025	0.061
36	0.0206	0.0538	0.021	0.055	0.02	0.052
37	0.0208	0.0594	0.024	0.07	0.016	0.044
38	0.0175	0.0629	0.022	0.086	0.011	0.029
39	0.0175	0.0584	0.026	0.086	0.005	0.018
40	0.0163	0.0535	0.026	0.086	0.002	0.006
41	0.0135	0.0466	0.022	0.077	0.001	0.002
42	0.0119	0.044	0.02	0.074	0	0
43	0.0059	0.0321	0.01	0.054	0	0
44	0.0053	0.025	0.009	0.042	0	0
45	0.0024	0.0143	0.004	0.024	0	0
46	0.0018	0.0053	0.003	0.009	0	0
47	0.0006	0.0012	0.001	0.002	0	0
Total	0.3046	0.6916	0.233	0.759	0.408	0.59

Table 9-14. Run SMS R3E (SCFE extraction using ethane).

Carbon no.	Feed		Bottoms		Dist.	
	n	iso	n	iso	n	iso
17	0	0				
18	8E-05	0			0.001	
19	8E-05	0			0.001	
20	0.0002	0			0.002	
21	0.0002	0			0.003	
22	0.0008	8E-05			0.004	0.001
23	0.001	0.0002			0.007	0.002
24	0.0019	0.0003			0.011	0.004
25	0.0028	0.0011			0.016	0.008
26	0.0038	0.0023			0.023	0.016
27	0.0056	0.0039			0.033	0.03
28	0.0073	0.0053	0.001		0.043	0.042
29	0.0099	0.0085	0.002	0.001	0.052	0.052
30	0.0112	0.0127	0.004	0.0	0.051	0.1
31	0.0128	0.0155	0.006	0.006	0.048	0.05
32	0.0137	0.0191	0.009	0.013	0.043	0.059
33	0.0151	0.0263	0.011	0.021	0.038	0.057
34	0.0163	0.0362	0.014	0.032	0.031	0.066
35	0.0175	0.0416	0.017	0.041	0.024	0.049
36	0.021	0.0556	0.022	0.059	0.015	0.035
37	0.0226	0.065	0.025	0.072	0.007	0.021
38	0.0214	0.0727	0.022	0.086	0.002	0.006
39	0.0221	0.0679	0.025	0.084	0.001	0
40	0.0201	0.0686	0.024	0.081	0	0
41	0.0169	0.0608	0.02	0.072	0	0
42	0.016	0.0629	0.019	0.084	0	0
43	0.0106	0.039	0.012	0.045	0	0
44	0.0069	0.0329	0.008	0.039	0	0
45	0.0037	0.0169	0.004	0.02	0	0
46	0.0023	0.0073	0.003	0.009	0	0
47	0.0009	0	0.001	0	0	0
Total	0.2848	0.7227	0.248	0.769	0.456	0.555

Table 9-15. Run PMR R1C (SCFE extraction using CO_2).

Carbon no.	Feed		Bottoms		Dist.	
	n	iso	n	iso	n	iso
16	5E-05	0			0.001	
17	5E-05	0			0.001	
18	5E-05	0			0.001	
19	0.0002	0			0.003	
20	0.0003	0			0.006	
21	0.0006	5E-05			0.011	0.001
22	0.001	0.0001			0.018	0.002
23	0.0014	0.0003			0.027	0.005
24	0.0031	0.0005	0.001		0.041	0.009
25	0.0043	0.0008	0.002		0.046	0.016
26	0.0056	0.0031	0.003	0.002	0.053	0.022
27	0.0061	0.0043	0.004	0.003	0.043	0.028
28	0.008	0.0076	0.006	0.006	0.043	0.037
29	0.0132	0.0191	0.011	0.017	0.052	0.056
30	0.0245	0.0373	0.022	0.0	0.069	0.1
31	0.039	0.0526	0.037	0.051	0.074	0.081
32	0.0413	0.0627	0.041	0.063	0.046	0.057
33	0.0458	0.0592	0.047	0.061	0.025	0.027
34	0.0364	0.0678	0.038	0.071	0.007	0.01
35	0.0351	0.0588	0.037	0.062	0.002	0.002
36	0.0294	0.0568	0.031	0.06		
37	0.0256	0.0511	0.027	0.054		
38	0.018	0.0483	0.019	0.051		
39	0.017	0.0379	0.018	0.04		
40	0.0123	0.0284	0.013	0.03		
41	0.0085	0.0152	0.009	0.016		
42	0.0047	0.0038	0.005	0.004		
43	0.0019	0	0.002	0		
44	0.0009	0	0.001	0		
45						
Total	0.3843	0.6157	0.374	0.626	0.569	0.432

Table 9-16. Run PMR R1E (SCFE extraction using ethane).

Carbon no.	Feed		Bottoms		Dist.	
	n	iso	n	iso	n	iso
16						
17						
18						
19						
20	0.0003	0			0.001	
21	0.0006	0			0.002	
22	0.0014	0			0.005	
23	0.002	0.0003			0.007	0.001
24	0.004	0.0008			0.014	0.003
25	0.0051	0.0023			0.018	0.008
26	0.0068	0.0025			0.024	0.009
27	0.0072	0.0037	0.001		0.023	0.013
28	0.0091	0.0076	0.002	0.002	0.027	0.022
29	0.0143	0.0173	0.005	0.008	0.038	0.041
30	0.0266	0.0351	0.013	0.0	0.061	0.1
31	0.0407	0.0531	0.026	0.039	0.078	0.089
32	0.041	0.0582	0.032	0.05	0.064	0.079
33	0.0437	0.0607	0.04	0.059	0.053	0.065
34	0.0369	0.0776	0.038	0.088	0.034	0.051
35	0.0338	0.0613	0.038	0.074	0.023	0.029
36	0.0284	0.0543	0.034	0.069	0.014	0.017
37	0.0247	0.0479	0.032	0.064	0.006	0.007
38	0.0178	0.0465	0.024	0.064	0.002	0.002
39	0.0161	0.0388	0.022	0.054	0.001	0
40	0.0108	0.0294	0.015	0.041		
41	0.0072	0.0194	0.01	0.027		
42	0.0043	0.0115	0.006	0.016		
43	0.0014	0.0022	0.002	0.003		
44	0.0007	0.0014	0.001	0.002		
45						
Total	0.3845	0.6319	0.341	0.681	0.495	0.507

Table 9-17. Run PMR R2E (SCFE extraction using ethane).

Carbon no.	Feed		Bottoms		Dist.	
	n	iso	n	iso	n	iso
16						
17						
18						
19	0.0002	0				
20	0.0003	0			0.001	
21	0.0007	0			0.002	
22	0.001	0.0002			0.004	
23	0.0016	0.0005			0.006	0.001
24	0.0029	0.0008			0.01	0.003
25	0.0038	0.0013			0.018	0.005
26	0.0049	0.002			0.023	0.008
27	0.0051	0.0043	0.001	0.002	0.03	0.012
28	0.0063	0.0066	0.002	0.003	0.026	0.016
29	0.0114	0.0156	0.006	0.01	0.028	0.025
30	0.0227	0.0328	0.015	0.0	0.039	0.044
31	0.0373	0.05	0.029	0.042	0.062	0.1
32	0.0401	0.0588	0.035	0.055	0.08	0.091
33	0.0436	0.0625	0.042	0.062	0.066	0.078
34	0.037	0.0641	0.038	0.069	0.052	0.065
35	0.0339	0.0645	0.037	0.073	0.032	0.039
36	0.0297	0.0584	0.034	0.068	0.018	0.021
37	0.0263	0.053	0.031	0.063	0.008	0.009
38	0.0192	0.051	0.023	0.061	0.002	0.002
39	0.0176	0.0427	0.021	0.051		
40	0.0125	0.031	0.015	0.037		
41	0.0084	0.0184	0.01	0.022		
42	0.005	0.005	0.006	0.006		
43	0.0017	0.0008	0.002	0.001		
44	0.0008	0	0.001	0		
45						
Total	0.374	0.6242	0.348	0.65	0.507	0.492

Table 9-18. Run PMR R3E (SCFE extraction using ethane).

Carbon no.	Feed		Bottoms		Dist.	
	n	iso	n	iso	n	iso
16						
17						
18						
19						
20	0.0002	0			0.001	
21	0.0007	0.0002			0.003	0.001
22	0.0011	0.0002			0.005	0.001
23	0.0018	0.0005			0.008	0.002
24	0.0032	0.0009			0.014	0.004
25	0.0043	0.0016			0.019	0.007
26	0.0064	0.0025	0.001		0.025	0.011
27	0.0067	0.0042	0.002	0.001	0.023	0.015
28	0.009	0.0077	0.004	0.003	0.026	0.024
29	0.0143	0.018	0.008	0.011	0.036	0.042
30	0.027	0.0367	0.018	0.0	0.058	0.1
31	0.0417	0.0537	0.032	0.044	0.075	0.087
32	0.0421	0.0593	0.036	0.053	0.063	0.081
33	0.0447	0.0617	0.042	0.061	0.054	0.064
34	0.0366	0.0623	0.038	0.067	0.032	0.046
35	0.0328	0.0625	0.036	0.072	0.022	0.03
36	0.0287	0.0552	0.033	0.066	0.014	0.018
37	0.0246	0.0475	0.03	0.059	0.006	0.008
38	0.0167	0.0446	0.021	0.057	0.002	0.002
39	0.0149	0.0372	0.019	0.048	0.001	0
40	0.0101	0.0294	0.013	0.038		
41	0.007	0.0186	0.009	0.024		
42	0.0039	0.0108	0.005	0.014		
43	0.0015	0.0031	0.002	0.004		
44	0.0008	0.0015	0.001	0.002		
45						
Total	0.381	0.6198	0.350	0.651	0.487	0.513

Appendix F. Simulations results used in CHAPTER 7.

F.1. Wax crystalliser simulations

Table 9-19. Stage profiles for wax crystalliser simulations.

Stage number	Temperature °C	Solid phase kg/h	Liquid phase kg/h	Heating/cooling duty[#] kW
		Cryst 5		
1	22.1	11950	13008	867
2	29.4	12642	14450	919
3 (Feed)	32.9	21883	15142	1558
4	36.3	22675	16050	1616
5	40.4	5833	16842	458
		Cryst 6		
1	22.1	4265	6251	315
2	27.9	4495	6766	332
3 (Feed)	31.0	13358	6995	944
4	34.9	13617	7527	963
5	37.0	13925	7784	985
6	40.4	5833	8096	429
		Cryst 7		
1	22.1	3123	5250	233
2	27.3	3252	5623	243
3	29.3	3342	5752	249
4 (Feed)	31.0	12150	5842	856
5	35.0	12375	6320	874
6	37.1	12633	6542	892
7	40.4	5833	6798	425

[#] The heating and cooling duties are approximately equal on each stage.

F.2. SPD simulations

Table 9-20. Stage profiles for SPD simulations. All SPD runs were done at a constant absolute pressure of 40 Pa.

Stage number	Temperature °C	Liquid flow kg/h	Vapour flow kg/h	Heating duty kW	Cooling duty kW
		SPD 4			
1	116.0	4055	5999	791	777
2 (Feed)	132.3	13017	6554	893	848
3	143.3	13408	7181	940	930
4	156.7	5833	7573	778	980
		SPD 5			
1	117.3	676	3075	401	398
2 (Feed)	128.6	9400	3177	429	411
3	139.9	9542	3567	466	462
4	145.9	9708	3712	485	481
5	156.4	5833	3871	398	501
		SPD 6			
1 (Feed)	124.9	8642	2500	332	324
2	135.9	8742	2811	366	364
3	139.9	8800	2905	378	376
4	142.8	8858	2962	385	383
5	146.5	8958	3021	394	391
6	155.7	5833	3124	321	404

F.3. SCFE simulations

Table 9-21. Stream data for simulation PFD1-30.

Stream no.	1	2	3	4	5	6	7
T (°C)	60	60	70	43.6	56	56	70
P (barA)	1	99	99	57	55.4	55	99
Solvent flow (ton/h)	0	0	172.6	172.6	172.6	11.03	10.11
Wax flow (ton/h)	8.33	8.33	29.5	29.5	29.5	30	27.5
Stream no.	8	9	10	11	12	13	14
T (°C)	56	56	56	70	28.9	55.4	237.8
P (barA)	55	55	55	99	1	1	55
Solvent flow (ton/h)	0.919	162.0	165.8	2.94	2.94	0.894	3.834
Wax flow (ton/h)	2.5	0.049	0.049	5.83	0	0	0
Stream no.	15	16	17	18	19	20	21
T (°C)	56	28	39.5	70	60	60	28
P (barA)	55	55	99	99	1	1	55
Solvent flow (ton/h)	3.834	165.78	165.78	165.784	0.008	0.016	0.025
Wax flow (ton/h)	0	0.05	0.05	0.049	2.5	5.83	0

Table 9-22. Stream data for simulation PFD2-30.

Stream no.	1	2	3	4	5	6	7
T (°C)	60	60	70	42.7	56	56	70
P (barA)	1	99	99	56.2	55	55	99
Solvent flow (ton/h)	0	0	172.6	172.6	172.6	11.03	10.11
Wax flow (ton/h)	8.33	8.33	29.5	29.5	29.5	30	27.5
Stream no.	8	9	10	11	12	13	14
T (°C)	56	56	70	28.9	55.4	237.8	56
P (barA)	55	55	99	1	1	55	55
Solvent flow (ton/h)	0.919	162.0	2.94	2.94	0.894	3.834	3.834
Wax flow (ton/h)	2.5	0.049	5.83	0	0	0	0
Stream no.	15	16	17	18	19	20	21
T (°C)	56	97.5	78.5	70	60	60	28
P (barA)	55	101	100	99	1	1	55
Solvent flow (ton/h)	165.78	165.78	165.78	165.78	0.008	0.016	0.025
Wax flow (ton/h)	0.05	0.05	0.05	0.05	2.5	5.83	0

Table 9-23. Stream data for simulation PFD3-30.

Stream no.	1	2	3	4	5	6	7
T (°C)	60	60	70	65.2	70.6	42.5	55.3
P (barA)	1	99	99	90	89.8	55.5	55.4
Solvent flow (ton/h)	0	0	172.6	172.6	172.6	172.6	172.60
Wax flow (ton/h)	8.33	8.33	29.5	29.5	29.5	29.5	29.50
Stream no.	8	9	10	11	12	13	14
T (°C)	56	70	56	56	56	80	74
P (barA)	55	99	55	55	55	55.1	54.5
Solvent flow (ton/h)	11.0	10.1	0.919	162.0	165.78	165.78	165.78
Wax flow (ton/h)	30.0	27.5	2.5	0.049	0.05	0.05	0.05
Stream no.	15	16	17	18	19	20	21
T (°C)	53.1	95.3	76	70	70	28.9	55.4
P (barA)	54.1	100	99.9	99	99	1	1
Solvent flow (ton/h)	165.78	165.78	165.78	165.78	2.94	2.94	0.894
Wax flow (ton/h)	0.05	0.05	0.05	0.05	5.83	0	0
Stream no.	22	23	24	25	26		
T (°C)	237.8	56	60	60	28		
P (barA)	55	55	1	1	55		
Solvent flow (ton/h)	3.834	3.834	0.008	0.016	0.025		
Wax flow (ton/h)	0	0	2.5	5.83	0		

Appendix G. Capital cost estimation results for SCFE plants.

The costs are given in 1996 US$. The Chemical Engineering Producers Price Index (CEPPI) for 1996 = 382, CEPPI(2001) = 396.

The costs of the wax feed pump (P1) and reflux pump (P2) includes a spare pump. The cost of the solvent pump in PFD1 is calculated for two pumps with a total capacity of 120% of the design case. The cost of the solvent compressor and electrical drive (CMP1) in PFD2 and PFD3 is calculated for two compressors with a total capacity of 120% of the design case.

Table 9-24. Equipment capital cost: PFD1-25.

Heat exchangers	Description	Type	Area (m^2)	Tube P (bar)	Shell P (bar)	Cost ($)
HX1	Feed heater	Double pipe	3	120		2756
HX2	Reflux heater	Double pipe	3	120		2756
HX3	Solvent cooler	Finned air cooler	1000	55		175962
HX4	Separator heater	Shell & tube, fixed head	79	75	10	35148
HX5	Solvent condenser	Shell & tube, fixed head	3377	75	10	660140
HX6	Solvent cooler	Shell & tube, fixed head	56	120	10	29268
Pumps/compressors			Duty (kW)	Suction (bar)	Discharge (bar)	
CMP1	Solvent recovery	Centrifugal	400	1	55	750455
P1	Wax feed pump	Reciprocating	30	10	120	377974
P2	Reflux pump	Reciprocating	75	55	120	927958
P3	Solvent pump	Reciprocating	652	55	120	3814599
Columns & vessels			Ø (m)	Height (m)	Pressure (bar)	
C1	Extraction column	Packed pressure vessel	2.17	25	120	1835411
V1	Extr. product vessel	Vessel	1.3	3.6	5	21840
V2	Wax product vessel	Vessel	1.6	4.8	5	33407
SEP1	Separator vessel	Pressure vessel with demister	2.60	5.77	75	328425
V3	Solvent storage/buffer	Pressure vessel	4	8.3	75	289064
Total bare module cost						9285163
Total installed cost						**13292000**

Table 9-25. Equipment capital cost: PFD1-30.

Heat exchangers	Description	Type	Area (m^2)	Tube P (bar)	Shell P (bar)	Cost ($)
HX1	Feed heater	Double pipe	3	120		2756
HX2	Reflux heater	Double pipe	3	120		2756
HX3	Solvent cooler	Finned air cooler	1000	55		175962
HX4	Separator heater	Shell & tube, fixed head	73	75	10	33604
HX5	Solvent condenser	Shell & tube, fixed head	3126	75	10	623860
HX6	Solvent cooler	Shell & tube, fixed head	52	120	10	28108
Pumps/compressors			Duty (kW)	Suction (bar)	Discharge (bar)	
CMP1	Solvent recovery	Centrifugal	400	1	55	750455
P1	Wax feed pump	Reciprocating	30	10	120	377974
P2	Reflux pump	Reciprocating	75	55	120	927958
P3	Solvent pump	Reciprocating	603	55	120	3571179
Columns & vessels			Ø (m)	Height (m)	Pressure (bar)	
C1	Extraction column	Packed pressure vessel	2.1	30	120	2136058
V1	Extr. product vessel	Vessel	1.3	3.6	5	21840
V2	Wax product vessel	Vessel	1.6	4.8	5	33407
SEP1	Separator vessel	Pressure vessel with demister	2.50	5.67	75	300607
V3	Solvent storage/buffer	Pressure vessel	4	8.8	75	300963
Total bare module cost						9287487
Total installed cost						**13247000**

Table 9-26. Equipment capital cost: PFD1-35.

Heat exchangers	Description	Type	Area (m^2)	Tube P (bar)	Shell P (bar)	Cost ($)
HX1	Feed heater	Double pipe	3	120		2756
HX2	Reflux heater	Double pipe	3	120		2756
HX3	Solvent cooler	Finned air cooler	1000	55		175962
HX4	Separator heater	Shell & tube, fixed head	70	75	10	32819
HX5	Solvent condenser	Shell & tube, fixed head	3000	75	10	605448
HX6	Solvent cooler	Shell & tube, fixed head	50	120	10	27519
Pumps/compressors			Duty (kW)	Suction (bar)	Discharge (bar)	
CMP1	Solvent recovery	Centrifugal	400	1	55	750455
P1	Wax feed pump	Reciprocating	30	10	120	377974
P2	Reflux pump	Reciprocating	75	55	120	927958
P3	Solvent pump	Reciprocating	579	55	120	3554355
Columns & vessels			Ø (m)	Height (m)	Pressure (bar)	
C1	Extraction column	Packed pressure vessel	2.06	35	120	2458876
V1	Extr. product vessel	Vessel	1.3	3.6	5	21840
V2	Wax product vessel	Vessel	1.6	4.8	5	33407
SEP1	Separator vessel	Pressure vessel with demister	2.5	5.6	75	298036
V3	Solvent storage/buffer	Pressure vessel	4	9.4	75	315248
Total bare module cost						9585409
Total installed cost						**13626000**

Table 9-27. Equipment capital cost: PFD1-40.

Heat exchangers	Description	Type	Area (m^2)	Tube P (bar)	Shell P (bar)	Cost ($)
HX1	Feed heater	Double pipe	3	120		2756
HX2	Reflux heater	Double pipe	3	120		2756
HX3	Solvent cooler	Finned air cooler	1000	55		175962
HX4	Separator heater	Shell & tube, fixed head	68	75	10	32287
HX5	Solvent condenser	Shell & tube, fixed head	2914	75	10	592808
HX6	Solvent cooler	Shell & tube, fixed head	49	120	10	27222
Pumps/compressors			Duty (kW)	Suction (bar)	Discharge (bar)	
CMP1	Solvent recovery	Centrifugal	400	1	55	750455
P1	Wax feed pump	Reciprocating	30	10	120	377974
P2	Reflux pump	Reciprocating	75	55	120	927958
P3	Solvent pump	Reciprocating	562	55	120	3360486
Columns & vessels			Ø (m)	Height (m)	Pressure (bar)	
C1	Extraction column	Packed pressure vessel	2.03	40	120	2789465
V1	Extr. product vessel	Vessel	1.3	3.6	5	21840
V2	Wax product vessel	Vessel	1.6	4.8	5	33407
SEP1	Separator vessel	Pressure vessel with demister	2.41	5.59	75	285908
V3	Solvent storage/buffer	Pressure vessel	4	10.1	75	331935
Total bare module cost						9713219
Total installed cost						**13757000**

Table 9-28. Equipment capital cost: PFD2-25.

Heat exchangers	Description	Type	Area (m^2)	Tube P (bar)	Shell P (bar)	Cost ($)
HX1	Feed heater	Double pipe	3	120		2756
HX2	Reflux heater	Double pipe	3	120		2756
HX3	Solvent cooler	Finned air cooler	1000	55		175962
HX4	Heat integrator	Shell & tube, fixed head	281	120	75	80648
HX5	Feed trim cooler	Shell & tube, fixed head	79	120	10	35476
Pumps/compressors			Duty (kW)	Suction (bar)	Discharge (bar)	
CMP1	Solvent recovery	Centrifugal	400	1	55	750455
CMP2	Solvent compressor	Centrifugal	1864	55	120	4002144
	CMP2 drive	Electric	1864			100830
P1	Wax feed pump	Reciprocating	30	10	120	377974
P2	Reflux pump	Reciprocating	75	55	120	927958
Columns & vessels			Ø (m)	Height (m)	Pressure (bar)	
C1	Extraction column	Packed pressure vessel	2.17	25	120	1835411
V1	Extr. product vessel	Vessel	1.3	3.6	5	21840
V2	Wax product vessel	Vessel	1.6	4.8	5	33407
SEP1	Separator vessel	Pressure vessel with demister	2.60	5.77	75	328425
V3	Solvent storage/buffer	Pressure vessel	4	8.3	75	289064
Total bare module cost						8965106
Total installed cost						**13089000**

Table 9-29. Equipment capital cost: PFD2-30.

Heat exchangers	Description	Type	Area (m^2)	Tube P (bar)	Shell P (bar)	Cost ($)
HX1	Feed heater	Double pipe	3	120		2756
HX2	Reflux heater	Double pipe	3	120		2756
HX3	Solvent cooler	Finned air cooler	1000	55		175962
HX4	Heat integrator	Shell & tube, fixed head	260	120	75	76643
HX5	Feed trim cooler	Shell & tube, fixed head	73	120	10	33918
Pumps/compressors			Duty (kW)	Suction (bar)	Discharge (bar)	
CMP1	Solvent recovery	Centrifugal	400	1	55	750455
CMP2	Solvent compressor	Centrifugal	1725	55	120	3718140
	CMP2 drive	Electric	1725			97615
P1	Wax feed pump	Reciprocating	30	10	120	377974
P2	Reflux pump	Reciprocating	75	55	120	927958
Columns & vessels			Ø (m)	Height (m)	Pressure (bar)	
C1	Extraction column	Packed pressure vessel	2.1	41.3	120	2136058
V1	Extr. product vessel	Vessel	1.3	3.6	5	21840
V2	Wax product vessel	Vessel	1.6	4.8	5	33407
SEP1	Separator vessel	Pressure vessel with demister	2.50	5.67	75	300607
V3	Solvent storage/buffer	Pressure vessel	4	8.8	75	300963
Total bare module cost						8957052
Total installed cost						**13010000**

Table 9-30. Equipment capital cost: PFD2-35.

Heat exchangers	Description	Type	Area (m^2)	Tube P (bar)	Shell P (bar)	Cost ($)
HX1	Feed heater	Double pipe	3	120		2756
HX2	Reflux heater	Double pipe	3	120		2756
HX3	Solvent cooler	Finned air cooler	1000	55		175962
HX4	Heat integrator	Shell & tube, fixed head	250	120	75	74706
HX5	Feed trim cooler	Shell & tube, fixed head	70	120	10	33125
Pumps/compressors			Duty (kW)	Suction (bar)	Discharge (bar)	
CMP1	Solvent recovery	Centrifugal	400	1	55	750455
CMP2	Solvent compressor	Centrifugal	1656	55	120	3577470
	CMP2 drive	Electric	1656			95941
P1	Wax feed pump	Reciprocating	30	10	120	377974
P2	Reflux pump	Reciprocating	75	55	120	927958
Columns & vessels			Ø (m)	Height (m)	Pressure (bar)	
C1	Extraction column	Packed pressure vessel	2.06	35	120	2458876
V1	Extr. product vessel	Vessel	1.3	3.6	5	21840
V2	Wax product vessel	Vessel	1.6	4.8	5	33407
SEP1	Separator vessel	Pressure vessel with demister	2.5	5.6	75	298036
V3	Solvent storage/buffer	Pressure vessel	4	9.4	75	315248
Total bare module cost						9146510
Total installed cost						**13222000**

Table 9-31. Equipment capital cost: PFD2-40.

Heat exchangers	Description	Type	Area (m^2)	Tube P (bar)	Shell P (bar)	Cost ($)
HX1	Feed heater	Double pipe	3	120		2756
HX2	Reflux heater	Double pipe	3	120		2756
HX3	Solvent cooler	Finned air cooler	1000	55		175962
HX4	Heat integrator	Shell & tube, fixed head	243	120	75	73342
HX5	Feed trim cooler	Shell & tube, fixed head	68	120	10	32588
Pumps/compressors			Duty (kW)	Suction (bar)	Discharge (bar)	
CMP1	Solvent recovery	Centrifugal	400	1	55	750455
CMP2	Solvent compressor	Centrifugal	1608	55	120	3477810
	CMP2 drive	Electric	1608			94761
P1	Wax feed pump	Reciprocating	30	10	120	377974
P2	Reflux pump	Reciprocating	75	55	120	927958
Columns & vessels			Ø (m)	Height (m)	Pressure (bar)	
C1	Extraction column	Packed pressure vessel	2.03	40	120	2789465
V1	Extr. product vessel	Vessel	1.3	3.6	5	21840
V2	Wax product vessel	Vessel	1.6	4.8	5	33407
SEP1	Separator vessel	Pressure vessel with demister	2.41	5.59	75	285908
V3	Solvent storage/buffer	Pressure vessel	4	10.1	75	331935
Total bare module cost						9378917
Total installed cost						**13498000**

Table 9-32. Equipment capital cost: PFD3-25.

Heat exchangers	Description	Type	Area (m^2)	Tube P (bar)	Shell P (bar)	Cost ($)
HX1	Feed heater	Double pipe	3	120		2756
HX2	Reflux heater	Double pipe	3	120		2756
HX3	Solvent cooler	Finned air cooler	1000	55		175962
HX4	Integrator exchanger	Shell & tube, fixed head	844	120	100	176258
HX5	Integrator exchanger	Shell & tube, fixed head	844	75	75	173530
HX6	Integrator exchanger	Shell & tube, fixed head	844	120	75	173530
HX7	Solvent trim cooler	Shell & tube, fixed head	34	75	10	22260
Pumps/compressors			Duty (kW)	Suction (bar)	Discharge (bar)	
CMP1	Solvent recovery	Centrifugal	400	1	55	750455
CMP2	Solvent compressor	Centrifugal	1850	55	120	3974814
	CMP2 drive	Electric	784			68121
P1	Wax feed pump	Reciprocating	30	10	120	377974
P2	Reflux pump	Reciprocating	75	55	120	927958
Turbines			Duty (kW)	Inlet P (bar)	Outlet P (bar)	
EX1	Expander 1	Axial turbine	194	100	90	253995
EX2	Expander 2	Axial turbine	872	90	55	615380
Columns & vessels			Ø (m)	Height (m)	Pressure (bar)	
C1	Extraction column	Packed pressure vessel	2.17	25	120	1835411
V1	Extr. product vessel	Vessel	1.3	3.6	5	21840
V2	Wax product vessel	Vessel	1.6	4.8	5	33407
SEP1	Separator vessel	Pressure vessel with demister	2.60	5.77	75	328425
V3	Solvent storage/buffer	Pressure vessel	4	8.3	75	289064
Total bare module cost						10203896
Total installed cost						**14971000**

Table 9-33. Equipment capital cost: PFD3-30.

Heat exchangers	Description	Type	Area (m^2)	Tube P (bar)	Shell P (bar)	Cost ($)
HX1	Feed heater	Double pipe	3	120		2756
HX2	Reflux heater	Double pipe	3	120		2756
HX3	Solvent cooler	Finned air cooler	1000	55		175962
HX4	Integrator exchanger	Shell & tube, fixed head	781	120	100	166525
HX5	Integrator exchanger	Shell & tube, fixed head	781	75	75	163948
HX6	Integrator exchanger	Shell & tube, fixed head	781	120	75	163948
HX7	Solvent trim cooler	Shell & tube, fixed head	31	75	10	21234
Pumps/compressors			Duty (kW)	Suction (bar)	Discharge (bar)	
CMP1	Solvent recovery	Centrifugal	400	1	55	750455
CMP2	Solvent compressor	Centrifugal	1712	55	120	3690714
	CMP2 drive	Electric	726			65602
P1	Wax feed pump	Reciprocating	30	10	120	377974
P2	Reflux pump	Reciprocating	75	55	120	927958
Turbines			Duty (kW)	Inlet P (bar)	Outlet P (bar)	
EX1	Expander 1	Axial turbine	179	100	90	242238
EX2	Expander 2	Axial turbine	807	90	55	587940
Columns & vessels			Ø (m)	Height (m)	Pressure (bar)	
C1	Extraction column	Packed pressure vessel	2.1	30	120	2136058
V1	Extr. product vessel	Vessel	1.3	3.6	5	21840
V2	Wax product vessel	Vessel	1.6	4.8	5	33407
SEP1	Separator vessel	Pressure vessel with demister	2.50	5.67	75	300607
V3	Solvent storage/buffer	Pressure vessel	4	8.8	75	300963
Total bare module cost						10132885
Total installed cost						**14796000**

Table 9-34. Equipment capital cost: PFD3-35.

Heat exchangers	Description	Type	Area (m^2)	Tube P (bar)	Shell P (bar)	Cost ($)
HX1	Feed heater	Double pipe	3	120		2756
HX2	Reflux heater	Double pipe	3	120		2756
HX3	Solvent cooler	Finned air cooler	1000	55		175962
HX4	Integrator exchanger	Shell & tube, fixed head	750	120	100	161688
HX5	Integrator exchanger	Shell & tube, fixed head	750	75	75	159186
HX6	Integrator exchanger	Shell & tube, fixed head	750	120	75	159186
HX7	Solvent trim cooler	Shell & tube, fixed head	30	75	10	20888
Pumps/compressors			Duty (kW)	Suction (bar)	Discharge (bar)	
CMP1	Solvent recovery	Centrifugal	400	1	55	750455
CMP2	Solvent compressor	Centrifugal	1643	55	120	3546554
	CMP2 drive	Electric	697			64273
P1	Wax feed pump	Reciprocating	30	10	120	377974
P2	Reflux pump	Reciprocating	75	55	120	927958
Turbines			Duty (kW)	Inlet P (bar)	Outlet P (bar)	
EX1	Expander 1	Axial turbine	172	100	90	236778
EX2	Expander 2	Axial turbine	774	90	55	573793
Columns & vessels			Ø (m)	Height (m)	Pressure (bar)	
C1	Extraction column	Packed pressure vessel	2.06	35	120	2458876
V1	Extr. product vessel	Vessel	1.3	3.6	5	21840
V2	Wax product vessel	Vessel	1.6	4.8	5	33407
SEP1	Separator vessel	Pressure vessel with demister	2.5	5.6	75	298036
V3	Solvent storage/buffer	Pressure vessel	4	9.4	75	315248
Total bare module cost						10287614
Total installed cost						**14955000**

Table 9-35. Equipment capital cost: PFD3-40.

Heat exchangers	Description	Type	Area (m^2)	Tube P (bar)	Shell P (bar)	Cost ($)
HX1	Feed heater	Double pipe	3	120		2756
HX2	Reflux heater	Double pipe	3	120		2756
HX3	Solvent cooler	Finned air cooler	1000	55		175962
HX4	Integrator exchanger	Shell & tube, fixed head	728	120	100	158232
HX5	Integrator exchanger	Shell & tube, fixed head	728	75	75	155784
HX6	Integrator exchanger	Shell & tube, fixed head	728	120	75	155784
HX7	Solvent trim cooler	Shell & tube, fixed head	29	75	10	20534
Pumps/compressors			Duty (kW)	Suction (bar)	Discharge (bar)	
CMP1	Solvent recovery	Centrifugal	400	1	55	750455
CMP2	Solvent compressor	Centrifugal	1596	55	120	3453730
	CMP2 drive	Electric	677			63340
P1	Wax feed pump	Reciprocating	30	10	120	377974
P2	Reflux pump	Reciprocating	75	55	120	927958
Turbines			Duty (kW)	Inlet P (bar)	Outlet P (bar)	
EX1	Expander 1	Axial turbine	167	100	90	232540
EX2	Expander 2	Axial turbine	752	90	55	564007
Columns & vessels			Ø (m)	Height (m)	Pressure (bar)	
C1	Extraction column	Packed pressure vessel	2.03	40	120	2789465
V1	Extr. product vessel	Vessel	1.3	3.6	5	21840
V2	Wax product vessel	Vessel	1.6	4.8	5	33407
SEP1	Separator vessel	Pressure vessel with demister	2.41	5.59	75	285908
V3	Solvent storage/buffer	Pressure vessel	4	10.1	75	331935
Total bare module cost						10504367
Total installed cost						**15208000**

Appendix H. List of publications

During his PhD studies the author of this work was involved with the preparation of the following papers:

1. Crause J.C., Nieuwoudt I. "The fractionation of paraffin wax mixtures", Industrial and Engineering Chemistry Research, 2000, 39(12), 4871-4876.

2. Nieuwoudt I., Crause C., Du Rand M. "Oligomer Fractionation with Supercritical Fluids" Journal of Supercritical Fluids, Submitted for publication, March 2001.

3. Nieuwoudt I., Crause J.C. "Fractionation of paraffin wax mixtures" 5th International Symposium on Supercritical Fluids, Atlanta, USA, April 2000, 12 pages.

4. Nieuwoudt I., Crause C., Du Rand M. "Oligomer Fractionation with Supercritical Fluids" 3rd International meeting on High pressure Chemical Engineering, March 2001, Hamburg, Germany, CD-Rom publication.

5. Nieuwoudt I., Crause C., Du Rand M. "Supercritical fractionation vs Competing processes: An operating cost comparison" 6th Conference on Supercritical Fluids and Their Applications, 9-12 Sept. 2001 Maiori, Italy, Accepted.

6. Nieuwoudt I., Crause C., Du Rand M., Schwarz C. "Wax fractionation with supercritical fluid extraction" International Solvent Extraction Conference, Cape Town, South Africa, March 2002, Accepted.

7. Crause J.C., Nieuwoudt I. "A comparison between supercritical extraction and short path distillation" Paper presented at: South African Institution of Chemical Engineers, Western Cape Branch, Chemical Engineering R&D '99, Cape Town, 22 October 1999, PS05, 1 page.